THE EFFECT OF FREESTREAM OSCILLATORY MOTION ON HEAT TRANSFER IN THE WAKE REGION OF A CYLINDER IN CROSSFLOW

by

ALEXANDER M. PETRIE M.Sc.; A.R.C.S.T.

Thesis submitted to the University of Strathclyde in accordance with the regulations governing the award of the Degree of Doctor of Philosophy in the School of Engineering.

Department of Mechanical Engineering,
Paisley College of Technology,
Paisley,
Scotland.

JUNE, 1970

SUMMARY

Local Heat transfer measurements have been completed around a cylinder in crossflow for a Reynolds Number range of 5000 to 35000. Fluctuations in the freestream are varied by placing grids of rods of different diameters upstream of the cylinder. It is shown that the heat transfer in the separated (wake) region is extremely sensitive to freestream turbulence.

Hot wire anemometer measurements using a single wire probe have also been obtained in the wake region. Local mean and fluctuating velocity distributions around the cylinder wall are in agreement with the heat transfer distribution. The mean velocity profile and the decay of turbulence near the wall has also been measured. A spectrum analysis of the hot wire signal indicates that most of the fluctuating motion occurs at the vortex shedding frequency. It is suggested that there is a resonant interaction between the freestream fluctuations and the vortex shedding which accounts for this sensitivity to heat transfer. This is also demonstrated qualitatively using a sound field at a frequency equal to an existing frequency within the wake.

It is also suggested that the vortex shedding motion may be described analytically by the self excited oscillation evolved by Van der Pol and that the inclusion of a simple forcing function is representative of the freestream fluctuations.

An attempt is made to relate the fluid motion in the separation region to the heat transfer. This is done by assuming the apparent viscosity to be a function of the turbulence energy and hence using the relationship between generation, diffusion and dissipation of turbulence. It is then a straightforward matter to

solve this turbulent energy equation with momentum and conserved property equations to obtain the heat transfer.

ACKNOWLEDGEMENTS

The author wishes to express his thanks to Professor H. C. Simpson, University of Strathclyde for his help, advice and encouragement throughout his supervision of this work.

Thanks are also extended to the Board of Governors, Dr. E. Kerr, Principal and Mr. J. Anderson, Head of Department of Mechanical Engineering of Paisley College of Technology for allowing the author time and all facilities available to study for this degree on a part time basis.

NOMENCLATURE

ρ	Density
μ	Viscosity
ν	Kinematic Viscosity
α	Thermal Conductivity
C_p	Specific Heat at Constant Pressure
D	Cylinder Diameter
θ	Degrees of Arc
t	Time
r_i, r_o	Inner and Outer Radius of Foil
R	Body Radius
n^*	Frequency
ω	Angular Frequency
Λ	Length Scale of Turbulence
q_w	Wall Heat Flux
$\frac{q_w}{\Delta T} = h$	Heat Transfer Coefficient
p	Pressure
Δp	$p - p_\infty$
$\frac{\Delta p}{\frac{1}{2}\rho \bar{u}_\infty^2}$	Pressure Coefficient
T	Temperature
ΔT	$T_w - T_G$
T_1	$\frac{T_w - T}{T_w - T_G}$
δ_T	$\int_{\bar{u}_G}^{\bar{u}} (1 - T_1)\, dy$

x	Distance Parallel to Wall*
y	Distance Normal to Wall*
X	x/D
η	y/y_G
a	$\frac{4\bar{u}}{D}$ A Time Constant
u, v	Total Velocity Components Parallel and Normal to Wall
$\bar{u}$, $\bar{v}$	Time Averaged Velocity Components Parallel and Normal to Wall
u', v'	Fluctuating Velocity Components Parallel and Normal to Wall
$\sqrt{\overline{u'^2}}, \sqrt{\overline{v'^2}}$	R.M.S. Velocity Components
k	$\frac{1}{2}\{\overline{u'^2} + \overline{v'^2} + \overline{w'^2}\}$
$\overline{q^2}$	$2k$
Tu	$\frac{\sqrt{\overline{u'^2}}}{\bar{u}}$
E	Instantaneous Voltage
ΔE	Instantaneous Voltage Difference above E_o
E_o	Voltage across Wire in Still Air
$\bar{E}_b$	Voltage Corresponding to Velocity $\bar{u}$
$\overline{\Delta E}$	Time Averaged Voltage Difference above E_o
e'	Fluctuating Voltage
$\sqrt{\overline{e'^2}}$	R.M.S. Voltage
A, n, K	Constants Used in Hot Wire Anemometer Equations
σ	$\frac{\mu C_p}{\alpha}$ Prandtl Number based on Freestream Properties

---

* The dimensions of these co-ordinates are indicated as they occur within the text.

Nu	$\frac{hD}{\alpha}$ Nusselt Number based on Freestream Properties
St	$\frac{q_w}{\rho C_p \bar{u}_G \Delta T}$ Stanton Number
Re	$\frac{\bar{u}D}{\nu}$ Reynolds Number
R'_e	$\frac{\sqrt{\overline{u'^2}}\, D}{\nu}$ Oscillating Reynolds Number
K	k/k_G
Y	y/y_G
U	$\bar{u}/\bar{u}_G$
Rosc	$\frac{k_G^{\frac{1}{2}}\, y_G}{\nu}$
Re_T	$\frac{\delta_T\, \bar{u}_G}{\nu}$
$u^*_{G,o}$	$\frac{\left[\sqrt{\overline{u'^2}}\right]_{G,o}}{\left\{\left[\sqrt{\overline{u'^2}}\right]_{G,o}\right\}_{FST\,=\,0}}$
$u^*_{G,2n_1}$	$\frac{\left[\sqrt{\overline{u'^2}}\right]_{G,2n1}}{\left\{\left[\sqrt{\overline{u'^2}}\right]_{G,2n}\right\}_{FST\,=\,0}}$
Nu^*	$\frac{\text{Heat Transfer With Freestream Turbulence}}{\text{Heat Transfer Without Freestream Turbulence}}$
F.S.T.	Freestream Turbulence
F(n)	Frequency Density Function
τ	Shear Stress in Equation (6.10)
	$\omega_n t$ in Equation (5.4)
m, e, k, A, B, n	Constants in Equation (5.1)
α, β, ω_n	Constants used in Equation (5.3)
ϵ	$\frac{\text{Input Force}}{\text{Spring Force}}$ in Equation (5.5)

y	$x/\sqrt{\frac{\varepsilon}{\beta}}$ A Function in Equation (5.5)
α', β', x_o, A, ψ	Constants in Equations (5.7)
E^*_D	Dissipative Energy in Equation (5.12)
E^*_e	Excitation Energy in Equation (5.13)
a, b, c	Constants in Equation (6.10)
Y, Y'	Constants in Equation (6.11)
P	$9.24\left[\left(\frac{\sigma}{\sigma_t}\right)^{0.75}-1\right]$ used in Equation (6.15)
a_1, L, G	Functions in Equation (6.18)
n, m	Indices used in Equation (6.30)
$\varphi(\eta)$	$-\bar{v}$ A Function in Equation (6.47)
$A_1, A_2, A_3, B, \sigma_\tau$, $C_\mu, \sigma_{k,t}, C_D$, A_μ, A_D	Constants in Equations (6.59), (6.60), (6.61)

SUBSCRIPTS

∞	Freestream Conditions
G	Conditions at Edge of Boundary Layer
t	Turbulent
ℓ	Laminar
o	Overall Turbulence Intensity
$2n_1$	Turbulence Intersity at Twice Natural Frequency
w	Conditions at Wall

CONTENTS

	PAGE
SUMMARY	i
ACKNOWLEDGEMENTS	iii
NOMENCLATURE	iv
CONTENTS	viii
LIST OF FIGURES	xiii
INTRODUCTION	1
1. A LITERATURE SURVEY	5
1.1 Acoustic Streaming	5
1.2 Natural Convection	7
1.3 Forced Convection	10
1.3.1 Discrete Frequencys	10
1.3.2 Random Motion	14
1.4 Flow in Ducts and Tubes	19
1.5 Flat Plates	20
1.6 Ultrasonics	21
1.7 General	21
1.8 Conclusions	22
2. THE EXPERIMENTAL APPARATUS	24
2.1 The Constant Heat Flux Cylinder	24
2.1.1 Construction of Probe	26
2.1.2 Corrections and Possible Sources of Error	27
2.1.3 Position of Cylinder in Rig	28
2.2 Wind Tunnel	29
2.3 Turbulence Generating Grid	29

2.4 Sound Producing Equipment 30

2.5 Anechoic Chamber 30

2.6 Cylinder Wall Static Pressure 31

3. EXPERIMENTAL TECHNIQUE AND INSTRUMENTATION 32

3.1 Velocity and Pressure Measurement 32

3.2 Thermal Power and Temperature Measurement 32

3.3 The Hot Wire Anemometer 34

3.3.1 Calibration of Probes 35

3.3.2 The Calculation of Freestream Turbulence 36

3.3.3 A Correction for Low Mean Velocity and High Turbulence Intensity 36

3.3.4 Effect of Turbulence Components 37

3.3.5 Electronic Signal Analysis 41

3.3.6 Correction for Proximity to a Solid Boundary 41

4. EXPERIMENTAL RESULTS 42

4.1 MEASUREMENT OF FREESTREAM TURBULENCE 43

4.1.1 Representation of Data 44

4.1.2 Repeatibility of Data 44

4.1.3 Turbulence Spectrum Survey 45

4.2 PRESSURE DISTRIBUTION AROUND CYLINDER 47

4.3 MEASUREMENT OF HEAT TRANSFER 48

4.3.1 Possible Sources of Error 49

4.3.2 Local Distribution of Heat Transfer 50

4.3.3 Effect of Turbulence Intensity 51

4.3.4 Overall Heat Transfer 52

4.3.5 Repeatability 52

4.3.6 Effect of Horizontal and Vertical Rods 53

4.3.7 Comparison With Available Data 53

4.3.8 Comparison With Existing Theory 54

4.3.9 Effect of Surface Temperature Variation 55

4.4 HOT WIRE ANEMOMETER MEASUREMENTS AT THE REAR STAGNATION POINT 56

4.4.1 Turbulence Variations Around the Wall 56

4.4.2 Steady Flow Profiles 57

4.4.3 Fluctuating Velocity Profiles 58

4.4.4 Turbulence Spectrum Survey 58

4.4.5 Repeatability 61

4.5 HOT WIRE ANEMOMETER MEASUREMENTS AT THE FRONT PORTION OF THE CYLINDER 62

4.6 CORRELATION OF EXPERIMENTAL DATA 63

4.6.1 Rear Stagnation Point Fluctuations 63

4.6.2 Relations Between Heat Transfer and Fluid Motion at Rear Stagnation Point 64

4.6.3 Relations Between Heat Transfer and Free-stream Conditions 65

4.6.4 Correlation of Heat Transfer at Front of Cylinder 65

4.7 SOUND AS A HEAT TRANSFER PROMOTER 66

4.7.1 Experimental Technique 66

4.7.2 Detectable Frequencies 67

4.7.3 Analysis of Fluid Flow 67

4.8 DISCUSSION OF RESULTS 69

4.9 CONCLUSIONS 75

5. A SIMULATION OF THE FREESTREAM TURBULENCE EFFECT IN THE WAKE REGION 76

5.1 Self Excited Systems 76

5.2 Use of Van der Pol's Equation 78

5.3 Method of Solution 79

5.4 Other Forms of Van der Pol's Equation 81

5.5 Forced Oscillations in Self Excited Systems 81

5.6 Possible Methods of Studying the Fluid Mechanic Equations to Investigate Resonance Effects 84

5.7 Van der Pol's Equation Related to the Experimental Data 86

5.8 Conclusions 88

6. THE PREDICTION OF HEAT TRANSFER FROM THE FLUID MECHANICS OF THE WAKE REGION 89

6.1 Method of Leontev and Riagen {C29} 89

6.2 Method of Spalding {C28} 91

6.3 The Turbulent Kinetic Energy Equation 95

6.3.1 Solution of Equation (6.21) 98

6.3.2 Solution of Equation (6.22) 100

6.4 A One Dimensional Theory for the Prediction of Heat Transfer 101

6.5 The Prediction of Heat Transfer at the Rear Stagnation Point 103

6.5.1 The Analogue Computer Solution 107

6.5.2 Boundary Conditions 110

6.5.3 Procedure for Solution 110

6.5.4 Heat Transfer Boundary Conditions 111

6.5.5 Discussion of Results 112

6.5.6 Conclusions 114

SUGGESTIONS FOR FURTHER WORK 115

APPENDIX A THE THEORY OF OPERATION OF A HOT WIRE ANEMOMETER 116

APPENDIX B THE EXPERIMENTAL DATA 120

APPENDIX C A RELATIONSHIP BETWEEN FREQUENCY SPECTRUM AND TURBULENCE SCALE 121

APPENDIX D

BIBLIOGRAPHY 128

LIST OF FIGURES

CHAPTER I

Acoustic streaming around a cylinder. 1.1

Effect of horizontal sound field on natural convection heat transfer. 1.2

Effect of sound field on forced convection heat transfer from cylinder in crossflow. 1.3

Van Zijnen functions. 1.4

Effect of turbulence on overall forced convective heat transfer from a cylinder in crossflow. 1.5

Effect of Turbulence on local heat transfer from a cylinder in crossflow. 1.6

Use of sound as a drying process. 1.7

CHAPTER 2

Details of the constant heat flux cylinder. 2.1

Schematic diagram required for equation (2.1). 2.2

Schematic diagram of wind tunnel. 2.3

Table of grid sizes. 2.4

Direction of sound field relative to cylinder and airstream. 2.5

Anechoic chamber. 2.6

CHAPTER 3

Thermocouple calibration curve. 3.1

The hot wire calibrator. 3.2

Effect of wall proximity on hot wire readings. 3.3

A hot wire calibration curve for the measurement of freestream turbulence. 3.4

A hot wire calibration curve for the measurement of low velocity's 3.5

CHAPTER 4

Variation of freestream turbulence with grid size	4.1.1
Repeatability of freestream turbulence data	4.1.2
Effect of grid size on freestream turbulence spectra	4.1.3
Effect of Reynolds number on freestream turbulence spectrum	4.1.4
Effect of grid size on freestream turbulence spectrum	4.1.5
Variation of static pressure around cylinder	4.2.1
Typical distributions of temperature and temperature gradient around cylinder	4.3.1
Effect of heat flux on local heat transfer	4.3.2
Effect of cylinder manufacturing tolerances on local heat transfer	4.3.3
Effect of freestream turbulence on local heat transfer	4.3.4
Effect of freestream turbulence on local heat transfer	4.3.5
Variation of heat transfer at rear stagnation point with freestream turbulence	4.3.6
Variation of overall heat transfer with freestream turbulence	4.3.7
Variation of overall heat transfer in the separation (wake) region	4.3.8
Variation of overall heat transfer at the front (boundary layer) region	4.3.9
Repeatability of experimental data	4.3.10
Heat transfer at rear stagnation point: a comparison between horizontal and horizontal + vertical rod grids	4.3.11
Distribution of local heat transfer: experimental data of other workers	4.3.12
A comparison between experimental data and available theories	4.3.13
Variation of mean and fluctuating velocity in the wake region of the cylinder	4.4.1
Variation of mean velocity ($\bar{u}_G$) at rear stagnation point with freestream turbulence	4.4.2
Non-dimensional mean velocity profiles at rear stagnation point	4.4.3

Variation of fluctuating velocity ($\sqrt{\overline{u_c^2}}$) at the rear stagnation point with freestream turbulence 4.4.4

A non-dimensional form of data presented in Fig. 4.4.4 4.4.5

Non-dimensional fluctuating velocity profile at rear stagnation point 4.4.6

Effect of freestream turbulence on the vortex shedding process in the wake region 4.4.7

A spectrum of turbulence at the rear stagnation point 4.4.8

Amplification of R.M.S. velocity with freestream turbulence (measured at 2 x vortex shedding frequency) 4.4.9

Effect of turbulence on fluctuations at front stagnation point 4.5.1

Effectiveness of freestream turbulence on rear stagnation point fluctuations 4.6.1

A correlation between freestream turbulence and the wake fluctuations 4.6.2

A correlation between the fluid motion and heat transfer at rear stagnation point 4.6.3

A correlation between rear stagnation point heat transfer and freestream motion 4.6.4

Local heat transfer (non-dimensional) on front portion of cylinder 4.6.5

A correlation of heat transfer data at front stagnation point 4.6.6

Variation of vortex shedding frequency with Reynolds number 4.7.1

'Other'frequencies detected in wake region 4.7.2

Interaction between a sound field and wake region fluid mechanics 4.7.3

The amplification of discrete frequencies in the wake region by means of an applied sound field 4.7.4

CHAPTER 5

An analogue computer circuit for the solution of Van der Pol's equation 5.1

Solutions of Van der Pol's equation 5.2

Effect of external excitation on the solution of Van der Pol's equation 5.3

Energy relationships derived from Van der Pol's equation 5.4

Potential flow representations of the wake motion 5.5

Variation of $\dot{y}_{max}$ with ϵ 5.6

Effect of external excitation on the solution of Van der Pol's equation 5.7

Van der Pol's equation: Variation of maximum amplification with external excitation at several values of ϵ 5.8

A relationship between theoretical and experimental data 5.9

CHAPTER 6

A prediction of heat transfer from fluid motion in the wake region using above relationship 6.1

L, G functions used in equation(6.19) 6.2

Coefficients for polynomical curve fitting for L, G functions 6.3

Solutions of Bradshaws equations 6.4

Solutions of Spaldings equations 6.5

A one-dimensional theory to predict heat transfer from fluid motion at rear stagnation point 6.6

Circuits for equations (6.68), (6.69), (6.70) 6.7

The solution of Hiemenz equation 6.8

A relationship between experimental heat transfer and turbulence at rear stagnation point 6.9

Variation of heat transfer with turbulence at rear stagnation point for a range of c_μ 6.10

Variation of c_μ with Rosc 6.11

Prediction of heat transfer at rear stagnation point: A comparison with experimental data 6.12

Variation of turbulent energy profiles with parameter c_μ 6.13

A comparison of theoretical and experimental turbulent profiles 6.14

A comparison of theoretical and experimental mean velocity profiles for $\epsilon = 2.0$ 6.15

A comparison of theoretical and experimental mean velocity profiles for $\epsilon = 3.0$ 6.16

APPENDIX A

Typical variations of n and A in the conventional form of Kings law A.1

APPENDIX B

Overall freestream turbulence intensity for all grids B.1

Freestream turbulence spectra for grids A, E, J, K, L B.2-B.6

Effect of freestream turbulence on local heat transfer B.7-B.11

Local distribution of mean and fluctuating velocity wake region of cylinder B.12

Mean and fluctuating velocity profiles at rear stagnation point with grids A, E, J. K, L B.13-B.17

Turbulence spectra at rear stagnation point using grids A, E, J, K, L B.18-B.22

INTRODUCTION

Many experiments have been performed in recent years to establish the effect of oscillatory fluid motion upon heat transfer. There are two main reasons for this interest. Firstly, it has been known for a long time that experimental results of heat transfer reported by several observers show divergences which exceed the experimental errors. It is clear that a systematic influence is at work and many such discrepancies can be explained by the effect which freestream turbulence has on the rate of heat transfer. Thus there is the problem of prediction of heat transfer under such conditions.

Secondly, there is a great practical need to improve heat transfer in most heat exchange equipment by any reasonable means possible. This is especially true for gaseous fluids where the heat transfer coefficients tend to be low thus leading to large components of heat exchange equipment.

Common devices used to improve heat transfer include the additions of studs or fins to heat exchanger tubes. As well as increasing the surface area, disturbances in the flow are created which produce turbulent fluctuations. It is well known to designers that the second row of tubes in a boiler is more effective than the first row and this fact was properly connected with the influence of the wake emanating from the first row of cylinders upon the flow pattern around those in the second row.

In recent years many experimenters have studied the effect of sound and vibration as a means of improving heat transfer. There is now ample evidence to show (see later) that in general an increase in average heat transfer may be obtained.

However, the inherent difficulty of conducting precise measurements has lead to results of sometimes doubtful validity. One important general conclusion can be drawn and that is that the influence of sound or vibrations upon heat transfer becomes appreciable only under circumstances in which the oscillation is of sufficient intensity to alter the fundamental character of the boundary layer in the neighbourhood of the heat transfer area. From the practical point of view the intensities of sound fields for which effects have been found are significantly higher than those encountered, even in a noisy engineering environment and exceed the normal discomfort level for humans.

One of the practical problems which originally inspired interest in the effects of sound on heat transfer was encountered in rocket propulsion motors. In certain cases a combustion instability of high amplitude occurred, the local heat transfer to the walls was drastically increased resulting in local overheating and eventual disintegration of the motor.

Other situations have occurred however where it has been advantageous to increase the rate of heat or mass transfer by means of sound or vibration. In particular in chemical and food processing industries when heat sensitive materials have to be dried the use of an ultrasonic sound field within a conventional system has been shown to be extremely effective. One other especially attractive situation is its use in medical machinery since it can reduce or eliminate the possibility of chemical or bacteriological contamination. This has already been used to advantage in artificial kidney machines.

All practical uses have so far been restricted to natural convection systems or systems where only a low steady flow exists. Large improvements can be expected in these regions and it can also be expected that substantial improvements are unlikely in forced convection where turbulent flows already exist. This has already been verified and therefore a practical use of sound or vibration in this region is most unlikely unless in very specialised high performance heat exchange equipment. There are however possibilities for its use in a scientific study of turbulence when the turbulence can be simulated in a controlled manner either at discrete frequencies or over restricted frequency bands.

The prediction of heat transfer, particularly in forced convection, has so far had to rely heavily on experimental data. Where general prediction methods are available a great deal of expertise in computing techniques is required and often large computer facilities, which can impose a financial limitation. Apart from the difficulties already mentioned there is a lack of knowledge concerning the mechanism of interaction in turbulent boundary layers. Since most problems involve turbulent boundary layers this restriction is a serious one although it has been partly resolved in recent years by use of the turbulent kinetic energy equation which relates the diffusion, dissipation and generation of turbulence within the boundary layer.

There is still a heavy reliance on experimental data however, much of which is obtained using hot wire anemometry. This can produce considerable errors since measurements are difficult and measuring techniques are frequently not fully understood by the operator. The analysis of the electrical signal can also lead to error since most hot wire probes are calibrated in low

turbulent flows then used for measurements in highly turbulent flows. When more than one component of turbulence is required the measuring technique and analysis of data become more complex. In addition the physical size of the probe prohibits measurement in close proximity to the wall which is the region of most interest.

Most experimenters so far have studied the variation of intensity of turbulence only. The possible effect of scale of turbulence, which, physically measures the average size of eddies in the stream is usually dismissed by the statement that the scale is chosen sufficiently small compared with the dimensions of the body. This is reasonable when one considers the two possibilities which can exist, (a) a very small body such as a hot wire probe placed in a large scale of turbulence stream is best treated as one immersed in a time dependent stream and (b) a body which is large compared with the size of the eddies is best analysed in terms of a turbulent quasi-steady flow.

Despite the amount of experimental data available there is a lack of knowledge concerning heat transfer in separated flows particularly in the wake region of cylinders in crossflow. This is important in the design of heat exchanger tube bundles. However, in this region all of the difficulties already mentioned seem to exist. It is a region of low steady flow and high turbulence intensity, it contains a mixture of periodic and turbulent fluctuations and the eddy size is likely to be of the same order as the body size. Despite these formidable difficulties there is much that can be done to resolve at least some of the problems. It is therefore proposed to investigate both heat transfer and fluid motion in such a region.

1. A LITERATURE SURVEY

Much time and effort has been spent in examining the effects of oscillations on heat transfer. The situations encountered are somewhat varied. Some tend to be of a practical nature such as the drying of heat sensitive materials while others are restricted to simple models such as single cylinders or flat plates. Experiment and theory range from free to forced convection, thus to attempt a complete classification is very difficult. One attempt by Richardson {B14}, which was confined to the effects of sound fields, has categories related by the body dimension to wavelength ratio with subdivisions for (a) oscillations alone (b) oscillations plus buoyancy effects and (c) oscillations plus steady forced flow. His survey however, is mostly concerned with free convection.

In this survey special emphasis is laid on forced convection around cylinders in crossflow and only a crude classification is used to indicate the natural development of work done in other areas of this large field.

1.1 ACOUSTIC STREAMING

It is well known that relative vibratory motion between a solid surface and a fluid medium can cause various types of non-oscillatory flows to arise in the fluid near the surface. These steady currents, which are superimposed upon the vibratory motion are referred to as acoustic streaming.

In 1931, Andrade {A1} performed a photographic study of isothermal streaming around a cylindrical obstacle placed at

the antinode of a standing wave using tobacco smoke. A vortex motion consisting of four loops was observed. It was noted that the direction of streaming was away from the cylinder along the line of sound propagation which passes through the centre of the cylinder. In 1932, Schlichting {A2} published the first mathematical solution to the problem of streaming around a cylinder. His solution predicted two regions of streaming in each quadrant: a thin layer next to the cylinder moving toward the surface towards the propagation axis and an outer streaming layer with its direction away from the surface along this axis. This is illustrated in Fig.1.1.

In more recent years however, substantial progress towards understanding the isothermal flow of viscous fluids in the presence of vibrations has been achieved. Isothermal flow studies have been made for three basically different physical situations: for the case of a vibrating solid surface in contact with an otherwise undisturbed fluid medium; for the case of a stationary surface in contact with a medium subjected to vibration (sound); and for the case of vibrations in a fluid in the absence of boundary surfaces. In all three cases steady currents arise within the fluid medium, which are superimposed upon the periodic motion. The general mathematical theory of isothermal streaming, beginning with the Navier-Stokes equation for a viscous incompressible fluid shows that streaming is generated by the combination of viscous and non-linear terms appearing in the equations. This is a characteristic of problems which are basically nonlinear.

The remainder of the references in this section investigate these effects as produced by changes of intensity and frequency of the sound wave producing the flow.

1.2 NATURAL CONVECTION

As early as 1938 Martinelli investigated the effect of vertical vibrations upon heat transfer from a horizontal tube immersed in a tank of water. At low Reynolds number the coefficient of heat transfer was unaffected resulting from the dominance of free convection in this range. However, for sufficiently intense vibrations the coefficient of heat transfer was increased by 400%.

During the last decade many investigators have studied this phenomenon, mostly with considerable success. Two systematic investigations have been undertaken, one by Fand and co-workers and the other by Richardson.

Extensive experimental data has been obtained by Fand {B2, B3, B5, B6, B7, B8} using a $\frac{3}{4}$ in. diameter cylinder in both horizontal and vertical sound fields in order to measure overall and local heat transfer. A qualitative analysis {B2} observed that a phenomenon, entitled by Fand as "thermoacoustic streaming", took place above a certain "critical sound pressure level". This streaming was characterised by two oscillating vortices in the upper two quadrants above the heated cylinder. Quantitative data {B5} in the frequency range 1100 - 6120 Hz showed that above a sound pressure level (S.P.L.) of 140 dB a rapid increase in heat transfer occurred. It also indicated from the data that for $L/D \geq 6$ (where L = half wavelength, D = cylinder diameter) the sound pressure level for vortex development was independent of frequency.

A correlation of the form

$$\frac{h_v}{h_o} = 2.95\ (D)^{\frac{1}{4}}\ (\Delta T)^{\frac{1}{12}}\ (af)^{\frac{2}{3}}$$

was shown to be valid at least in the frequency range 100 - 1500 Hz {B6}. In this range the overall heat transfer was increased three-fold.

In order to achieve a better understanding of the physical mechanism of interaction between free convection and sound fields, local heat transfer coefficients around the circumference of a horizontal cylinder subjected to a transverse horizontal sound field were measured {B7}. At a frequency of 1500 Hz and a S.P.L. of 140 dB, maximum increases recorded on the lower and upper portion of the circumference were 250% and 1500% respectively as illustrated in FIG 1.2. The bottom loop 0^{o} - 97^{o} is a region of laminar boundary layer flow while in the upper loop 97^{o} - 180^{o} an oscillating vortex occurs. Although the development is not fully understood it is clear that this vortex motion by bringing in cold air causes the large measured increase in heat transfer over the upper part of the cylinder. The reason for the increase over the bottom half is less apparent as there is no obvious change in flow. The flow velocities however, are greater with sound, which is similar to imposing a low speed crossflow. Thus the boundary layer thickness is reduced, the thermal gradient at the surface increased and hence the local heat transfer improved. The observed convergence of the streamlines however, does not appear to be sufficient to account for the large observed increases and it is believed that the major part of the increase is due to acoustically induced fluctuations within the laminar boundary layer.

The differential equations which govern the coupling of vibrations and free convection have been studied {B3} and it was deduced that (i) the presence of harmonic oscillations modify the steady flow solution only when pressure gradients are present, (ii) the modifying forces have their most pronounced effect on the fluid closest to the surface, (iii) the product $a\omega$ (where a = amplitude of vibration and ω = circular frequency) is a measure of the magnitude of the influence of vibrations on free convection and agrees well with experimental correlations.

Both experimental and theoretical work has been done by Richardson {B9, B10, B11, B12, B13, B14} along similar lines to that of Fand. Experimentally the main difference lies in the fact that an optical technique was used to measure temperature gradients around the circumference of the cylinder instead of local surface temperature. Several interesting points were observed. It was concluded that the "critical sound pressure level" had no intrinsic fluid mechanical significance and in a study of vertical transverse vibrations around a horizontal cylinder local increases occurred at sound intensities below those for which comparable changes in average heat transfer were found. With a sufficiently intense vertical sound field, the boundary layer at the bottom of the cylinder was found to thicken, become unstable and then finally bubble up repeatedly into the top flume.

In his first theoretical study {B13}, Richardson considers the case of oscillations transverse to the cylinder using a standing sound wave of much greater wavelength than the cylinder diameter. The effect of natural convection is not taken into account, i.e. the contribution of buoyancy forces are omitted. The flow pattern then reduces to two regions of streaming in each

quadrant as in FIG 1.1, an inner dc layer and an outer layer. Three limiting case are then considered: (i) convection by outer streaming at small streaming Reynolds number. By considering the limit as the Prandtl number approaches zero the effect of the inner streaming motion is ignored. In this instance $\delta_{outer} >> \delta_{thermal} >> \delta_{ac}$ where δ represents the appropriate boundary layer thickness. (ii) convection by inner streaming as the Prandtl number approaches infinity and (iii) convection by outer streaming at large streaming Reynolds number. The trends indicated by the experimental data available illustrate the correctness of the calculations. In {B14} his analysis restores the influence of buoyancy into the calculations and illustrative solutions are obtained from the coupled momentum and energy equations which are valid only in the region near the lower stagnation point of the cylinder.

1.3 FORCED CONVECTION

Much experimental data is available investigating the effect of free stream turbulence on heat transfer and more recently this problem has been tackled using sound fields. For convenience this section is divided into two parts. The first dealing with the effect of discrete frequencies in the form of either sound waves or mechanical vibration on heat transfer and the second dealing with the more common random motion or turbulence effects. Most papers are concerned with cylinders in crossflow.

1.3.1 DISCRETE FREQUENCIES

Several experimenters have attempted to improve heat transfer by forced convection with sound or vibration but very few seem to

have used any systematic approach or producedany general conclusions. All have used a circular cylinder in either crossflow or parallel flow and most have vibrated the cylinder mechanically rather than vibrate the surrounding medium, consequently the applied frequencies are low, usually in the region of 0 - 150 Hz.

Anantanararanan {C1} using a parallel airflow has claimed an improvement of 130% in the freestream velocity range 10 - 20 m/s at frequencies varying from 75 - 120 Hz. His results however are of doubtful validity. Haughey {C6} obtained improvements of 20% during condensation of ethanol vapour.

Of interest in this report is the work of Fand and Cheng {C5} who have studied the effect of a standing sound field around a cylinder in crossflow in the Reynolds number range 590 - 10750. This is a continuation of work done by Fand in natural convection. Some of their results are plotted in FIG 1.3 and suggest that acoustic vibration increases the overall heat transfer rate in two regions. The first corresponds to the lowest experimental crossflow (Re ~ 1000) and the second to the highest crossflow (Re ~ 10000) with a minimum value occurring between the two extremes. The results also show that the percentage increase in overall heat transfer is greater in natural convection than for a Reynolds number of 1000. There are two possible reasons for this difference.

Firstly in the case of forced convection a vortex flow occurs in the absence of sound therefore in this case the addition of sound acts to amplify an effect already present whereas in the case of natural convection there is no vortex flow to start with and hence vortices created by sound have a relatively greater effect on the rate of heat transfer.

Secondly, the ratio of the vibrational velocity to the steady component of the velocity in the laminar boundary layer is much lower for Reynolds numbers of 1000 than for natural convection; thus, with crossflow the vibration represents a weaker disturbance and its effect on heat transfer from the lowest portion of the cylinder is correspondingly less than for the case of natural convection.

It was also shown that (Nu)v/(Nu)o (i.e. the ratio of heat transfer with sound to heat transfer without sound) decreases to about unity when Re → 5000. This is to be expected and the reasons for it are the same as are given above to explain the reduction of the effect of sound on heat transfer when Re → 1000.

The increases in heat transfer at Re ~ 10000 constitutes the most important result of this investigation. From local measurements it was shown that the injection of sound did not change the position of the separation point nor did it cause transition from laminar to turbulent boundary layer flow. It therefore follows that the sound field augmented the heat transfer rate by modifying the laminar boundary layer (0^{o} - 100^{o}) and by changing the flow in the wake of the cylinder (100^{o} - 180^{o}). The mechanics of interaction in the region of the laminar boundary layer is likely to be similar as that encountered in "thermoacoustic streaming" and free stream turbulence but the interaction in the wake cannot be the same as occurs in thermoacoustic streaming as it has been shown that this ceases to have effect at Re ~ 5000.

The mechanism appears to be a type of resonance between the acoustic oscillation and the vortices which are normally shed from the cylinder. This kind of resonance has been proposed by ZIJNEN {C18} to explain observations concerning the effect of freestream turbulence on heat transfer (See Section 1.3.2). Local measurements of heat transfer have shown that an improvement of 5% is achieved around the front portion of the cylinder and approximately 50% improvement in the separated flow region at the rear of the cylinder.

Richardson {C8} has discussed this mechanism which causes an increase in heat transfer in separated flows in the light of recent publications investigating the wake behind a cylinder. He suggests that the conclusions of Fand and Cheng are difficult to accept since the Strouhal frequency is about one tenth of the applied frequency. However, recent investigations by Bloor {G6} have shown that at a Reynolds number greater than 1000 the separated boundary layer is laminar and exhibits a dominant fundamental frequency upon which is superimposed a single frequency (designated the transition frequency) inside the wake. This frequency was found to be a function of the fundamental frequency and could be detected up to a Reynolds number of 4.5×10^4 although only outside the wake. This transition frequency corresponded to the applied frequency in Fand's experiments. Other investigators {G8} have shown that in the Reynolds number range $3 \times 10^3 - 5 \times 10^4$ the region in which vortex formation occurs was progressively reduced in size and that the position of turbulence approached closer to the cylinder. Gerrard {G9} has demonstrated that the wake is sensitive to acoustical disturbance at a frequency

equal to the transition frequency. The fluctuating velocity at the shoulder of the cylinder was found to increase by a factor of 2.5 when excited by a sound wave of magnitude u'/U_∞ = 0.01%. Richardson has also detected frequencies of values about half of Fands applied sound field in the inner near wake and claims that it is possible that the sound field could couple significantly into this flow since the field provides a massive disturbance of u'/U_∞ = 10% and significantly affect the heat transfer.

Kezios {C7} has investigated the effect of vibrating a cylinder in crossflow at the Strouhal frequency and his results have shown that maximum improvement in heat transfer was obtained when the excitation frequency coincided with the Strouhal frequency. Overall increases of about 20% were recorded.

1.3.2 RANDOM MOTION

It has long been realised that the influence of turbulence on the rate of heat transfer is very important in many engineering applications. It may lead to methods of controlling the heat transfer from solid bodies to fluid streams, whether in the direction of increasing them, for example in boilers or heat exchangers and thus improving their efficiency or in the direction of reducing them in order to protect the metal walls from deteriorating and burning out at high temperatures.

Several earlier experiments measuring local heat transfer {C13, C14} indicated wide discrepancies which may be at least partly due to the variation of turbulence in the freestream. Initial attempts to examine the effects of turbulence produced improvements up to 25% in overall measurements. Attempts were made to relate the changes in heat transfer to changes in skin friction {C15}

but concluded that while the skin friction on the front portion of the cylinder in crossflow remained unaltered by an increase in turbulence, local heat transfer rates were increased by 33%. Kestin and Maeder {C17} performed experiments to determine whether the role of the increased turbulence was to shift the point of laminar separation in subscritical flow, at the point of transition in supercritical flow and thus effecting or change in heat transfer. It was concluded that this was not the case and that the varying freestream turbulence affected local rates of heat transfer. Experiments covered the range $128 \times 10^3 < Re < 308 \times 10^3$ and overall improvements of 22% were detected.

Zijnen {C18} made a systematic investigation of the effects of scale, Λ, and the intensity of turbulence, Tu, in the range $2000 < Re < 25800$ using cylinders in crossflow. Increases of 38% were measured. From the correlation of the data

$$\frac{(Nu)_{TURBULENT}}{(Nu)_{LAMINAR}} = 1 + (Re.Tu)\ \psi\ \left(\frac{\Lambda}{D}\right)$$

the functions and ψ being illustrated in FIG 1.4, one interesting feature is that an optimum value of the influence of turbulence on heat transfer exists, at least for this range of tests. This has a striking similarity to the "apparent" resonance of the vortex shedding as suggested earlier. Kestin {C24}, by using a cylinder with tripping wires to fix the position of transition by changes due to turbulence thus leaving the flow pattern unaffected confirmed that the intensity of turbulence exerted a local effect on the rate of heat transfer but it was impossible to discern whether the local influence was important inside the laminar boundary layer, the turbulent boundary layer or the wake. The range of the experiments and the results are shown in FIG 1.5.

Further work to measure the local effects unmistakably demonstrated that the effects of turbulence intensity were confined to the laminar boundary layer and that these effects were unmistakably high reaching a value of 80% at the stagnation point. It should be remembered that the flow near the stagnation point of a blunt body is not fixed and performs oscillations in time, shifting from location to location around its theoretical position. (Once again the possibility occurs that the turbulence may be acting to amplify existing oscillations).

No correlation was given due to difficulties which Kestin points out. Firstly, techniques of measuring turbulence are not always mastered by experimenters and consequently errors of an order of magnitude are not uncommon. Secondly, there is no uniformity regarding the location of the measuring station. Thirdly, it has been shown that the intensity as well as the scale of turbulence may vary throughout the flow field and are affected by the details of the model present. Finally, the definition of turbulence may not constitute a sufficient criterion of similarity as nothing is said about the frequency spectrum. In spite of the failure to obtain a correlation, Kestin has summarized existing data in the form of qualitative statements:-

(i) Freestream turbulence may affect heat (and mass) transfer rates both locally and through an effect on the flow configuration.

(ii) The local effect is most pronounced on a laminar boundary layer near the stagnation point of a cylinder; it is absent in the case of a flat plate with zero pressure gradient and it does not occur when the boundary layer is turbulent or when the flow is separated, regardless of pressure gradient.

(iii) The combination of freestream turbulence and pressure gradient

seems to have some effect on the laminar boundary layer on flat plates.

(iv) The local effect does not seem to produce any measurable changes in drag and presumably not in skin friction.

(v) The local effect seems to consist of an increase in heat transfer rates with turbulence intensity.

Related experimental work which measures heat transfer in separated flows has also been completed {C17,C24} although no effect of freestream turbulence has been investigated. However, Richardson {C22} in an attempt to correlate the heat transfer data in these regions provides two correlation equations to include all available data and it is possible that at least part of this variation may be accounted for by freestream turbulence effects, which although contradictory to Kestin's conclusions do take into account the so called resonance effect observed by Zijnen. The correlation for the separated region is given by

$$Nu = \begin{cases} 0.057\ Re^{2/3} \\ 0.084\ Re^{2/3} \end{cases}$$

The problem of fluctuations superimposed on a steady velocity has also been studied mathematically. Lighthill {C14} examined the response of laminar skin friction and heat transfer to fluctuations superimposed on a steady velocity and predicted a change in phase relation between the skin friction and heat transfer. Gersten {C25} tackled a similar problem and in determining second order effects showed that time independent terms appeared which altered the nett wall shear stress and heat transfer. This is expected since the laminar boundary layer equations are non-linear and hence the average profile will, in general, differ from the steady state profile.

However, it has been calculated that the effect is several orders of magnitude smaller than the observed phenomenon.

STAGNATION POINT HEAT TRANSFER Another attack on this complex problem centres on the fact that vorticity carried by turbulent motion constitutes one of its most important physical characteristics.

Sutera {C21, C28} has theorized that vorticity amplification by stretching is possible, and perhaps the dominant underlying mechanism responsible for this sensitivity of the stagnation point heat transfer to small changes in freestream turbulence. A mathematical model is presented for a steady, basically plane stagnation point flow into which is steadily transported disturbed unidirectional vorticity having the only orientation susceptable to stretching. The resulting velocity and temperature fields in the stagnation point boundary layer are analysed assuming the fluid to be incompressible and to have constant properties. This theory bears a qualitative resemblance with the phenomena observed and reproduces approximately their order of magntiude. In spite of this the theory fails to explain the qualitative similarity between the effects of sound and turbulence and provides no sure guide to the particular quantitative characteristic of a turbulent stream to be used in any correlations. Thus the task of explaining the detailed mechanics of time observed phenomena remains unaccomplished.

SEPARATION ZONE HEAT TRANSFER The problems associated with calculating the heat transfer in separation zones are even more complex as outlined in a review by Hanson {C23}. No velocity fluctuation measurements exist at present for the flow immediately

behind a bluff body which might assist in calculations for this region. Only two papers are available which have tackled this problem.

The first, by Leontev {C27} attempts to use boundary layer theory in the eddy separation region behind a cylinder by assuming the existence of two stationary vortices, which is likely to be an oversimplified assumption.

The second is a one dimensional theory by Spalding {C28} who has obtained a power law relation between the Stanton number and the Reynolds number expressing the law of heat transfer for a wall adjacent to a region of turbulent separated flow. The derivation is based on Prandtls law of dissipation, diffusion and generation of turbulent kinetic energy. The result is expressed in the form

$$\left(\frac{\bar{U}_G D}{\nu}\right)^{0.4} St = \frac{3.2\left(\frac{k_G}{\bar{u}_G}\right)^{0.6}\left(\frac{D}{y_G}\right)^{0.4}}{P + 15.5}$$

Both references are discussed in greater detail later to assist in the development of the theory.

1.4 FLOW IN DUCTS AND TUBES

The practical significance of oscillations in rocket motors has lead to studies in tubes in which the flow oscillations are generated acoustically. A major experimental program was carried out by Jackson, two references being {D1, D9} and this is adequately described by Richardson {B14}. Briefly, the conclusions were that in the region of the tube wall covered with a laminar boundary layer, the local heat transfer coefficient exhibited a spatially periodic ripple with maxima at velocity antinodes and minima at velocity nodes, the average being scarcely different

from that found in the absence of sound. For conditions where the wall was covered by a turbulent boundary layer, the positions of maxima and minima were reversed and the average heat transfer was smaller than found in the absence of sound.

Theoretical investigations on the effects of acoustic oscillations on combustion have been completed {D8, D10, D12} which indicate that the acoustic combustion instability of a solid fuel rocket depends vitally on the response of the burning propellant surface to a sound field. This response can be significantly non-linear and could lead to severe oscillations. Other references related to this problem are {D13, D14}. Finally, the work of Low and Hodgin {D7} who studied the ablation of napthalene indicated that improvements in mass transfer occurred with increase in amplitude of the sound field but decreased with increase in frequency. The mass transfer was observed to increase at an antinode and to decrease at a node.

1.5 FLAT PLATES

The flat plate is also a hardy perennial in convection analysis and it is not surprising that some investigators have turned to this in an attempt to understand the influence of oscillations on laminar flows {E1, E2}. It has been shown however by analytical and experimental studies that the influence of oscillation is weak at least for small oscillations. Feiler {E3} claims improvements of up to 65% in what appears to be a highly turbulent flow. No mention is made of pressure gradient which has already been shown to be a requirement for improvements in heat transfer.

1.6 ULTRASONICS

This last section which concerns the use of ultrasonics to enhance heat and mass transfer is of interest, not for its relevance to this thesis but because of the practical applications tested successfully with pilot-plant, particularly in the chemical process industry. Several investigators are mentioned in the literature, in particular, Boucher {F3} has used the technique to improve the desorption rate of water from Silicone Gel. Tests at 6.8 kHz and 152 dB (S.P.L.) obtained a considerable saving in drying time compared to conventional equipment, FIG 1.7. A highly heat sensitive hormone powder has also been dried in one third of the time taken by conventional means. Other workers have used ultrasonic agitation to assist liquid/solid extraction {F1} and the absorption of gases into liquids, {F6, F7}.

Of particular interest are the experiments of Howkins {F8} who demonstrated the possibility of using ultrasonic energy to significantly increase the rate of dialysis of urea. The amplitude of sound used was sufficiently low to avoid damage to living cells. An increase in the dialysis rate of 3 to 5 times was obtained at 14 kHz and approximately 0.02 W/m^2. This tends to suggest that medical machinery offer considerable scope for use of sound and vibration since oscillations can be applied without the risk of bacteriological or chemical contamination. The principal limitation appears to be the damage that can be caused to living cells by over intense agitation.

1.7 GENERAL

From this brief survey of the effects of oscillation on heat

and mass transfer it will now be apparent that the range of situations where this effect can occur are many and the mechanisms involved are complex. Before any predictions of heat or mass transfer can be made detailed knowledge of the fluid mechanics in the relevant systems is required. It is for this purpose that the list of references in this section are compiled, particular attention being paid to flow in the wake region of cylinders in crossflow. These references are only mentioned directly as they occur within the text.

1.8 CONCLUSIONS

There is now ample evidence to show that the effect of oscillations on heat transfer can result in considerable improvements in many cases. The simple divisions in the literature survey have shown that most common engineering components in heat exchange equipment have been studied to a greater or less extent. General conclusions are difficult to make because the wide variety of geometries involves several different mechanisms which affect heat transfer. The work can however be divided into two categories.

The first concerns practical applications where heat transfer may be improved using oscillatory flows. Natural convection avails itself to large improvements or situations where only a low speed flow exists. Sound is the preferable choice of fluctuation source rather than mechanical vibration. For human safety ultrasonic frequencies are desirable but care has to be taken that no damage is done to cellular structures involved, especially in medical applications. All applications are highly specialised and so far any prediction of oscillatory effects has relied upon experimental data.

The second category which is mainly concerned with the prediction of the effect of fluctuations rather than with improvements is restricted to forced convection, normally with random oscillations rather than periodic. Prediction methods are now concerned with laminar and turbulent boundary layers and separated flows. Very little progress has been made in developing theories to calculate the effect of turbulence on heat transfer in these regions although there has been limited success with stagnation point heat transfer. Most calculations have still to rely on empirical correlations. often based on steady flow theory. No theories are yet available which attempt to understand the basic mechanism in the wake region of circular cylinders where a mixture of periodic and turbulent flow exists. Some experimental data are available demonstrating the sensitivity of this region to freestream turbulence and the suggestion that some type of resonance occurs is plausible.

2. THE EXPERIMENTAL APPARATUS

The experimental program was primarily concerned with measuring the sensitivity, to freestream turbulence, of the wake region behind a cylinder, using the heat transfer from the cylinder and a hot wire anemometer as the two means of measurement and to determine the controlling parameters which govern the interaction. This was achieved by having a cascade of horizontal, constant diameter rods upstream of the heated cylinder, the rod dimensions being such that the predominant frequency generated was in the same range as the vortex shedding frequency of the test cylinder. The stagnant region near the cylinder in the wake was considered to be sufficiently thick to permit accurate probing with the hot wire anemometer.

Qualitative measurements were also obtained in the same region using a sound field to investigate the excitation of existing discrete frequencies (at a higher range than the vortex shedding frequency) when subjected to external forcing.

Measurements were also recorded of the heat transfer around the remainder of the cylinder and also, using the hot wire probe, the mean and fluctuating velocities near the edge of the boundary layer in this region. Accurate probing within the layer was of course impossible since the thickness of the stagnant region produced by the 0.75 in. diameter cylinder in the velocity range tested was of the order of 0.006 in.

2.1 THE CONSTANT HEAT FLUX CYLINDER

The experimental determination of local heat transfer

coefficients requires that measurements be made of the local heat flux and surface temperature. Many devices which have been used to effect these measurements on the outer surface of a cylinder have employed electrical heating on account of the ease with which heat flux may be measured and controlled. They can be classified broadly as isothermal surface devices or constant heat flux devices. Where direct heating is employed to create an isothermal surface, several independently controlled heaters have to be used. If large circumferential variations in surface coefficient are present a large number of separate heaters are required to achieve a uniform surface temperature, thus complicating the design.

Under conditions of constant heat flux, variations in surface heat transfer coefficient appear as variations in surface temperature. Large variations in surface coefficient would therefore create large temperature variations which result in unacceptable errors due to axial or circumferential heat conduction. By generating heat in a thin conducting film, located at the outer surface of a cylinder, these errors can however be minimized. Giedt {C13} reports the successful use of a device of this type formed by winding a nickel strip 1 in wide x 0.002 in thick around the outer surface of a non-conducting cylindrical former. The spiral joint between the edges of the helically wound strip does however, constitute a discontinuity in surface heat flux, which may be a disadvantage. The design used in this thesis is similar to the Giedt probe except that the width of the metal foil is made approximately equal to the circumference of the probe, giving a seam parallel to the axis of the probe (i.e. corresponding to a helix of infinite pitch).

2.1.1 CONSTRUCTION OF PROBE

Stainless steel foil of a mean thickness of approximately 0.002 in. and having an overall tolerance of ± 0.75% was found to be commercially available and was used in the construction of the probe. Basically the instrument comprised of a sheet of stainless foil, two cylindrical copper conductors and five surface mounting thermocouples. (Later probes were constructed with thirteen thermocouples attached to the inner surface thus facilitating local measurements at 5^{o} intervals around one half of the cylinder). The components are shown in FIG 2.1

The foil was first cut to the size required and preformed so that when positioned inside a .75 in. bore tube it took up the shape of a 0.75 in. O.D. cylinder. This latter operation involved rolling the foil between cylinders of differing diameters, commencing with the largest diameter and working down in size until the required shape was obtained. A 0.75 in. strip at either end of the foil was then tinned and a thin coating of Araldite applied to the inner surface. When the resin was set, thermocouples were attached to predetermined positions on the inner surface of the foil and secured in position by a second application of resin.

With the thermocouple wire leading out from one end, the foil was clamped between two semi-circular sections of 0.75 in. bore tubing and the free end soldered to the stepped end of one conductor. Care was taken during soldering to cool the foil to prevent damage to the resin. The thermocouple wires were then lead through the filling hole and after aligning both conductors the remaining joint was soldered.

The outer surface of the foil was now coated with silicone grease to prevent sticking of the Araldite during the filling operation. A 0.75 in. bore cylinder was then slid over the foil and Araldite poured into the filling hole. Care was taken to ensure that all air bubbles were removed. This was done by adding a little Araldite at a time to the hole and allowing some to leave via the drain hole.

2.1.2 CORRECTIONS AND POSSIBLE SOURCES OF ERROR

Since under steady state conditions the direction of heat flux is essentially outwards from the probe, temperature gradients in the region of the inside surface can be expected to be weak. Errors due to conduction along the thermocouple leads and due to imprecise knowledge of the exact location of the heat junction will therefore be small. A correction is however, required for the temperature drop, ΔT_c, through the stainless steel foil. This can be calculated from the equation given by McAdam {G18}

$$\Delta T_c = \frac{q_w}{2\pi L \alpha}\left[\frac{1}{2} - \frac{r_i^2}{r_o^2 - r_i^2}\,\mathrm{Log}\,\frac{r_o}{r_i}\right]$$

where L, α, r_o and r_i are the length, thermal conductivity, external radius and internal radius of the foil. For the probe described this reduces to $\Delta T_c \approx q_w/2700$ where q_w is the power consumed in watts. For most cases ΔT_c will clearly be negligible.

The variation in thickness of the foil was ± 0.75%. Errors due to non-uniform heat generation resulting from variations in thickness will therefore be of this order.

Non-uniform heat generation, resulting from the variation of electrical resistivity and conduction errors are two other possible sources created by circumferential and axial temperature

gradients. Giedt however gives a method for evaluating these errors in particular due to circumferential temperature gradients. By considering the elemental strip of foil shown in FIG 2.2, an expression for the heat transferred to the air blown across the heated cylinder may be obtained by considering as follows:-

$$\left\{\begin{matrix}\text{HEAT}\\ \text{GENERATED}\\ \text{BY}\\ \text{CURRENT}\end{matrix}\right\} + \left\{\begin{matrix}\text{HEAT}\\ \text{CONDUCTED}\\ \text{INTO}\\ \text{ELEMENT}\end{matrix}\right\} = \left\{\begin{matrix}\text{HEAT}\\ \text{CONDUCTED}\\ \text{OUT OF}\\ \text{ELEMENT}\end{matrix}\right\} + \left\{\begin{matrix}\text{HEAT}\\ \text{CONVECTED}\\ \text{TO}\\ \text{AIR}\end{matrix}\right\} + \left\{\begin{matrix}\text{HEAT}\\ \text{CONDUCTED}\\ \text{INTO}\\ \text{CYLINDER}\end{matrix}\right\} + \left\{\begin{matrix}\text{HEAT}\\ \text{LOST}\\ \text{BY}\\ \text{RADIATION}\end{matrix}\right\}$$

which may be presented mathematically as

$$\frac{VI\,dx}{\pi D} + \left[\alpha l t \frac{dT}{dx}\right] = \left[\alpha l t\left\{\frac{dT}{dx} + \frac{d}{dx}\left(\frac{dT}{dx}\right)dx\right\}\right] + h\,l\,dx\,\Delta T$$

resulting in

$$h = \frac{q_w}{\Delta T} + \frac{0.17\alpha}{\Delta T} \cdot \frac{d^2\Delta T}{d\theta^2} \qquad (\text{BTU/HR.FT}^2{}^{\circ}\text{F}) \qquad (2.1)$$

The second term on the right hand side represents the effect of heat conduction along the foil. Its effect on h in general amounts to only a few per cent except near maximum and minimum points where it may be as much as 15%.

By plotting the temperature distribution around the cylinder an estimate of the gradient $\frac{dT}{d\theta}$ may be obtained. A similar plot of $\frac{dT}{d\theta}$ versus θ results in determining the position of maxima and minima corrections.

2.1.3 POSITION OF CYLINDER IN RIG

The probe was rigidly held in the horizontal plane on the centreline of the duct and normal to the airstream. When using the cylinders with only five thermocouples it was necessary to rotate the probe to measure the local variation of temperature at 15° intervals.

2.2 WIND TUNNEL

2.2 WIND TUNNEL

The tunnel used was of the open circuit type, the air supply being provided by a 4500 c.f.m. centrifugal fan powered by a 10 h.p., 3 phase motor. A schematic diagram is shown in FIG 2.3. On leaving the fan the air was passed through a honeycomb section and a series of wire mesh screens to smooth the flow. By means of a diffuser section the cross-section of the tunnel was increased to 9 ft^2 where fine wire mesh screens reduced the turbulence level still further. A suitable contraction shape reduced the tunnel section to a 1 ft^2 test section. Originally the tunnel was part of a rig to study the effect of sound fields on forced convection heat transfer and for this purpose an open test section was used, the whole test section being enclosed in an anechoic chamber.

The air supply was controlled by means of a simple butterfly valve at the fan inlet. A maximum velocity of 95 ft/s at the test section was available and the intensity of turbulence in the clear tunnel was approximately 0.7%. The rotational speed of the fan, 2890 rpm, corresponding to a frequency of 3630 Hz for the 12 blade impeller was not detectable on the spectrum analysis of the turbulence.

2.3 TURBULENCE GENERATING GRID

Grids of regularly spaced, horizontal cylindrical rods varying in diameter from $\frac{1}{8}$ in. to $\frac{3}{4}$ in. were used to generate in a controlled manner a relatively high level of turbulence upstream of the cylinder. The grids were situated at the entrance of the working section. Vertical movement was possible to ensure that maximum benefit was obtained at the test cylinder position, this was particularly desirable with the grids made from the large

diameter rods. The longitudinal intensity of turbulence produced by the grids ranged to more than 10%. The complete range of grids available is tabulated in FIG 2.4.

2.4 SOUND PRODUCING EQUIPMENT

The investigation of the coupling between a sound field and the discrete frequencies other than the vortex shedding frequency in the cylinder wake required a frequency range of 650 to 8000 Hz. This was obtainable by means of GOODMANS "MIDAX" horns, each of output 25 watts. A 300 watt DERRITRON solid state power amplifier was available to power 12 of these horns simultaneously in parallel. Great difficulty was obtained in obtaining a uniform sound field over a sufficiently large area to extract quantitative data. Several unsuccessful attempts resulted in measuring the coupling in a qualitative way using a bank of six horns placed directly above the heated cylinder. The direction of the sound relative to the flow in shown in FIG 2.5.

2.5 ANECHOIC CHAMBER

The anechoic chamber enclosing the test section was of simple construction. It consisted of two chipboard cubes one inside the other and completely isolated from each other by a mineral wool filing. The complete structure was isolated from the floor by a layer of mineral wool. A schematic diagram is shown in FIG 2.6. An 8 in. layer of acoustic rubber lined the inner walls to represent acoustic wedges, leaving a final working volume of $(6.5\ ft)^3$. The duct inlet and outlet were also isolated from the chamber using acoustic rubber.

2.6 CYLINDER WALL STATIC PRESSURE

To provide another method of checking the variation of velocity around the cylinder and also to locate the separation point, the wall static pressure around the cylinder was measured. A separate cylinder having the same diameter as the heated test cylinder was constructed to measure the static pressure. This was placed in the same position in the test section as the heated cylinder and it was a simple matter to rotate it and record the static pressure at different locations around the cylinder.

3. EXPERIMENTAL TECHNIQUE AND INSTRUMENTATION

3.1 VELOCITY AND PRESSURE MEASUREMENT

A Pitot-Static tube was located in the test section in the plane of the cylinder (with and without the test cylinder in position) to measure the uniformity of the velocity field. For the range of flows possible uniformity was within a few percent. During tests the Pitot-Static tube was used to provide a quick assessment of the mainstream flow. The impact orifice of the tube was 0.05 in. diameter and its design was according to B.S. 1042. The viscous effects for a Pitot-Static tube become important only for Reynolds Numbers less than 10, which corresponded in this case to a freestream velocity of 0.39 ft/s. Since the lowest freestream velocity of interest was 10 ft/s, the viscous effects were ignored.

All pressure measurements, from the Pitot-Static tube and the wall static pressure around the cylinder, were measured by means of a Betz Manometer having an overall range of 10 in.H_2O and a resolution of 0.05 in.H_2O.

3.2 THERMAL POWER AND TEMPERATURE MEASUREMENT

An A.C. electric current was used to supply electrical power to the test cylinder. Because of the uniformity in thickness of the foil, thus uniform electrical resistance, the power dissipated was easily obtained by measuring the voltage drop across the foil and the current passing through it. Initially an A.C. potentiometer was used to measure the voltage drop across the foil, the current passing through it (which was recorded as a voltage drop across a

"TINSLEY" 0.001 Ω standard resistance) and the power factor Cos Φ (i.e. the phase angle between voltage and current). For a range of current up to 50 amps the power factor remained constant at 0.98. During tests the power was measured more conveniently by means of a "SANGAMO-WESTON" ammeter having a maximum error of 0.25% (at full scale deflection) and an "AC" transistorised battery voltmeter to measure the voltage across the foil. The leads which were attached to the foil for this purpose were cemented into grooves on the surface of the copper conductors to prevent any localised disturbance in the flow.

The measurement of thermocouple e.m.f's was by means of a "CAMBRIDGE" Vernier Potentiometer capable of reading to within 0.1 μV. A "HEWLETT PACKARD" Null Detector was used instead of the more conventional mirror galvanometer, having a full scale deflection of 3 μV and being accurate to within 2%.

All the thermocouples used were manufactured from the same reel of commercial Copper/Constantan thermocouple wires of thickness 40 S.W.G. A representative sample was chosen from the batch for calibration purposes.

Each thermocouple calibrated was immersed into an oil-filled capillary tube and the tubes were immersed in a large insulated bath of water. The tubes were spaced sufficiently far apart to allow the circulation of water. The water was heated slowly with an electrical immersion heater and stirred constantly. Every few degrees, between 65°F and 120°F, the heater was switched off and when conditions were steady, the temperature was measured with a calibrated N.P.L. thermometer. The thermal e.m.f's were also noted.

A typical calibration curve is shown in FIG. 3.1. (The variation in e.m.f's recorded from the sample set of thermocouples did not exceed 2 μV at any temperature).

A check on the calibration of the thermocouples was performed before each test by measuring the airstream temperature with the thermocouples in the test cylinder and comparing with the air temperature measured with the N.P.L. thermometer.

3.3 THE HOT WIRE ANEMOMETER

The hot wire anemometer is the principal tool for turbulence research today. It is especially valuable for the measurement of a fluctuating flow field. With it such a flow field can be resolved in space and time with a sensitivity that is unavailable at present by any other means. Its use in incompressible flow has become standard practice, but so far has been confined mainly to low speed flow with small relative fluctuations. It is most suitable for measurements of low velocities and of boundary layer velocity profiles where its small physical dimensions offer the minimum disturbance possible. The main advantages of the hot wire are its short time response and the fact that its transient response can be made adequate up to very high frequencies.

There are at present two basic methods of hot wire operation. The constant current method (CC), is used mainly for measurement of small fluctuations because of its relatively low noise level. In studying relatively large fluctuations or transient flows starting from rest, the non-linearity of the hot wire is particularly apparent. In these cases, the constant temperature (CT) or constant resistance method is utilised because it allows suitable linearization of the

signal. As both methods have different merits, the preference of one over the other depends upon the particular application. Commercially available hot wire systems are of the C.C. or C.T. type.

For the present work a "THERMO-SYSTEMS" (MODEL 1010 A) constant temperature type was available with single wire probes, the sensing element being made from 0.00015 in. diameter tungsten wire. The theory behind the operation of a hot wire anemometer which is now fairly standard is described in Appendix A.

3.3.1 CALIBRATION OF PROBES

In this work no explicit corrections for aspect ratio, end losses and other non-linear effects of the probe are made, but instead these effects are accounted for by means of a calibration for each particular wire used. All probes used were calibrated in a special calibrator manufactured by "THERMO-SYSTEMS", FIG. 3.2. A low turbulence intensity air-stream was supplied from an air bottle and control was by a simple needle valve. It was possible to calibrate each probe for three ranges of mean velocity (i) $0 < \bar{u} < 4$ ft/s (ii) $4 < \bar{u} < 10$ ft/s and (iii) $10 < \bar{u} < 300$ ft/s by locating the probe at different positions in the calibrator. The velocity in each section was obtained by measuring the static pressure in the largest chamber and by reference to a supplied calibration chart. Typical calibration curves are shown in FIGS 3.4 and 3.5 for a probe in the freestream and rear stagnation point velocity ranges respectively. For the lower flow range it was noted that the index n acquired a larger value which is in accord with the data supplied in FIG A.1. (See Appendix A).

3.3.2 THE CALCULATION OF FREESTREAM TURBULENCE

The following expressions were used to calculate the mean and fluctuating velocity in the mainstream.

$$\bar{E}_b^2 = E_o^2 + A\bar{u}^n \tag{3.1}$$

$$\frac{\sqrt{\overline{u'^2}}}{\bar{u}} = \frac{2\bar{E}_b^2}{n(\bar{E}_b^2 - E_o^2)} \times \frac{\sqrt{\overline{e'^2}}}{\bar{E}_b} \tag{3.2}$$

which of course are only valid when $u'/\bar{u} << 1$. At the rear stagnation point where $u'/\bar{u} \sim 1$ other relationships are necessary and these are described in the next section.

3.3.3 A CORRECTION FOR LOW MEAN VELOCITY AND HIGH TURBULENCE INTENSITIES

In order to obtain reliable measurements of turbulence intensity when dealing with low velocity flows and relatively high intensities it is necessary to linearize the hot wire equation in a suitable manner. A method which is used by Sadeh {G12} has been chosen as suitable for measurements near the rear stagnation point and is outlined below.

Let the total voltage across the wire be expressed as

$$E = E_o + \Delta E \tag{3.3}$$

where ΔE is the total instantaneous increase in the voltage above its level at zero velocity. The instantaneous AC voltage e' caused by the fluctuation is

$$e' = E - \bar{E} = \Delta E - \overline{\Delta E} \tag{3.4}$$

Now consider low flows where $\Delta E/E_o < 1$ (for present work this ratio is of order 0.2). The total velocity normal to the wire is

$$U = \bar{u} + u' \tag{3.5}$$

and the relationship between instantaneous voltage and velocity is

$$E^2 = E_o^2 + AU^n \tag{3.6}$$

By substituting (3.3) into (3.6) and by neglecting second order terms in ΔE, equation (3.6) reduces to

$$2E_o \cdot \Delta E = A U^n \tag{3.7}$$

thus

$$U = \left[\frac{2E_o \cdot \Delta E}{A}\right]^{\frac{1}{n}} \tag{3.8}$$

Now even with large fluctuations present $e' << \overline{\Delta E}$. Therefore, by substituting (3.4), (3.5) into (3.8) and neglecting second order terms in e', then

$$\bar{u} + u' = \left[\frac{2E_o}{A}\right]^{\frac{1}{n}} (\overline{\Delta E})^{\frac{1}{n}} \left[1 + \frac{e'}{n\,\overline{\Delta E}}\right] \tag{3.9}$$

The mean and fluctuating velocities thus become

$$\bar{u} = \left[\frac{2E_o}{A}\right]^{\frac{1}{n}} (\overline{\Delta E})^{\frac{1}{n}} \tag{3.10}$$

$$\sqrt{\overline{u'^2}} = \left[\frac{2E_o}{A}\right]^{\frac{1}{n}} \left[\frac{\overline{\Delta E}^{\frac{1}{n}-1}}{n}\right] \times \sqrt{\overline{e'^2}} \tag{3.11}$$

thus

$$\frac{\sqrt{\overline{u'^2}}}{\bar{u}} = \frac{1}{n} \cdot \frac{\sqrt{\overline{e'^2}}}{\overline{\Delta E}} \tag{3.12}$$

where both $\sqrt{\overline{e'^2}}$ and $\overline{\Delta E}$ are easily obtainable.

3.3.4 EFFECT OF TURBULENCE COMPONENTS

So far it has been assumed that all the turbulent fluctuations are parallel to the direction of the mean velocity. This greatly simplifies the relationship between the measured fluctuating voltage and the fluctuating velocity. Also, since only a single wire is then necessary to obtain all the required information, the complex and difficult measurements involved with two wire probes is avoided.

For the flow region of interest however, it cannot be assumed that the fluctuations are parallel to the wall and indeed the effect of the normal component has to be taken into account.

It is now necessary to write equation (3.5) in the form

$$U = [(\bar{u} + u')^2 + v'^2]^{\frac{1}{2}} \tag{3.13}$$

Expanding this in the form of a series gives

$$U = \bar{u}\left[1 + \frac{u'}{\bar{u}} + \frac{v'^2}{2\bar{u}^2} - \frac{u'v'^2}{2\bar{u}^3} + \text{----}\right] \tag{3.14}$$

Equation (3.9) may now be modified to include the effect of v', the component normal to the wall, thus:-

$$\bar{u}\left[1 + \frac{u'}{\bar{u}} + \frac{v'^2}{2\bar{u}^2} - \frac{u'v'^2}{2\bar{u}^3}\right] = \left[\frac{2E_o}{A}\right]^{\frac{1}{n}}(\Delta E)^{\frac{1}{n}}\left[1 + \frac{e'}{n\Delta E}\right] \tag{3.15}$$

The steady and fluctuating components of the signal may be separated by time averaging equation (3.15). This leads to:-

$$\bar{u}\left[1 + \frac{\overline{v'^2}}{2\bar{u}^2} - \frac{\overline{u'v'^2}}{2\bar{u}^3}\right] = \left[\frac{2E_o}{A}\right]^{\frac{1}{n}}(\overline{\Delta E})^{\frac{1}{n}} \tag{3.16}$$

By substracting (3.16) from (3.15)

$$\bar{u}\left[\frac{u'}{\bar{u}} + \frac{v'^2 - \overline{v'^2}}{2\bar{u}^2} - \frac{u'v'^2 - \overline{u'v'^2}}{2\bar{u}^3}\right] = \left[\frac{2E_o}{A}\right]^{\frac{1}{n}}(\overline{\Delta E})^{\frac{1}{n}}\left[\frac{e'}{n\overline{\Delta E}}\right] \tag{3.17}$$

A comparison of (3.16), (3.17) with (3.10), (3.11) shows the interlinking of terms resulting from the addition of the v' component. The fluctuating voltage signal e' will now also include the effect of u' and v' so that a single wire may not be used to measure the mean velocity under such conditions. Equation (3.16) also shows that calibration of the hot wire anemometer in a low turbulence flow (as in the calibrator) to permit subsequent use in a highly turbulent conditions must lead to some error in the measurement of mean flow rate unless additional terms are included.

If the mean square voltage is measured then

$$\overline{e'^2} = K\bar{u}^2\left[\frac{u'}{\bar{u}} + \frac{v'^2 - \overline{v'^2}}{2\bar{u}^2} - \frac{u'v'^2 - \overline{u'v'^2}}{2\bar{u}^3}\right] \tag{3.18}$$

where

$$K = \left[\frac{A}{2E_o}\right]^{\frac{2}{n}}\left[\frac{n}{\overline{\Delta E}^{1/n-1}}\right]^2$$

After expansion this simplifies to

$$\overline{e'^2} = K\bar{u}^2\left[\frac{\overline{u'^2}}{\bar{u}^2} + \frac{\overline{v'^4} - (\overline{v'^2})^2}{4\bar{u}^4} + \frac{\overline{u'v'^2}}{\bar{u}^3} - \frac{\overline{u'^2v'^2}}{\bar{u}^4} + \cdots\right] \tag{3.19}$$

which is correct to fourth order terms.

It is now apparent, that in order to extract a correct value for $\bar{u}$, $\sqrt{\overline{u'^2}}$ and $\sqrt{\overline{v'^2}}$ it is necessary to determine experimentally the magnitudes of $\overline{v'^2}$, $\overline{u'\,v'^2}$, $\overline{u'^2}$, $\overline{v'^4}$, $\overline{u'^2v'^2}$ which involves at least a two wire probe. The choice therefore lies between an X wire probe or a single wire probe. With the former choice there is a reasonable chance of estimating the required components of velocity provided one accepts that present day electronics may not be capable of complete evaluation of the required correlations. There is also the disadvantage that the physical size of the probe restricts measurements to a reasonable distance from the wall. With the latter choice one must accept the limitations of a single wire probe but at least measurements in close proximity to the wall are feasible. Since it is heat transfer from the wall that is of interest, most of which is likely to occur close to the wall, a single wire probe seems the appropriate choice.

Having accepted that the above restrictions will lead to errors it is of interest to attempt a possible estimation of their magnitude.

One approach is to consider the fluctuations as purely harmonic (which is not unreasonable since there is a strongly periodic motion at the rear stagnation region). Thus:-

$$\left.\begin{aligned} u' &= u'_{max.} \sin \omega t \\ v' &= v'_{max} \sin \omega t \\ q'^2 &= u'^2 + v'^2 \end{aligned}\right\} \qquad (3.20)$$

Time averages of the fluctuating components are now easily evaluated and reduce to

$$\begin{aligned} \overline{u'^2} &= \tfrac{1}{2}(u'_{max.})^2 & \overline{u'^4} &= \tfrac{3}{4}(u'_{max.})^4 \\ (\overline{u'^2})^2 &= \tfrac{1}{4}(u'_{max.})^4 & \overline{u'^3} &= 0 \end{aligned} \qquad (3.21)$$

By considering the fluctuating vector q'^2 in several positions relative to the main stream direction, equations (3.16) and (3.19) can be solved simultaneously to obtain $\bar{u}$ and q'^2. By choosing experimental values of $\overline{E}$ and e'^2 the table below shows values of $\bar{u}$, q'^2 and Tu for q'^2 parallel, normal and at 45^o to the wall

	$\sqrt{\overline{u'^2}} = 0$	$\sqrt{\overline{u'^2}} = \sqrt{\overline{v'^2}}$	$\sqrt{\overline{v'^2}} = 0$
$\bar{u}$	.505	.903	.985
$\sqrt{\overline{q'^2}}$	.65	.55	.592
Tu	1.29	.608	.602

Taking these results at their face value suggests that errors involved by assuming that only a fluctuating component parallel to the wall exists may not be serious provided the magnitude of the normal component does not exceed that of the tangential component. This result requires experimental verification before any faith may be placed in it.

3.3.5 ELECTRONIC SIGNAL ANALYSIS

Both time averaged voltage and fluctuating voltage were recorded in order to analyse the velocity field. The former was obtained from the hot wire anemometer system directly while the latter required a separate R.M.S. meter. The r.m.s. voltage was recorded on magnetic tape for later analysis of the frequency spectrum. A "NAGRA III KUDELSKI" portable tape recorder was used for this purpose. Recording speed was normally 15 in/s and a flat response was available from 30-18000 Hz. A "BRUEL & KJERR" 2107 Constant Percentage Bandwidth frequency analyser and level Recorder were then used to obtain a spectrum analysis of all signals.

3.3.6 CORRECTION FOR PROXIMITY TO A SOLID BOUNDARY

When using a hot wire probe for velocity measurements close to a solid boundary errors may be introduced if the effect of the boundary on the rate of heat loss from the wall is ignored. From the information available {H2} it is suggested that the correction depends upon the ratio b/a, where b is the distance from the wall and a the wire radius. This correction is reproduced in graphical form in FIG. 3.3. This shows that a calibration curve for each position near the wall would be required for $b/a < 100$. For the present work no correction was required.

No information is as yet available for wires in close proximity to heated walls and it was assumed also to ignore any effects since the wall temperature was never more than $25^{o}F$ above the freestream temperature.

4. EXPERIMENTAL RESULTS

The main purpose of the experimental program was to obtain quantitative evidence concerning the sensitivity of heat transfer, in the separated flow region in the wake of the cylinder to free-stream turbulence. Data have been obtained by measuring local heat transfer and by use of a hot wire anemometer. A spectrum analysis has been completed with the hot wire data to confirm that a resonant interaction occurs between the flow in the wake and the freestream fluctuations.

The close relationship between the effects of turbulence and the effects of sound on heat transfer justified the time spent in obtaining quantitative information to demonstrate this resonant type of interaction. This qualitative information was obtained in a frequency range which was an order of magnitude greater than the vortex shedding frequency.

Local Heat transfer data in the laminar boundary layer region on the front portion of the cylinder is also presented together with a limited amount of hot wire data. The effect of freestream turbulence on pressure distribution around the cylinder is also presented.

4.1 MEASUREMENT OF FREESTREAM TURBULENCE

The conventional hot wire anemometry techniques already discussed have been used to measure the freestream turbulence produced by the grids. Measurements were restricted to a single wire probe thus assuming that the fluctuations were parallel to the direction of the mainstream. This was not considered a serious restriction since intensities of only 10% were recorded, thus this simplifying assumption was regarded as satisfactory. The mean and fluctuating velocities were calculated from the following relationships.

$$\bar{u} = \left[\frac{\bar{E}_b^2 - E_o^2}{A}\right]^{\frac{1}{n}} \qquad (4.1.1)$$

and

$$\sqrt{\overline{u'^2}} = \frac{2\,\bar{u}\,\bar{E}_b}{\bar{E}_b^2 - E_o^2} \times \sqrt{\overline{e'^2}} \qquad (4.2.2)$$

In the development of the theory, the turbulent kinetic energy k is used as a measure of the turbulence. This is defined below as

$$k = \frac{1}{2}\left\{\overline{u'^2} + \overline{v'^2} + \overline{w'^2}\right\} \qquad (4.3.3)$$

Since the components $\sqrt{\overline{v'^2}}$ and $\sqrt{\overline{w'^2}}$ have already been assumed to be much smaller than $\sqrt{\overline{u'^2}}$, the turbulent energy is now effectively defined as

$$k = \frac{1}{2}\left\{\overline{u'^2}\right\} \qquad (4.1.4)$$

The uniformity of the turbulence in the test section was measured in the plane of the test cylinder (without the cylinder present) and parallel to the grids. A variation of only a few percent was recorded except for grids K and L, that is, the grids

constructed from the largest diameter rod, where a variation of 20% was recorded. This was not surprising since the measuring station was only 15 diameters downstream of the grid which was an insufficient distance to allow diffusion of the large vortices throughout the stream. A much greater distance would be required for uniformity but as this would be at the expense of a reduction in turbulence intensity it was not desirable for the present experiments.

4.1.1 REPRESENTATION OF DATA

The turbulent fluctuations are presented in non-dimensional form as a fluctuating Reynolds number $\sqrt{\bar{u}^2}\,D/\nu$. This is simply the product of Re.Tu and when plotted against Reynolds number conveniently provides the intensity of turbulence as the gradient of the curve. The data is presented in graphical form in FIG.4.1.1 showing the intensity to be constant for each grid. (For the raw data see Appendix B).

4.1.2 REPEATABILITY

The repeatability of measurements was very good for the range of turbulence intensity from 0.675% to 5.78% as shown in FIG. 4.1.2. For reasons already stated the variation for grids K and L was much greater and is given in the table below.

GRID	K	L
MIN. Tu%	8.05	9.43
MAX. Tu%	9.65	11.5

4.1.3 TURBULENCE SPECTRUM SURVEY

So far only the overall intensity of turbulence produced by the grids has been presented. It was necessary for the present investigation to examine the distribution of this turbulent motion in the frequency spectrum to determine its effect on the strongly periodic wake fluctuations. The spectrum analysis of the hot wire signal was obtained, using the frequency analyser, in logarithmic form. Typical distributions, presented linearly, for convenience, are plotted in FIG. 4.1.3 in the frequency range 30 - 2000 Hz. The most noticeable feature is the sharp peak at the low frequency end of the spectrum, evidently due to the vortex shedding frequency from the grids. This is more apparent for the larger grids where the strong periodic fluctuations have not had time to decay before reaching the measuring station. Sometimes the first harmonic of this frequency was also detectable, suggesting an interchange of energy from the low frequency part of the spectrum to higher values. For the smaller grids the motion was more random up to 1000 Hz. (All raw data is tabulated in Appendix B).

The data can be presented in a more convenient way by considering the mean square energy, $\overline{u'^2}$, per unit mass as a function of frequency.

$$\overline{u'^2} = \overline{u'^2}\left\{\int_0^\infty F(n)\,dn\right\} \qquad (4.1.5)$$

where F(n) is the fraction of energy within the frequency interval n to n + dn, that is, the fraction of energy per unit frequency. The function F(n) is known as the frequency density function. The normalised energy over a frequency interval o to n is

$$\frac{\overline{u'^2(n)}}{\overline{u'^2}} = \int_0^N F(n)\,dn \qquad (4.1.6)$$

since the normalised energy over all frequencies, that is, the total energy is by definition equal to unity. The data can now be presented in dimensionless form by defining a dimensionless frequency

$$n = \frac{n^*}{a} \qquad (4.1.7)$$

where n* is the dimensional frequency and $a = 4\bar{u}_\infty/D$. The effect of Reynolds number on spectral distribution can now be seen in FIG. 4.1.4 and the distribution produced by different grids in FIG. 4.1.5. In the later FIG. it is quite apparent that the turbulent energy is spread over a larger frequency range as the grid size increases.

4.2 PRESSURE DISTRIBUTION AROUND CYLINDER

Before examining the local variation of heat transfer and velocity distribution around the cylinder it is an instructive exercise to examine the local variation in pressure around the cylinder. This assists in locating the separation point and indicates whether the addition of turbulence in the freestream merely increases the mean velocity and hence the local shear stress and heat transfer.

For the range of grids and Reynolds numbers tested the pressure coefficient was plotted from 0^{o} (front stagnation point) to 180^{o} (rear stagnation point). The distribution was as expected, a continuous decrease in pressure up to the separation point and then an almost constant value to the rear stagnation point. From 0^{o} to 40^{o} and 140^{o} to 180^{o} the pressure distribution was the same for all grids. The only variation in pressure with grid size occurred between 40^{o} and 140^{o} with the largest grid. All the data is plotted in FIG 4.2.1 for the range of flows and grids. Apparently the velocity distribution is independent of freestream turbulence for most parts of the cylinder. This is confirmed in a later chapter by hot wire measurements. A similar distribution of local heat transfer is observed but with a definite benefit resulting from turbulence effects. This improvement is likely to result from some mechanism other than a simple increase of mean velocity, possibly by a combination of the diffusion, dissipation and generation properties of the turbulence within the boundary layer. This will be discussed in detail later.

4.3 MEASUREMENT OF HEAT TRANSFER

The following procedure was adopted for measurement of local heat transfer around the cylinder. For each required crossflow the cylinder was heated slowly for all epoxy resin to reach its final temperature without any sudden expansion. Whenever possible the maximum cylinder temperature was kept below $50^{o}C$ in order to prolong the life of each cylinder. If this temperature was exceeded for long periods the resin became pliable and tended to detach itself from the foil, this being especially noticeable in the region of the thermocouple junctions. When this occurred the cylinder was replaced. This temperature limit was sometimes incompatible with the errors likely to result from measurement of small temperature differences (occurring at the maximum heat transfer position) and a compromise had to be made. Steady conditions were determined by observing the variation of e.m.f. from the hottest part of the cylinder which usually required about twenty minutes. Once steady conditions were attained the thirteen e.m.f.'s were measured, repeating the first few as a check. The power being supplied to the cylinder and the airstream temperature were noted before and after the e.m.f. readings, the average value being used in the calculations. Tests were done in the Reynolds number range from 4000 to 35000 for the complete range of grids. As far as possible the heat flux was maintained at one value but as already stated this depended upon the maximum and minimum temperatures measured during each test. The effect of heat flux variation is discussed later.

Before and after each series of tests the temperature of the unheated cylinder was compared with the measured airstream temperature. This provided a check on the thermocouple calibration and also to check if all thermocouples were in working order.

4.3.1 POSSIBLE SOURCES OF ERROR

During all tests the minimum temperature difference was $8C^{o}$. Using the thermometers available which were calibrated in 0.1 C^{o} the estimated maximum error was in the region of 2.5%. This was considered satisfactory for the present work.

A correction was required to account for the conduction of heat around the cylinder and has been shown to be dependent upon $\frac{d^2T}{d\theta^2}$. This required a graphical construction and was obtained by plotting first the local temperature versus θ, the position around the cylinder, then by measuring the slope at several points around this curve. A typical construction is shown in FIG. 4.3.1 and it is immediately apparent that the maximum value of $\frac{d^2T}{d\theta^2}$ occurs at the separation point and is negative. Attempts to measure this accurately proved rather difficult because of the small differences involved and in practice the best approximation was a visual inspection of the slope, $\frac{dT}{d\theta}$, near the separation point which was adjusted by eye. For all cases the correction, which was a reduction in heat transfer of 10-15%, was the same order of magnitude as found by other workers {C13}. Corrections to all other areas of the distribution were considered small enough to be neglected.

The requirement to limit the maximum and minimum temperature differences necessitated a variation in heat flux during the tests. This varied between 200 and 400 $Btu/ft^2\ ^{o}F$ and the changes in

temperature distribution due to the effect of heat flux was measured at several Reynold's numbers, one being plotted in FIG. 4.3.2. Nowhere was the variation greater than 3.5% which was considered satisfactory, being at the limits of accuracy of the temperature measurement. Because of this limitation in the manufacture of the cylinders no information was obtained to determine the effect of heat flux over a much larger range.

A similar test was performed to measure the effect of manufacturing tolerances of the cylinders. This was of the order of 5% and it is doubtful if it could be improved using the present techniques of manufacture. A typical variation is shown in FIG. 4.3.3.

4.3.2 LOCAL DISTRIBUTION OF HEAT TRANSFER

The local distribution of heat transfer is plotted non-dimensionally as a series of Nusselt Number (Nu) versus θ curves. Nusselt Number was chosen instead of the more logical Stanton number since it tends to be the most common parameter used making it easier to compare with other data. Difficulty was experienced in locating the position of minimum heat transfer at the separation point directly from the heat transfer distribution. Use was made of the pressure distribution (discussed earlier) from which it was observed that the separation region varied between 70^{o} and 80^{o} from the front stagnation point depending upon the level of freestream turbulence. Once located, this assisted in "correcting" the local distribution as described. The actual measured distribution in this region is shown by a broken line, as in FIG. 4.3.4 and FIG. 4.3.5. These graphs are typical of the effect of Reynold's number and turbulence intensity on local

heat transfer. (A complete set of data is provided in Appendix B). For all grids a similar pattern was recorded. The highest rate of heat transfer occurred at the front stagnation point followed by a rapid decrease to the separation point corresponding to the increase in boundary layer thickness. In the eddy separation region a weak temperature gradient corresponding to the weak pressure gradient until the freestream turbulence was increased sufficiently and then a more substantial gradient was observed from the separation region to the rear stagnation point. This is likely to be the result of the diffusion of turbulence from the oscillations in the wake towards the wall rather than by a convection process. A similar situation must exist at the separation region since conventional boundary layer theory predicts zero shear stress and hence no heat transfer. This is obviously false as shown by the data. It is shown later that a possible mechanism to account for this effect is a relationship between the turbulent generation by the maximum shear stress, now remote from the wall, and its diffusional and dissipation properties.

4.3.3 EFFECT OF TURBULENCE INTENSITY

The data have demonstrated the sensitivity of heat transfer to freestream turbulence at all positions around the cylinder. For a detailed study it is convenient to divide the local distribution into two parts. The first being the front region of the cylinder in the laminar boundary layer which is strongly dependent on velocity gradient, where it is necessary to examine the entire distribution. In the second region, in the wake of the cylinder, the heat transfer presents only a weak variation with θ.

For this reason, only the heat transfer at the maximum position has been studied in detail, that is, at the stagnation point. In this region a different type of flow exists from that at the front of the cylinder, namely a low speed steady flow with an oscillatory motion of the same order of magnitude superimposed upon it. The variation of heat transfer at the rear stagnation point is shown in FIG. 4.3.6 and a maximum improvement of 70% was attained. The data exhibits a linear variation, for all grids, with Reynold's number which is unexpected but is possibly the result of the short range of tests covered. To assist in the correlation of experimental data the results are extrapolated to determine the variation of heat transfer with Reynold's number for zero free-stream turbulence.

4.3.4 OVERALL HEAT TRANSFER

From the local heat transfer data it is a simple task to integrate each curve to determine overall heat transfer. This has been done for the two regions of interest by choosing a division at the position of separation. This was taken as 80^{o} from the front stagnation point. This data is presented in FIGS. 4.3.7, 4.3.8, 4.3.9.

4.3.5 REPEATABILITY

To check the repeatability of the experiments a comparison was made of data obtained from the same cylinder. Only the heat transfer at the front and rear stagnation points is compared in FIG. 4.3.10. Differences of only a few percent were detectable.

This also checked that the position of grids K and L relative to the cylinder had no measureable effect upon heat transfer.

4.3.6 EFFECT OF HORIZONTAL AND VERTICAL RODS

The sensitivity of the heat transfer in the wake region to fluctuations in the mainstream is now apparent. It is assumed that the directions of these fluctuations is in the plane of the test cylinder cross section. To determine if the wake region is sensitive to fluctuations parallel to the cylinder axis, grids were constructed from horizontal plus vertical rods. Thus vortices were also generated in this plane also. For two grid sizes, producing intensities of 2.63% and 5.78%, no effect of the vertical grids was detected with the equipment available as illustrated in FIG. 4.3.11.

It therefore appears that the direction of the freestream fluctuations is significant.

4.3.7 COMPARISON WITH AVAILABLE DATA

Several sources of experimental data exist with which to compare the present data and this can be grouped into three sections.
(a) Local Distributions of Heat Transfer: All the data available covering the present range of tests is shown in FIG. 4.3.12. It is not surprising that there is a large variation making a comparison difficult. Information regarding the experimental conditions is usually sparse and many variables can account for the differences. A lack of knowledge about turbulence conditions has already been shown to be important. The relative size of the turbulence scale to the cylinder diameter may also have an effect and lastly the method

chosen for heating (either a constant heat flux surface or a constant temperature surface) will be shown later to play an important part in standardising data. One example from the present data is superimposed on FIG. 4.3.12 and may be compared with the data of Fand and Cheng who used the same cylinder diameter and claimed to have a low turbulence airstream. Agreement appears to be reasonable in the separated region but in the laminar region there is a divergence of agreement. It is reasoned later that this is a result of the pressure gradient and the constant heat flux surface.

(b) Overall Heat Transfer: The correlation of overall heat transfer data given by McAdams is reputed to correspond to a free-stream turbulence of 1%. Comparing this with corresponding data in FIG. 4.3.7 produces differences of 25% which once again can be explained by the low heat transfer on the front region of the cylinder.

(c) Heat Transfer in Separated Region: Richardson has provided a correlation of experimental data behind bluff bodies as an upper and lower limit. No details are given about freestream turbulence levels but they are unlikely to have been greater than 3%. Thus agreement with the present data in FIG. 4.3.8 appears satisfactory.

4.3.8 COMPARISON WITH EXISTING THEORY

There are no theories available which will predict the heat transfer in the present problem by accounting for the effect of turbulence. A theory by Schlichting predicts the heat transfer in the laminar portion of the cylinder by assuming a constant temperature surface.

It agrees well with some data and serves to highlight the differences produced by the present data, FIG 4.3.13. In the separated flow region a theory by Leontev based on boundary layer theory is almost certain to be inadequate as no account has been taken of the fluctuating motion.

4.3.9 EFFECT OF SURFACE TEMPERATURE VARIATION

The claim that the variation of surface temperature has an important effect on heat transfer distribution has yet to be discussed. It has been demonstrated {G16} for flow inside tubes that a 16% difference in heat transfer exists between a constant temperature surface and a constant heat flux surface and it is claimed that this difference is accounted for by the difference in surface temperature variation. In this particular example with zero pressure gradient, the constant heat flux profile is greater than that of constant temperature. In another example {G17} the authors have studied heat transfer in accelerating boundary layers. The surface temperature is allowed to vary as $\bar{u}^{\beta}$. It has been predicted that the thermal boundary layer now penetrates the velocity layer thus causing a reduction in Stanton number. There is obviously no simple solution to this problem but the foregoing examples provide a plausible explanation for the discrepancies encountered in the experimental measurements. An attempt is made in Appendix D to investigate the effect of surface heating at the Stagnation Point but significant advances are restricted by the lack of experimental temperature profiles.

4.4 HOT WIRE ANEMOMETER MEASUREMENTS AT THE REAR STAGNATION POINT

It is now clear that the heat transfer in the wake region is extremely sensitive to freestream turbulence effects. A study of the fluid motion in this region requires the use of the hot wire anemometer which is the only suitable means of measurement available. Measurements in this region are obviously complex and interpretation of results difficult. The choice between a single wire probe or a X wire probe has already been discussed. For measurements in a low steady flow with a large turbulence intensity, the relationships between velocities (mean and fluctuating) and the voltage signal have already been derived and are shown below

$$\bar{u} = \left[\frac{2E_0}{A}\right]^{\frac{1}{n}} (\bar{E}_b - E_0)^{\frac{1}{n}} \qquad (4.4.1)$$

$$\sqrt{\overline{u'^2}} = \left[\frac{2E_0}{A}\right]^{\frac{1}{n}} \frac{(\bar{E}_b - E_0)^{\frac{1}{n}-1}}{n} \times \sqrt{\overline{e'^2}} \qquad (4.4.2)$$

Measurements were taken at several positions around the cylinder wall. The thickness of the boundary layer was determined by noting the variation in readings as the normal distance of the probe from the wall increased. By this means both mean velocity and fluctuating velocity profiles were obtained as well as the variation in boundary layer thickness around the wall. During these tests each probe was never used for more than one hour of continuous operation before being recalibrated.

4.4.1 TURBULENCE VARIATIONS AROUND THE WALL

Having located the edge of the boundary layer the variation of the mean and fluctuating components of velocity can now be studied.

Typical data are plotted in FIG. 4.4.1 covering the range of Reynolds number testd for the most turbulent freestream case (grid K). Apparently there is very little variation around the wall until at least 40^{o} from the rear stagnation point. This is similar to the pressure distribution and heat transfer distribution in this region. Measurements were taken up to 55^{o} from the rear stagnation point, where a sharp increase in both time average and r.m.s. voltage signal was observed. This was due to the probe being close to the free shear region and of course the relationships (4.4.1) and (4.4.2) are invalid since the flow is no longer parallel to the surface of the cylinder. The thickness of the boundary layer appears to be independent of freestream effects, being 0.15 in. thick at the rear stagnation point and decreasing rapidly to 0.1 in. over the remainder of the surface. Because of the invariance of all the variables around the cylinder wall, it was considered sufficient at this stage to examine only the variations normal to the wall at one position, namely the rear stagnation point.

4.4.2 STEADY FLOW PROFILES

The variation of mean velocity with freestream turbulence at the edge of the boundary layer is shown in FIG. 4.4.2. For the range of Reynolds numbers examined the mean velocity is approximately $\frac{1}{5}$ to $\frac{1}{10}$ of the freestream velocity depending upon the intensity of turbulence. The mean velocity profile can be non-dimensionalised in the usual manner (subscript G refers to conditions at the edge of the boundary layer) and the data are presented in FIG. 4.4.3. The data collapse fairly well on to a

"Power Law" profile for most of the boundary layer thickness. A rapid increase in the scatter of data occurs close to the wall, which is to be expected. The best fit profile, assuming a power law relationship has an index between 0.2 and 0.167. There is no evidence to show that this index is a function of freestream turbulence. It is interesting to note that this profile lies between the laminar case expected for low velocity flows, and the well known "$\frac{1}{7}$ Power Law" relationship for turbulent flows.

4.4.3 FLUCTUATING VELOCITY PROFILES

The overall magnitude of the r.m.s. fluctuations at the rear stagnation point are plotted in FIG. 4.4.4. For convenience in correlating the data (see later), the magnitude of these fluctuations with zero freestream turbulence has been extrapolated from the data. It is also convenient to present the data as a fluctuating Reynolds number

$$(Re')_{\infty} = \frac{\sqrt{\overline{u_o^2}}\,D}{\nu}$$

as shown in FIG. 4.4.5. The decay of turbulence towards the wall is represented by the ratio $\sqrt{\overline{u^2}}/\sqrt{\overline{u_o^2}}$ and is plotted in FIG. 4.4.6, having a similar form to the mean velocity profile. The scatter of data is much greater although a $\frac{1}{6}$ index in a power law provides a reasonable fit. No effect of mean velocity profiles, which serves to generate turbulence can be detected but this is likely to be obscured by the massive turbulence level in the wake.

4.4.4 TURBULENCE SPECTRUM SURVEY

So far the analysis has been confined to examination of the

overall turbulence level which has now been shown to be extremely sensitive to freestream turbulence. It has already been suggested that some sort of resonance occurs between the vortex shedding frequency and the freestream conditions. It is therefore necessary to examine the turbulence in closer detail via the frequency spectrum in order to confirm or reject this hypothesis. This analysis was completed in the same way as the freestream turbulence spectrum survey. It is immediately obvious that there is a strongly periodic component within the spectrum corresponding to twice the normal vortex shedding frequency. This is the direct result of measuring the fluctuations at the rear stagnation point which experiences the effect of vortices shed from both sides of the cylinder. Care was taken to record the fluctuating signal for a sufficient length of time to ensure a reliable recording. It is immediately obvious that the freestream fluctuations affect only the periodic component of the spectrum by amplifying the signal (FIG 4.4.7). No significant alteration of the turbulence component was observed.

This situation is analogous to the simple mechanical vibration of a spring/mass system with an oscillating force applied. The amplitude of motion of the mass is dependent upon the magnitude and frequency of the forcing function. In this problem the free-stream fluctuations represent the forcing function. With the available data it is not easy to separate the effect of magnitude (intensity) from the frequency (or scale) of the turbulence. However, most of the turbulent energy in the freestream is contained in the lower frequency range which includes the vortex shedding frequency.

Thus it is likely that the effect observed is primarily the result of the turbulence intensity. A much larger range of experiments would be required, such as {C18}, in order to separate the effect of frequency. For completeness a total typical spectrum recorded at the rear stagnation point is plotted linearly in FIG. 4.4.8.

The most suitable way to examine the data for the complete range of Reynolds number is to examine the amplification of the fluctuations at twice the vortex shedding frequency, with intensity of freestream turbulence. By choosing the fluctuations at this frequency (by using zero freestream turbulence values as a datum, which were evaluated by extrapolating available data) the results are as shown in FIG 4.4.9. It is immediately apparent that the freestream turbulence is most effective at low Reynolds numbers. This can be explained qualitatively for two reasons. Firstly, the datum magnitude increases with Reynolds number and therefore for the same freestream intensity there is likely to be relatively less amplification. Secondly, as the Reynolds number increases there is an increase in the turbulent component of the spectrum. Since the effective viscosity may be considered a function of turbulent energy it will become more and more difficult to amplify the periodic component. This implies that as the Reynolds number increases, and the vortex shedding frequency becomes less detectable, the effect of freestream turbulence will progressively decrease. In the limit, this is in agreement with the experimental work of Kestin {C24} who observed no improvement in heat transfer in the separated region for a Reynolds number range $1.5 \times 10^5 < Re < 2.6 \times 10^5$. It also appears from FIG. 4.4.9 that the appearance of a maximum benefit includes an effect of frequency of the freestream oscillations.

4.4.5 REPEATABILITY

Several tests were repeated and all results were found to be within 5% of each other provided care was taken to calibrate the hot wire probes frequently.

4.5 HOT WIRE ANEMOMETER MEASUREMENTS AT THE FRONT PORTION OF THE CYLINDER

There is not a great deal of analysis that can be done using the hot wire data at the front of the cylinder. The main restriction is the thinness of the boundary layer which does not permit accurate probing near the wall. However, it was possible to assess the distribution of mean and fluctuating components of velocity around the wall. As expected there was an increase in mean velocity from front stagnation point to region of separation. Very little variation in fluctuating component was detected around the wall and it is sufficient to show how this parameter was effected by freestream Reynolds number and turbulence intensity at the front stagnation point only. The results are plotted in FIG. 4.5.1 and are similar in form to those already measured in the freestream.

No further analysis has been completed in this region.

4.6 CORRELATION OF EXPERIMENTAL DATA

Three sections of experimental work have now been completed. The results indicate the sensitivity of heat transfer to freestream turbulence. Only the effects in the wake region will be dealt with in detail. It is now necessary to derive relationships between the heat transfer and the fluid motion in this region from the experimental evidence. The following correlations are obtained from FIG. 4.1.1, the freestream turbulence data; FIG. 4.3.6, the heat transfer data; and FIG. 4.4.5, the turbulence intensity data at the rear stagnation point. The accuracy and repeatability of this data has already been discussed and was found satisfactory except for the freestream turbulence data using the larger grids. This has been taken into account in the correlations. All Reynolds numbers are based on cylinder diameter and freestream viscosity, fluid properties being measured at freestream temperature and pressure. Only overall turbulence measurements are considered.

4.6.1 REAR STAGNATION POINT FLUCTUATIONS

A useful first step in the data reduction was the formation of a new parameter $U^*_{g,o}$, which is the ratio of the turbulent fluctuations with freestream turbulence present to the fluctuations when no freestream turbulence is present. This illustrates the effectiveness of the freestream fluctuations at low Reynolds number and demonstrates the effect of the resonant interaction. It is reasonable to expect a greater benefit in a region where the fluctuations are strongly periodic and also that this effect will decrease as the amount of turbulence increases (with increasing Reynolds number).

The data in FIG. 4.6.1 may now be related to the turbulence intensity using FIG. 4.1.1 by crossplotting the data to arrive at a series of $U^*_{G,o}$ versus $R'e_\infty$ curves for the range of Reynolds number. These curves then collapsed on to the single line in FIG. 4.6.2 by division of the abscissa of each curve by the corresponding Re^2_∞. Using standard curve fitting procedures, the data can now be evaluated using the following relationships

$$\frac{\sqrt{\overline{u'^2_{G,o}}}D}{\nu} = 0.026\,(Re)^{1.01}_\infty \qquad (4.6.1)$$

$$u^*_{G,o} = 0.283\left[\frac{(R'e)_\infty}{(Re_\infty/10^4)^2}\right]^{0.303} \qquad (4.6.2)$$

Equations (4.6.1) and (4.6.2) may now be combined to give

$$\frac{\sqrt{\overline{u'^2_{G,o}}}D}{\nu} = 1.96\,(Re)^{0.707}_\infty \times Tu^{0.303} \qquad (4.6.3)$$

4.6.2 RELATION BETWEEN HEAT TRANSFER AND FLUID MOTION AT REAR STAGNATION POINT

By a similar process a new heat transfer parameter Nu*, which is a measure of the effectiveness of the freestream turbulence on heat transfer, may be formed, being, the ratio of heat transfer with freestream turbulence to the heat transfer with no freestream turbulence. From FIG. 4.3.6 the following empirical relationship was obtained.

$$(Nu)_{FST=0} = 0.196\,(Re)^{0.564}_\infty \qquad (4.6.4)$$

After some manipulation of the graphical evidence the experimental data collapsed satisfactorily on to the single line shown in FIG.4.6.3 which can be represented by the equation

$$u^*_{G,o} = 0.288\left[\frac{Nu^* - 1}{(Re_\infty/10^4)^{1.67}}\right]^{0.307} \qquad (4.6.5)$$

$$= 28.8\left[\frac{Nu^* - 1}{(Re)_\infty^{1.67}}\right]^{0.307} \qquad (4.6.6)$$

4.6.3 RELATION BETWEEN HEAT TRANSFER AND FREESTREAM CONDITIONS

By using a similar graphical manipulation as above a direction relationship between heat transfer at the rear stagnation point and the freestream motion was obtained. The results are plotted in FIG. 4.6.4 and may be represented by the equation

$$\frac{Nu^* - 1}{(Re)_\infty^{1.67}} = 0.000478\left[\frac{(Re')_\infty}{(Re)_\infty^2}\right]^{0.986} \qquad (4.6.7)$$

i.e. $$Nu^* = 1 + 0.000478\,(Re)_\infty^{0.694} \times (Tu)^{0.986} \qquad (4.6.8)$$

4.6.4 CORRELATION OF HEAT TRANSFER DATA AT FRONT OF CYLINDER

The well known parameter developed from dimensional analysis for the laminar boundary layer is the $Nu/\sqrt{Re}$ group. It is now apparent that when a wide variation in freestream turbulence is present this is unsuitable for the correlation of data as indicated in FIG. 4.6.5 by plotting local heat transfer for several Reynolds numbers and turbulence levels. By adopting similar processes to the rear stagnation point, a correlation between the heat transfer at the front stagnation point and freestream motion is shown to collapse all data on to a single line (FIG. 4.6.6) which is represented by the equations below.

At the front stagnation point,

$$(Nu)_{F.S.T.=0} = 0.263\,(Re)_\infty^{0.547} \qquad (4.6.9)$$

From FIG. 4.6.6,

$$Nu^* = 1 + 3.15\times10^{-5}\left[\frac{(Re')_\infty}{(Re)_\infty^5}\right]^{1.37} \qquad (4.6.10)$$

$$= 1 + 3.15\times10^{-5}\,(Re)_\infty^{0.625}\,Tu^{1.37} \qquad (4.6.11)$$

4.7 SOUND AS A HEAT TRANSFER PROMOTER

It has now been demonstrated that for certain ranges of freestream Reynolds number the wake region is sensitive to freestream turbulence, the sensitivity resulting from a type of resonant interaction between the freestream fluctuations and the vortex shedding frequency. So far, this phenomenon has been demonstrated for low frequency amplification. Several attempts have been made to use a sound field for improving heat transfer. While this is likely to be impractical commercially, at least for forced convection, it is likely to prove useful in simulating turbulence at either discrete frequencies or in octave bands. Experimental work discussed in the literature survey tends to have chosen the frequency of the applied sound field at random. The remainder of this section is devoted to demonstrating qualitatively that by correct choice of the sound frequency to match discrete frequencies which exist in the wake region, a resonant condition similar to that at the vortex shedding frequency results.

4.7.1 EXPERIMENTAL TECHNIQUE

It has already been stated that it was extremely difficult to obtain a uniform sound field hence the restriction to qualitative data. The first part of the experiment consisted of detecting discrete frequencies in various parts of the wake using the hot wire probe. The probe was then positioned at various positions around the cylinder wall in the wake, it was then a simple matter to measure the fluctuations with and without the sound field.

This process was repeated for several crossflows and corresponding frequencies. Heat transfer data was also obtained at these frequencies but improvements were only in the region of 8% at the rear of the cylinder. No improvement was detected on the front portion of the cylinder.

4.7.2 DETECTABLE FREQUENCIES

Several discrete frequencies were detectable in the wake using the hot wire probe, the predominant one being the Strouhal or vortex shedding frequency which could be detected both inside and outside the wake. Near the rear stagnation point a signal at twice the frequency was detectable, receiving fluctuations from both sides of the cylinder. At the edge of the wake, between the separation point and the appearance of the first vortex, two other frequencies were measured. The first, corresponded to the "transition" frequency discussed by Bloor {G6} and the second, which was approximately half the "transition" frequency has already been observed by Richardson {C8}. The comparison of measurements with other data was in good agreement, as shown in FIG. 4.7.1 and 4.7.2.

4.7.3 ANALYSIS OF FLUID FLOW

No significant changes in the overall measurement of fluctuations was observed in the freestream when the sound field was applied as a result of the small increases involved. A study was thus made of the complete spectrum with and without the addition of the sound field. For each flow and frequency used the difference in the freestream spectrum was also noted. Typical effects of the sound field near the wall are illustrated in FIG. 4.7.3 with an

applied sound field of 1100 Hz, the effect of sound addition being indicated by the broken line. The results were not always a straightforward amplification at the applied frequency. Sometimes amplification at half the applied frequency was also detected. Depending upon the distance the sound penetrated the wake there could be very little effect at the single frequency but instead a small increase over a larger range.

The most convenient method of illustrating the phenomena around the cylinder wall, was to plot the difference in spectra at each station as indicated in FIG. 4.7.4. The increase in fluctuation level in the freestream is also indicated. Clearly, a small increase in the freestream motion can result in large alterations at all positions in the wake. The maximum benefit appears to be about 50^{o} from the rear stagnation point. All measurements were taken at 0.1 in. from the wall.

Unfortunately only qualitative data is available but nevertheless it does confirm previous experiments by illustrating this resonance phenomenon.

4.8 DISCUSSION OF RESULTS

Several sections of experimental work have now been completed and the data have been analysed to determine the effects of freestream turbulence on heat transfer with special emphasis on the wake region of the cylinder. The most straightforward measurements were those of heat transfer, being obtained using standard equipment which was easy to operate.

Three possible sources of error were considered with reference to measurements being made in the wake region. Firstly, the temperature gradient around the cylinder which induced a conduction error around the foil, required a correction to be made in the region of the separation point (approximately a reduction of 10-15%). This correction, which was a function of $\frac{d^2T}{d\theta^2}$ was not required in the wake region. Secondly, the requirement to vary the heat flux produced a maximum error of only 3% ... which occurred at the front stagnation point. Thirdly, manufacturing tolerances resulted in a variation of data from different cylinders which was of the order of 5%. Since a complete set of data was always obtained from one cylinder, this error was ignored. Thus the accuracy of the data in the wake region was satisfactory.

The analysis of the heat transfer data was conveniently divided into two sections, the front portion of the cylinder up to the separation point and from separation point to rear stagnation point. No attempt was made to determine whether the boundary layer on the front portion of the cylinder was laminar or turbulent but there was no evidence of this from the local heat transfer distribution in this region.

The location of the separation region was not precisely determined. This region is known to oscillate around a mean position and its sensitivity to freestream fluctuations which has been demonstrated by {G8} was confirmed by the variation of heat transfer in this region.

In the wake region the weak variation of heat transfer around the wall justified restricting the analysis to only the rear stagnation point.

A comparison of the experimental results with other available data does at first glance give cause for concern. However, the lack of background information, particularly turbulence levels, can account for most of the discrepancies. Largest differences however, which occurred at the front stagnation region may be explained satisfactorily by the difference in heating surfaces as the illustrative examples in Appendix D suggest. This can also account for the differences between the present data and that quoted in McAdams {G18}. The reasonably good agreement between the present experiments and Richardsons data {C22} may be partly due to the weak temperature gradient around the wall in this region.

The scarcity of theories to predict heat transfer in separated flows accentuates the complexity of the mechanism involved. From the results it is apparent that no conventional steady state theory is likely to adequately predict the results. With the information available the best attack is likely to include a relationship between the diffusion, dissipation and generation of turbulence energy near the cylinder wall. This is suggested by the variation in heat transfer at the separation region where the shear stress is now remote from the wall and the mechanism

suggested is the most likely means of effecting heat transfer.

The difficulties encountered in measuring turbulence, in particular when low steady velocities and large fluctuations are present, the analysis of the data and the choice between single wire and X wire probes, has already been discussed. The assumption that the steady flow velocity is parallel to the wall is reasonable up to about 50^{o} from the rear stagnation point. Beyond this point, the flow is being swept into the mainstream and hence there is a sharp change in direction. This was easily detected from the hot wire probe signal when a sharp rise in mean voltage was observed. Thus no analysis could be made in the region of the separation point. This was not considered a serious restriction.

The lack of available data for comparison restricts ones confidence in the results. The acceptance of the results at their face value is not however outrageous. While one admits that there are defects, there is also useful information to be gained from the analysis. The distribution of mean velocity and turbulent energy around the cylinder is shown to have an almost constant value which is in agreement with the heat transfer and pressure distributions in the same region. It is observed that an increase in mean velocity occurs with increasing freestream turbulence and it is suggested that this may be a form of acoustic streaming being produced by the action of the vortex shedding.

The constant boundary layer thickness is in keeping with the weak velocity gradient around the cylinder. The value of $y_G/D \approx 0.133$ is of the same order of magnitude as suggested by Spalding {C30}. The mean velocity profile indicates that turbulence is generated near the wall. Unfortunately measurements were

restricted to distances corresponding to $y/y_G > 0.2$ because of available equipment. The decay of turbulence in the boundary layer appears to follow a similar profile as the mean velocity. Close to the wall the results are scattered but this may partly be due to turbulence generation near the wall. Measurements within the boundary layer showed remarkably good repeatability provided care was taken to recalibrate the probes at frequent intervals. Thus the main restriction is in the analysis of the electrical signal which is unlikely to be improved upon until further knowledge of measurements in this type of flow is available.

The study of the interaction between the freestream turbulence and the fluctuations in the wake requires a detailed look at the turbulence structure. The turbulence spectrum obtained using the frequency analyser is sufficient to present a picture of what happens and it's useful to relate the mechanism into mechanical vibration terms. In the wake itself, a strongly periodic vibration is detected superimposed upon a turbulent background. The oscillation is of the self excited type, that is, energy is provided which keeps the oscillation at a constant intensity level. There is a linear increase in frequency of the periodic part of the spectrum with Reynolds number together with some increase in the turbulent part of the spectrum. Over the short range of tests completed the periodic component however always predominates. The existence of small oscillations in the freestream produces an amplification in the spectrum at the natural frequency of the self-excited system, the amount depending upon the frequency and intensity of the forcing oscillation. This is plainly observed in the analysis of the data.

It is assumed that most of the amplification is due to the intensity of the freestream turbulence. This is not an unreasonable assumption since examination of the turbulence spectrum in the freestream suggests that most of the energy is contained at the low frequency end of the spectrum in every case, thus it can be considered that any "effective frequency" which may exist is likely to remain constant.

The data shows that the greatest effect of freestream turbulence is at low Reynolds numbers which is not surprising when one considers that the relative effect of penetrating the stagnant region in the wake by the fluctuating motion will be more effective when the freestream velocity is low and there is little turbulence in the wake. It is not clear from the spectra whether a large increase in intensity at one frequency is better than the same increase in energy being spread over a large frequency range. As the periodic component becomes less predominant with increasing Reynolds number, the relative effect of the freestream turbulence is also less. Eventually no effect is likely to be detected (as confirmed by Kestin {C24} in the Reynolds number range at 200×10^5).

The data have been correlated successfully for the short range of Reynolds number tested using only the overall intensity measurements and by referring all data to the zero freestream turbulence case. The data collapse fairly well on to the curves illustrated, the dependence of Nusselt number on Reynolds number at zero freestream turbulence being similar to Richardsons correlation.

The amplification of predominant frequencies in the wake region has also been examined using the more sophisticated method

of sound waves. The application of a sound field at the same frequency as that detected in the wake has produced similar results. Qualitatively there is a clear demonstration that a small forcing oscillation applied at the same frequency as the natural frequency of the system can produce a large amplification of intensity.

4.9 CONCLUSIONS

1. The heat transfer in the wake region is strongly sensitive to the freestream turbulence for the range of Reynolds number tested.

2. The effect of the freestream turbulence is greatest when the vortex shedding frequency is the predominant fluctuation. The effect is likely to become negligible once the wake fluctuations are completely random.

3. The interaction between the freestream fluctuations and the fluctuations in the wake is a form of resonance.

4. The fluctuating velocity at the rear stagnation point is of the same order of magnitude as the steady flow velocity as far as can be determined by the present analysis.

5. The fluctuating and mean velocity profiles around the wall are in agreement with the pressure and heat transfer distributions.

5. A SIMULATION OF THE FREE STREAM TURBULENCE EFFECT IN THE WAKE REGION

There is now sufficient experimental evidence based on hot wire anemometer measurements to show that the sensitivity of heat transfer to freestream turbulence is due to the amplification of the vortex shedding oscillations. This is the result of a resonance between these oscillations in the wake and the fluctuations in the freestream. Once this fluid motion has been established it is then possible to predict the heat transfer. This is discussed in the next chapter. A comprehensive study of the wake region is obviously extremely complex and is unlikely to be resolved until a complete solution of Navier-Stokes equations is available. However, a simplified attack is possible by considering the fluid motion as a self-excited vibration. An analysis is then possible by using equations already derived to describe mechanical and electrical vibrations of this type. In the following paragraphs these equations are described together with the effect of including an external forcing function.

5.1 SELF-EXCITED SYSTEMS

A self-excited vibration may be defined as one in which the alternating force which sustains the motion is created or controlled by the motion itself; thus when the motion stops the alternating force disappears. This may be compared to a forced vibration where the alternating force sustaining the motion exists independently of the motion and persists even when the vibratory motion has stopped.

A self-excited vibration may also be defined as a free vibration with negative damping. With a linear positive viscous damping force, the force is proportional to the velocity of vibration and directed opposite to it. When the damping force is negative, it is also proportional to the velocity but has the same direction as the velocity. Thus instead of diminishing the amplitude of the free vibration, the negative damping will produce an increase. This may be examined by studying the differential equation for a single degree of freedom system having negative damping.

$$m\ddot{x} - c\dot{x} + kx = 0 \tag{5.1}$$

The solution to this equation may be written down immediately.

$$x = e^{\frac{ct}{2m}}\left\{A\cos nt + B\sin nt\right\} \tag{5.2}$$

This is clearly a vibration with an exponentially increasing amplitude, becoming infinitely large with time.

A consideration of the energy relations also serves to provide an additional understanding of the system. With positive damping, the damping force does negative work, being always opposed to the direction of the velocity and the kinetic energy is reduced during each cycle of the vibration. In the case of negative damping, the damping force (which is now the driving force) does positive work on the system thus increasing the kinetic energy during each cycle. It is clear that a self-excited vibration cannot exist without an extraneous source of energy. With a truly linear self-excited system the amplitude would become infinitely large with time.

In most practical cases however, the mechanisms of self-excitation and of damping exist simultaneously and separately. In all cases either the input force or the damping force in the system (or both) are non-linear and the input and dissipation curves intersect thus a maximum amplitude is reached.

5.2 USE OF VAN DER POL'S EQUATION

The above notions can be written in mathematical form. By modifying the damping coefficient to be a function of amplitude in such a way that it may be either positive or negative the following equation results.

$$\ddot{x} - (\alpha - \beta x^2)\dot{x} + \omega_n^2 x = 0 \qquad (5.3)$$

where x is a displacement, α and β are positive constants, and ω_n is the natural frequency of the system. The "dot" notation represents differentiation with respect to time. This is the simplest form of equation describing a self-excited system and was first studied by Van der Pol {G19}.

Before studying the solutions of this equation it is useful to reduce the three characteristics to one by means of a suitable non-dimensionalising process. The term ω_n may be removed by substitution of $\tau = \omega_n t$ so that,

$$\frac{d^2x}{dt^2} = \omega_n^2 \frac{d^2x}{d\tau^2} \quad , \quad \frac{dx}{dt} = \omega_n \frac{dx}{d\tau}$$

Thus,

$$\ddot{x} - \frac{\alpha}{\omega_n}\left[1 - \frac{\beta}{\alpha}x^2\right]\dot{x} + x = 0 \qquad (5.4)$$

where the "dots" now signify differentiation with respect to τ .

Also, by replacing $x = y\sqrt{\frac{\alpha}{\beta}}$, the equation (5.4) reduces to

$$\ddot{y} - \epsilon(1 - y^2)\dot{y} + y = 0 \qquad (5.5)$$

where $\epsilon = \frac{\alpha}{\omega_n}$

Thus, a damping coefficient has been introduced which is negative for small values of amplitude. The value of ϵ may be considered as the ratio of the maximum negative damping force to the maximum spring force.

$$\epsilon = \frac{\text{INPUT FORCE}}{\text{SPRING FORCE}}$$

5.3 METHOD OF SOLUTION

The solutions of non-linear equations are few except in special circumstances. The method used by Van der Pol was a graphical technique. Equation (5.5) can be rewritten in the form

$$\frac{dv}{dy} = \epsilon(1 - y^2) - \frac{y}{v} \qquad (5.6)$$

where $v = \frac{dy}{dt}$

A solution may now be found by mapping out a diagram with directional lines representing $\frac{dv}{dy}$ over a range of v and y. Having this whole field of tangents, a solution may be found by starting from any arbitrary point (that is, with an initial displacement y and velocity v) and constructing a curve following the tangents. This however is a very tedious process and solutions are much more easily obtained by use of an analogue computer. One possible circuit to provide the required solution is shown in FIG. 5.1 together with suitable potentiometer settings. It is not considered necessary to outline the scaling techniques which produce these settings.

The solutions were recorded in two forms using the X-Y plotter. Firstly, as y versus t, where the amplitude y was seen to build up to a maximum value and secondly by plotting the phase plane trajectory, that is $\dot{y}$ versus y. This second method was found to be the most convenient and easiest to interpret, consequently only this method was used throughout. The solution now forms a spiral which is asymptotic to a limiting value (known as the limit cycle). Depending upon the initial condition the spiral may approach the limit cycle either from the inside or the outside. The value of the limit cycle is however unaffected. This can be explained by a straightforward physical reasoning. If initially, more energy is being put into the system than is absorbed, the amplitude increases. If however the damping forces exceed the input forces the amplitude will decrease. This limit cycle solution is illustrated in FIG. 5.2 for several values of ϵ . For the case when $\epsilon = 0$ the non-linear term in equation (5.5) vanishes thus reducing to an equation of simple harmonic motion, being represented by a circle (or ellipse depending on the scaling factors) in the phase plane solution. As the value of ϵ increases the limit cycle is found to become more and more distorted, and while remaining periodic it is certainly no longer sinusoidal. Other interesting features of the solution are that the amplitude of the oscillation remains constant throughout the complete range of ϵ , the value of $\dot{y}$ being the only variable to change. Finally, the maximum velocity does not occur at the zero displacement position as in the case of simple harmonic motion.

5.4 OTHER FORMS OF VAN DER POL'S EQUATION

One other form of Van der Pol's equation has been used in the solution of a similar problem {G13} to investigate the oscillations of cylinders due to the wake motion. This is written in the form

$$\ddot{x} - (\alpha - \beta \dot{x}^2)\dot{x} + \omega_n^2 x = 0 \qquad (5.6)$$

Apparently this is similar to equation (5.3) except that the damping coefficient is dependent upon the magnitude of the velocity instead of the displacement. It was a simple matter to examine the solution of this equation using the analogue computer. Not surprisingly a phase change within the solution resulted and instead of having constant amplitude at all values of ϵ, the reversed occurred, the maximum velocity remained constant while the amplitude varied. There is no doubt that this is a valid solution but for the present problem the former presentation seems a more reasonable simulation of the physical situation and hence this form will be adopted.

5.5 FORCED OSCILLATIONS IN SELF-EXCITED SYSTEM

The analysis of motion of non-linear oscillations subjected to external excitation is a difficult task, and one which until now, has not been accomplished except in a few special cases. The difficulty arises mainly from the fact that the superposition principle no longer holds for non-linear systems, so that the total solution cannot be obtained from a synthesis of the particular solutions. This means that the general solution cannot be found by simple superposition of the natural motions and the forced motions.

Many new non-linear effects can also appear which make the trends in solution behaviour difficult to predict.

Before deciding if the equation derived by Van der Pol can successfully describe the wake oscillations behind the cylinder it is also necessary to examine the addition of a periodic external excitation in equation (5.3) to determine what phenomena may be expected as a result of an externally imposed excitation. It can then be decided whether the results are representative of the effect of freestream turbulence on the wake motion. A similar analysis has already been completed in {G19} and the main results are described below.

A harmonic excitation term is added to a slightly modified form of equation (5.4)

$$\ddot{x} - (\alpha' - \beta' x^2)\dot{x} + x = x_0 \cos \eta \tau \qquad (5.7)$$

where $\eta = \omega/\omega_n$, ω being the frequency of external excitation. After some algebraic manipulation this equation can be linearised into a form whose solution is known {G19}

$$x = A \cos(\eta\tau - \psi) \qquad (5.8)$$

The amplitude, A, of the oscillation is now given by

$$A^2\left[(1-\eta^2)^2 + \eta^2\left(\frac{\beta'}{4}A^2 - \alpha'\right)^2\right] = x_0^2 \qquad (5.9)$$

and

$$\tan \psi = \frac{\eta\left(\frac{1}{4}\beta' A^2 - \alpha'\right)}{1-\eta^2} \qquad (5.10)$$

The resonance curves $A(\eta)$ corresponding to various x_0 values are now plotted in FIG. 5.3. As often occurs in the solution of non-linear equations not all the branches of the resonance curves correspond to stable, that is physically realisable solutions. The

The procedure involved for stability evaluation is complex and only the results are indicated in FIG. 5.3. All the parts of the resonance curves lying below the dotted curve cannot be physically realised which is to say they are unstable. The horizontal part of this limit curve is given by

$$A = \left(\frac{2\alpha}{\beta}\right)^{\frac{1}{2}} \tag{5.11}$$

and the remaining portion is the geometric locus of all points on the resonance curves where vertical tangencies exist. The plausibility of this result can be demonstrated by considering an energy balance. The damping energy which, because of the potentiality for self-excitation, may also become excitation energy, is given by

$$E_D^* = \left(\frac{\beta'}{4}A^2 - \alpha'\right)\pi\eta A^2 \tag{5.12}$$

This is plotted in FIG. 5.4 against A. For the self-excitation amplitude ($A = A_o$) the E_D^* curve cuts the A-axis. The energy supplied by the excitation is

$$E_e^* = \pi x_o A \sin\psi \tag{5.13}$$

For the simplest case $\eta = 1$, the E_e^* curve is a straight line and therefore

$$E_e^* = \pi x_o A \tag{5.14}$$

This straight line is plotted in FIG. 5.4. There is a balance of energy at the intersection of the E_D^* and E_e^* curves for one (and only one) A value which is located above A_o. This amplitude belongs to the upper parts of the resonance curves in FIG. 5.3.

The associated motion is stable, since for smaller amplitudes energy is pumped into the oscillation, while for greater amplitudes energy is withdrawn. Thus, in both cases any disturbance is again neutralised.

Some of the properties of Van der Pol's equation have now been described and the rest of this chapter is devoted to relating this equation and its properties to the physical problem.

5.6 POSSIBLE METHODS OF STUDYING THE FLUID MECHANIC EQUATIONS TO INVESTIGATE RESONANCE EFFECTS

To derive a mathematical model which satisfactorily describes the resonance effect observed is extremely difficult and is unlikely to be resolved in the near future if at all. The logical starting point which is the Navier-Stokes equation has been attempted by reducing the equations to a one dimensional form. Even in this simplest state the evaluation of an equation which may be self excited is complex and has been unfruitful. The main difficulty is the lack of knowledge on the solution of non-linear equations having self excited properties since their reduction to a form similar to the Van der Pol equation is remote.

One other possibility is to consider a potential flow model {G20} and examine the flow at the rear stagnation point as follows.

The effect of a single vortex of variable strength is considered and it is shown that a peak value is obtained while the vortex is still close to the cylinder and at that instant the vortex is assumed to join the vortex street and remain constant beyond this point.

This is equivalent to the vortex breaking away as observed in practice. At the same instant a similar vortex of opposite sign is assumed to start growing on the opposite side of the cylinder and to grow until it reaches a maximum when it joins the vortex street.

By considering a two dimensional cylinder, radius a, in a uniform stream of velocity $\bar{u}$ (Fig. 5.5), with a single vortex strength $-K_o$ at point Z_o close to the cylinder, the complex potential is

$$w = -\bar{u}\left(z + \frac{a^2}{z}\right) - iK_o \log(z - z_o) + iK_o \log\left(\frac{a^2}{z} - z_o\right) \tag{5.15}$$

The velocity components (u,v) at any point (x,y) are given by

$$u = \bar{u} - \frac{\bar{u}a^2(x^2-y^2)}{(x^2+y^2)^2} + \frac{K_o(y-y_o)}{(x-x_o)^2+(y-y_o)^2} - \frac{a^2K_o\{y(xx_o+yy_o-a^2)+x(yx_o-xy_o)\}}{(x^2+y^2)\{(xx_o+yy_o-a^2)^2+(yx_o-xy_o)^2\}} \tag{5.16}$$

$$v = -\frac{2\bar{u}a^2xy}{(x^2+y^2)^2} - \frac{K_o(x-x_o)}{(x-x_o)^2+(y-y_o)^2} + \frac{a^2K_o\{x(xx_o+yy_o-a^2)-y(yx_o-xy_o)\}}{(x^2+y^2)\{(xx_o+yy_o-a^2)+(yx_o-xy_o)^2\}} \tag{5.17}$$

By assuming that the vortex moves parallel to the x axis, that is, v = 0 at (x_o, y_o). Then,

$$K_o = \frac{2\bar{u}y_o(x_o^2+y_o^2-a^2)}{(x_o^2+y_o^2)} \tag{5.18}$$

Since there is no vertical motion of vortices

$$\frac{dx_o}{dt} = u = \frac{\bar{u}(x_o^2+y_o^2-a^2)}{x_o^2+y_o^2} \tag{5.19}$$

and therefore

$$t = \frac{1}{\bar{u}}\int\left(\frac{x_o^2+y_o^2}{x_o^2+y_o^2-a^2}\right)dx_o \tag{5.20}$$

By assuming values for y_o at a point near the rear stagnation point it is a straightforward matter to calculate the variation in velocity as the vortex moves downstream.

The maximum velocity obtained during the downstream motion of the vortices was found to be approximately ten times larger than the measured r.m.s. values. The effect of the freestream fluctuating motion was included by replacing $\bar{u}$ in equation (5.18) by a steady and fluctuating component, that is, $\bar{u} + u'$, where u' was a simple sinusoidal motion $\lambda \mathrm{Sin}\omega t$. Based on the available experimental data λ is approximately $0.1\bar{u}$ which produced an amplification in the wake of the order of 20%. It is clear that this greatly simplified model is inadequate for the prediction of local flow details.

A slightly more complex model which consisted of two vortices spaced as indicated in FIG. 5.5 also produced inadequate results.

It is therefore suggested that this technique is also likely to be unfruitful at least until more knowledge about the vortex shedding process is known.

5.7 VAL DER POL'S EQUATION RELATED TO THE EXPERIMENTAL DATA

The three parameters α, β, ω_n in Van der Pol's equation have already been reduced to one, ϵ , by means of a non-dimensionalising process. The resulting form of the equation, (5.5), is now used for the remainder of the analysis. It is now necessary to relate the physical parameters to the equation (5.5) by means of ϵ . This can be accomplished by considering the maximum value of $\dot{y}$ for each value of ϵ as a measure of the fluctuating velocity in the wake.

This relationship is plotted in FIG. 5.6. There is no way available at present to relate the flow conditions to absolute values of ϵ but the relative variation may be examined using the following dimensional considerations

$$\frac{dy}{dt} \propto \omega_n \frac{dy}{d\tau} \propto (Re)_\infty \frac{dy}{d\tau} \tag{5.23}$$

Also

$$\epsilon \propto \frac{1}{(Re)_\infty} \tag{5.24}$$

Using the above relationships together with the experimental data, it has been found that for the range of data available ϵ appears to be approximately constant. Further examination of the distortion of the limit cycles (FIG. 2) with ϵ suggests that as small a value as possible is desirable since this is approaching sinusoidal motion.

Equation (5.5) may now be modified to include an external excitation. Hence,

$$\ddot{y} - \epsilon(1-y^2)\dot{y} + y = \frac{y_0}{\omega_n^2} \sin \frac{\omega}{\omega_n} \tau \tag{5.25}$$

where

$$y_0 = \frac{|a|}{\sqrt{\alpha/\beta}}$$

$|a|$ = ACCELERATION AMPLITUDE

$= |x_0|$ OR $|v_0|$ FOR SINUSOIDAL MOTION

The solutions of this equation are similar in form to those in FIG. 5.3 and have been plotted in FIG. 5.7 for one value of ϵ. For convenience the ordinates of the graph is the ratio of $(\dot{y})$max. when external excitation is present to $(\dot{y})$ max. with no external excitation. Once again the lack of experimental information does not permit an absolute relationship between y_0/ω_n^2 and the corresponding parameter in freestream turbulence (although a crude relationship is devised in FIG. 5.9) and therefore y_0/ω_n^2 is presented

in machine units meantime. Only the stable solutions are presented in FIG. 5.7, this being determined by observations of the $\dot{y}$ versus t trace, unstable solutions producing non-periodic oscillatory traces. Only the maximum amplification is of interest and this has been plotted in FIG. 5.8 for a range of η_o/ω_n^2 and several ϵ. The abscissae is observed to be of the same form as $\sqrt{\overline{u'^2}}/\bar{u}_\infty^2$ and in the experimental section this has been written as $(Re')_\infty/(Re)_\infty^2$. It can therefore be claimed that one value of ϵ in FIG 5.8 corresponds to the correlation of experimental data in FIG. 4.6.2. By a process of trial and error the data is best predicted if a value of $\epsilon = 1.5$ is used and the relationship between η_o/ω_n^2 and $(Re')_\infty/(Re)_\infty^2$ in FIG. 5.9 is adopted. It is of interest to note that the value of ϵ results in a periodic motion which is not too different from a sinusoidal type.

5.8 CONCLUSIONS

It now appears that the resonant interaction between the wake motion and the freestream motion can be crudely simulated using an equation which was originally developed for self-excited motion of electrons. ~~It has been shown by comparing this equation with a modified form of the Navier-Stokes equation that this is realistic.~~ An absolute relationship between the experimental data and the theory is unobtainable with the present state of knowledge but a simple minded relationship has been obtained meantime. The analogue computer which provides a speedy means of solving non-linear equations does not help in the detection of all possible solutions. It is possible that other equations exist which can adequately describe self-excited oscillations.

6. THE PREDICTION OF HEAT TRANSFER FROM THE FLUID MECHANICS OF THE WAKE REGION

There appears to be no theory currently available which can be used to predict adequately local heat transfer in turbulent separated flows, based on a knowledge of the flow. It is unlikely that any significant advance from the present position of the theory will be made until there is a better understanding of the basic mechanism behind the formation of eddies and of factors which provoke instability. The region of interest is one of characteristically large velocity fluctuations rather than large steady velocities being further complicated by the fact that it contains a mixture of turbulent and periodic motion. Clearly a suitable theory will have to be based on the fluctuating motion and for this purpose use of the turbulent kinetic energy equation has distinct advantages. Nevertheless it is worthwhile to examine steady state theories as they will be shown to be useful in the construction of the equations.

6.1 METHOD OF LEONTEV AND RIAGEN {C29}

An attempt is made to extend the analytical method involving boundary layer theory to heat transfer calculations in the eddy separation region. It is assumed that the surface of the cylinder is wetted by the relatively stable turbulent return flow, and there is the growth of a layer which obeys boundary layer theory. It is also assumed that the velocity gradient at right angles to the surface in the turbulent eddy has no effect on the development of this layer. The starting point for the theory is the two dimensional incompressible conserved property equation.

$$\rho c_p\left(\frac{\partial T}{\partial t} + u\frac{\partial T}{\partial x} + v\frac{\partial T}{\partial y}\right) = \frac{\partial}{\partial y}\left(\alpha\frac{\partial T}{\partial y}\right) \qquad (6.1)$$

This can now be integrated across the boundary layer and after some algebraic manipulation is re-written in the form

$$\delta_T\left(\frac{1}{c_p\Delta T}\cdot\frac{\partial \bar{u}_c}{\partial t} + \frac{1}{\Delta T}\cdot\frac{\partial \Delta T}{\partial x} + \frac{1}{\bar{u}_G}\cdot\frac{\partial \bar{u}_c}{\partial x}\right) + \frac{\partial \delta_T}{\partial x} = \frac{q_w}{\rho c_p \bar{u}_c \Delta T} \qquad (6.2)$$

where $\delta_T = \int \frac{\bar{u}}{\bar{u}_G}\left(1 - T_1\right)dy \quad ; \quad T_1 = \frac{T_w - T}{T_w - T_G} \quad ; \quad \Delta T = T_w - T_G$

The subscripts G and w refer to conditions at the edge of the boundary layer and at the wall respectively. q_w is the heat flux at the wall.

For steady incompressible flow, the first and third terms on the left hand side of the equation can be neglected. The velocity at the edge of the boundary layer is now defined by

$$\bar{u}_G = A\,\bar{u}_\infty \tanh \alpha X \qquad (6.3)$$

where X = x/D. It is not quite clear how this expression is derived but is likely to have an experimental basis. The constants A and α are given numerical values 2.93 and 1.12. Equation (6.2) can now be non-dimensionalised

$$\frac{d(Re)_T}{dX} + \frac{(Re)_T}{\Delta T}\cdot\frac{d\Delta T}{dX} = \frac{1}{2}(Re)_D\,St \qquad (6.4)$$

where $(Re)_T = \frac{\bar{u}_G \delta_T}{\nu} \quad ; \quad (Re)_D = \frac{\bar{u}_G D}{\nu} \quad ; \quad (Re)_\infty = \frac{\bar{u}_\infty D}{\nu}$

$$St = \text{Stanton Number} = \frac{q_w}{\rho c_p \bar{u}_G \Delta T} = \frac{0.22}{\sigma^{4/3}(Re)_T}$$

It is now a simple matter to calculate the $(Re)_T$ profile around the cylinder for the case of a constant heat flux surface and a constant temperature surface. For the condition of constant heat flux, equation (6.4) is written in the form

$$\frac{d}{dX}\left(\Delta T \cdot (Re)_T\right) = \frac{1}{2}\cdot\frac{D q_w}{\nu \rho c_p} \qquad (6.5)$$

Hence, $$(Re)_T = \sqrt{0.11}\,(Re)_\infty^{0.5}\,\sigma^{-\frac{4}{3}}\sqrt{X} \qquad (6.6)$$

It is now a simple matter to relate this function to the heat transfer variation in the form of Nusselt number using the empirical relationship for Stanton number. Hence,

$$Nu = \sqrt{0.44A\alpha}\,(Re)_\infty^{0.5}\,\sigma^{\frac{1}{3}}\left(\frac{\tanh \alpha X}{\alpha X}\right)^{\frac{1}{2}} \qquad (6.7)$$

For the sake of completeness, the equivalent expression derived by assuming a constant temperature is given below.

$$Nu = \sqrt{0.22A\alpha}\,(Re)_\infty^{0.5}\,\sigma^{\frac{1}{3}}\,\frac{\tanh \alpha X}{\sqrt{\log \cosh \alpha X}} \qquad (6.8)$$

A comparison has already been made between equation (6.7) and the experimental data in FIG. 4.3.13. The poor agreement is not surprising, mainly because of the sensitivity of this region to freestream turbulence. One important contradiction however, is the difference between $(Re)_\infty^{\frac{1}{2}}$ term in the solution with the $(Re)_\infty^{\frac{2}{3}}$ predicted experimentally by Richardson {C22}. Finally, the main restriction in this theory is the exclusion of the turbulence effect.

6.2 METHOD OF SPALDING {C28}

This contribution is restricted to a one dimensional theory. A power law relation is derived between the Stanton number and the Reynolds number, expressing the law of heat transfer for a wall adjacent to a region of turbulent separated flow. The derivation is based on Prandtl's proposal for the laws of dissipation, diffusion and generation of turbulent kinetic energy. The constants appearing in these laws are determined by reference to experimental

data for the fluid mechanic properties of constant stress and linear stress layers.

The agreement between the resulting predictions and the experimental data of other workers is sufficiently good to suggest that the actual mechanism of heat transfer within separated flows has much in common with that which is postulated. Closer agreement can only be expected after the present one-dimensional analysis is superceded by a two-dimensional one.

One of the characteristic features of separated flows is that the locations of maximum shear stress are remote from the wall. A consequence of this feature is that the turbulence which is generated in the remote high shear region of a separated flow must be conveyed to the vicinity of the wall by the action of convection and diffusion; the turbulence intensity in the vicinity of the wall, which is a main determinant of heat transfer, is governed by the interaction of these two factors together with turbulence dissipation.

By defining the turbulent kinetic energy as

$$k = \frac{1}{2}\{\overline{u'^2} + \overline{v'^2} + \overline{w'^2}\} \qquad (6.9)$$

and using Prandtls terms which represent dissipation, generation and diffusion of turbulence, then,

Rate of dissipation per unit volume $= a\rho\frac{k^{3/2}}{y}$

Rate of generation per unit volume $= \tau\frac{d\bar{u}}{dy}$

Rate of diffusion into unit volume $= b\rho\frac{d}{dy}\left(k^{1/2}y\frac{dk}{dy}\right)$

where $\frac{\tau}{\rho} = \nu_t\frac{d\bar{u}}{dy}$; $\nu_t = c k^{1/2} y$

Hence in the fully turbulent region

$$a\frac{k^{3/2}}{y} - b\frac{d}{dy}\left(k^{\frac{1}{2}}y\frac{dk}{dy}\right) - \frac{\tau}{\rho}\frac{d\bar{u}}{dy} = 0 \qquad (6.10)$$

For the region near the wall, that is $y < y_o$, where viscous effects are no longer negligible

$$\frac{y_o k_o^{1/2}}{\nu} = Y \quad ; \quad \frac{y_o}{k_o}\left(\frac{dk}{dy}\right)_o = Y' \tag{6.11}$$

where Y and Y' are constants. By applying equation (6.10) to the point of reattachment of a turbulent boundary layer where the wall shear stress is zero, and hence the generation term is zero, a general solution may be written down immediately which after some manipulation becomes

$$\left(\frac{k_1}{k_o}\right)^{\frac{3}{2}} \approx \frac{[1 + (3/2m)Y']}{2} \cdot \left(\frac{y_1}{y_o}\right)^m \tag{6.12}$$

where $m = (3a/2b)^{\frac{1}{2}}$ and the subscript 1 denotes conditions at a distance much greater than y_o from the wall. To relate the above to the heat transfer, the following parameter is derived,

$$\frac{\nu}{\bar{u}_c y_o} \approx \left(\frac{1 + (3/2m)Y'}{2}\right)^{\frac{-1}{m+3}} \times \left(Y\right)^{\frac{-3}{m+3}} \times \left(\frac{k_1^{1/2}}{\bar{u}_c}\right)^{\frac{3}{m+3}} \times \left(\frac{D}{y_1}\right)^{\frac{m}{m+3}} \times \left(\frac{\bar{u}_c D}{\nu}\right)^{\frac{-m}{m+3}} \tag{6.13}$$

At this stage heavy reliance is placed upon experimental data from which the values of the constants are chosen

$$a = 0.313; \quad b = 0.1173; \quad C = 0.2 \tag{6.14}$$

After some algebraic manipulation, the Stanton number is derived from equation (6.13)

$$\left(\frac{\bar{u}_c D}{\nu}\right)^{0.4} \cdot St = \frac{3.2\left(\frac{k_1^{1/2}}{\bar{u}_c}\right)^{0.6}\left(\frac{D}{y_1}\right)^{0.4}}{P + 15.5} \tag{6.15}$$

where $P = 9.24\left[\left(\frac{\sigma}{\sigma_t}\right)^{0.75} - 1\right]$. For air $P = -1.98$ and $\sigma = 0.72$. Thus, in terms of Nusselt number, equation (6.15) becomes

$$Nu = 0.17\left(\frac{D}{y_1}\right)^{0.4}\left(\frac{k_1^{1/2}}{\bar{u}_c}\right)^{0.6}(Re)_\infty^{0.6} \tag{6.16}$$

Taking $D/y_1 = 10$ which was used by Spalding and is also representative of the present experimental data, the heat transfer and fluid mechanic data may now be compared. An unexpected result is the ineffectiveness of the turbulence intensity in its present form to produce an improvement in heat transfer. Closer examination of the data shows that the ratio $k_1^{1/2}/\bar{u}_e$ is approximately constant suggesting that the dependence of heat transfer on turbulence will be a function of the turbulent energy level and not on the conventional turbulence intensity ratio. The results are plotted in FIG 6.1.

There now appear to be two possible attacks on the solution to this problem. The first method which ignores the effect of the fluctuating motion is clearly inadequate in its present form. The latter theory offers distinct advantages as a mechanism to relate turbulent energy to heat transfer. The most suitable approach to the present problem appears to be a combination of both theories.

By choosing a suitable model to describe the steady flow at the rear stagnation point, the turbulent energy can be incorporated by means of the effective viscosity. The decay of turbulence within the boundary layer region will then be controlled by the turbulent energy equation. This requires the simultaneous solution of three partial differential equations.

Before discussing the solution procedure a study of the various forms of the turbulent energy equation is desirable.

6.3 THE TURBULENT KINETIC ENERGY EQUATION

The turbulent kinetic energy equation has been used in the calculation of boundary layer development. Most present day methods involving calculations with turbulent boundary layers assume that the shear stress profile at a given distance from the origin of the boundary layer is uniquely related to the mean flow conditions at that station, the simplest version of this assumption being the "mixing length" or eddy viscosity theory which states that the shear stress at a point depends on the mean velocity gradient at that point. Bradshaw and Ferris {G10} argue that the shear stress $\tau = -\rho \overline{u'v'}$ is closely related to the turbulent kinetic energy $\frac{1}{2}\rho\{\overline{u^2}+\overline{v^2}+\overline{w^2}\}$ and that the latter, being governed by the turbulent kinetic energy equation is not determined uniquely by the local mean flow conditions. This argument has already been put forward by Dryden (1946). Bradshaw {G10} shows that there is a much closer connection between the shear stress profile and the other parameters describing the turbulence structure than between the shear stress profile and mean velocity profile. In fact it is assumed that the turbulent intensity is directly proportional to the local shear stress, that the dissipation rate is determined by the local shear stress and a length scale, and that the diffusion energy is directly proportional to the local shear stress with a factor depending on the maximum value of shear stress. The method is similar to the work of Townsend (1961, 1965) and Glushko (1965) who used the turbulent kinetic energy equation to calculate $\overline{q^2}$ and then made the assumption that the eddy viscosity ν_t is given by $(\overline{q^2})^{\frac{1}{2}} L/\nu_t$ = Constant.

The turbulent kinetic energy equation for a two dimensional incompressible mean flow, outside the viscous sublayer is

$$\frac{1}{2}\rho\left(\bar{u}\frac{\partial \overline{q^2}}{\partial x} + \bar{v}\frac{\partial \overline{q^2}}{\partial y}\right) - \tau\frac{\partial \bar{u}}{\partial y} + \frac{\partial}{\partial y}\left(\overline{p'v'} + \frac{1}{2}\rho\overline{q^2 v'}\right) + \rho\epsilon = 0 \qquad (6.17)$$

ADVECTION GENERATION DIFFUSION DISSIPATION

where $\overline{q^2} = 2k = \overline{u'^2} + \overline{v'^2} + \overline{w'^2}$

$$\tau = -\rho\overline{u'v'} \qquad \epsilon = \nu\left(\frac{\partial u_i}{\partial x_j}\right)^2$$

This can be regarded as an equation for the advection or rate of change of turbulent kinetic energy along a mean streamline through a point providing all the other terms are known at that point. The following parameters are now defined.

$$a_1 = \frac{\tau}{\rho\overline{q^2}} \quad ; \quad L = \frac{1}{\epsilon}\left(\frac{\tau}{\rho}\right)^{\frac{3}{2}} \quad ; \quad G = \frac{\left(\frac{\overline{p'v'}}{\rho} + \frac{1}{2}\overline{q^2 v'}\right)}{\left(\frac{\tau_{max}}{\rho}\right)^{\frac{1}{2}}\cdot\frac{\tau}{\rho}} \qquad (6.18)$$

so that equation (6.17) becomes

$$\bar{u}\frac{\partial}{\partial x}\left(\frac{\tau}{2a_1\rho}\right) + \bar{v}\frac{\partial}{\partial y}\left(\frac{\tau}{2a_1\rho}\right) - \frac{\tau}{\rho}\cdot\frac{\partial \bar{u}}{\partial y} + \left(\frac{\tau_{max}}{\rho}\right)^{\frac{1}{2}}\frac{\partial}{\partial y}\left(G\frac{\tau}{\rho}\right) + \frac{1}{L}\left(\frac{\tau}{\rho}\right)^{\frac{3}{2}} = 0 \qquad (6.19)$$

which for the purpose of comparison is more conveniently written in terms of k thus,

$$\bar{u}\frac{\partial k}{\partial x} + \bar{v}\frac{\partial k}{\partial y} - 2a_1 k\frac{\partial \bar{u}}{\partial y} + (2a_1)^{\frac{3}{2}}k_{max}^{\frac{1}{2}}\frac{\partial}{\partial y}(Gk) + \frac{(2a_1)^{\frac{3}{2}}k^{\frac{3}{2}}}{L} = 0 \qquad (6.20)$$

where a_1, L and G are functions of $\frac{y}{y_G}$ which depend on the shape of the shear stress profile. The functions a_1 and G are dimensionless while L has the dimensions of length, this being the most important of the three functions because over most of the boundary layer the dissipation of energy is much larger than the advection or diffusion.

These functions are obtained from experimental measurements which, at present are not of high accuracy. The value of a_1 is chosen as constant at 0.15 while the functions L and G are plotted in FIG. 6.2. Best fit curves have been obtained for computing purposes and the coefficients for each function are tabulated in FIG. 6.3.

For the region of interest it has already been shown experimentally that $\frac{\partial k}{\partial x} \sim 0$ and also $\frac{\partial \bar{u}_c}{\partial x} \sim 0$. For this reason the advection terms are ignored. Equation (6.20) now reduces to

$$\frac{(2a_1)^{\frac{3}{2}} k^{\frac{3}{2}}}{L} + (2a_1)^{\frac{3}{2}} k^{\frac{1}{2}} \frac{\partial (Gk)}{\partial y} - 2a_1 k \frac{\partial \bar{u}}{\partial y} = 0 \qquad (6.21)$$

DISSIPATION DIFFUSION GENERATION

At this stage it is observed that there are differences in form between each term in equation (6.21) and the equation describing the turbulent energy used by Spalding {C28} which is

$$\frac{a\, k^{\frac{3}{2}}}{y} - b \frac{d}{dy}\left(k^{\frac{1}{2}} y \frac{dk}{dy}\right) - c k^{\frac{1}{2}} y \left(\frac{d\bar{u}}{dy}\right)^2 = 0 \qquad (6.22)$$

It is not surprising that differences occur since the derivation of the laws of dissipation, generation and diffusion of turbulence are largely based on experimental evidence. The present state of knowledge is insufficient to determine the correct theory, the choice being dependent largely upon each particular problem. The following paragraphs provide a brief comparison of each term.

(i) DISSIPATION: Both functions L and G are constructed to include the viscous region near the wall. In the viscous region L varies linearly with y but there is a non-linear variation in

the turbulent region which is likely to lead to differences between each solution. The constant in equation (6.21) has a value of 0.4 compared with 0.313 in equation (6.22).

(ii) GENERATION: The different forms of generation term can be compared by considering the turbulence $k \propto y^{2m}$ and $\bar{u} \propto y^{n}$ Both forms are identical, except for the experimental constants, provided m is equal to n which is a plausible assumption based on the available experimental evidence. It therefore appears that either form is acceptable for the present work.

(iii) DIFFUSION: The differences occurring with this expression is based on the assumption that the form used by Bradshaw in equation (6.21) is physically more realisable than the more conventional gradient diffusion form in equation (6.22). This is based on work by Townsend (1956) who has argued that at least part of the turbulent diffusion of energy is effected by the large eddy formations. Since, in the present problem large eddies comprise a most important part of the turbulence, the former expression could be the most suitable.

However, the evidence upon which both theories is based is insufficient to ensure confidence without examination of the solution of each equation in relation to the experimental data.

6.3.1 SOLUTION OF EQUATION (6.21)

For the purpose of comparison it is sufficiently accurate to use the same values of the constants a, b and c as for equation (6.22).

Equation (6.21) now becomes

$$a\frac{k^{3/2}}{L} - b k_G^{1/2}\frac{d}{dy}(Gk) - ck\frac{d\bar{u}}{dy} = 0 \qquad (6.23)$$

It is assumed that the maximum turbulence level occurs at the edge of the boundary layer. The following method of non-dimensionalising has been used.

$$K = \frac{k}{k_G} \quad ; \quad Y = \frac{y}{y_G} \quad ; \quad U = \frac{\bar{u}}{\bar{u}_G}$$

where subscript G refers to conditions at the edge of the boundary layer. Thus,

$$a\frac{K^{3/2}}{L} - b\frac{d}{dY}(GK) - c\frac{\bar{u}_G}{k_G^{1/2}}\cdot\frac{dU}{dY} = 0 \qquad (6.24)$$

A knowledge of the mean velocity is now required before a solution of (6.24) is obtained. This can be achieved by simultaneous solution of (6.24) with the momentum equation or by assuming a velocity profile based on experimental evidence. The latter method is more convenient at this stage of the analysis. By choosing $U = Y^n$, (6.24) becomes,

$$a\frac{K^{\frac{3}{2}}}{L} - b\frac{d}{dY}(GK) - cn\frac{\bar{u}_G}{k_G^{1/2}}KY^{n-1} = 0 \qquad (6.25)$$

A straight forward solution procedure using the Runge-Kutta technique is now adopted after rewriting (6.25) in the form

$$\frac{dK}{dY} = \frac{\left(a\frac{K^{3/2}}{L} - cn\frac{\bar{u}_G}{k_G^{1/2}}KY^{n-1}\right)\frac{1}{b} - K\frac{dG}{dY}}{G} \qquad (6.26)$$

The solutions are plotted in FIG. 6.4 for different values of index n in the generation term. The comparison between experiment and theory is poor and it is suggested that this is mainly due to the source of data used in the synthesis of the L and G functions. Clearly, different L, G functions are necessary before satisfactory agreement can be achieved.

6.3.2 SOLUTION OF EQUATION (6.22)

By using the same non-dimensionalising procedure and the same experimental mean velocity profile, equation (6.22) becomes,

$$a\frac{K^{3/2}}{Y} - b\frac{d}{dY}\left(K^{1/2}Y\frac{dK}{dY}\right) - g n^2 K^{\frac{1}{2}} Y^{2n-1} = 0 \qquad (6.27)$$

where $$g = c\left(\frac{\bar{u}_c}{k_c^{1/2}}\right)^2$$

By substituting $Z = K^{3/2}$ and after some algebraic manipulation equation (6.27) becomes

$$Y^2\frac{d^2Z}{dY^2} + Y\frac{dZ}{dY} - \frac{3a}{2b}Z + \frac{3gn^2}{2b}Z^{\frac{1}{3}}Y^{2n} = 0 \qquad (6.28)$$

which is conveniently solved using standard finite difference techniques. The finite difference equations are

where

$$\left.\begin{aligned} &A_1 Z_{i-1} + A_2 Z_i + A_3 Z_{i+1} = NL \\ &A_1 = 2Y_i^2 - hY_i \\ &A_2 = -4Y_i^2 - 2h^2 \times \frac{3a}{2b} \\ &A_3 = 2Y_i^2 + hY_i \\ &NL = -2h^2 \times \frac{3gn^2}{2b} \times Z_i^{0.353} \times Y_i^{2n} \end{aligned}\right\} \qquad (6.29)$$

The results are plotted in FIG. 6.5. For the special case of DIFFUSION = DISSIPATION there is complete agreement between the solution of equation (6.28) and the analytical solution (described by Spalding in {C28}). Using the experimental values for a, b and c agreement between theory and experiment is poor. However by modifying the value of c = 0.77 satisfactory agreement was obtained.

This difference in the value of a constant is acceptable in view of the lack of knowledge of the type of flow being examined.

Based on the present state of knowledge the form of turbulent energy equation presented in (6.22) appears to give best agreement with the experimental data for the least alteration to the form of the equation. Therefore it is the form which is chosen to assist in the solution of the present problem.

6.4 A ONE DIMENSIONAL THEORY FOR THE PREDICTION OF HEAT TRANSFER

Before proceeding with the solution of the turbulent energy equation to predict heat transfer it is instructive to relate the experimental fluid mechanic measurements to the experimental heat transfer using a technique similar to that in {C28}. By starting from the experimental velocity profiles in the turbulent region of the boundary layer

$$\frac{\bar{u}}{\bar{u}_G} = \left(\frac{y}{y_G}\right)^n \quad ; \quad \left(\frac{k}{k_G}\right)^{\frac{1}{2}} = \left(\frac{y}{y_G}\right)^m \tag{6.30}$$

which are valid in the range $y_o < y < y_G$. It is assumed that in the region $y < y_o$, the shear stress is constant. By using the relationship given by Bradshaw {G10} $\frac{\tau}{\rho} = a_1 \bar{q}^2$, then at y_o, the turbulent energy k_o is given by

$$k_o = \frac{\nu \bar{u}_G}{0.3 y_o}\left(\frac{y_o}{y_G}\right)^n \tag{6.31}$$

This can be re-written in terms of the conditions at the edge of the boundary layer

$$(y_o)^{n-2m-1} = \frac{0.3 k_G (y_G)^{n-2m}}{\nu \bar{u}_G} \tag{6.32}$$

which after some algebraic manipulation leads to

$$\frac{\nu}{\bar{u}_c y_o} = (0.3)^{\frac{1}{2m+1-n}} \times \left(\frac{k_c^{1/2}}{\bar{u}_c}\right)^{\frac{2}{2m+1-n}} \times \left(\frac{D}{y_c}\right)^{\frac{2m-n}{2m+1-n}} \times \left(\frac{\nu}{\bar{u}_c D}\right)^{\frac{2m-n}{2m+1-n}} \tag{6.33}$$

The fluid motion may now be related to the heat transfer via

$$\frac{q}{\tau} = \frac{c_p}{\sigma} \frac{\frac{dT}{dy}}{\frac{d\bar{u}}{dy}} \tag{6.34}$$

from which

$$T_w = \frac{q_w \sigma}{c_p} \int_0^{y_c} \frac{1}{\tau} \cdot \frac{d\bar{u}}{dy} dy = \frac{q_w \sigma}{c_p} \left[\int_0^{y_o} \frac{1}{\tau} \cdot \frac{d\bar{u}}{dy} dy + \int_{y_o}^{y_c} \frac{1}{\tau} \cdot \frac{d\bar{u}}{dy} dy \right] \tag{6.35}$$

In the region $0 < y < y_o$, $\tau = \nu \rho \frac{\bar{u}_o}{y_o}$ and

therefore $$\int_0^{y_o} \frac{1}{\tau} \frac{d\bar{u}}{dy} dy = \frac{y_o}{\rho \nu} \tag{6.36}$$

The second integral which is valid in the turbulent region becomes

$$\int_{y_o}^{y_c} \frac{1}{\tau} \cdot \frac{d\bar{u}}{dy} dy = \frac{y_o}{\rho \nu} \cdot \frac{n}{n-2m} \left[\left(\frac{y}{y_c}\right)^{n-2m} - 1 \right] \tag{6.37}$$

Provided $y_c >> y_o$ the second integral is very small and may be neglected. Thus,

$$q_w = \frac{c_p T_w \rho \nu}{\sigma y_o} \tag{6.38}$$

which can easily be related to the Nusselt number, hence

$$Nu = (0.3)^{\frac{1}{2m+1-n}} \times \left(\frac{k_c^{1/2}}{\bar{u}_c}\right)^{\frac{2}{2m+1-n}} \times \left(\frac{D}{y_c}\right)^{\frac{2m-n}{2m+1-n}} \times \left(\frac{\bar{u}_c D}{\nu}\right)^{\frac{1}{2m+1-n}} \tag{6.39}$$

Replacing m and n by the experimental values (6.39) becomes,

$$Nu = 0.397 \left(\frac{k_c^{1/2}}{\bar{u}_c}\right)^{1.54} \times \left(\frac{D}{y_c}\right)^{0.231} \times (Re)_\infty^{0.77} \times \left(\frac{\bar{u}_c}{\bar{u}_\infty}\right)^{0.77} \tag{6.40}$$

Agreement between the above theory and the experiment heat transfer is surprisingly good considering the crudeness of the assumptions. There is still the restriction however that the effect of turbulence cannot be evaluated due to the almost constant value of the ratio $k_c^{1/2}/\bar{u}_c$

6.5 THE PREDICTION OF HEAT TRANSFER AT THE REAR STAGNATION POINT

It is now clear that the complete solution of the time dependent Navier-Stokes equations would be necessary to resolve this problem which is impractical at this stage. It seems likely however that the more conventional approach, which lumps together the time dependent terms in these equations into a single term (the apparent viscosity) may still be a suitable approach at least as a first approximation. The equation set is now simplified to time-independent equations together with an additional equation (turbulent kinetic energy equation) which accounts for the variation of the apparent viscosity in the boundary layer.

The Navier-Stokes equations may now be written in the form,

$$\bar{u}^* \frac{\partial \bar{u}^*}{\partial x^*} + \bar{v}^* \frac{\partial \bar{u}^*}{\partial y^*} = -\frac{1}{\rho} \frac{\partial \bar{p}^*}{\partial x^*} + \frac{\partial}{\partial x^*}\left[(\nu + \nu_t)\frac{\partial \bar{u}^*}{\partial x^*}\right] + \frac{\partial}{\partial y^*}\left[(\nu + \nu_t)\frac{\partial \bar{u}^*}{\partial y^*}\right] \qquad (6.41)$$

$$\bar{u}^* \frac{\partial \bar{v}^*}{\partial x^*} + \bar{v}^* \frac{\partial \bar{v}^*}{\partial y^*} = -\frac{1}{\rho} \frac{\partial \bar{p}^*}{\partial y^*} + \frac{\partial}{\partial x^*}\left[(\nu + \nu_t)\frac{\partial \bar{v}^*}{\partial x^*}\right] + \frac{\partial}{\partial y^*}\left[(\nu + \nu_t \frac{\partial \bar{v}^*}{\partial y^*}\right] \qquad (6.4.2)$$

where the * indicates "having dimensions". The conserved property equation has also to be solved simultaneously with (6.41) and (6.42),

$$\bar{u}^* \frac{\partial T^*}{\partial x^*} + \bar{v}^* \frac{\partial T^*}{\partial y^*} = \frac{\partial}{\partial x^*}\left[\left(\frac{\nu}{\sigma} + \frac{\nu_t}{\sigma_T}\right)\frac{\partial T^*}{\partial x^*}\right] + \frac{\partial}{\partial y^*}\left[\left(\frac{\nu}{\sigma} + \frac{\nu_t}{\sigma_T}\right)\frac{\partial T^*}{\partial y^*}\right] \qquad (6.43)$$

The problem is now reduced to a steady flow with a fluctuating component being included via the apparent viscosity, .
There is sufficient experimental evidence to indicate that the velocity and temperature gradients in the wake region are weak, therefore at this stage in the analysis only the rear stagnation point is considered. A stagnation point flow solution has already been obtained by Hiemenz for laminar flow and this is now modified to include the apparent viscosity term.

At this stage in the analysis the same non-dimensional groups used by Hiemenz are adopted. Thus,

$$\left.\begin{aligned} x &= \sqrt{\frac{a}{\nu}}\, x^* \qquad \bar{u}^* = \sqrt{a\nu}\,\bar{u} \qquad T = \frac{T_w - T^*}{T_w - T_\infty} \\ \eta &= \sqrt{\frac{a}{\nu}}\, y^* \qquad \bar{v}^* = \sqrt{a\nu}\,\bar{v} \end{aligned}\right\} \qquad (6.44)$$

where $a = \frac{4\bar{u}_c}{D}$

= a reciprocal time constant

The velocity distribution in frictionless potential flow in the neightbourhood of the stagnation point is given by

$$\bar{u} = ax \qquad \bar{v} = -ay \qquad (6.45)$$

In potential flow the pressure is given by Bernoullis equation. If p_s denotes the stagnation pressure and p is the pressure at any arbitrary point, then

$$p_s - p = \tfrac{1}{2}\rho(\bar{u}^2 + \bar{v}^2) = \tfrac{1}{2}\rho a(x^2 + y^2) \qquad (6.46)$$

For viscous flow the following assumptions are made.

$$\bar{u} = x\,\varphi'(\eta) \quad ; \quad \bar{v} = -\varphi(\eta) \tag{6.47}$$

where ' denotes differentiation with respect to

also $$p_s - p = \tfrac{1}{2}\rho a^2 (x^2 + F(\eta)) \tag{6.48}$$

Therefore, by non-dimensionalising equations (6.41), (6.42), (6.43) and by substituting into these equations (6.47) the following equations result after some algebraic manipulation

$$\frac{d}{d\eta}\left[\left(1+\frac{\nu_t}{\nu}\right)\varphi''\right] + \varphi\varphi'' - \varphi'^2 + 1 = 0 \tag{6.49}$$

$$\frac{d}{d\eta}\left[\left(1+\frac{\nu_t}{\nu}\right)\varphi''\right] - \varphi\varphi'' + \frac{1}{2}F' = 0 \tag{6.50}$$

$$\frac{d}{d\eta}\left[\left(1+\frac{\nu_t}{\nu}\right)T'\right] + \sigma\varphi T' = 0 \tag{6.51}$$

The corresponding boundary conditions are

$$\eta = 0 : \quad \varphi = 0 , \ \varphi' = 0 , \ F = 0 , \ T = 1$$

$$\eta = \eta_e : \quad \varphi' = 1 , \ \varphi'' = 0 , \ T = 0$$

Since the function F does not appear in the first equation, (6.49) may be solved directly (provided $\frac{\nu_t}{\nu}$ is known) and the value of φ obtained from this solution can be substituted into equation (6.51). For laminar flow the equations reduce to those derived by Hiemenz thus,

$$\varphi''' + \varphi\varphi'' - \varphi'^2 + 1 = 0 \tag{6.52}$$

$$\varphi''' - \varphi\varphi'' + \frac{1}{2}F' = 0 \tag{6.53}$$

$$T'' + \sigma\varphi T' = 0 \tag{6.54}$$

It is now necessary to relate the variations of ν_t to η using a suitable form of the turbulent energy equation. A modified version of equation used by Spalding is presented by Wolfshtein {G14} which, by including two exponential terms ℓ_μ and ℓ_D is claimed to be valid in the viscous layer at the wall. This is an approximation which is based on information obtained from boundary layers on flat plates and therefore may not be of high accuracy in the present situation. It does however simplify the solution procedure and will be used until more accurate information is available. The equation is now presented as follows

$$\left.\begin{aligned} &\frac{d}{dy^*}\left[\left(\nu + \frac{\nu_t}{\sigma_{k,t}}\right)\frac{dk}{dy^*}\right] + \nu_t\left(\frac{d\bar{u}}{dy^*}\right)^2 - \frac{C_D k^{\frac{3}{2}}}{\ell_D} = 0 \\ &\text{where} \quad \nu_t = C_\mu k^{\frac{1}{2}} \ell_\mu \\ &\ell_\mu = y^*(1 - e^{-A_\mu R}) \quad ; \quad R = \frac{k^{1/2} y^*}{D} \\ &\ell_D = y^*(1 - e^{-A_D R}) \end{aligned}\right\} \qquad (6.55)$$

Equation (6.55) may now be written in non-dimensional form using the same groups as in (6.41) and (6.42). It is more reasonable however to non-dimensionalise this equation in the same manner as for (6.21) and (6.22). That is, by using conditions at the edge of the boundary layer,

$$\eta = \frac{y}{y_G} \quad ; \quad u = \frac{\bar{u}}{\bar{u}_G} \quad ; \quad K = \frac{k}{k_G} \qquad (6.56)$$

The difference in the different forms of non-dimensionalising will be taken into account at a later stage in the analysis. Thus (6.55) becomes

$$\left.\frac{d}{d\eta}\left[\left(1 + \frac{1}{\sigma_{k,t}}\frac{\nu_t}{\nu}\right)\frac{dK}{d\eta}\right] + \frac{\bar{u}_G^2}{k_G}\cdot\frac{\nu_t}{\nu}\left(\frac{du}{d\eta}\right)^2 - \frac{k_G y_G}{\nu}\cdot\frac{C_D K^{3/2}}{\eta(1 - e^{-A_D R})} = 0 \right|$$

$$\left.\begin{aligned} \frac{\nu_t}{\nu} &= \frac{k_c^{1/2} y_c}{\nu} \, c_\mu K^{\frac{1}{2}} \eta \left(1 - e^{-A_\mu R}\right) \\ R &= \frac{k_c^{1/2} y_c}{\nu} \, K^{\frac{1}{2}} \eta \end{aligned}\right\} \qquad (6.57)$$

By putting $R_{osc} = \frac{k_c^{1/2} y_c}{\nu}$ the main equation in (6.56) becomes

$$\frac{d}{d\eta}\left[\left(\frac{1}{R_{osc}} + \frac{1}{R_{osc}\sigma_{k,t}} \cdot \frac{\nu_t}{\nu}\right)\frac{dK}{d\eta}\right] + \frac{1}{R_{osc}} \cdot \frac{\bar{u}_c^2}{k_c} \cdot \frac{\nu_t}{\nu}\left(\frac{dU}{d\eta}\right)^2 - \frac{c_D K^{3/2}}{\eta\left(1 - e^{-A_D R}\right)} = 0 \qquad (6.58)$$

For the present range of experiments R_{osc} was of the order of 300 and hence the term $1/R_{osc}$ is neglected. By replacing the function $K^{1/2}\eta\left(1 - e^{-A_\mu R}\right)$ by V the three equations to be solved simultaneously may now be written as

$$\frac{d}{d\eta}\left[A_1 V \frac{dK}{d\eta}\right] + B V \left[\varphi''\right]^2 - \frac{c_D K^{3/2}}{\eta\left(1 - e^{-A_D R}\right)} = 0 \qquad (6.59)$$

$$\frac{d}{d\eta}\left[A_3 V \varphi''\right] + \varphi\varphi'' - \varphi'^2 + 1 = 0 \qquad (6.60)$$

$$\frac{d}{d\eta}\left[A_2 V T'\right] + \sigma \varphi T' = 0 \qquad (6.61)$$

where $V = K^{\frac{1}{2}} \eta \left(1 - e^{-A_\mu R}\right)$ and

$$A_1 = \frac{c_\mu}{\sigma_{k,t}} \; ; \; A_2 = \frac{c_\mu R_{osc}}{\sigma_T} \; ; \; A_3 = c_\mu R_{osc} \; ; \; B = \frac{c_\mu \bar{u}_c^2}{k_c}$$

6.5.1 THE ANALOGUE COMPUTER SOLUTION

The facilities available dictated that the most efficient way to obtain a solution was by means of an analogue computer. There is no doubt that there is some sacrifice in accuracy in comparison to a digital machine but this was not considered a serious restriction for the present problem since the main purpose was to establish the suitability of these

equations for application to separated flow problems. The main advantage of the analogue computer was the ease with which non-linear equations could be solved together with the benefits of a graphical solution for determining the effectiveness of the various parameters.

Before attempting to solve the equation set there are two modifications which must be made to the equations. The first, is concerned with the division by zero at $\eta = y/y_c = 0$. It is necessary to start the solution at $\eta = 1$, thus reversing the direction in which the solution is generated. It is convenient at this stage to modify the method of non-dimensionalising y^* in (6.41) and (6.43) for compatibility with the technique used in (6.55). This is done as follows,

Let
$$\eta = \frac{y^*}{y_G} = \epsilon \frac{y^*}{\sqrt{\frac{\nu}{a}}} \tag{6.62}$$

A new dependent variable can now be chosen to accommodate the above modifications

Let
$$\tau = 1 - \frac{1}{\epsilon}\eta \tag{6.63}$$

Thus
$$\frac{d}{d\eta} = -\frac{1}{\epsilon}\frac{d}{d\tau} \quad ; \quad \frac{d^2}{d\eta^2} = \frac{1}{\epsilon^2}\frac{d^2}{d\tau^2} \tag{6.64}$$

Substitution of (6.64) in (6.60) and (6.61) leads to the following equations

$$\varphi_\tau'' = \frac{-\epsilon}{A_3 \nu}\int\left\{\varphi_\tau'^2 - \varphi_\tau\varphi_\tau'' - \epsilon^2\right\} d\tau \tag{6.65}$$

$$T_\tau' = \frac{\epsilon}{A_2 \nu}\int \sigma T_\tau' \varphi \, d\tau \tag{6.66}$$

A similar process can be used to modify equation (6.59) thus

$$\frac{dK}{d\tau} = \frac{1}{A_1 V}\int\left\{\frac{C_D K^{3/2}}{(1-\tau)(1-e^{-DK^{1/2}(1-\tau)})} - BV[\varphi_\tau'']^2\right\}d\tau \qquad (6.67)$$

where $$V = K^{\frac{1}{2}}(1-\tau)(1-e^{-EK^{1/2}(1-\tau)})$$

and $$E = A_\mu R_{osc} \quad ; \quad D = A_D R_{osc}$$

The ' now denotes differentiation with respect to τ .

The second modification requires a scaling between the physical variables and the representative voltages in the computer. The following symbols in square brackets are now the computer variables which represent the physical variables, the letters a, b, c, d, e, f, g being scaling constants.

Thus, $$\varphi_\tau \equiv \left[\frac{\varphi_\tau}{4}\right] \; ; \; \varphi_\tau' \equiv \left[\frac{\varphi_\tau'}{a}\right] \; ; \; \varphi_\tau'' \equiv \left[\frac{\varphi_\tau'''}{b}\right]$$

$$T_\tau \equiv \left[\frac{T_\tau}{e}\right] \; ; \; T_\tau' \equiv \left[\frac{T_\tau'}{d}\right] \; ; \; V \equiv [V]$$

$$K \equiv [K] \; ; \; K^{1/2} \equiv [K^{1/2}] \; ; \; K^{3/2} \equiv [K^{3/2}]$$

$$K^{\frac{1}{2}}(1-\tau) \equiv [K^{\frac{1}{2}}(1-\tau)] \; ; \; 1-e^{\frac{E}{D}K^{1/2}(1-\tau)} \equiv [1-e^{-\frac{E}{D}K^{1/2}(1-\tau)}]$$

$$K_\tau' \equiv \left[\frac{K_\tau'}{c}\right] \; ; \; A_{2,3} \equiv \left[\frac{A_{2,3}}{g}\right] \; ; \; A_1 \equiv \left[\frac{A_1}{2}\right]$$

$$B \equiv \left[\frac{B}{f}\right] \; ; \; C \equiv [C]$$

By substituting the new variables into equations (6.65), (6.66) and (6.67) the resultant equation set is now in a suitable form for solution by means of the analogue computer. The additional equation (6.71) is required for compatibility in integration

$$\left[\frac{\varphi_\tau''}{b}\right] = \frac{-\epsilon}{g\left[\frac{A_3 V}{g}\right]}\int\left\{\frac{a^2}{b}\left[\frac{\varphi_\tau'}{b}\right]^2 - 4\left[\frac{\varphi_\tau}{4}\right]\left[\frac{\varphi_\tau''}{b}\right] - \frac{\epsilon^2}{b}\right\}d\tau \qquad (6.68)$$

$$\left[\frac{T'_\tau}{d}\right] = \frac{4\sigma}{g\left[\frac{A_2 V}{g}\right]}\int\left[\frac{\phi_\tau}{4}\right]\left[\frac{T'_\tau}{d}\right] d\tau \qquad (6.69)$$

$$\left[\frac{K'}{c}\right] = \frac{1}{\left[\frac{A_1 V}{2}\right]}\int\left\{\frac{1}{2c}\cdot\frac{[c][K^{3/2}]}{[1-\tau]\left[1-e^{-DK^{1/2}(1-\tau)}\right]} - \frac{b^2 f}{2c}\left[\frac{B}{f}\right][V]\left[\frac{\phi''_\tau}{b}\right]^2\right\} d\tau \qquad (6.70)$$

$$\left.\begin{aligned}\left[\frac{\phi'_\tau}{a}\right] &= \frac{b}{a}\int\left[\frac{\phi''_\tau}{b}\right] d\tau \quad ; \quad \left[\frac{\phi_\tau}{4}\right] = \frac{a}{4}\int\left[\frac{\phi'_\tau}{a}\right] d\tau \\ \left[\frac{T_\tau}{e}\right] &= \frac{d}{e}\int\left[\frac{T'_\tau}{d}\right] d\tau \quad ; \quad [K] = c\int\left[\frac{K'}{c}\right] d\tau\end{aligned}\right\} \qquad (6.71)$$

The analogue circuits used for the solution of these equations are illustrated in FIG. 6.7(a) and (b)

6.5.2 BOUNDARY CONDITIONS

$$\eta = 0 : \quad K = 0 ; \quad \phi'_\tau = 0 ; \quad \phi_\tau = 0 ; \quad T_\tau = 1$$

$$\eta = 1 : \quad K = 1 ; \quad \phi'_\tau = 0.999 ; \quad T_\tau = 0$$

6.5.3 PROCEDURE FOR SOLUTION

The following procedure was adopted for the solution of equations (6.68), (6.69) and (6.70). The solution of (6.70) was first obtained by starting the computation at $\eta = 1$, $K = 1$ and adjusting the initial slope of the equation until the remaining boundary condition was satisfied. A similar process was required to solve (6.68). The speed at which this equation was computed was matched to the computation speed of (6.70). This required an iterative process due to the coupling of these equations by the ϕ''_τ term. It was found however that for the range of variables considered this coupling produced a negligible effect on the final solution and was eventually neglected.

The solution of (6.69) was then straightforward.

One difficulty encountered during the solution was the generation of the exponential function. This required the use of a diode function generator which required resetting for each value of E and D. From the initial calculations values of E or D greater than 0.5 made a negligible difference on the final solution. It was therefore considered sufficiently accurate to have one exponentional function with a time constant of 0.5 for all solutions.

6.5.4 HEAT TRANSFER BOUNDARY CONDITIONS

The calculations in Appendix D demonstrate that the heat transfer is dependent upon the type of surface heating employed and on the velocity gradient around the wall. With the present problem the velocity gradient in the separation region is weak and it is suggested that the differences between constant temperature and constant heat flux surfaces will be small. The following calculations are based on constant temperature conditions. The relationship between Nusselt number and temperature gradient is then derived as follows.

$$q_w = \alpha \left(\frac{dT^*}{dy^*}\right)_{y=0}$$

By non-dimensionalising this equation in the same manner as (6.43), then

$$q_w = \alpha \frac{\Delta T}{y_c} \left(\frac{dT}{d\eta}\right)_{\eta=0}$$

where $\Delta T = T_w - T_c$

Thus

$$Nu = \frac{D}{y_c} \left(\frac{dT}{d\eta}\right)_{\eta=0} \qquad (6.72)$$

6.5.5 DISCUSSION OF RESULTS

Before analysing the data the accuracy of the solutions was checked by comparing the solution of the equations for the special case when $\nu_t = 0$ (that is, laminar flow) which could then be compared with the numerical solution obtained by Hiemenz. A comparison of $(\varphi'')_{\eta=0}$ was as follows

PRESENT SOLUTION $\quad (\varphi'')_{\eta=0} = 1.227$

HIEMENZ SOLUTION $\quad (\varphi'')_{\eta=0} = 1.233$

The difference of 0.5% was considered to be extremely good and sufficiently accurate for the present analysis. The solutions of the equations for this case plotted in FIG. 6.8.

The initial solutions were evaluated using the experimental constants recommended by Wolfshtein and which are tabulated below.

$$C_\mu = 0.22 \qquad C_D = 0.416 \qquad \sigma_{k,t} = 1.53$$

$$A_\mu = 0.016 \qquad A_D = 0.263 \qquad \sigma_T = 0.9$$

Throughout the analysis the Prandtl number σ was fixed at 0.7. The value of $\epsilon = 2.0$ was based on the laminar flow boundary layer thickness $(= 2.4\sqrt{\frac{\nu}{a}})$ at the front stagnation point. The experimental heat transfer data was plotted as a function of the turbulent energy, FIG. 6.9, and this was converted into a temperature gradient form using equation (6.72) and by assuming $y_G = 0.15$ IN. as constant over the range of tests.

Only the temperature gradient at the wall is of interest and this has been calculated for the experimental range of Rosc. It is immediately obvious that the constants used by Wolfshtein are unsuitable for the immediate problem. This is not surprising since they are likely based on flat plate boundary layer analysis.

Either C_μ or σ_T must be altered to suit the experimental data. Alteration of the latter term was unrealistic since the reduction required to accommodate the experimental results exceeded the lower limit of this term (which is 0.7, the laminar value), therefore it was decided leave σ_T unaltered and modify only C_μ to suit the experimental data. The required range of C_μ to encompass the experimental data is plotted in FIG. 6.10 from which it is evident that C_μ must be assigned as a variable before agreement can be obtained. By introducing $C_\mu = f(R_{osc})$ which effectively is a function of $k_G^{\frac{1}{2}}$ is the simplest choice. This is not unreasonable since C_μ is the factor attached to the diffusion term in the turbulent energy equation and it has already been proposed by Bradshaw (see equation (6.19)) that this factor is a function of the turbulent energy.

By plotting the values of C_μ at the intersection of the experimental data line with the constant C_μ lines against Rosc (FIG. 6.11) the following relationship may be evaluated

$$C_\mu = 0.051 (R_{osc})^{0.5} \qquad (6.73)$$

which is shown to give good agreement between theory and experiment in FIG. 6.12.

Having established the value of C_μ it is a straightforward process to adjust the value of $\sigma_{k,t}$ to obtain agreement between the theoretical turbulence profiles and the experimental data. The effect of C_μ on the turbulence decay is plotted in FIG. 6.13 using the value $\sigma_{k,t} = 1.53$. The range of C_μ covering the experimental values of Rosc is tabulated on next page.

Rosc	50	100	150	200	250
C_μ	.36	.51	.624	.72	.805

A simple modification to $\sigma_{k,t} = 0.5$ enables a satisfactory agreement to be obtained as indicated in FIG. 6.14.

Finally, the mean velocity profiles ϕ' are compared with experiment in FIG. 6.15. This can be modified to suit the data by using $\epsilon = 3.0$ as indicated in FIG. 6.16. It is now implied that the boundary layer thickness at the rear stagnation point is of the same order of magnitude as with a laminar flow.

It now appears that the equations discussed can satisfactorily predict the heat transfer from the fluid motion in the wake region of a cylinder. Although heavy reliance has had to be placed on numerical constants this technique is unlikely to be improved until more detailed knowledge of the flow in such a region is available.

6.5.6 CONCLUSIONS

1. The equations discussed in this section of the thesis may be used to satisfactorily predict the heat transfer from the fluid motion in the wake region.
2. For the diffusion term in the turbulent kinetic energy equation, it is necessary to include a factor which is a function of the turbulent energy at the edge of the boundary layer.
3. The constants used in the equations which provide the best agreement with the experimental data are as follows

$$C_\mu = 0.051 (R_{osc})^{0.5} \qquad \sigma_{k,t} = 0.5$$

$$\epsilon = 3.0 \qquad \sigma_T = 0.9$$

SUGGESTIONS FOR FURTHER WORK

1. A study of the effect of low velocity, high turbulence flows on the hot wire signal, from a wire calibrated in a low turbulence airstream.
2. The effect of turbulence components on the hot wire signal in highly turbulent flows.
3. The decay of turbulence near the wall in the wake region.
4. A theoretical study of the effect of fluctuating motion at a stagnation point flow.
5. An improved turbulent energy equation which is valid in both turbulent and viscous layers.
6. Further studies to determine the differences between heat transfer from constant temperature and constant heat flux surfaces.

APPENDIX A

THE THEORY OF OPERATION OF A HOT WIRE ANEMOMETER

The hot wire anemometer probe consists of a fine electrically heated wire which is cooled by the flow being measured. The use of a heated wire to measure fluctuations in a fluid stream is based on the fact that the characteristic time for the wire flow, i.e. the time it takes for a particle to move a distance equal to the wire diameter, is very small compared with the period of fluctuations in the flow. The flow about the wire behaves as though it were a steady flow at any instant. Hence the relationship between wire temperature and heat transfer from the wire is at any instant the same in the unsteady fluctuating flow as it would be in a steady flow having the same instantaneous properties.

From both experimental and dimensional considerations the heat transfer by convection from a finite heated wire placed normal to the mainstream of an incompressible fluid of constant Prandtl Number and constant specific heat ratio at low velocities can be expressed in a functional form as

$$Nu = f\left\{(Re)_D, Gr, \frac{T_w}{T_{wc}}, T_\infty, \frac{L}{D}\right\} \tag{A1}$$

where Nu is the Nusselt number, $(Re)_D$ the Reynolds number based on wire diameter, Gr the Grashof number, Tw/T_{wc} the ratio of the heated wire temperature to the cold wire temperature, T_∞ the free-stream temperature and L/D the length to diameter ratio of the wire.

The last three terms are included to account for non-linearities in some of the parameters (viscosity, thermal conductivity) and non-uniformities in heat loss from the wire. The heat transfer by radiation and the effects of the molecular nature of the flow are omitted. The former can be neglected unless the density, ρ, is very small or the wire temperature exceeds $1000^{o}K$. The molecular effects are small enough to be treated as a correction to the continuum heat transfer. (This is less than 0.5% for low velocities and completely ignored).

In this work no explicit corrections for aspect ratio, end losses and other non-linear effects are made, but instead these effects are accounted for by means of a calibration for each particular wire used. For practical purposes, the behaviour of a given wire under specific working conditions is of interest and not some ideal wire under ideal conditions. All fluid properties are evaluated at freestream temperature and free convection effects have been ignored since the flow velocities are sufficiently large.

The simplified and operational form of the relation for heat transfer from a wire placed normal to a flow (King's Law) may be written as

$$E_b^2 = E_o^2 + A U^n \qquad \text{(A2)}$$

where E_o corresponds to the voltage across the wire in still air, E_b is the instantaneous voltage corresponding to the instantaneous velocity U. A and n depend on the wire configuration, material and on the properties of the air. Furthermore, both A and E_o depend on the chosen resistance ratio Rw/Rwc. The resistance ratio indicates the degree of wire overheating. As it increases so does

the wire operating temperature. The higher the ratio the more sensitive the hot wire is, since the rate of heat transfer has increased, but at the same time the more rapidly the wire can burn out. For a chosen resistance ratio, E_o is constant and as the former increases so does E_o. By calibration of each probe at a chosen resistance ratio the data obtained using the calibration curve is only correct when the same resistance ratio is employed.

For the purpose of data analysis it is necessary to write the relationship between voltage and velocity in a suitable form, the most common being equation (A2), where frequently the index n is chosen equal to 0.5. It has been suggested however {H4} that n and A are not constants but in fact vary with mean velocity. This variation for a typical probe is shown in FIG. A.1. It seems that n is very sensitive to mean velocity for low flows and thus the relationship now implied is

$$E_b^2 = E_o^2 + f_1(\bar{u}) \cdot u^{f_2(\bar{u})} \tag{A3}$$

which is rather cumbersome. There is no apparent reason why this form of equation is used when other forms such as the one suggested below could satisfy requirements equally well. As many terms as required could then be included.

$$E = \frac{a_1 + a_2 u + a_3 u^2 + \cdots}{1 + b_2 u + \cdots} \tag{A4}$$

For the work in this thesis measurements in two ranges of flow were required, namely the range of freestream velocity and the corresponding range of mean velocity at the rear stagnation point, the latter being of the order of one tenth of the freestream range.

Equations (A2) and (A4) were used initially for curve fitting and the former was found to be as suitable as any other for each range of measurements.

To derive an expression which relates the fluctuating velocity component to the fluctuating voltage component, equation (A2) is written in the form

$$(\bar{E} + e')^2 - E_o^2 = A(\bar{u} + u')^n \qquad \text{(A5)}$$

where $\bar{E}$ and $\bar{u}$ denote time averaged values. The mean velocity is given by $\bar{u}$ and the mean voltage $\bar{E}$ across the wire is the DC voltage necessary to balance the bridge under steady state conditions. The fluctuating component of the velocity is u'(which is assumed parallel to $\bar{u}$) and the corresponding fluctuating voltage across the wire is e', that is, the A.C. voltage. By neglecting the quadratic and higher order terms in the binomial expansions of $(\bar{E} + e')^2$ and $(\bar{u} + u')^2$, the turbulence intensity Tu, defined by $\sqrt{\overline{u'^2}}/\bar{u}$ is given by

$$Tu = \frac{\sqrt{\overline{u'^2}}}{\bar{u}} = \frac{2\bar{E}^2}{n(\bar{E}^2 - E_o^2)} \cdot \frac{\sqrt{\overline{e'^2}}}{\bar{E}} \qquad \text{(A6)}$$

where $\sqrt{\overline{u'^2}}$ and $\sqrt{\overline{e'^2}}$ are the r.m.s. values.

This expression is only applicable for small fluctuations, that is, when $u'/\bar{u} \ll 1$. As already explained in the main part of the thesis this expression is acceptable for the measurement of freestream turbulence intensity but in the region of the rear stagnation point, where $u'/\bar{u} \sim 1$, another relationship was necessary.

APPENDIX B

TABLES OF EXPERIMENTAL DATA

Tables of raw data are presented in FIGS B1 - B22 details of which are listed under "Contents".

APPENDIX C

A RELATIONSHIP BETWEEN FREQUENCY SPECTRUM AND TURBULENCE SCALE

In this thesis the detailed analysis of turbulence has been studied by looking at the spectrum of turbulence measured at a fixed point in the fluid. Another method, which can be related to the above, is to define a length L, which may represent in some definite way the size of an eddy. This is done by measuring the velocity at two points close together compared with the size of the eddy. It is clear that a high degree of correlation will exist in this case and if the velocity at two points far apart are measured the correlation is likely to be small. If the correlation R_y between the values of u' at two points a distance y apart in the direction of the y coordinate has been determined for various values of y, then the R_y versus y curve will represent, from a statistical point of view, the distribution of u' along the y axis. If $R_y = 0$ at $y = Y$ then a length L can be defined such that

$$L = \int_0^Y R_y \, dy \tag{C1}$$

L may be taken as a possible definition of the average size of the eddies. Also, by definition, R_y is defined as

$$R_y = \frac{\overline{u_1' u_2'}}{\sqrt{\overline{u_1'^2}}\sqrt{\overline{u_2'^2}}} \tag{C2}$$

It is now possible to determine a relationship between the spectrum of turbulence measured at a fixed point and the correlation between simultaneous values of velocity measured at two points.

It has been shown mathematically that a relationship between R_y and F(n) exists in the form

$$R_y = \int_0^\infty F(n) \cos \frac{2\pi n y}{\bar{u}} \, dy \qquad (C3)$$

which may be transformed into

$$F(n) = \frac{4}{\bar{u}} \int R_y \cos \frac{2\pi n y}{\bar{u}} \, dy \qquad (C4)$$

Thus R_y and $\frac{\bar{u} F(n)}{2\sqrt{2\pi}}$ are Fourier transforms of one another.

Thus the scale of turbulence is now

$$L = \int_0^Y \int_0^N F(n) \cos \frac{2\pi n y}{\bar{u}} \, dn \, dy \qquad (C5)$$

In practice the evaluation of this integral using experimental data is likely to be tedious and not very accurate.

APPENDIX D

THE EFFECT OF SURFACE HEATING ON HEAT TRANSFER

Differences have been shown to exist between the experimental heat transfer measurements using a constant heat flux surface and those obtained using an isothermal surface. It is proposed to demonstrate in this Appendix, by means of several examples, that the variation in surface heating is a plausible reason which can account for the differences which occur. It is not intended that accurate predictions can be made from the calculations but that they are merely illustrative examples.

Information is already available {G16} for heat transfer in fully developed laminar flow inside tubes which predicts the effect of constant heat flux and constant temperature surface heating. The results are as follows

	Nusselt Number
Constant Heat Flux	4.364
Constant Temperature	3.658

The 16% difference has been explained simply by the slightly different shape of the generalised temperature profile which results.

Launder {G17} has studied heat transfer in accelerating boundary layers. His paper presents theoretical solutions of turbulent velocity and thermal boundary layers in flow between converging planes where the wall temperature varies as the free-stream velocity raised to a positive exponent. The solutions

clearly illustrate that as the wall temperature variation is made less rapid the thermal boundary layer penetrates progressively further beyond the velocity boundary layer causing the Stanton number to decrease.

Both of the above considerations are restricted to boundary layer flows and have shown that the type of surface heating is important although the effect is the opposite from that measured experimentally in the present problem. It is likely however that these boundary layer theory predictions are inapplicable for stagnation point flow.

D.1 STAGNATION POINT FLOW

In an attempt to show that the heat transfer at a stagnation point is dependent upon the type of surface heating and that any differences which occur are at least in qualitative agreement with experimental measurements available, the conserved property equation, written in the form below is chosen as a starting point.

$$\frac{dR_T}{dX} + R_T\left\{\frac{1}{\bar{u}_c}\cdot\frac{d\bar{u}_c}{dX} + \frac{1}{\rho}\cdot\frac{d\rho}{dX} + \frac{1}{R}\cdot\frac{dR}{dX} + \frac{1}{\Delta T}\cdot\frac{d\Delta T}{dX}\right\} = \frac{q_w(X)}{\rho c_p \bar{u}_c(X)\Delta T(X)} \qquad (D.1)$$

where x = Distance measured around cylinder from the stagnation point

X = x/D

R_T = $\dfrac{\bar{u}_\infty\, \delta T}{\nu}$

δ_T = Thermal layer thickness

R = Body Radius

q_w = Wall heat flux

$\bar{u}_G$ = Velocity at edge of boundary layer

ΔT = $T_w - T_\infty$

$\bar{u}_G$, ΔT, q_w may be functions of x.

In potential flow theory the velocity around the cylinder is described by the equation

$$\bar{u}_G = \bar{u}_\infty \sin 2X \tag{D.2}$$

Hence $$\frac{1}{\bar{u}_G} \cdot \frac{d\bar{u}_G}{dX} = 2 \cot 2X \tag{D.3}$$

For incompressible flow the density term may be neglected and in the region of the stagnation point the effect of body radius may also be neglected. Equation (D.1) now reduces to

$$\frac{dR_T}{dX} + R_T\left\{2\cot 2X + \frac{1}{\Delta T} \cdot \frac{d\Delta T}{dX}\right\} = \frac{q_w(X)}{\rho c_p \bar{u}_G(X) \Delta T(X)} \tag{D.4}$$

It is now apparent that different solutions for the equation will be obtained depending upon which function for q_w (x) and ΔT (x) are chosen.

D.1.1 CONSTANT HEAT FLUX SURFACE

The heat transfer at the stagnation point for this boundary condition may now be calculated as follows.

Let q_w (x) = Q_w, a constant

By multiplying (D.4) by ΔT (x) it becomes

$$\frac{d}{dX}(R_T \Delta T) + (R_T \Delta T) \cdot 2\cot 2X = \frac{Q_w}{\rho c_p \bar{u}_\infty \sin 2X} \tag{D.5}$$

which is of the form $\frac{dy}{dx} + Py = Q$ and therefore the integrating factor is $e^{2\int \cot 2X\, dX} = e^{\log \sin 2X} = \sin 2X$

$$\frac{d}{dX}\left\{R_T \Delta T \sin 2X\right\} = \frac{Q_w}{\rho C_p \bar{u}_\infty} \tag{D.6}$$

$$R_T = \frac{Q_w}{\rho C_p \Delta T \bar{u}_\infty \sin 2X}\int dX = \frac{Q_w X}{\rho C_p \Delta T \bar{u}_\infty \sin 2X} \tag{D.7}$$

i.e. $$[R_T]_{q_w = \text{Const.}} = [St]_{q_w = \text{Const.}} \times X \tag{D.8}$$

D.1.2 CONSTANT TEMPERATURE SURFACE

By adopting a similar procedure to the above equation (D.4) may be solved with this alternative boundary condition. Thus,

$$\frac{d}{dX}(R_T \Delta T) + (R_T \Delta T) \times 2\cot 2X = \frac{q_w(X)}{\rho C_p \bar{u}_\infty \sin 2X} \tag{D.9}$$

$$R_T = \frac{1}{\rho C_p \Delta T \bar{u}_\infty \sin 2X}\int q_w(X)\, dX \tag{D.10}$$

It is now necessary to choose a suitable function for q_w (x) which will represent the variation of heat transfer around the wall. A simple first approximation is

$$q_w(X) = Q_w \cos 2X \tag{D.11}$$

By substituting this expression into (D.10), the integral may now be evaluated.

$$[R_T]_{\Delta T = \text{Const.}} = [St]_{\Delta T = \text{Const.}} \times \frac{1}{2}\sin 2X \tag{D.12}$$

D.1.3 A COMPARISON OF DATA

The effect of the two boundary conditions may now be compared

$$\frac{[R_T]_{\Delta T=\text{CONST.}}}{[R_T]_{q_w=\text{CONST.}}} = \frac{[St]_{\Delta T=\text{CONST}} \times \frac{1}{2}\sin 2X}{[St]_{q_w=\text{Const}} \times X} \qquad (D.13)$$

At the front stagnation point (x = 0) the equation (D.13) reduces to

$$\frac{[R_T]_{\Delta T=\text{CONST.}}}{[R_T]_{q_w=\text{CONST.}}} = \frac{[St]_{\Delta T=\text{CONST.}}}{[St]_{q_w=\text{CONST.}}}$$

It is now apparent that no further progress can be made until experimental data is available to determine the shape of the temperature profiles at the front stagnation point. All that can be said is that differences will result from any variation in temperature profile which may occur thus producing different values of thermal layer thickness.

BIBLIOGRAPHY

ACOUSTIC STREAMING

A. 1 ANDRADE : Proc. Roy. Soc. A134, 445 (1931)
On the circulation caused by vibration of air around a tube.

A. 2 SCHLICHTING : Physikalische Zeit 33, 97 (1932)
Berechnung ebener periodischer Grenz - schichtstromungen.

A. 3 WEST : Proc. Roy. Soc. B64, 483 (1951)
Circulations occurring in acoustic phenomena.

A. 4 WESTERVELT : J. Ac. Soc. Am. 25, 1, 60 (1953)
The theory of flow generated by a sound field.

A. 5 ANDRES, INGARD : J. Ac. Soc. Am. 25, 928 (1953)
Acoustic streaming at high and low Reynolds number.

A. 6 RANEY, CORELLI, WESTERVELT : J. Ac. Soc. Am. 26, 1006 (1954)
Acoustical streaming in the vicinity of a cylinder.

A. 7 HOLTSMARK, et al : J. Ac. Soc. Am. 26, 26 (1954)
Boundary layer flow near a cylindrical obstacle in an oscillating incompressible fluid.

A. 8 MAWARDI : J. Ac. Soc. Am. 28, 2, 239 (1956)
On thermoacoustic transduction in a potential flow.

A. 9 NYBORG : J. Ac. Soc. Am. 30, 4, 329 (1958)
Acoustic Streaming near a boundary.

A.10 WESTERVELT : J. Ac. Soc. Am. 32, 337 (1960)
Effect of sound waves on heat transfer.

NATURAL CONVECTION

B. 1 KUBANSKII : Sor. Phys. - Acoustics 5, 49 (1959)
The effect of acoustic streaming on convective heat exchange.

B. 2 FAND, KAYE : J. Ac. Soc. Am. 32, 579 (1960)
Acoustic streaming near a heated cylinder.

B.3 DOUGALL, CHIANG, FAND. : A. R. L. TN148 USAF Aero Lab. (1961) A study of the differential equations of coupled vibrations and free convection.

B.4 FAND, KAYE : Proc. Int Heat Trans. Con. - Colorado (1961) Influence of vertical vibrations on free convection heat transfer coefficients.

B.5 FAND, KAYE : J. Heat Trans. 83, p133 (1961) The influence of sound on free convection from a horizontal cylinder.

B.6 FAND, PEEBLES : Trans. A. S. M. E. 84, 3 (1962) A comparison of the influence of mechanical and acoustic vibration on free convection from a horizontal cylinder.

B.7 FAND, et al : Trans. A. S. M. E. 84, 245 (1962) The Local heat transfer coefficient around a heated cylinder in an intense sound field.

B.8 FAND : J. Ac. Soc. Am. 34, 12, 1887 (1962) Mechanism of interaction between vibrations and heat transfer.

B.9 RICHARDSON : J. Ac. Soc. Am. 36, 2323 (1964) Influence of sound upon local heat transfer from a cylinder.

B.10 LEE, RICHARDSON : J. Mech. Eng. Sci. 7, 2, 127 (1965) Effect of sound on heat transfer from a horizontal cylinder at large wavelengths.

B.11 BURDOKOV : J. App. Mech. Tech. Phys. (USA) Jan-Feb p112 (1965) Heat transfer from a cylinder in a sound field at Grashof numbers approaching zero.

B.12 RICHARDSON : ARL 66-0235 (1966) The effect of vibrations and oscillations on heat transfer from a cylinder.

B.13 RICHARDSON : Heat Trans. Sym. - Chicago (1966) Local details of the influence of a vertical sound field on heat transfer from a circular cylinder.

B.14 RICHARDSON : A. M. R. 20, 3, (1967)
Effects of sound and vibration on heat transfer.

B.15 RICHARDSON : J. Fluid Mech. 30, 2, 337 (1967)
Heat transfer from a circular cylinder by acoustic streaming.

B.16 DAVIS, RICHARDSON : Brown U. AF1754/3 (1967)
Natural convection from a horizontal cylinder in the presence of a sound field giving large streaming Reynolds number.

B.17 BOGDANOFF : Princeton U. Tech. Rpt. 483-f (1967)
A study of the mechanism of heat transfer in oscillating flow.

B.18 RICHARDSON : A. R. L. - USAF F33615-67C-1754 (1968)
Local effects of horizontal and vertical sound fields on natural convection from a horizontal cylinder.

B.19 BORISOV : Sov. Phys. - Acoustics 14, 2 (1968)
Critical sound pressure for heat and mass transfer process stimulated by acoustic oscillations.

FORCED CONVECTION

Part I

C.1 ANANTANARAYANAN : Trans. A. S. M. E. 80, 1426 (1958)
Effect of vibration on heat transfer from a wire to air in parallel flow.

C.2 SCREENIVASAN : Int. J. Heat Mass Trans. 3, (1961)
Effect of vibration on heat transfer from a horizontal cylinder to a normal airstream.

C.3 KUBANSKII : Sov. - Phys. - Acoustics 7, 290 (1962)
Forced flow heat transfer from a heat exchange surface with a resonant system in the wall.

C.4 FUSSELL : 5th Nat. H.T. Con. - Houston (1962)
Sonic effect on convective heat and mass transfer rates between air and a transverse cylinder.

C.5 FAND, CHENG : Int. J. Heat & Mass Trans. 6, 571 (1963)
The influence of sound on heat transfer from a cylinder in crossflow.

C.6 HAUGHEY : Trans. Inst. Chem. Eng. 43, T40 (1965)
Heat transfer during condensation on a vibrating tube.

C.7 KEZIOS : A. S. M. E. 66-HT/WA-43 (1966)
Effect of vibration on heat transfer from a cylinder in normal flow.

C.8 RICHARDSON : Chem. Eng. Sci. 21, 609 (1966)
The influence of sound on heat transfer in separated flows.

C.9 MORI, TOKUDA : Int. Heat Trans. Sym. - Chicago (1966)
The effect of oscillation on instantaneous local heat transfer in forced convection from a cylinder.

C.10 SUGANO : Chem. Eng. Sci. 23, 7, 707 (1968)
Effect of transverse vibration upon the rate of mass transfer from horizontal cylinders.

C.11 FAIRCLOTH, SCHAETZLE: A.S.M.E. HT Feb. 140 (1969)
Effect of vibration on heat transfer for flow normal to a cylinder.

C.12 FAND : Trans A. S. M. E. H.T. Feb (1969)
Formation of calcium sulphate scale on a heated cylinder in crossflow and its removal by acoustically induced vibration.

Part II

C.13 SCHMIDT, WENNER : N. A. C. A. Tech. Mem. 1050 (1943)

C.14 WINDING, CHENEY : Ind. Eng. Chem. 40, 1087 (1948)
Heat and Mass transfer in tube banks.

C.15 GIEDT : Trans. A. S. M. E. 71, 4, 375 (1949)
Investigation of variation of point unit heat transfer coefficient around a cylinder normal to an air stream.

C.16 LIGHTHILL : Proc. Roy. Soc. 224 A (1954)
The response of laminar skin friction and heat transfer to fluctuations in the stream velocity.

C.17 KESTIN, MAEDER : N. A. C. A. 4018 (1957)
Influence of turbulence on the transfer of heat from cylinders.

C.18 ZIJNEN : App. Sci. Res. p205 (1958)
Heat transfer from horizontal cylinders to a turbulent air flow.

C.19 SEBAN, et al : J. Aero Sp. Sci. 26, 809 (1959)
Heat transfer to separated and reattached subsonic turbulent flows downstream of a step.

C.20 GRIBBEN : Trans. A.S.M.E. 28, 3, 339 (1961)
The laminar boundary layer on a hot cylinder fixed in a fluctuating stream.

C.21 SUTERA, et al : J. Fluid Mech. 16, 497 (1963)
On sensitivity of heat transfer in stagnation point boundary layer to free stream vorticity.

C.22 RICHARDSON : Chem. Eng. Sci. March (1963)
Heat and Mass transfer in turbulent separated flows.

C.23 CHERVYAKOV : Inzhen-Fiz. Zh. 6, 8, 10, (1963)
An experimental of the effect of vibration on heat and mass transfer to a cylinder in a turbulent airflow.

C.24 KESTIN : Advances in Heat Transfer 3, 1-32 (1964)
The effect of free stream turbulence on heat transfer rates.

C.25 HANSON, RICHARDSON : Sym. on Separated Flows (A.S.M.E.) Philedelphic (1964)
Mechanics of turbulent separated flows as indicated by heat transfer: A Review.

C.26 SOGIN : A.S.M.E. J. Heat Trans. p200 (1964)
A summary of local heat transfer from the rear of bluff obstacles to low speed airstream.

C.27 GERSTEN : Brown U. AF 33(615)-1263 (1965)
Heat transfer in laminar boundary layer with oscillating flow.

C.28 SUTERA : J. Fluid Mech. 21, 3, 513 (1965)
Vorticity amplification in stagnation point flow and its effect on heat transfer.

C.29 LEONTEV, RIAGEN : U.S.S.R. J. App. Math & Phys. 6, p111 (1966)
Heat transfer in the eddy separation zone for a cylinder in crossflow.

C.30 SPALDING : J. Fluid Mech. 27, 1, 97 (1967)
Heat transfer from turbulent separated flows.

DUCTS AND TUBES

D.1 JACKSON, et al : Trans. A.S.M.E. 81, 68 (1959)
Free, forced convections and acoustic vibrations in a constant temperature vertical field.

D.2 LEMLICH : J. Heat Trans. A.S.M.E. p385 (1961)
A musical heat exchanger.

D.3 LEMLICH, HWU : A.I.Ch.E. J. 7, 102 (1961)
The effect of acoustic vibration on forced convective heat transfer.

D.4 LEMLICH : Chem. Eng. Sci. May 15, p171 (1961)
Vibration and pulsation boost heat transfer.

D.5 KUBANSKII : Sor. Phys. - Acoustics 8, 1, 62 (1962)
Acceleration of convective heat exchange by acoustic streaming.

D.6 MATHEWSON, SMITH : Preprint 20, 5th Nat. H.T. Con. - Houston (1962)
Effect of sonic pulsation on forced convective heat transfer to air and on film condensation of Isopropanal.

D.7 LOW, HODGINS : Can. J. Chem. Eng. 41, 241 (1963)
The effect of acoustic turbulence on mass transfer at a column wall.

D.8 BIRD, HART, McLURE : A.I.A.A. J. 3, 2248 (1965)
Finite acoustic oscillations and erosive burning in solid fuel rockets.

D.9 JACKSON, PURDY : J. Heat Trans. A.S.M.E. 87, 507 (1965)
Resonant pulsating flow and convective heat transfer.

D.10 CULICK : Astronautica Acta 12, 2 (1966)
Acoustic oscillations in solid propellant rocket chambers.

D.11 KOSHKIN, et al : Heat Trans. Sym. - Chicago (1966)
Unsteady heat transfer in tubes resulting from changes in heat flows, gas mass flow rate, and acoustic resonance.

D.12 MURPHREE : STAR 5, 9-N67-202 63*// (1967)
Acoustic and heat transfer aspects of launch vehicle turbulence.

D.13 DENT : A.I.Ch.E. J. 13, 6, 1114 (1967)
The calculation of heat transfer for combustion driven transverse oscillations in a gas air burner.

D.14 CHIANG, et al : Trans A. S. M. E. E, 36, 2, 159 (1969)
Analysis of pulsating flows in infinite and finite conical nozzles.

FLAT PLATES

E.1 NICKERSON : W. A. D. C. TR57-481 A. S. T. I. A. Doc. AD 210, 477 (1958)
The effect of free stream oscillations on the laminar boundary layer on a flat plate.

E.2 BAILEY, et al : Int. H.T. Con. - Colorado (1961)
Effect of flow pulsations on heat transfer by forced convection from a flat plate.

E.3 FEILER, YEAGER : N. A. S. A. TR-142 (1962)
Effect of large amplitude oscillations on heat transfer.

ULTRASONICS

F.1 THOMSON, SUTHERLAND : Ind. Eng. Chem. 47, 1167 (1955)
Ultrasonic insulation effect on liquid solid extraction.

F.2 ROBINSON, McLURE : Am. Cer. Bull. 37, 399 (1958)
Effects of ultrasonics on heat transfer by convection.

F.3 BOUCHER : Chem. Eng. 66, 151 (1959)
Ultrasonics boosts heatless drying.

F.4 ZUKAUSKAS : Inz. Fiz. Zh. 4, 58 (1961)
Investigation of the effect of ultrasonic waves on heat transfer from a body in a fluid.

F.5 LARSON, LONDON : A. S. M. E. 62-HT-44 (1962)
A study of the effects of ultrasonic vibrations on convective heat transfer to liquids.

F.6 TUDOZE : Int. Chem. Eng. 4, (1964)
Increasing the rate of absorption by the use of pulsations.

F.7 TUDOZE : Int. Chem. Eng. 4, (1964)
Increasing the rate of absorption by the use of pulsations.

F.8 HOWKINS, ZELTMANN : Proc. 19th Con. Eng. Med. & Bio. San Franscisco (1966) The use of ultrasonic energy to increase the rate of hemodialysis in artificial kidney machines.

F.9 ANISOVITCH : Izv. ACAD NAVK BSSR 2, 95 (1966) Heat transfer between a rod and a box in a process of high frequency drying.

F.10 SIRNOVYAN : Inz-Fiz. Zh. 10(4), 542 (1966) On the simultaneous acoustic and high frequency drying of capillary porous materials.

F.11 GUREVICH : N. A. S. A. TT-F-432 (1967) Non stationary heat and mass transfer.

GENERAL

G.1 ROSHKO : N. A. C. A. TN 2913 (1953) On the development of turbulent wakes from vortex sheets.

G.2 ROSHKO : N. A. C. A. TN 3169 (1954)

C.3 KEMP : J. Aero/Space Sci. 26, 543 (1959) Vorticity interaction at an axis-ymetric stagnation point in a viscous incompressible fluid.

G.4 STUART : J. Aero/Space Sci. 26, 124 (1959) The viscous flow near a stagnation point when the external flow has uniform vorticity.

G.5 KUETHE, et al : A. G. A. R. D. Con. London (1960) Stagnation point fluctuations on bodies of revolution with hemispherical noses.

G.6 BLOOR : J. Fluid Mech. 19, 290 (1964) The transition in the wake of a circular cylinder.

G.7 PUTNAM : A. S. M. E. 64-WA/HT-21 (1964) Flow induced noise and vibration in heat exchangers.

G.8 GERRARD : J. Fluid Mech. 22, 1, (1965) A disturbance sensitive Reynolds number range of the flow past a circular cylinder.

G.9 GERRARD : J. Fluid Mech. 25, 401 (1966)
The mechanics of the formation region of vortices behind bluff bodies.

G.10 BRADSHAW, et al : J. Fluid Mech. 28, 3, 593 (1967)
Calculation of boundary layer development using the turbulent energy equation.

G.11 CHEN : J. R. Ae.S. 71, 211 (1967)
Frequency of Karman vortex streets in tube banks.

G.12 SADEH, et al : A.R.L. - U.S.A.F. 33 (615)-1263 (1968)
An investigation of vorticity amplification in stagnation flow.

G.13 HARTLEN, et al : U. Toronto U.T.Mech.E. TP6809 (1968)
Vortex excited oscillations of a circular cylinder.

G14 WOLFSHTEIN : Int. J. Heat Mass Trans. 12, 301 (1969)
The velocity and temperature distribution in one dimensional flow with turbulence augmentation and pressure gradient.

G.15 PETERKA, RICHARDSON : J. Fluid Mech. 37, 2, 265 (1969)
Effects of sound on separated flows.

G16 KAYS : McGraw-Hill
Convective Heat and Mass Transfer.

G.17 LAUNDER, LOCKWOOD : Trans. A.S.M.E. (HT) May 1969
An aspect of Heat Transfer in Accelerating Turbulent Boundary Layers.

G.18 McADAM : McGraw-Hill, New York
Heat Transmission

G.19 MAGNUS : Blackie & Son, Glasgow.
Vibrations

G.20 ALEXANDER : Sym. on Wind Effects on Buildings and Structures. Loughborough U. 1968
A Theory for the oscillating lift on a circular cylinder.

HOT WIRE ANEMOMETRY

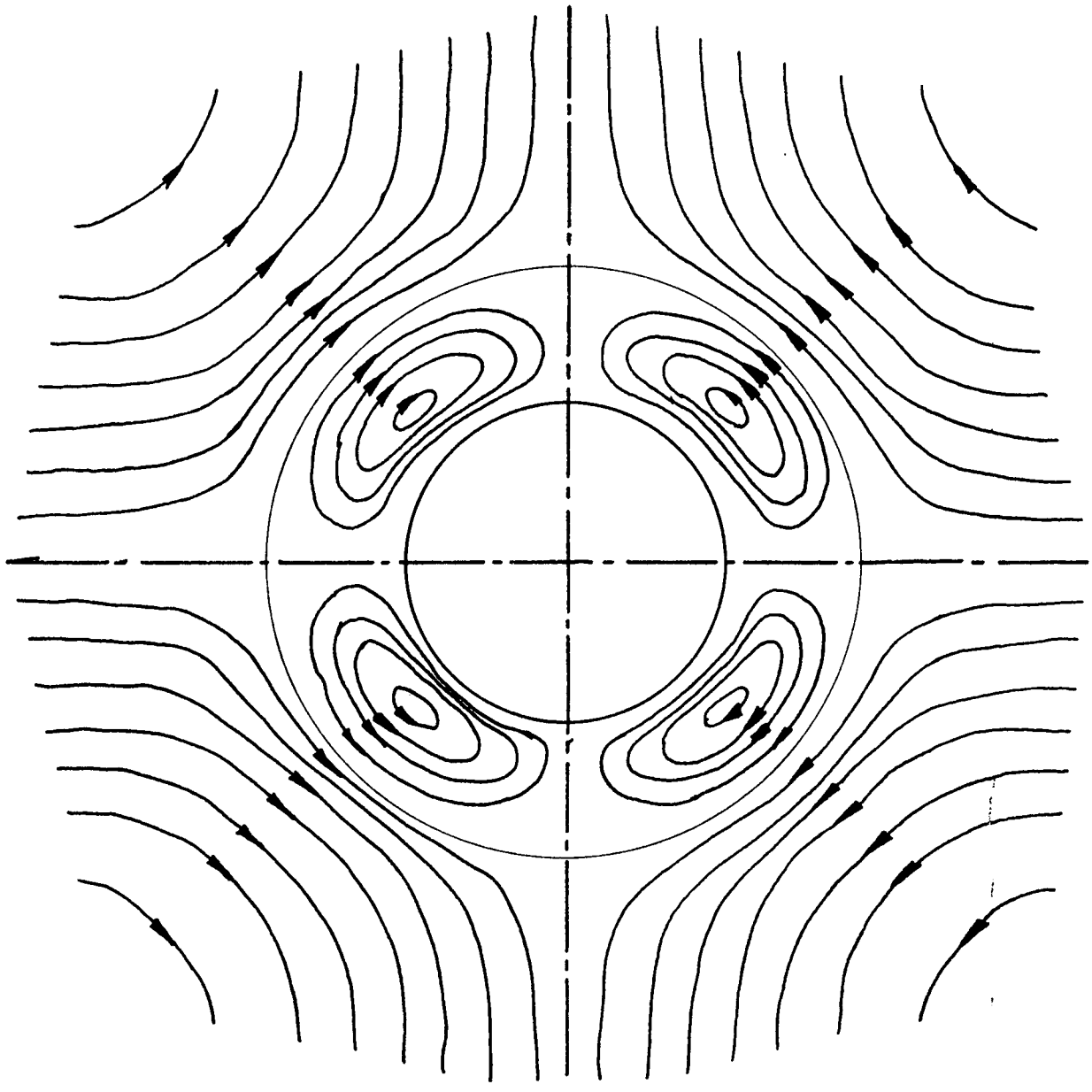
H.1 HINZE : McGraw-Hill. New York (1959)
Turbulence: An introduction to its mechanism and theory.

H.2 WILLS : J. Fluid Mech. 12, 3, 388 (1962)
The correction of hot wire readings for proximity to a solid boundary.

H.3 RHEN : A.I.A.A. Student J. 4, 1, 24 (1966)
Investigation of effects of surface proximity and resulting wire to surface heat transfer on hot wire anemometer data.

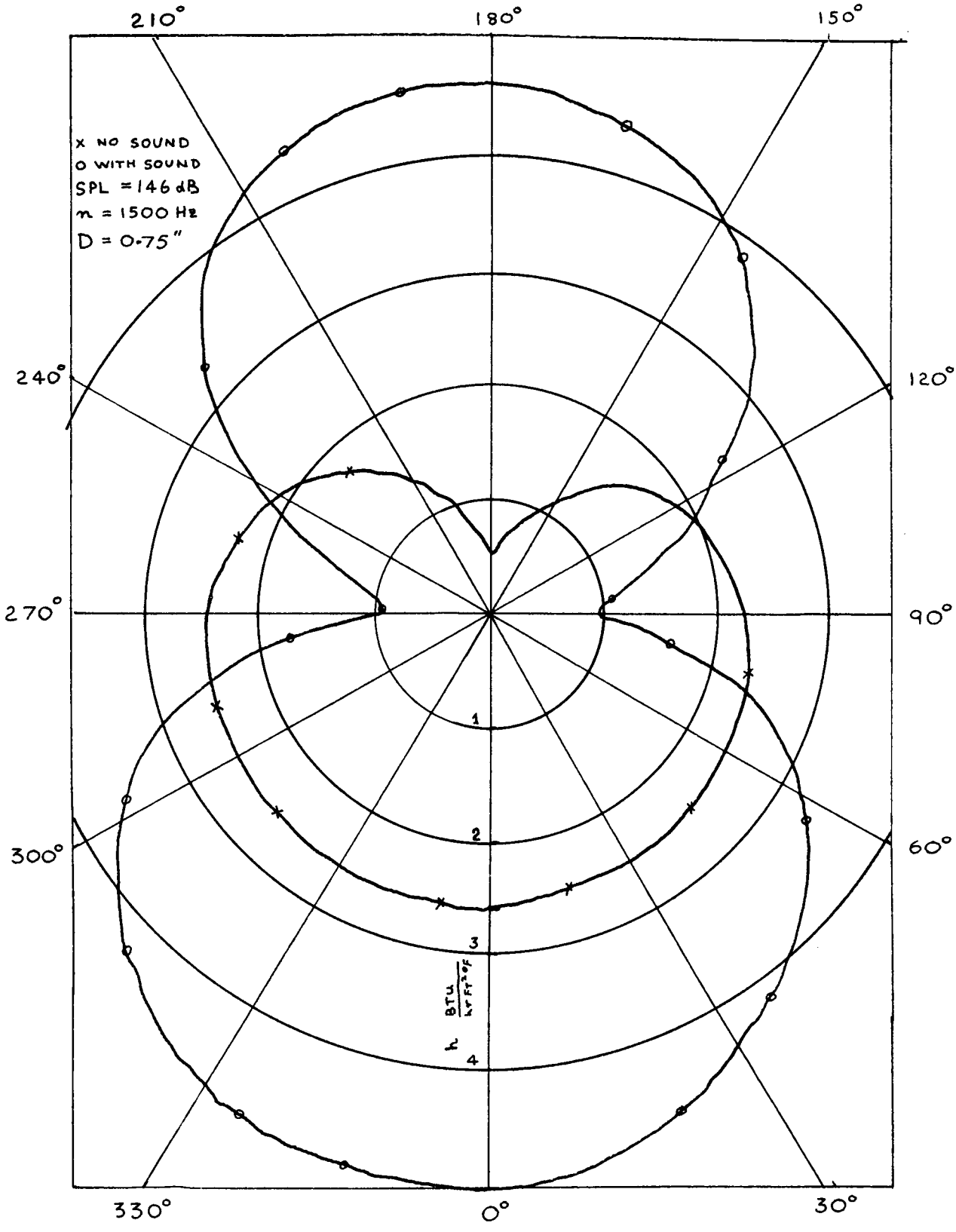
H.4 TURNER : N.P.L. Sym. Nov. (p9) (1968)
Non-linear convections for the response of a hot wire anemometer in highly turbulent flows.

H.5 FREYMOUTH : Rev. Sci. Inst. 40, 2, 258 (1969)
Non-linear control theory for constant temperature hot wire anemometer.



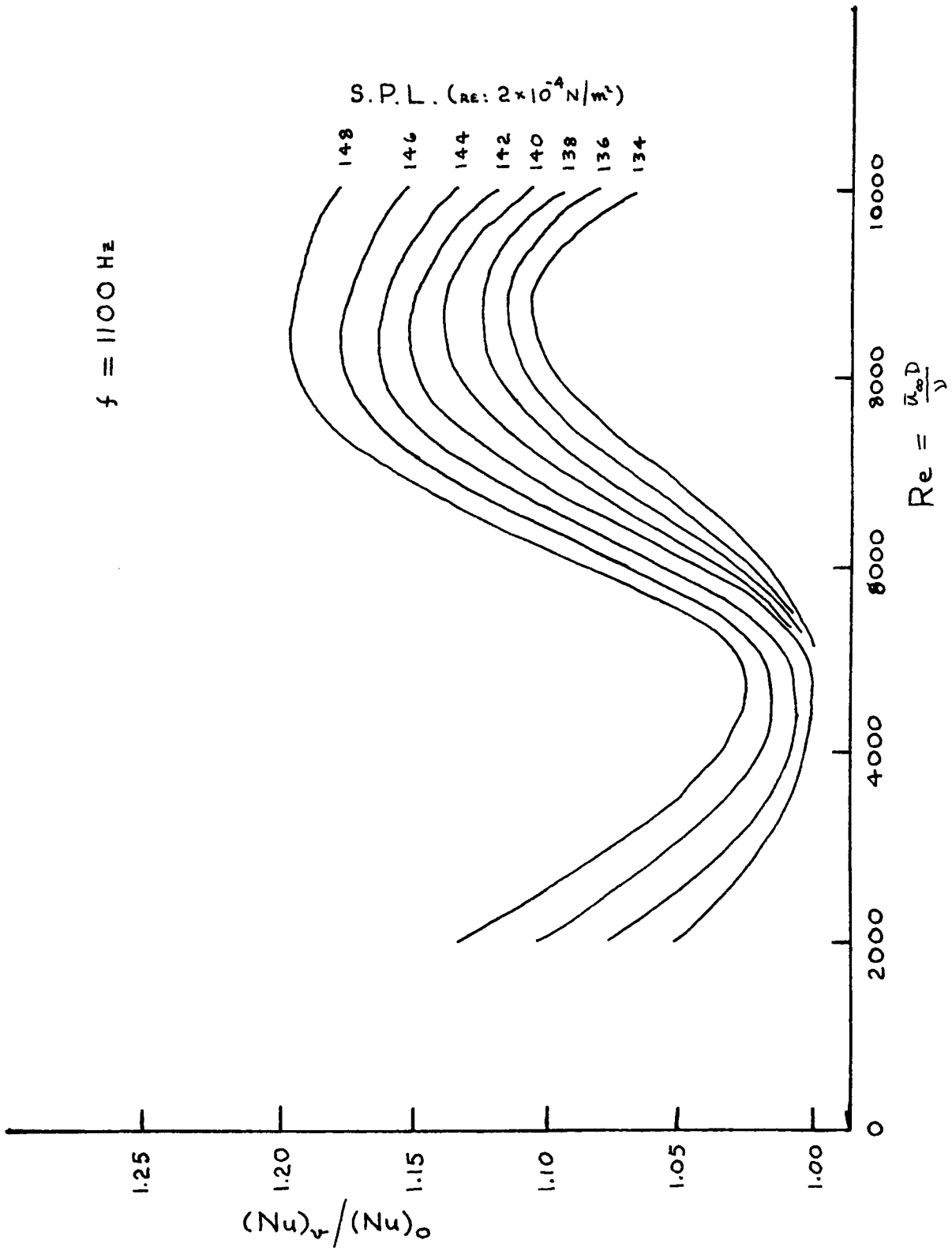
ACOUSTIC STREAMING AROUND A CYLINDER

FIG.1.1



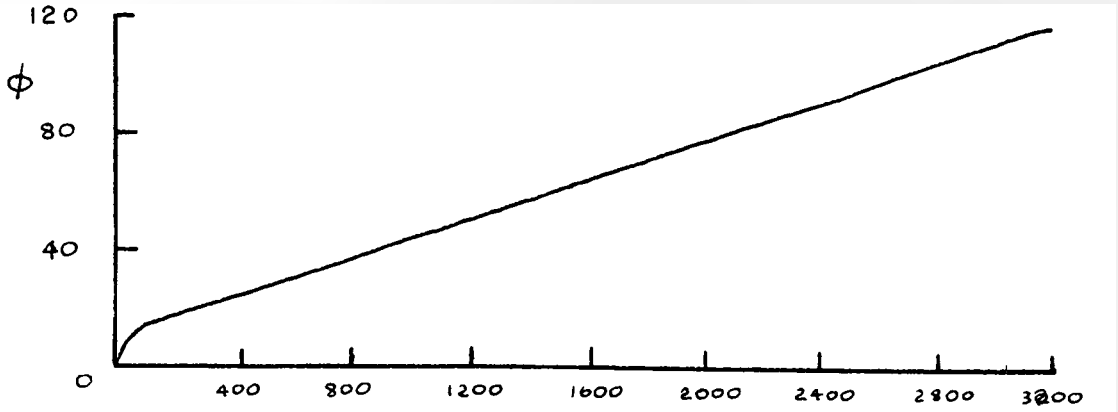
EFFECT OF HORIZONTAL SOUND FIELD ON NATURAL CONVECTION HEAT TRANSFER

FIG.1.2

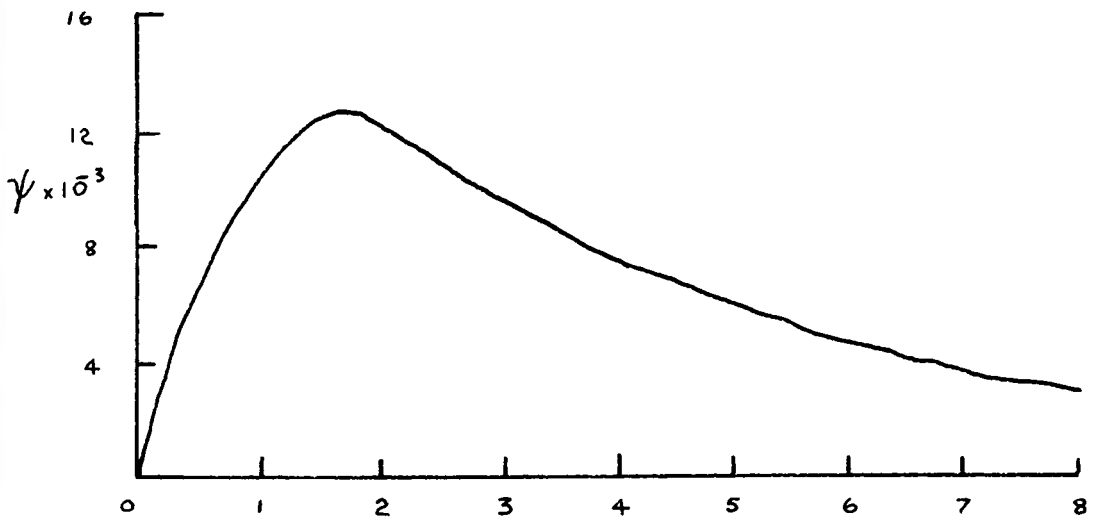


EFFECT OF SOUND FIELD ON FORCED CONVECTION HEAT TRANSFER FROM CYLINDER IN CROSS FLOW

FIG 1.3



CORRELATION PARAMETER $Re \times Tu = \frac{u'D}{\nu}$

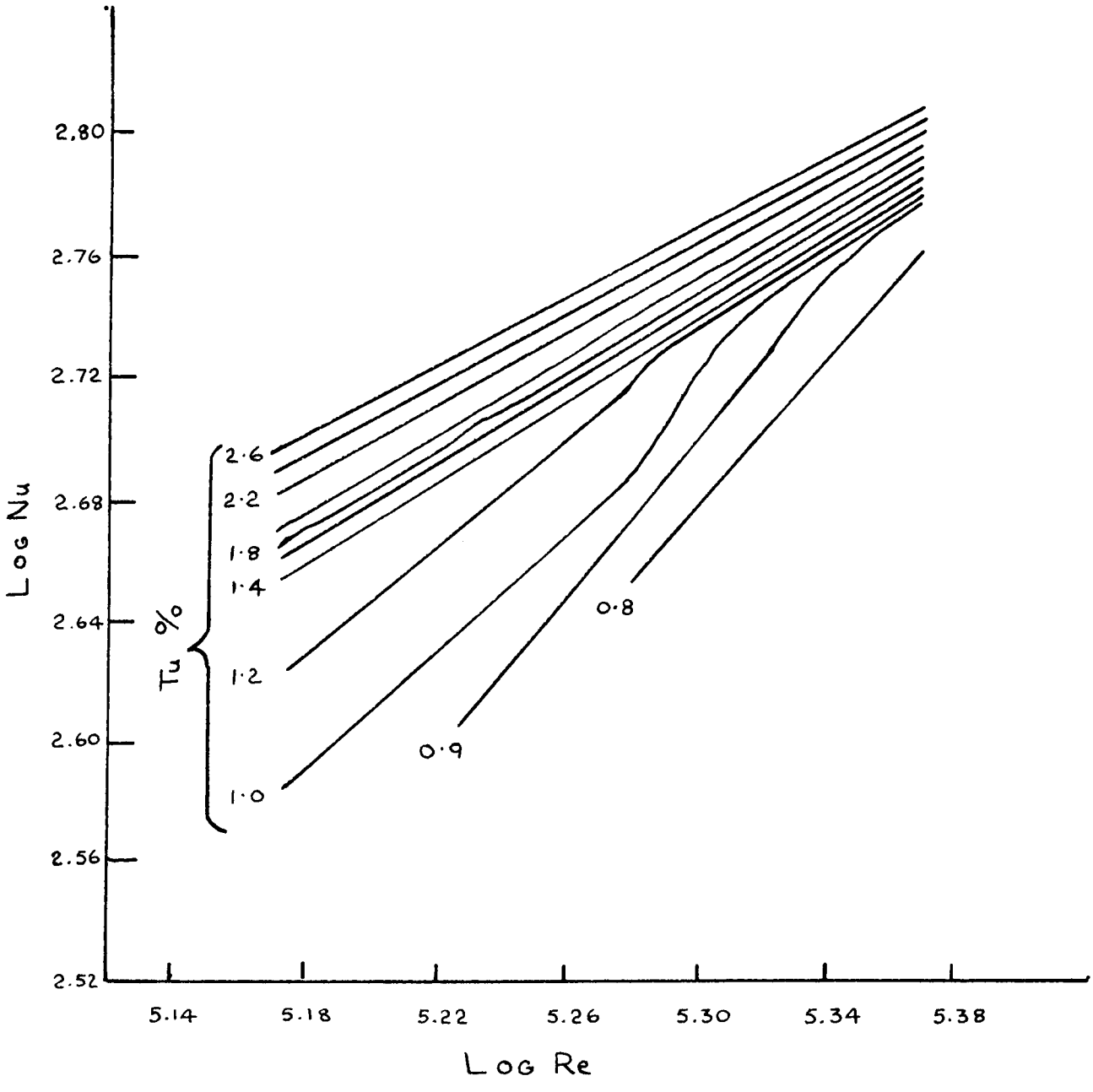


RELATIVE SCALE $\frac{Lx}{D}$

$$Nu^* = 1 + \phi(Re \times Tu) \times \psi(Lx/D)$$

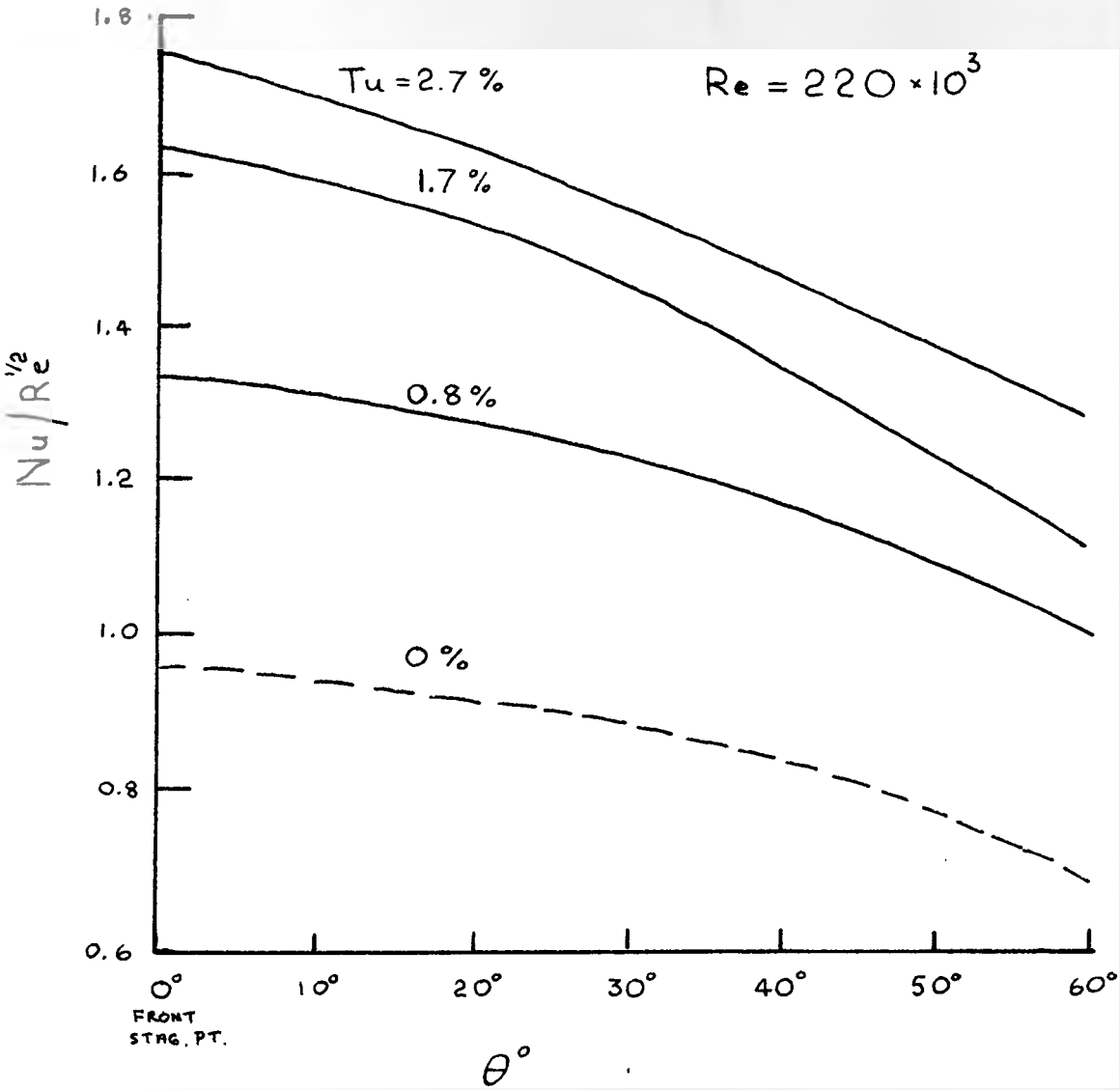
VAN ZIJNEN FUNCTIONS

FIG 1.4



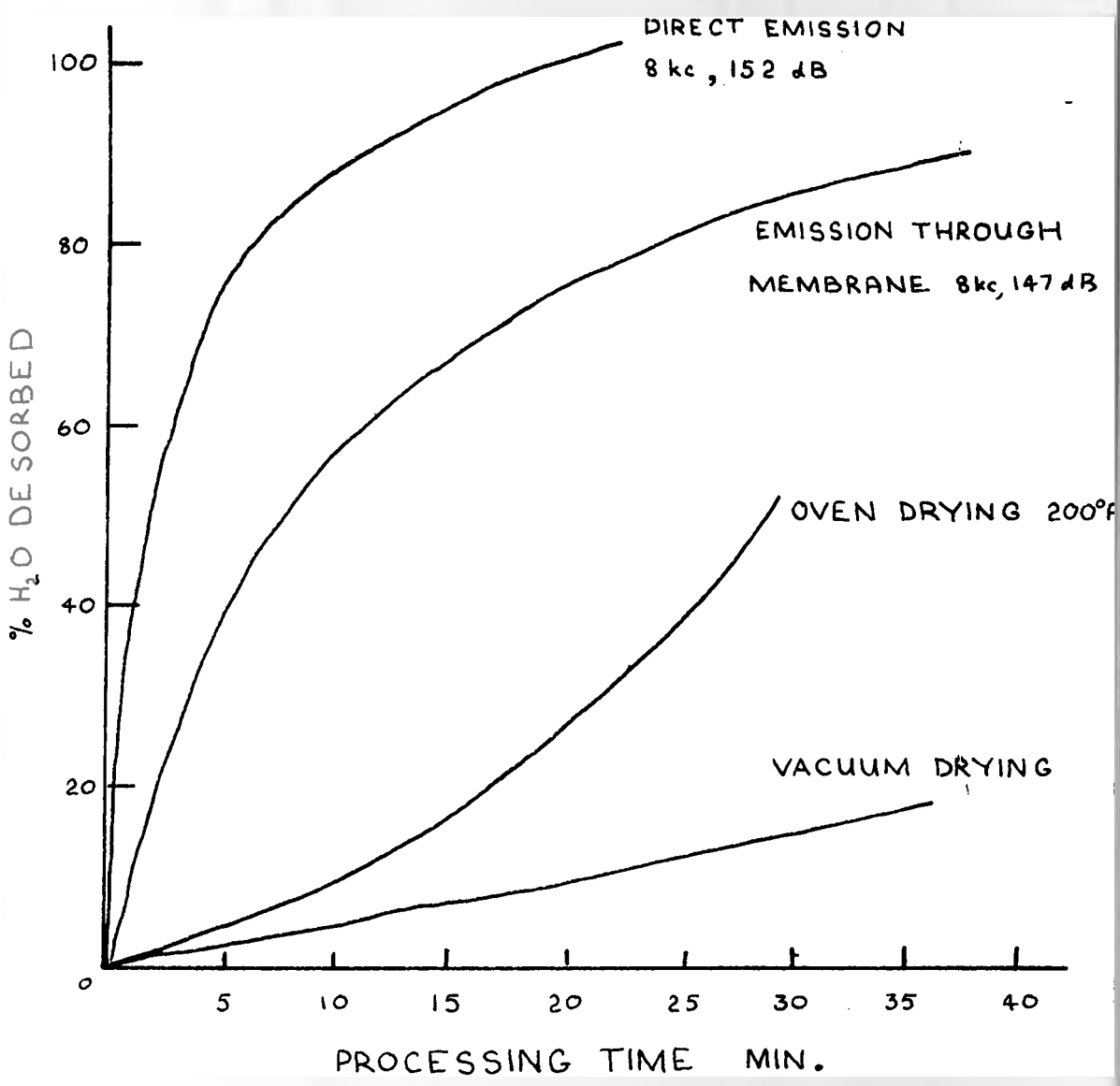
EFECT OF TURBULENCE ON OVERALL FORCED CONVECTIVE HEAT TRANSFER FROM A CYLINDER IN CROSSFLOW

FIG 1.5



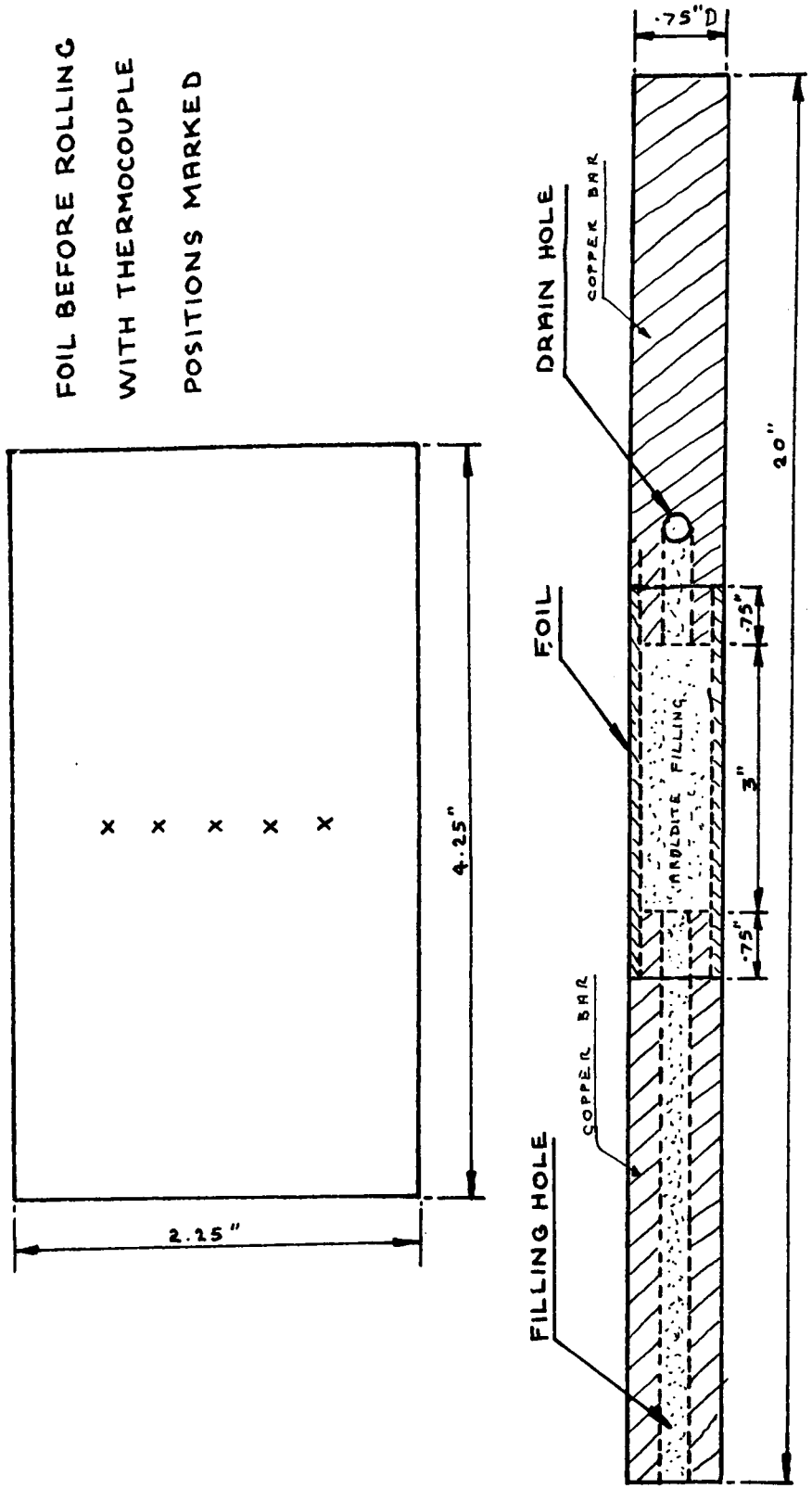
EFECT OF TURBULENCE ON LOCAL HEAT TRANSFER FROM A CYLINDER IN CROSSFLOW

FIG 1.6



THE USE OF SOUND AS A DRYING PROCESS

FIG 1.7



DETAILS OF THE CONSTANT HEAT FLUX CYLINDER

FIG 2.1

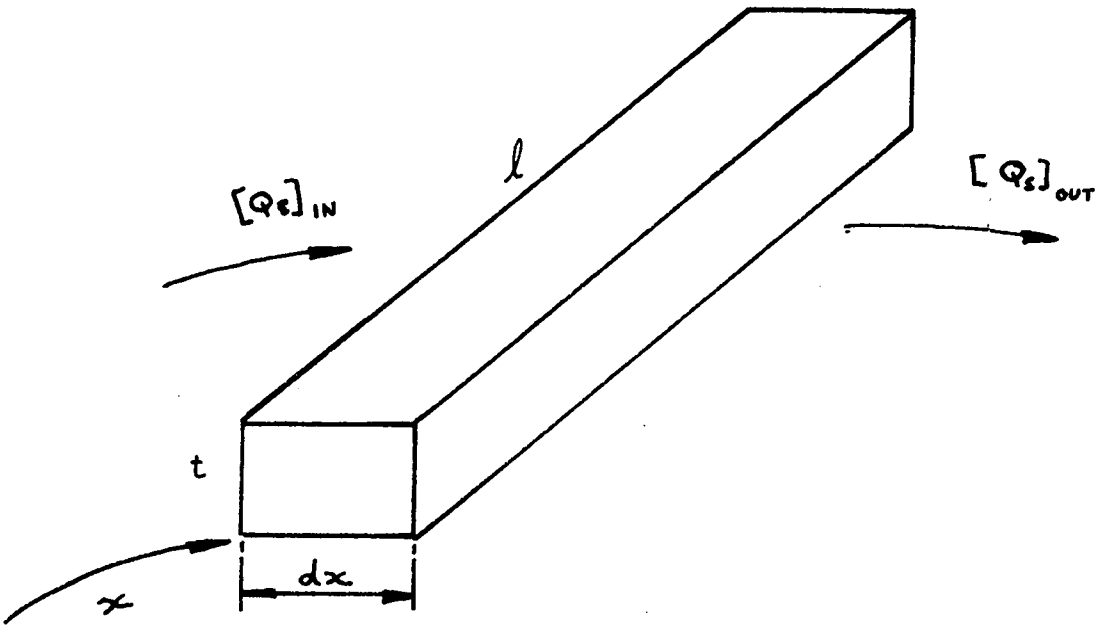
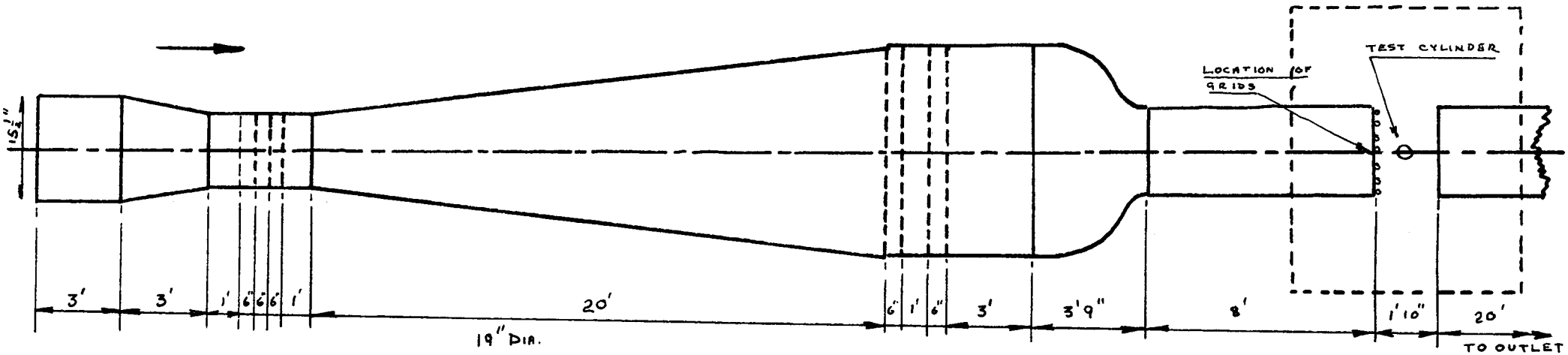
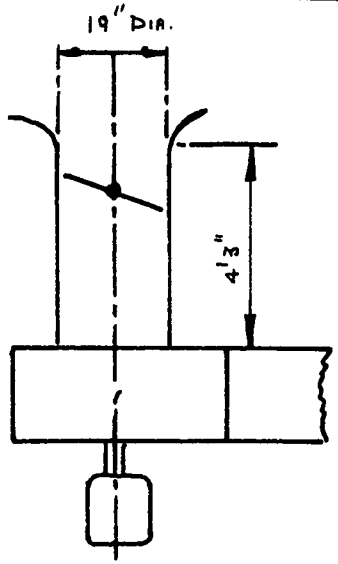


FIG 2.2



ELEVATION



PLAN

DETAIL OF FAN INLET

SCHEMATIC DIAGRAM OF WIND TUNNEL

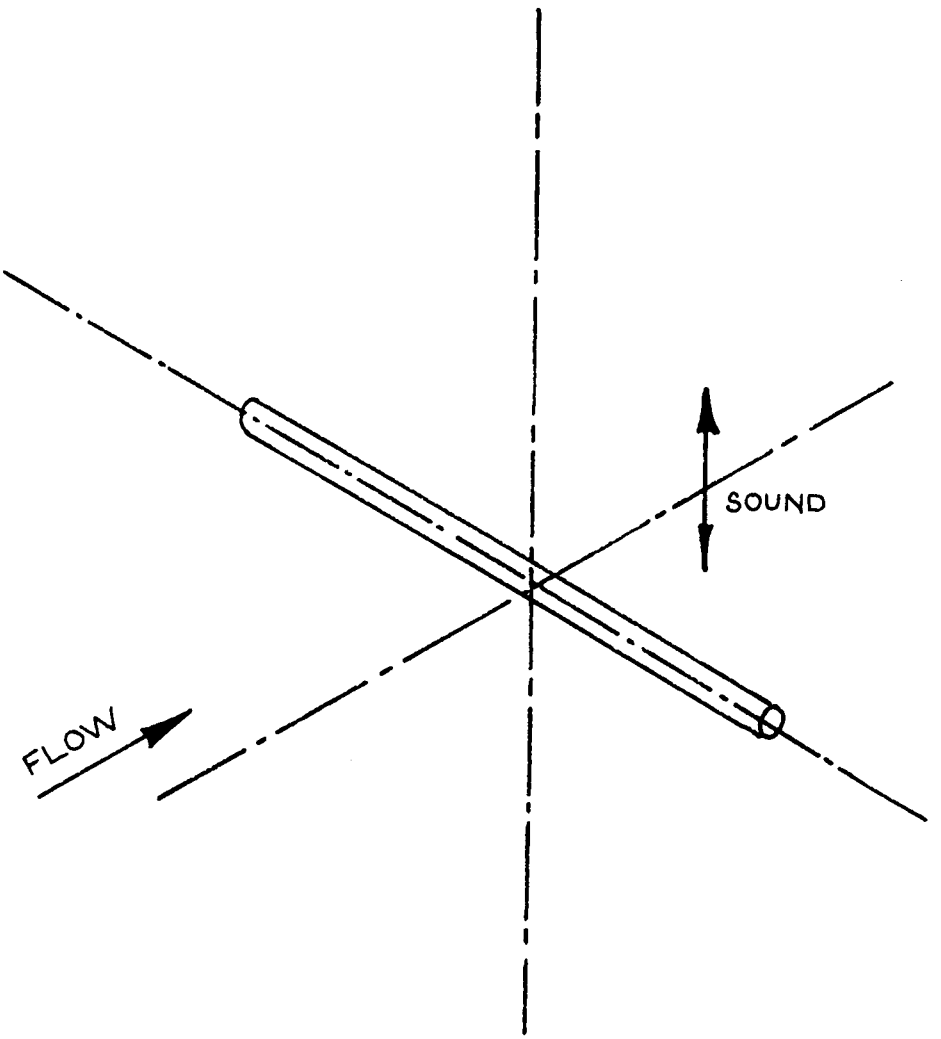
FIG 2.3

GRID	WIRE DIA (IN)	SPACE (IN)
E *	1/8	3/8
I	1/8	1/4
J	1/4	1/4
K	1/2	1/2
L	3/4	3/4
M	3/16	3/16
N *	1/4	1/4
P	3/8	3/8

* GRIDS E + N ARE CONSTRUCTED FROM HORIZONTAL + VERTICAL RODS OF ABOVE DIMENSIONS

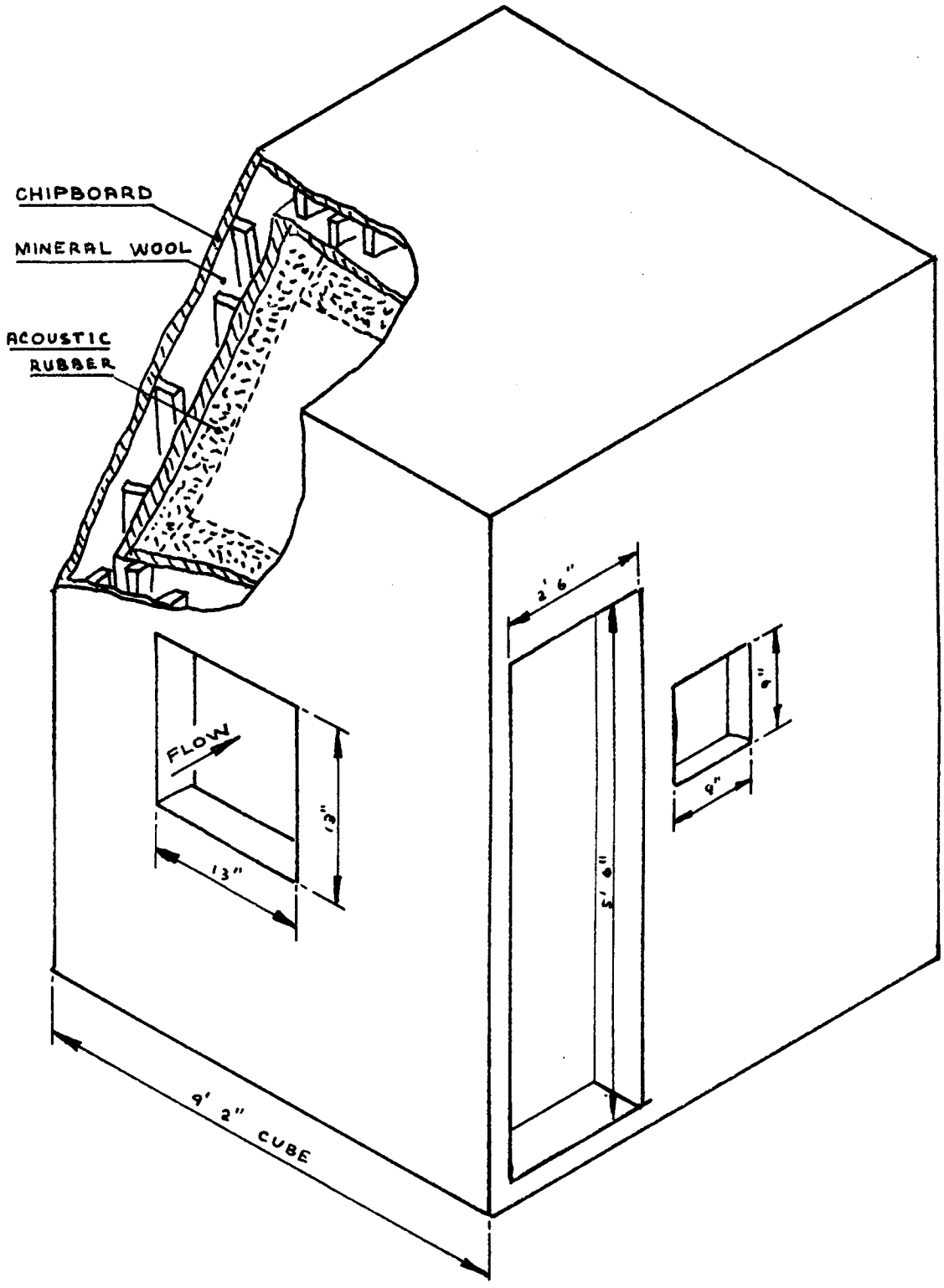
TABLE OF GRID SIZES

FIG 2.4



DIRECTION OF SOUND FIELD RELATIVE TO CYLINDER AND AIRSTREAM

FIG 2.5



ANECHOIC CHAMBER

FIG 2.6

THERMOCOUPLE CALIBRATION CURVE

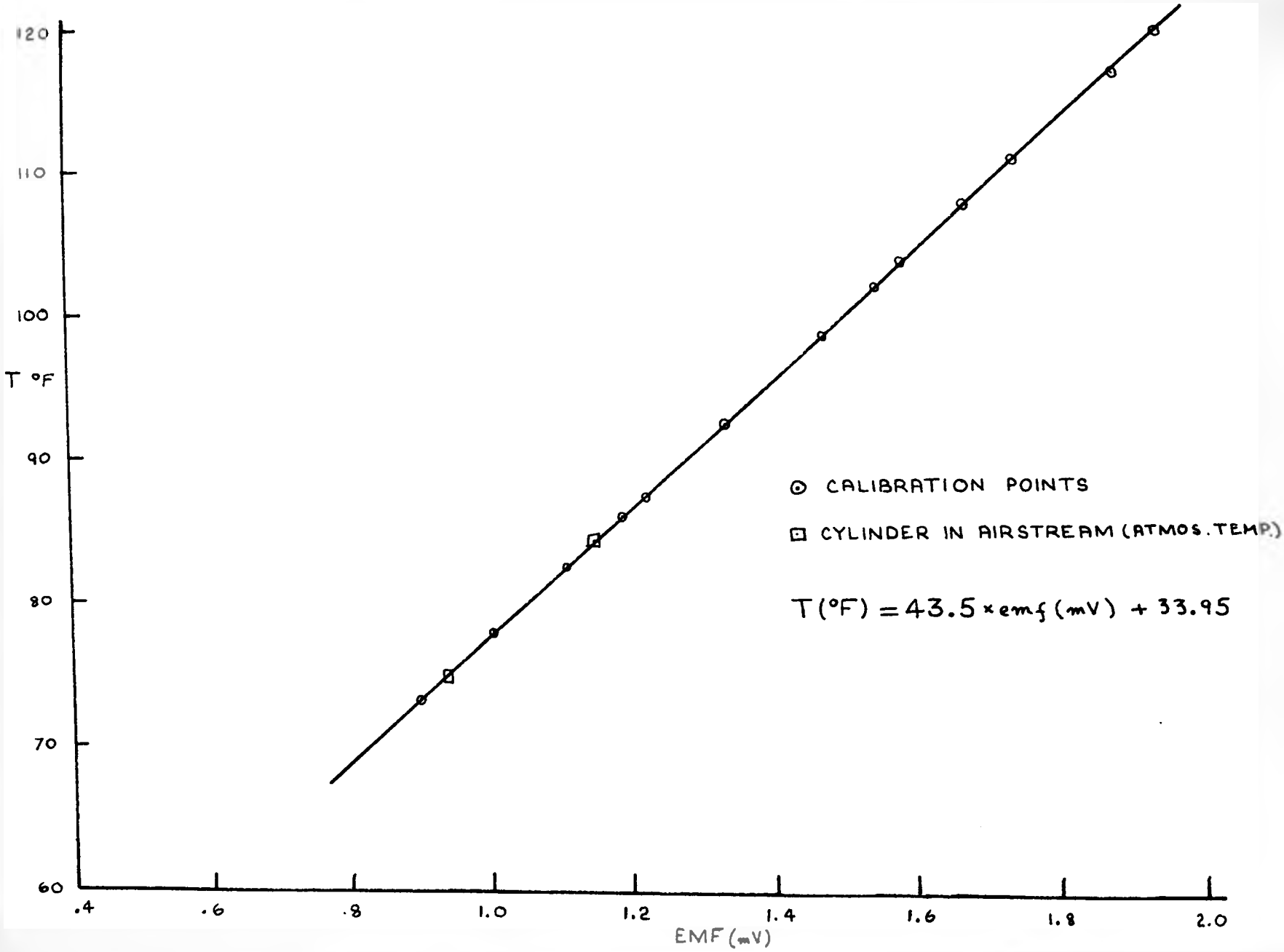
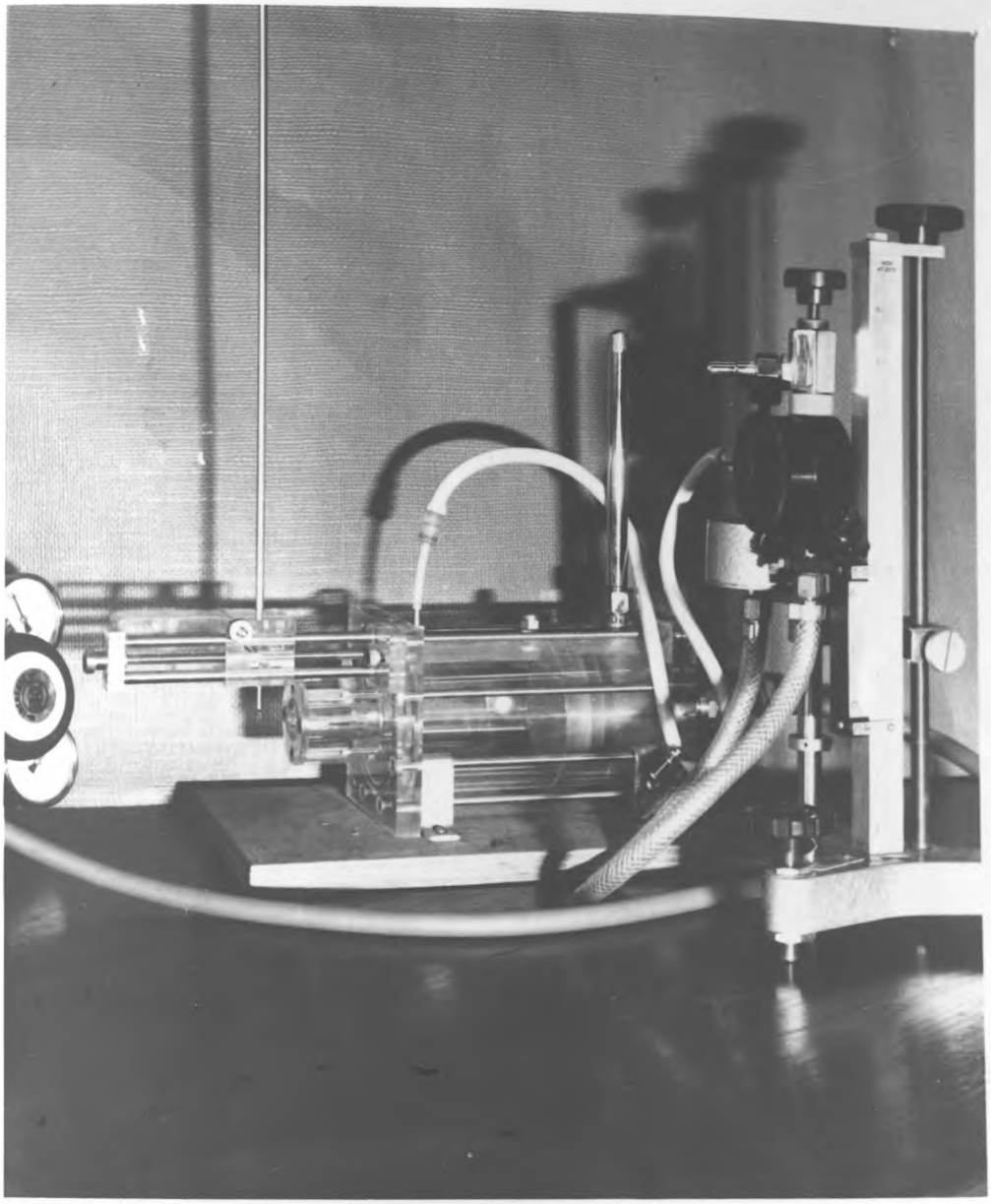
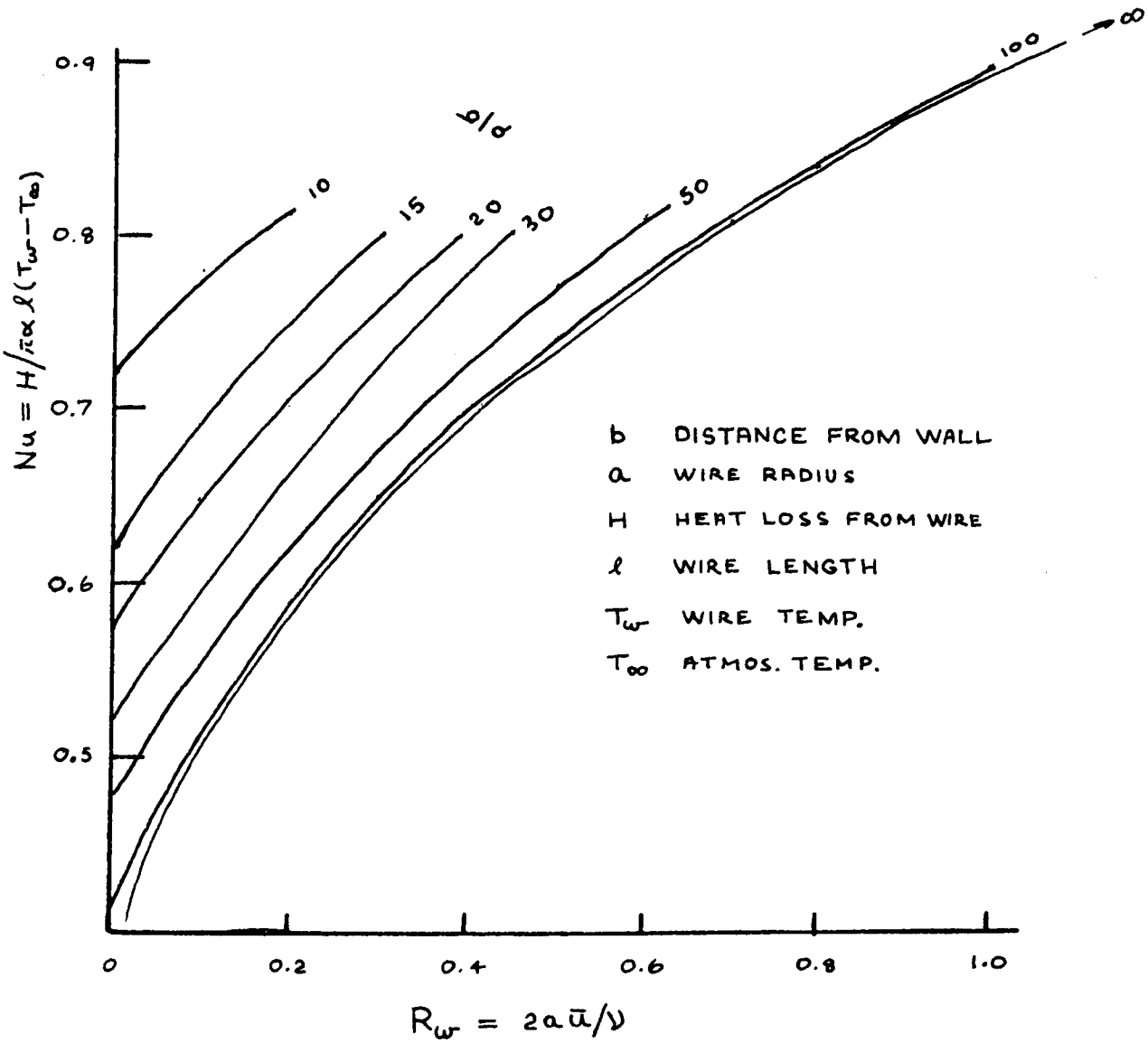


FIG 3.1



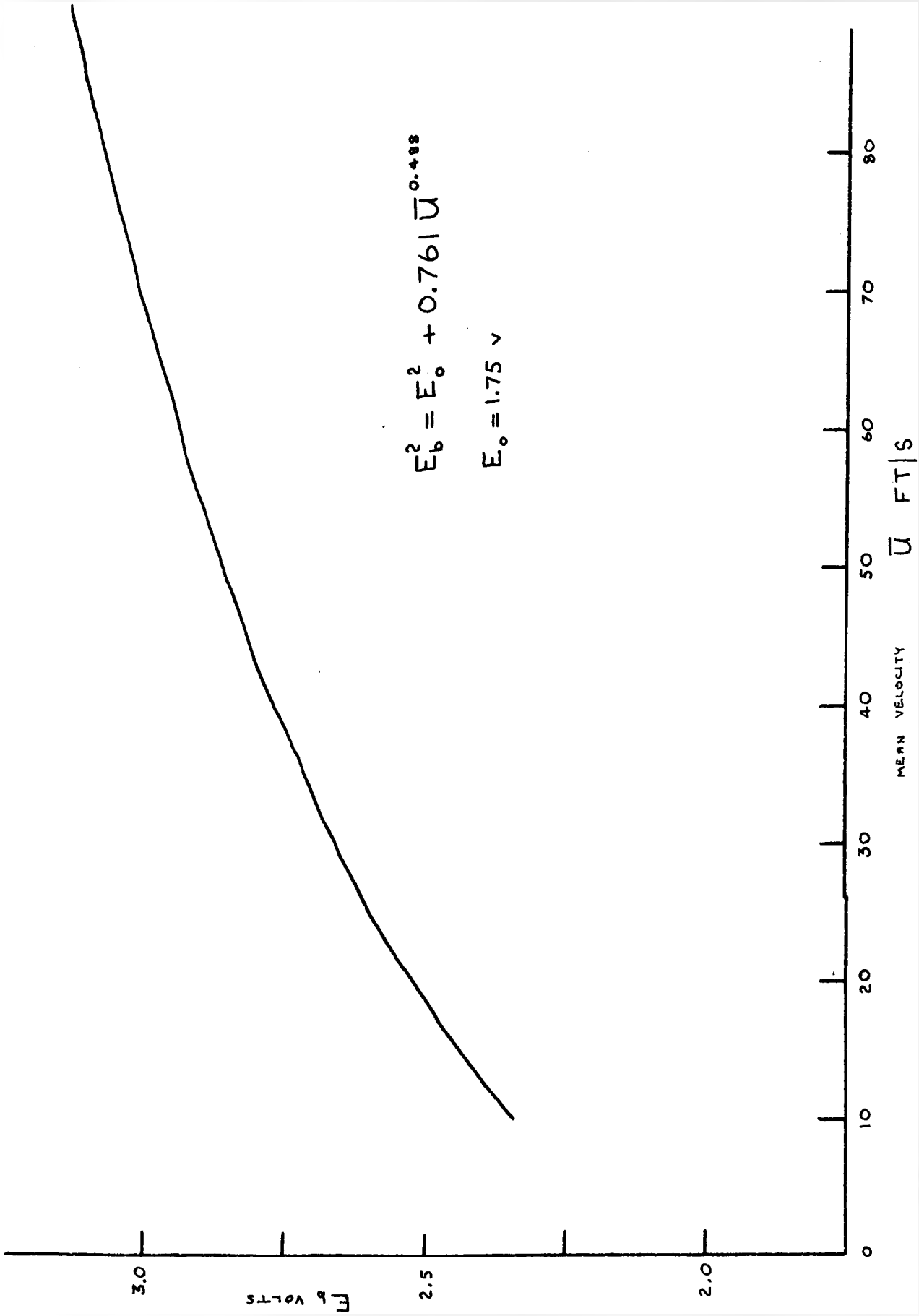
THE HOT WIRE CALIBRATOR

FIG 3.2



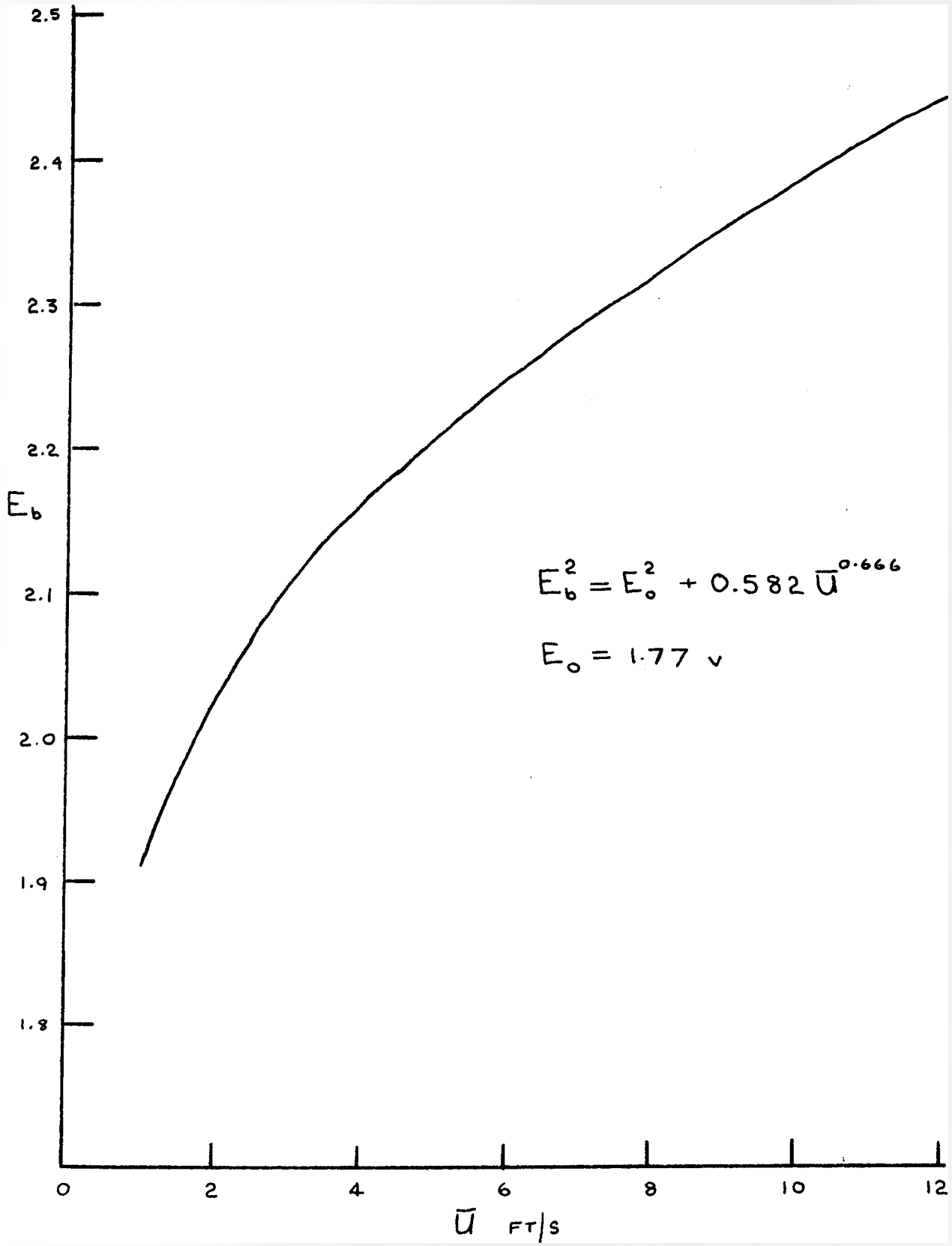
EFFECT OF WALL PROXIMITY ON HOT WIRE READINGS

FIG 3.3



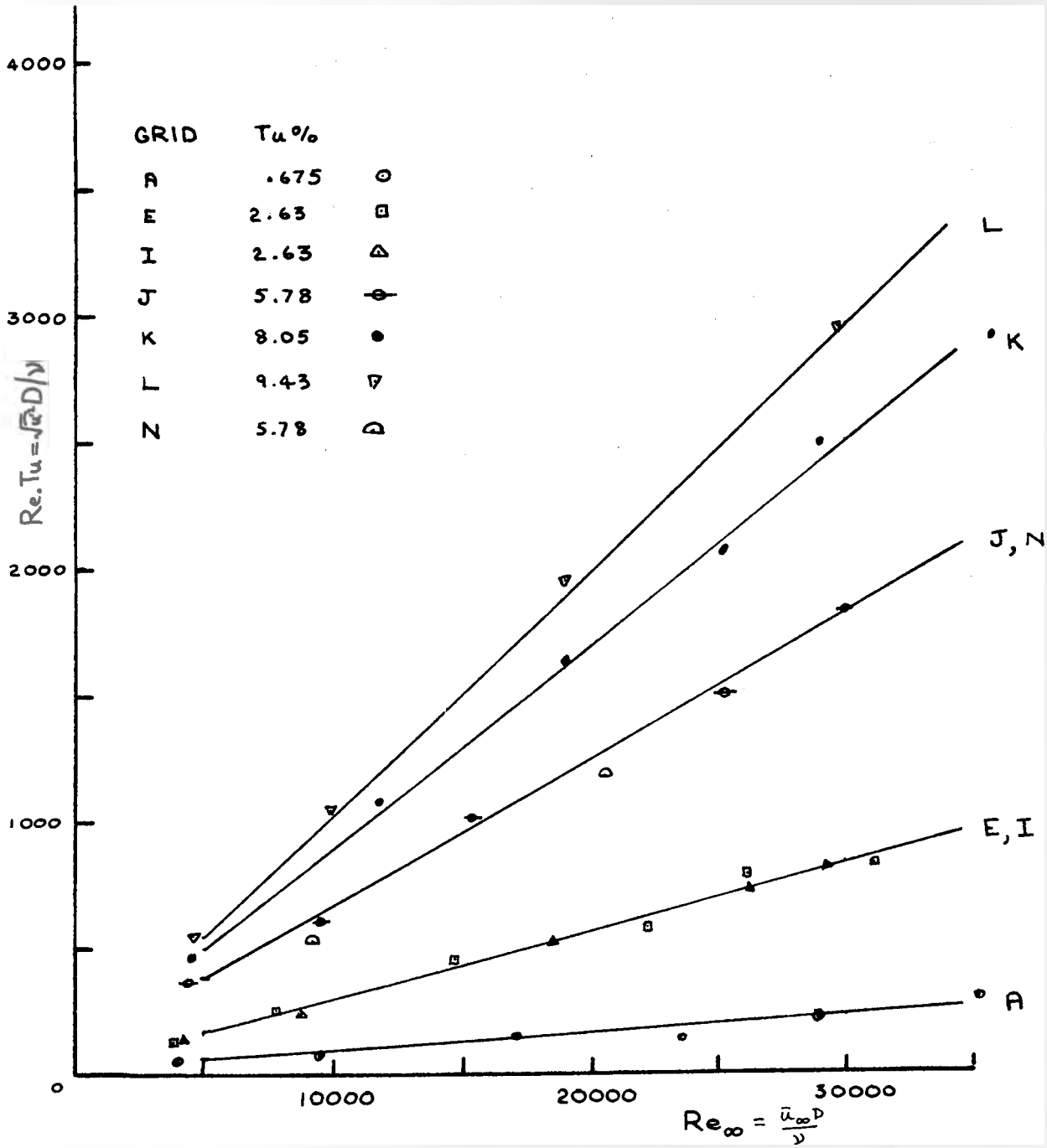
A HOT WIRE CALIBRATION CURVE FOR THE MEASUREMENT OF FREE STREAM TURBULENCE

FIG 3.4



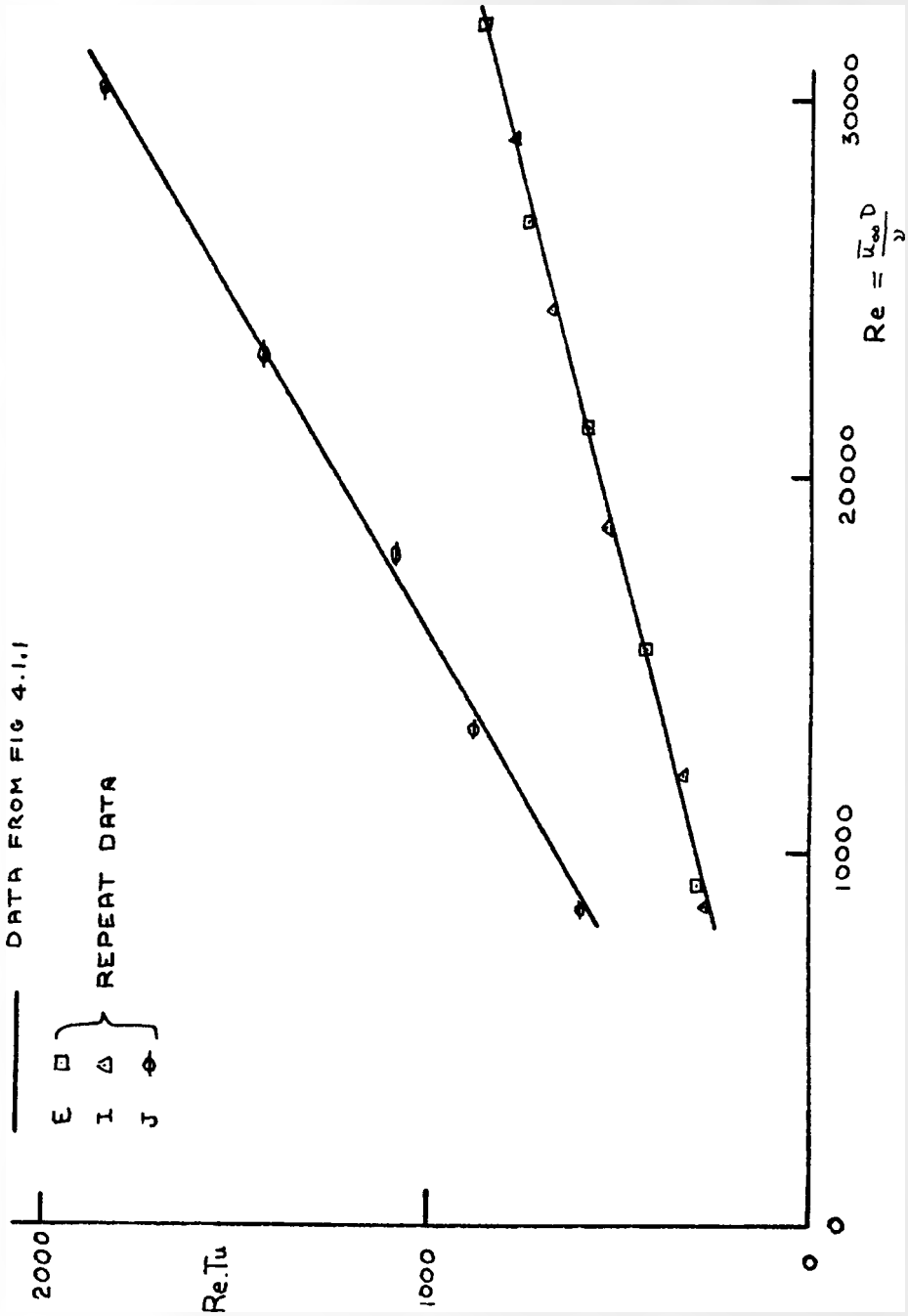
A HOT WIRE CALIBRATION CURVE FOR THE MEASUREMENT OF LOW VELOCITY'S

FIG 3.5



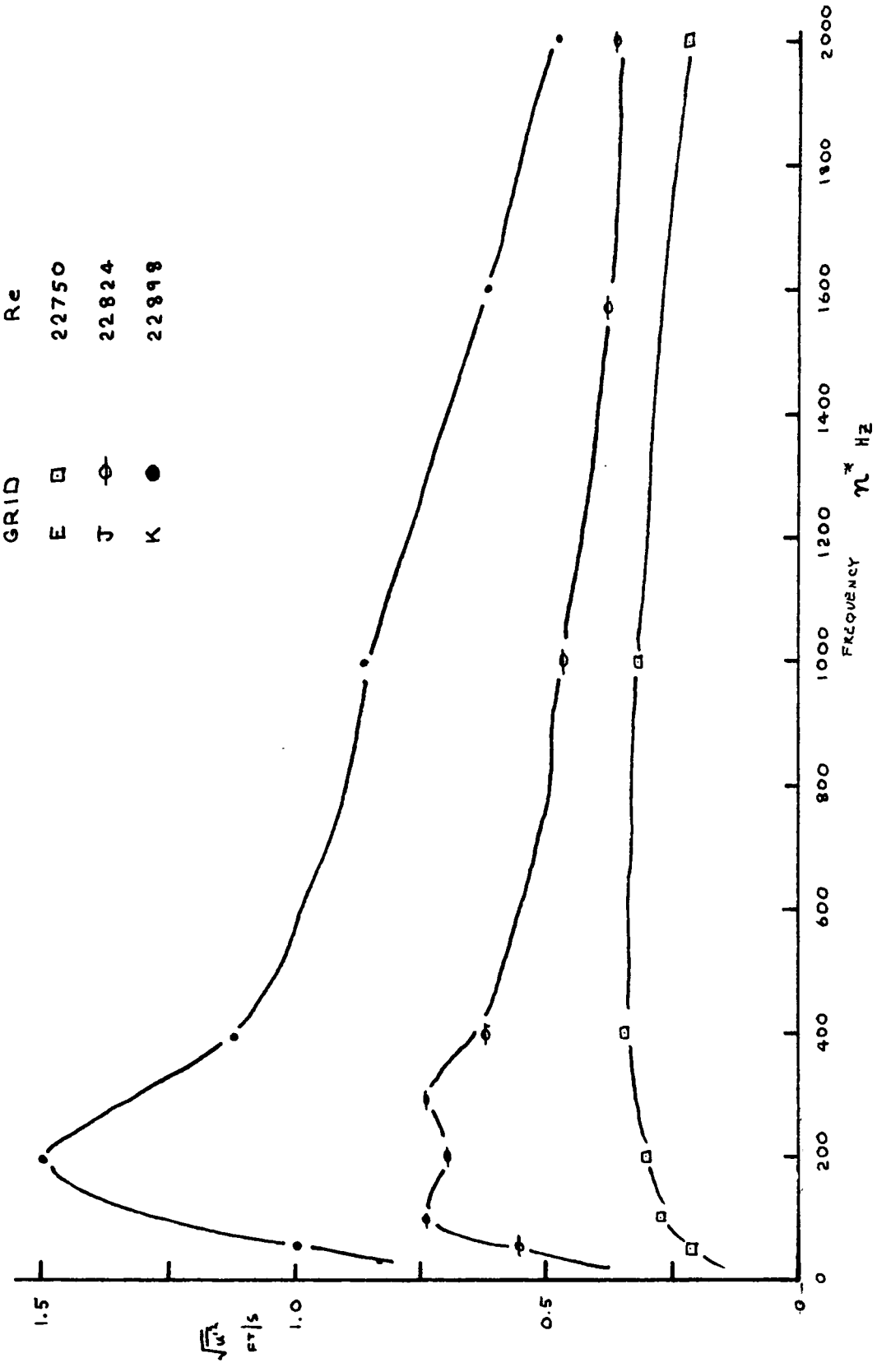
VARIATION OF FREE STREAM TURBULENCE WITH GRID SIZE

FIG 4.1.1



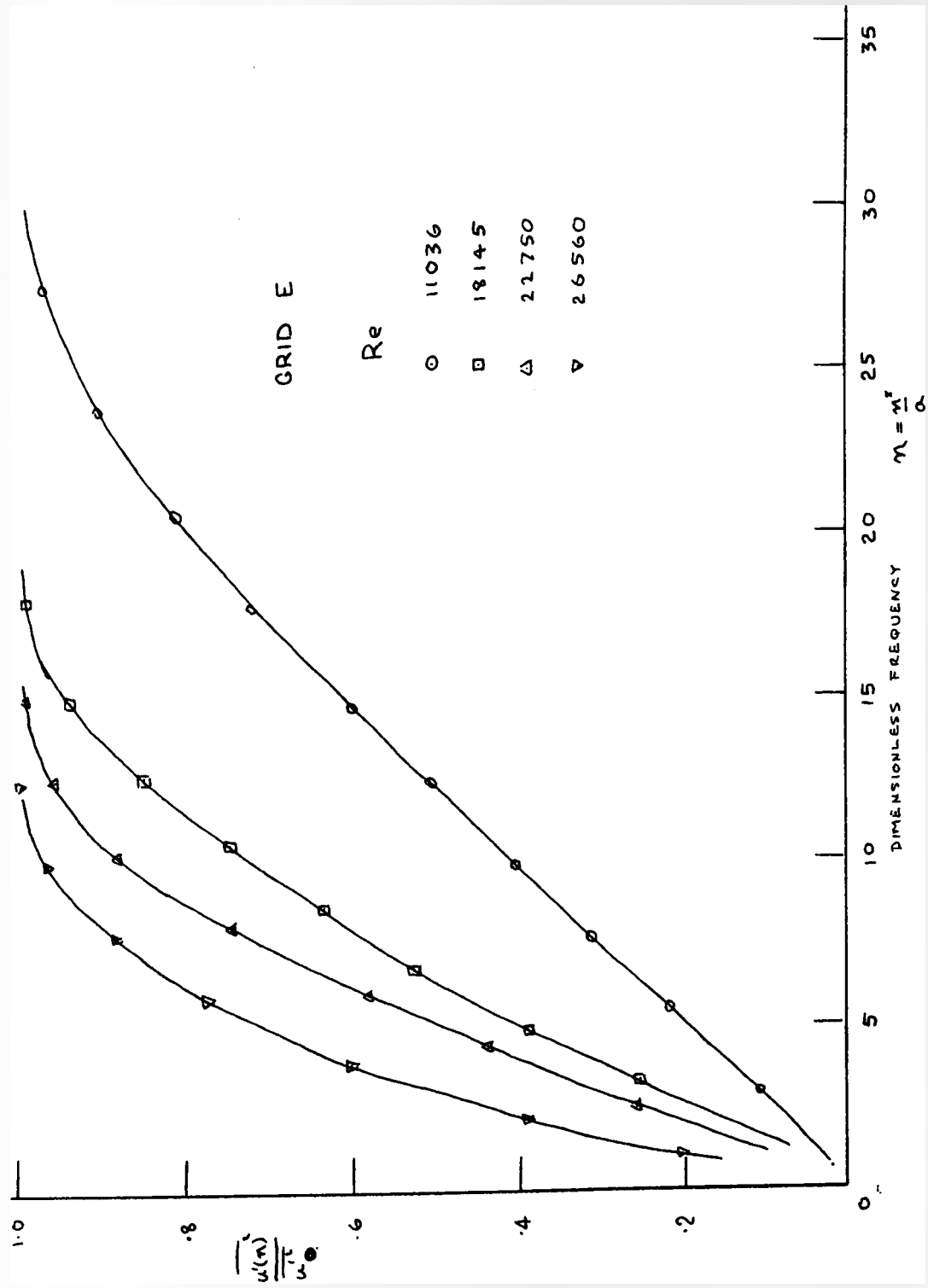
REPEATABILITY OF FREE STREAM TURBULENCE DATA

FIG 4.1.2



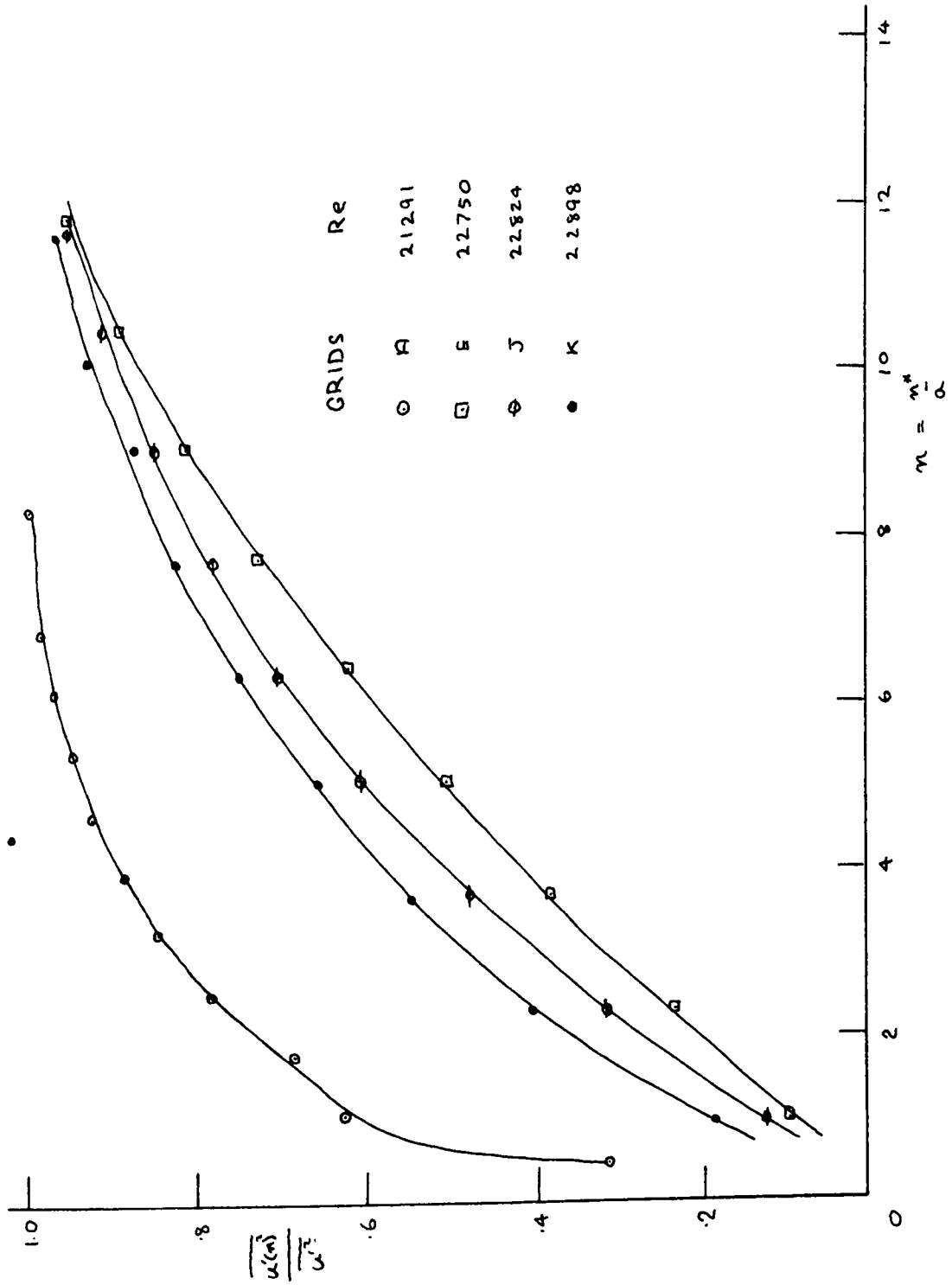
EFFECT OF GRID SIZE ON FREE STREAM TURBULENCE SPECTRA

FIG 4.1.3



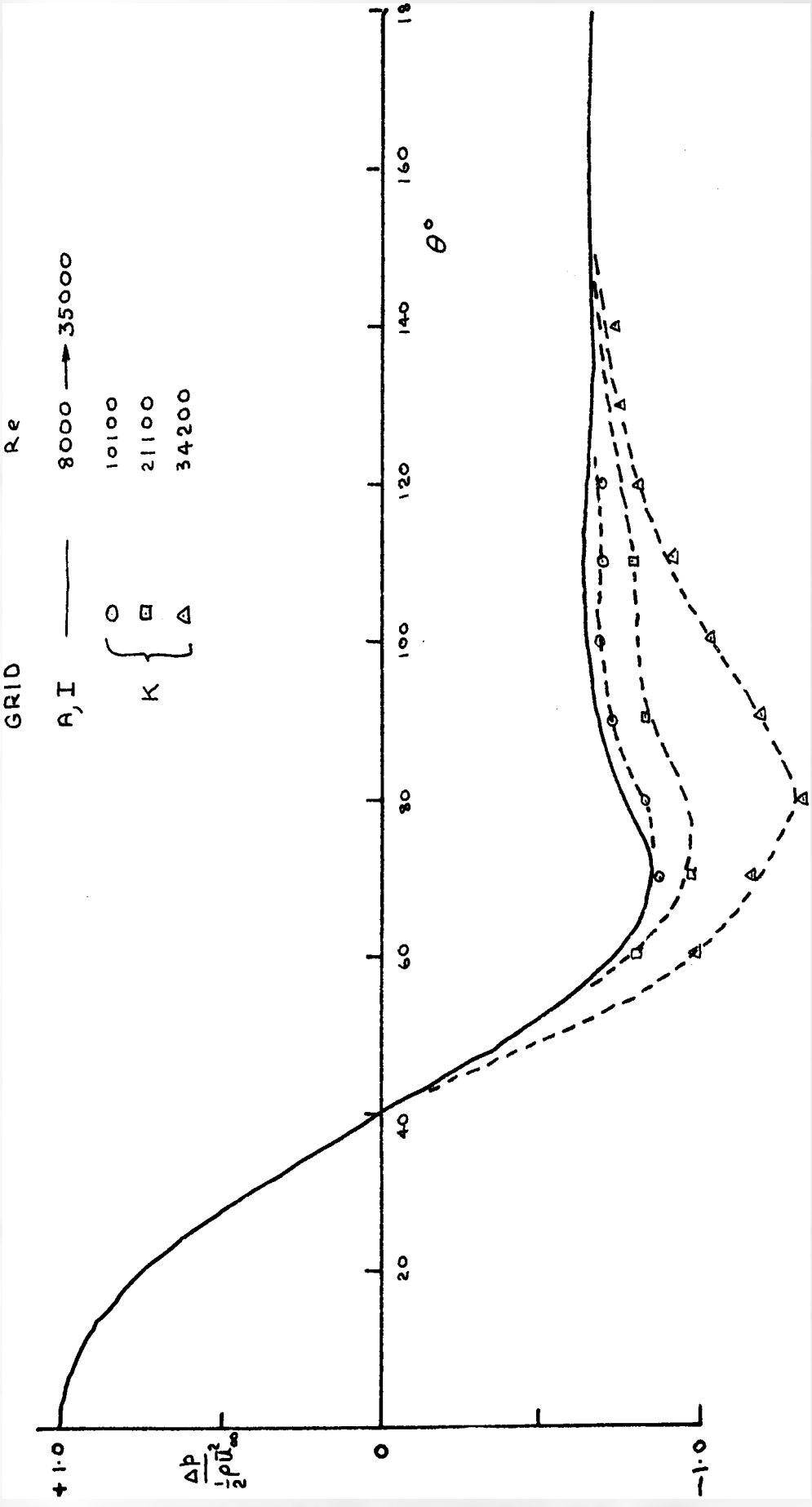
EFFECT OF REYNOLDS NUMBER ON FREESTREAM TURBULENCE SPECTRUM

FIG 4.1.4



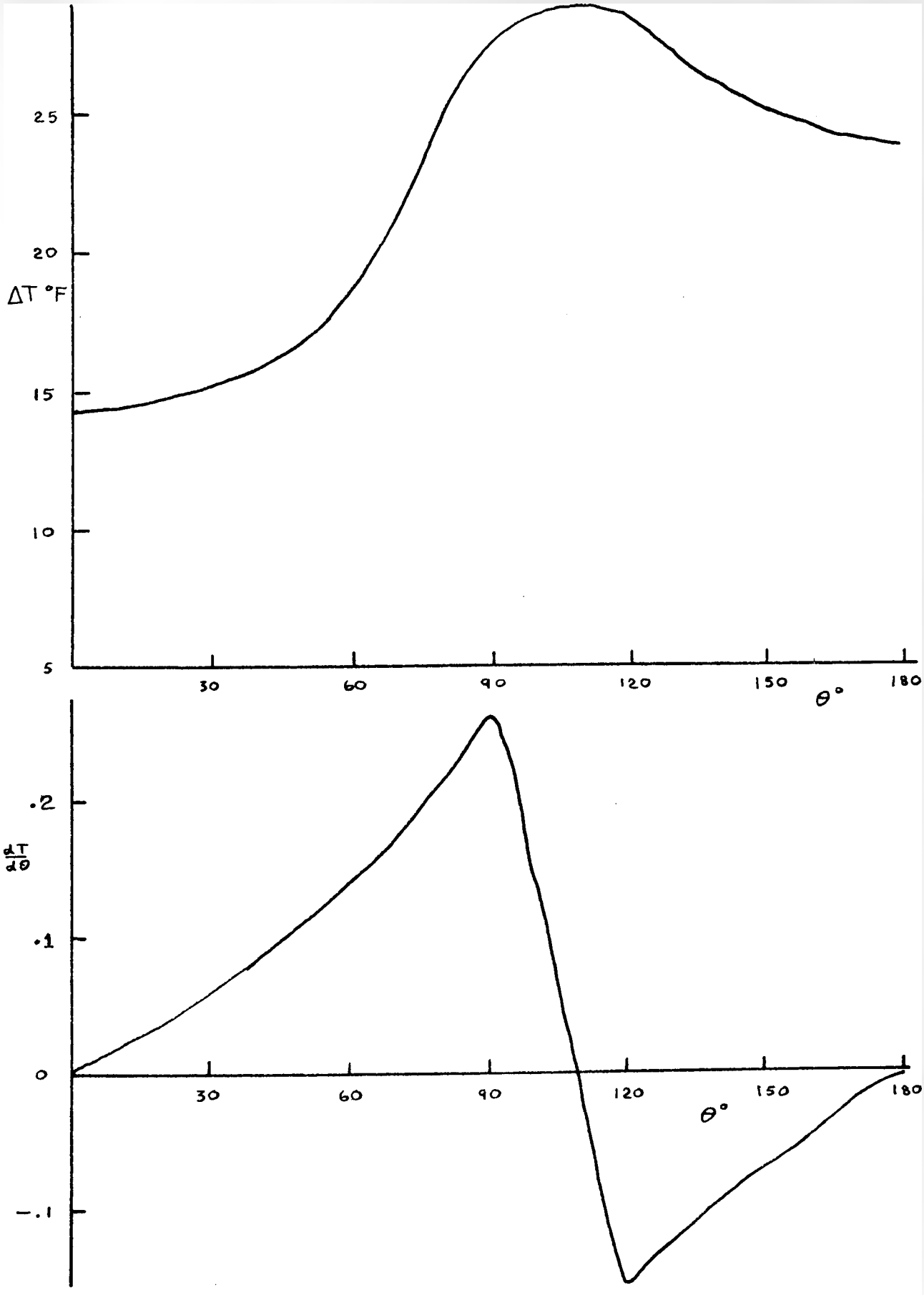
EFFECT OF GRID SIZE ON FREESTREAM TURBULENCE SPECTRUM

FIG 4.1.5



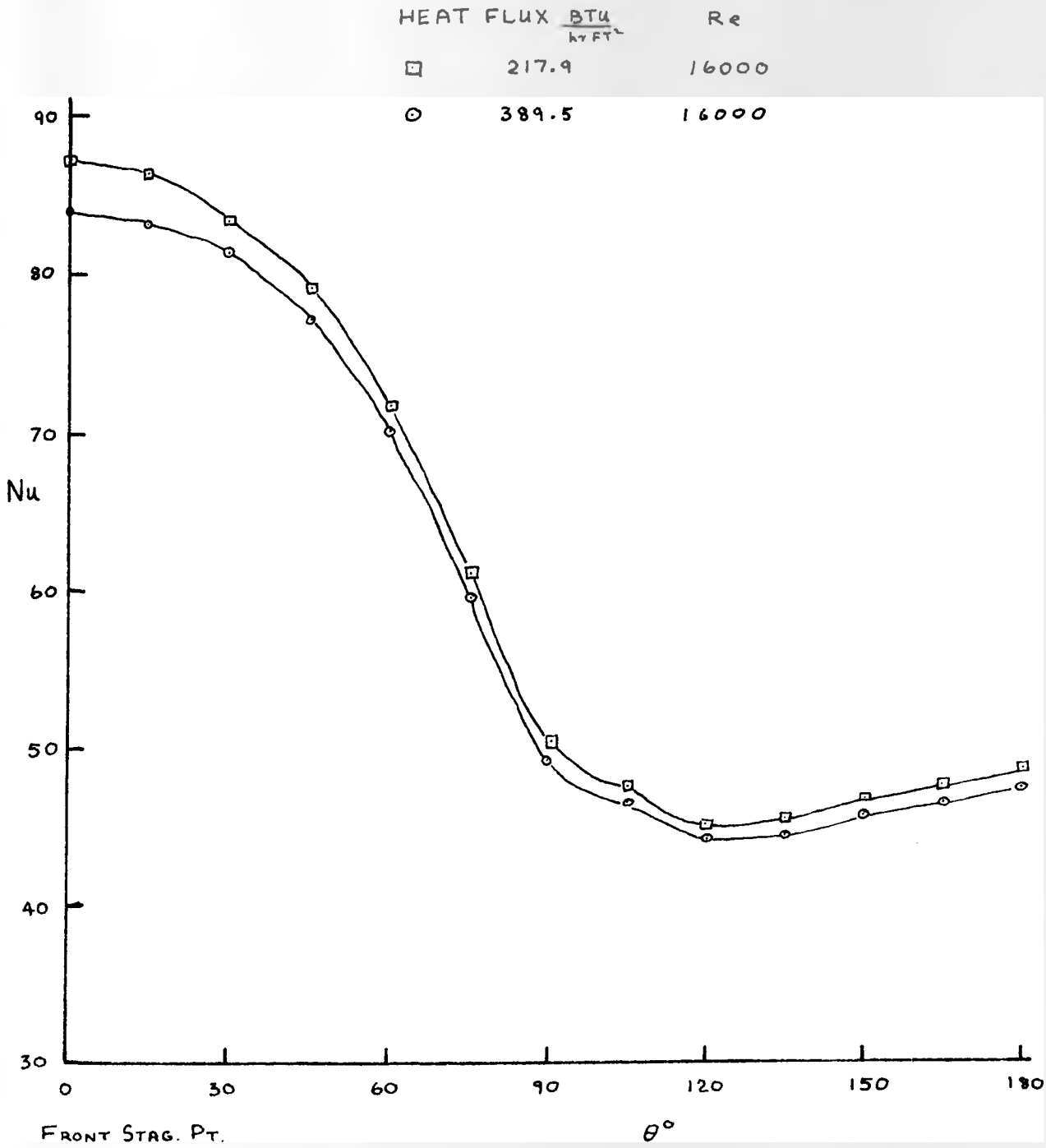
VARIATION OF STATIC PRESSURE AROUND CYLINDER

FIG 4.2.1



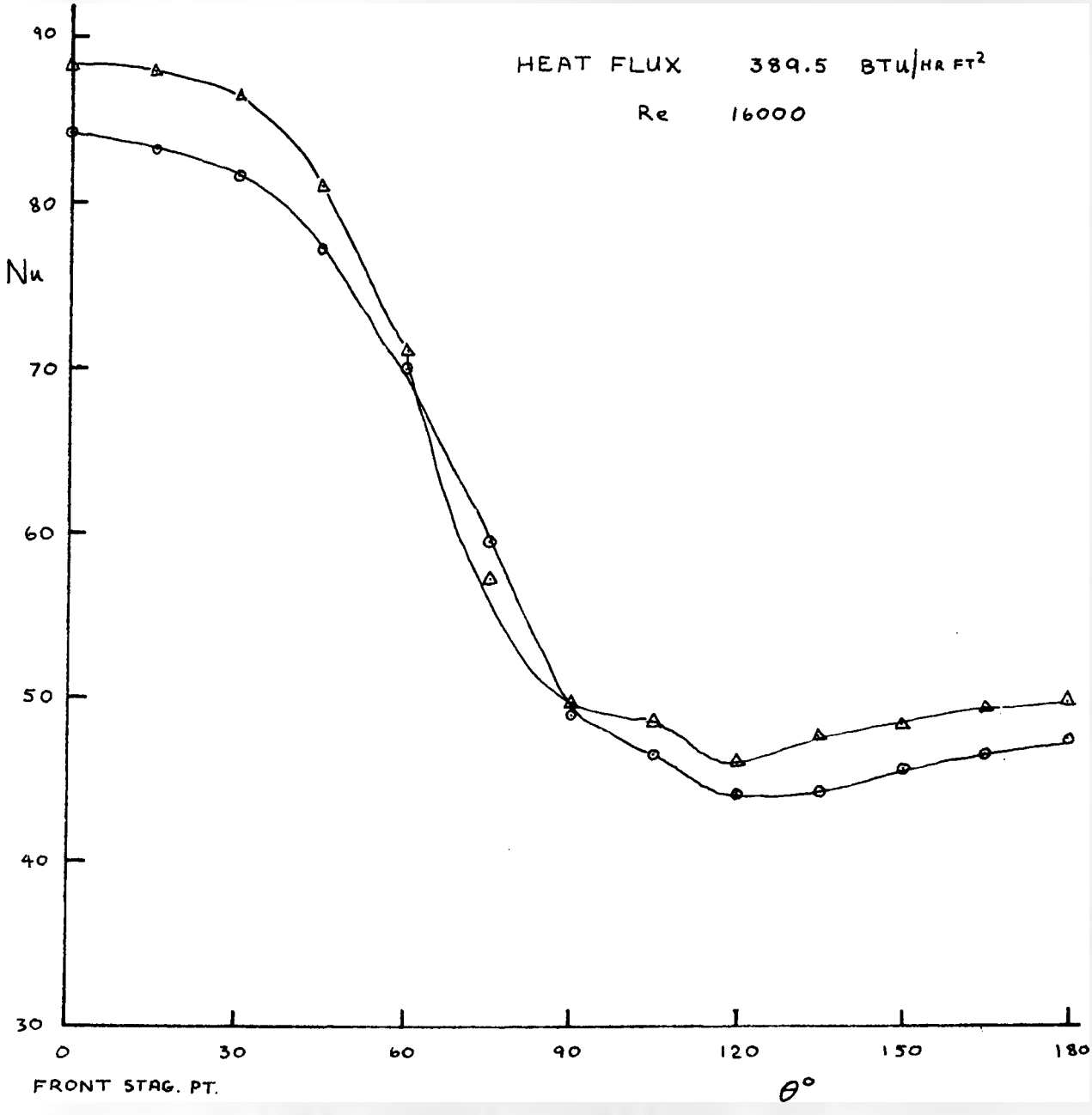
TYPICAL DISTRIBUTIONS OF TEMPERATURE AND TEMPERATURE GRADIENT AROUND CYLINDER

FIG 4.3.1



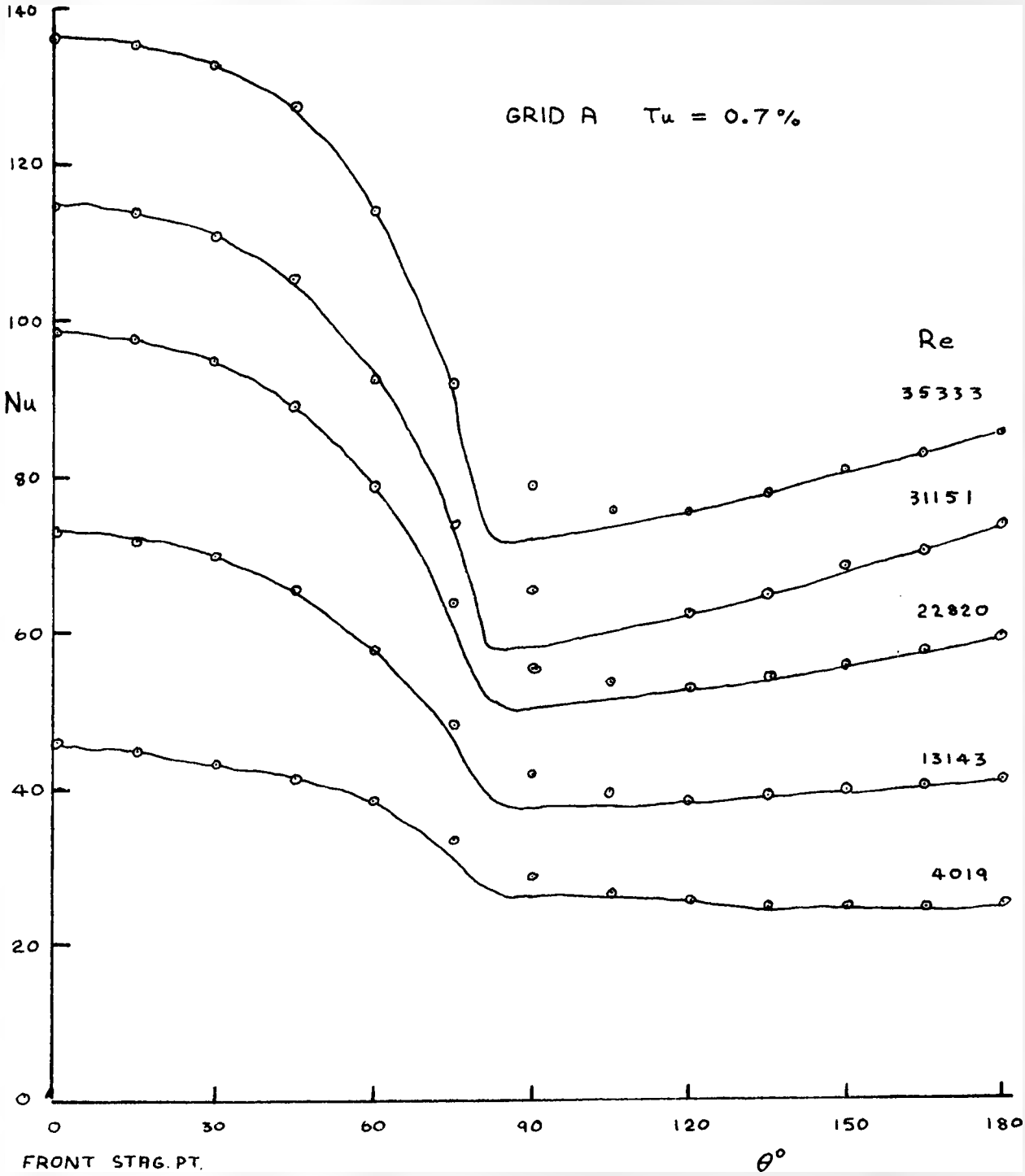
EFFECT OF HEAT FLUX ON LOCAL HEAT TRANSFER

FIG 4.3.2



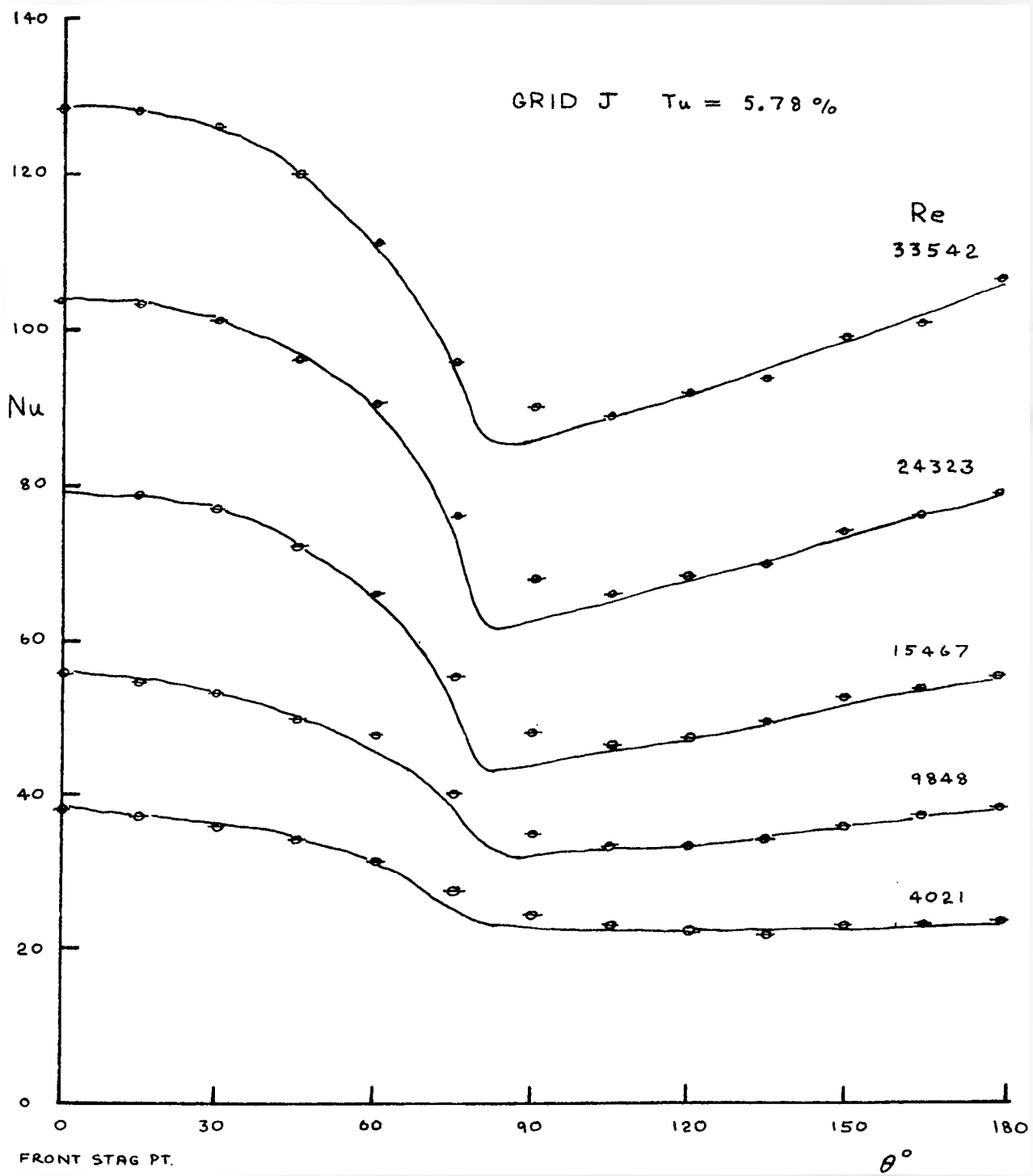
EFFECT OF CYLINDER MANUFACTURING TOLERANCES ON LOCAL HEAT TRANSFER

FIG 4.3.3



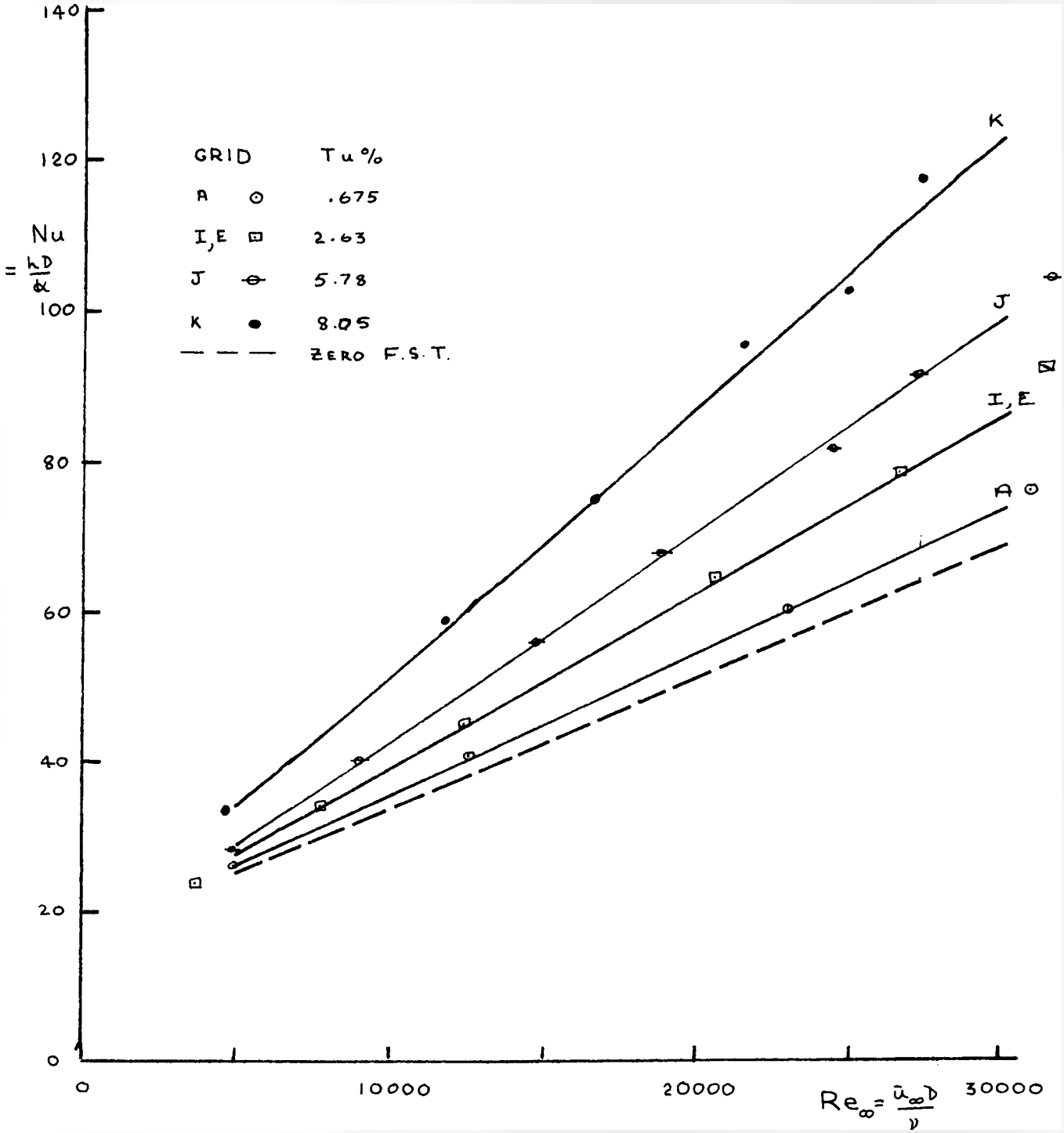
EFFECT OF FREE STREAM TURBULENCE ON LOCAL HEAT TRANSFER

FIG 4.3.4



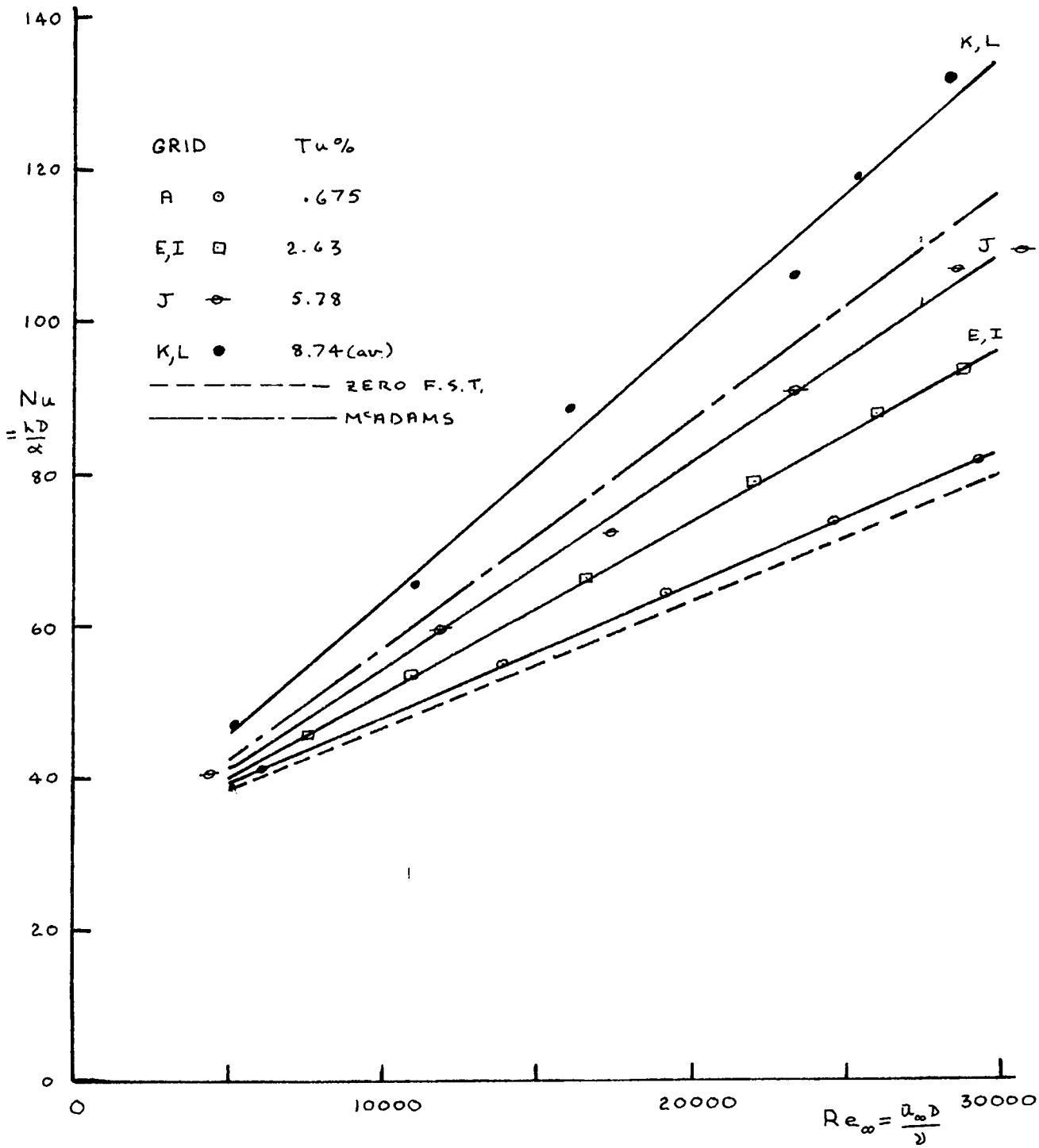
EFFECT OF FREE STREAM TURBULENCE ON LOCAL HEAT TRANSFER

FIG 4.3.5



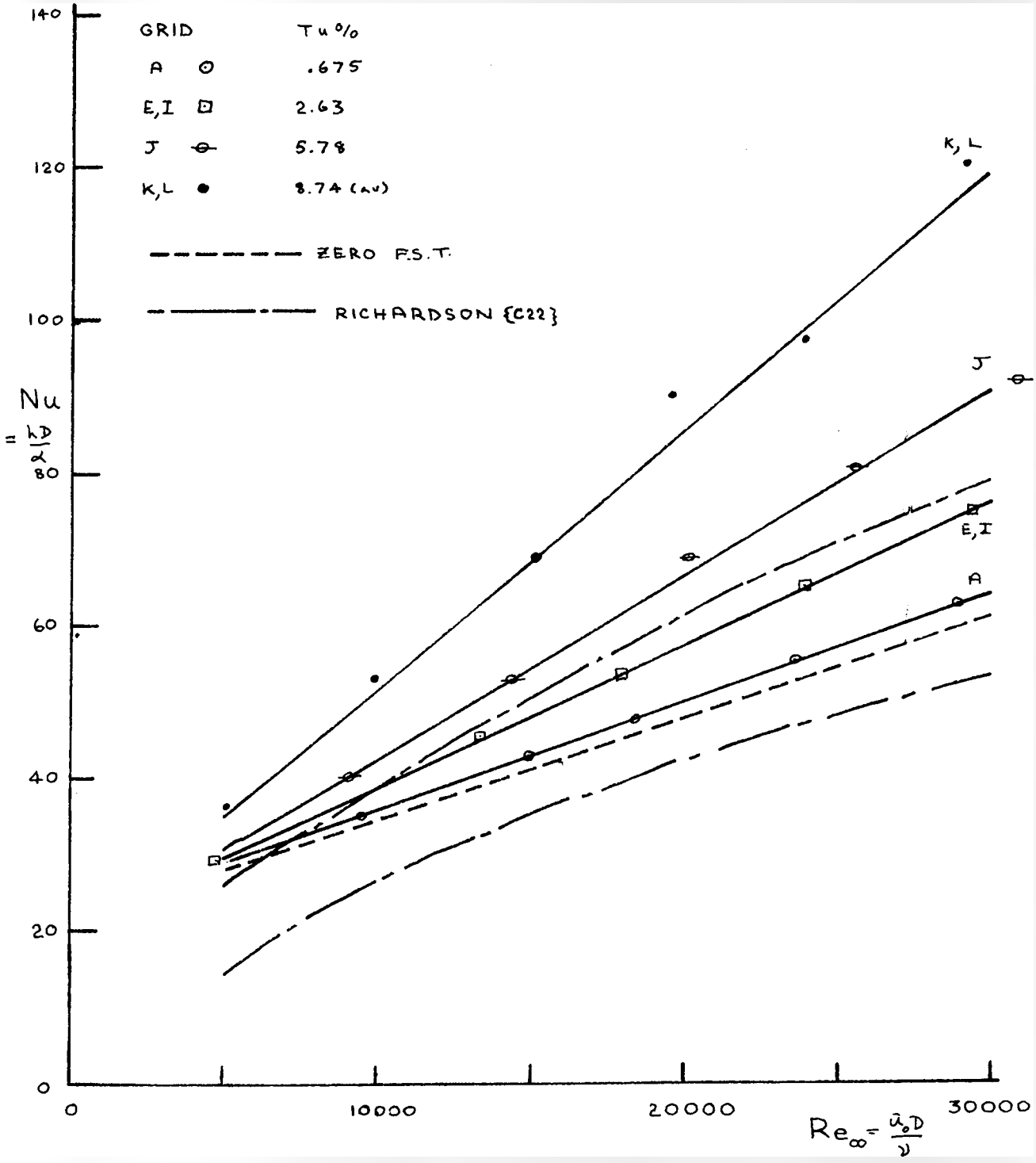
VARIATION OF HEAT TRANSFER AT REAR STAGNATION POINT WITH FREE STREAM TURBULENCE

FIG 4.3.6



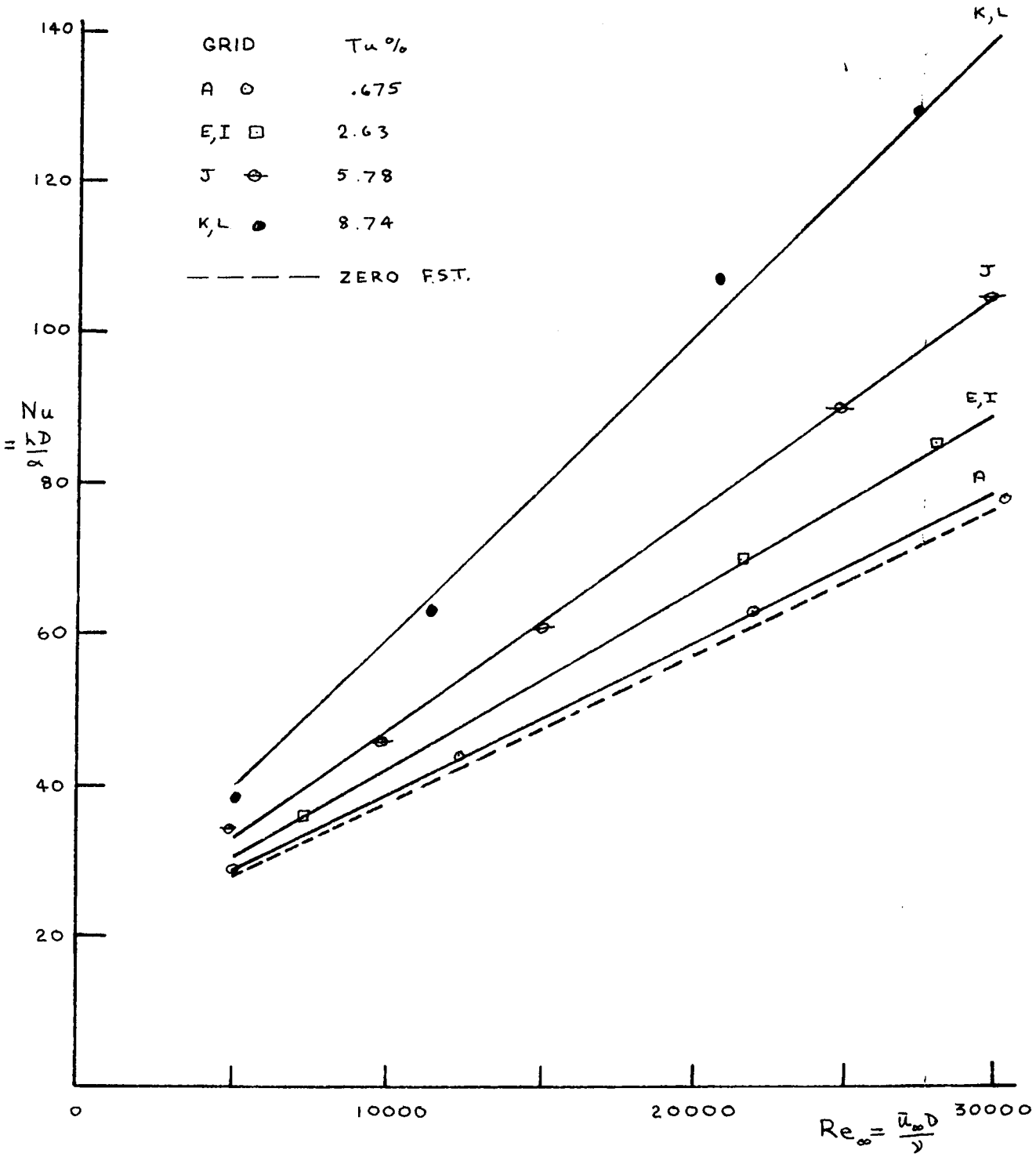
VARIATION OF OVERALL HEAT TRANSFER WITH FREE STREAM TURBULENCE

FIG 4.3.7



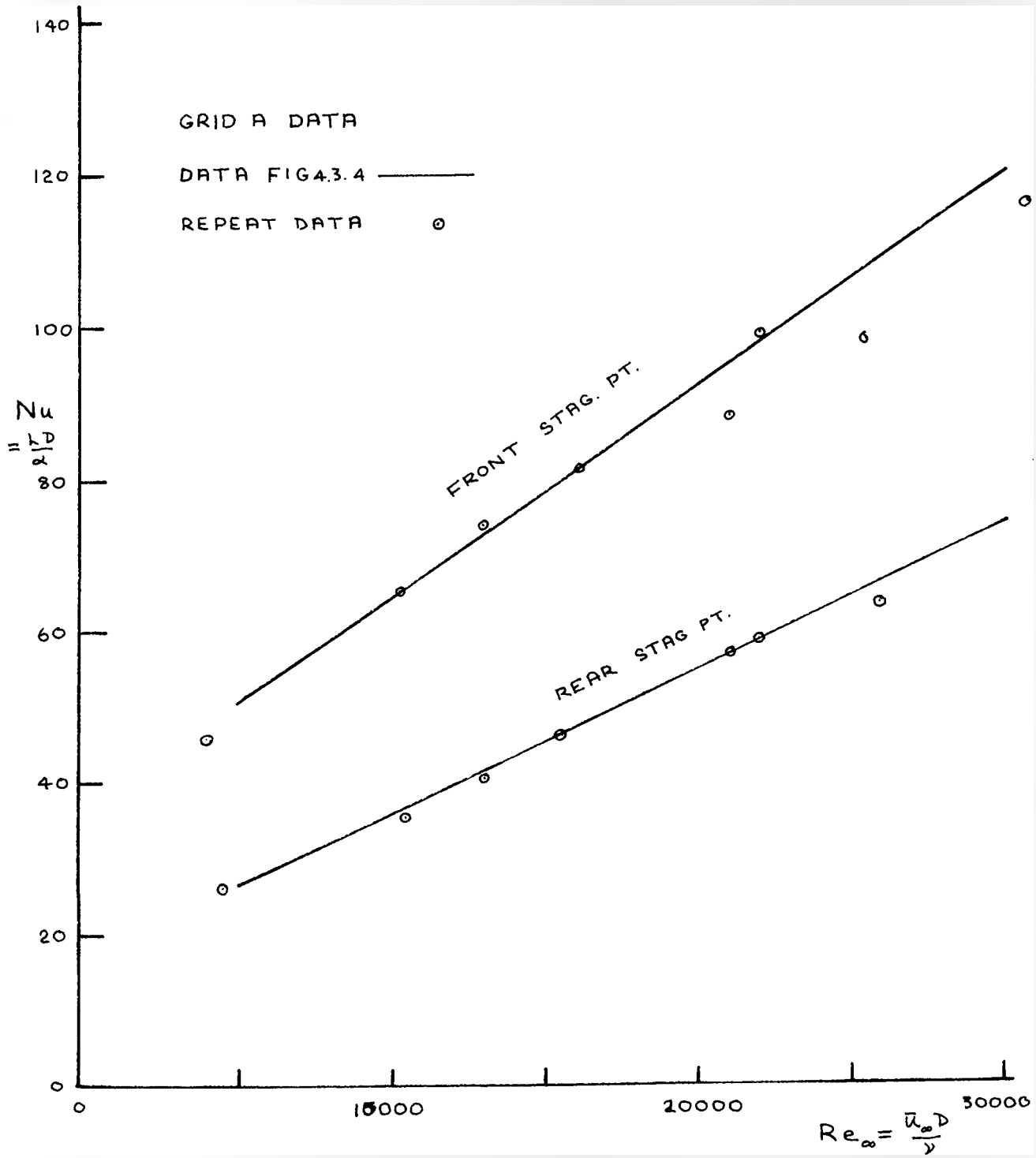
VARIATION OF OVERALL HEAT TRANSFER IN THE SEPARATION (WAKE) REGION

FIG 4.3.8



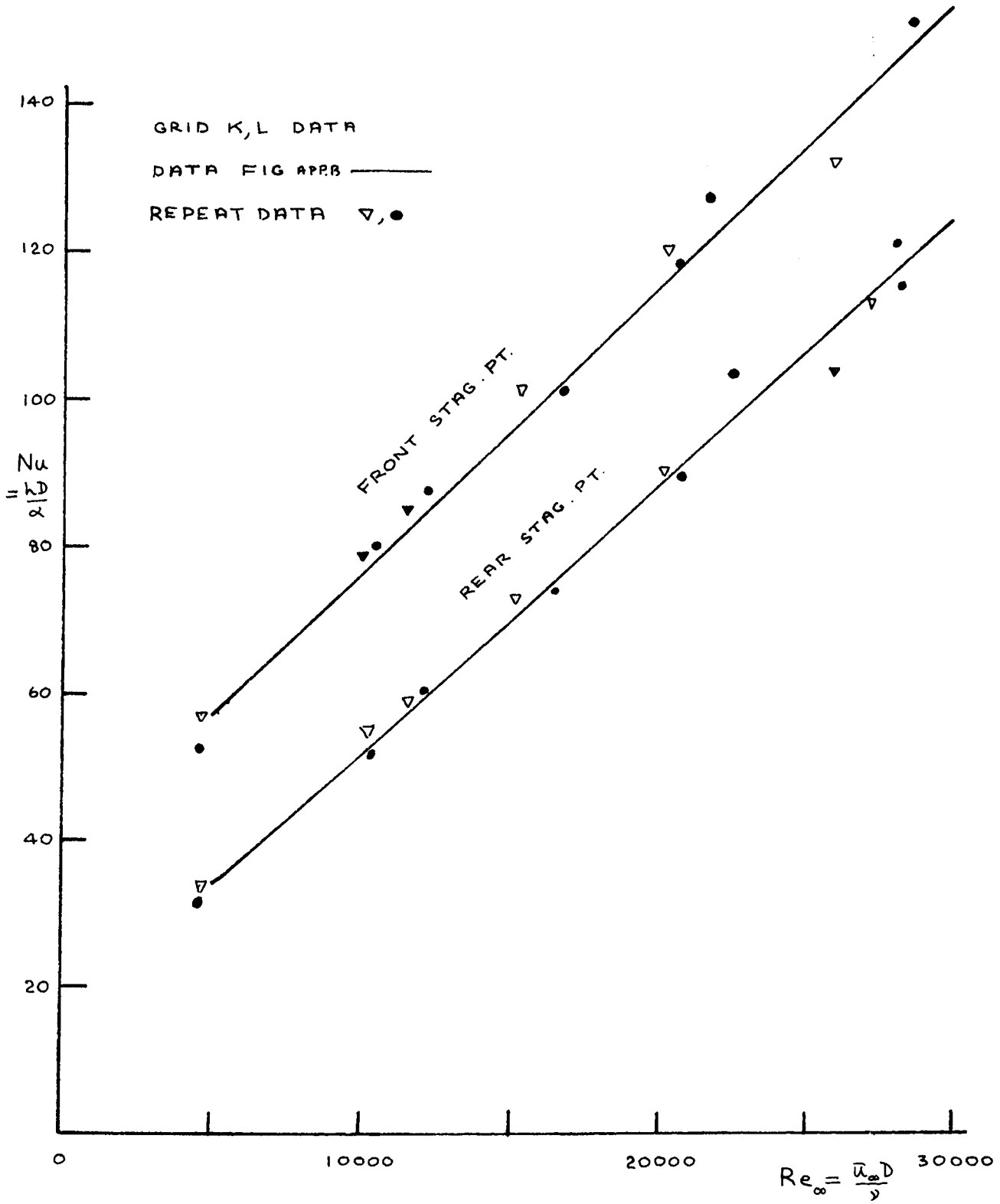
VARIATION OF OVERALL HEAT TRANSFER AT THE FRONT (BOUNDARY LAYER) REGION

FIG4.3.9



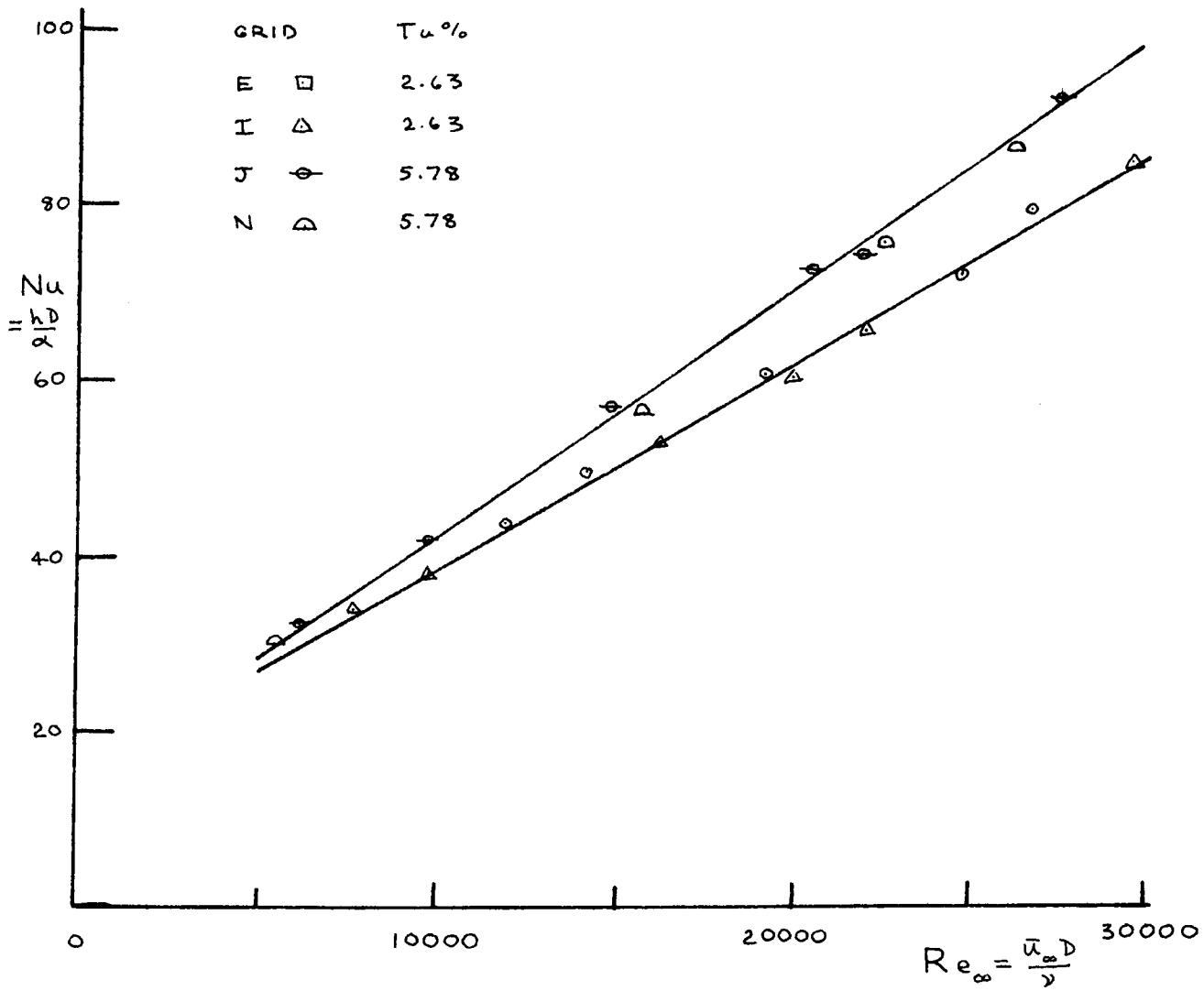
REPEATABILITY OF EXPERIMENTAL DATA

FIG 4.3.10a



REPEATABILITY OF EXPERIMENTAL DATA

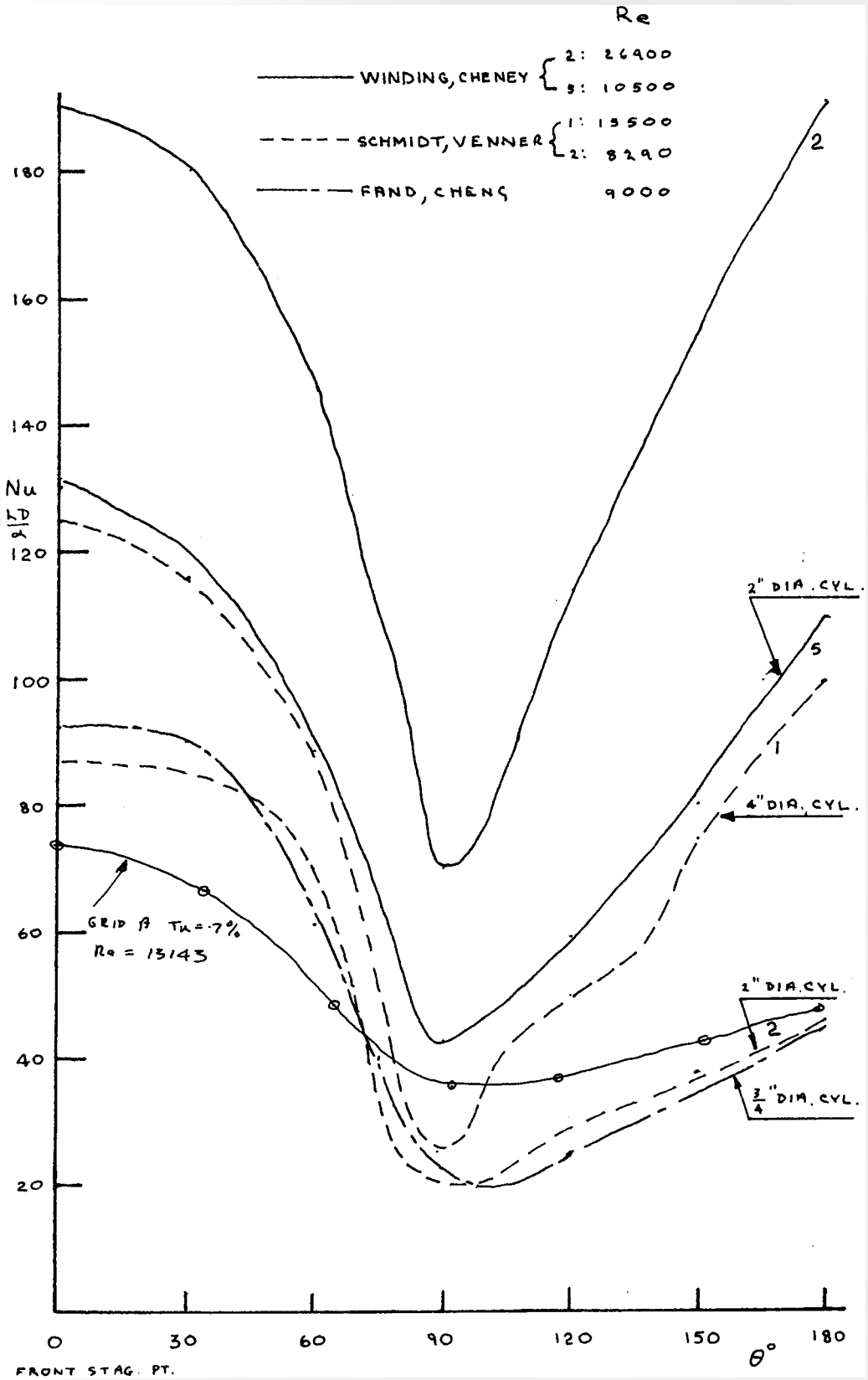
FIG4.3.10b



HEAT TRANSFER AT REAR STAGNATION POINT:

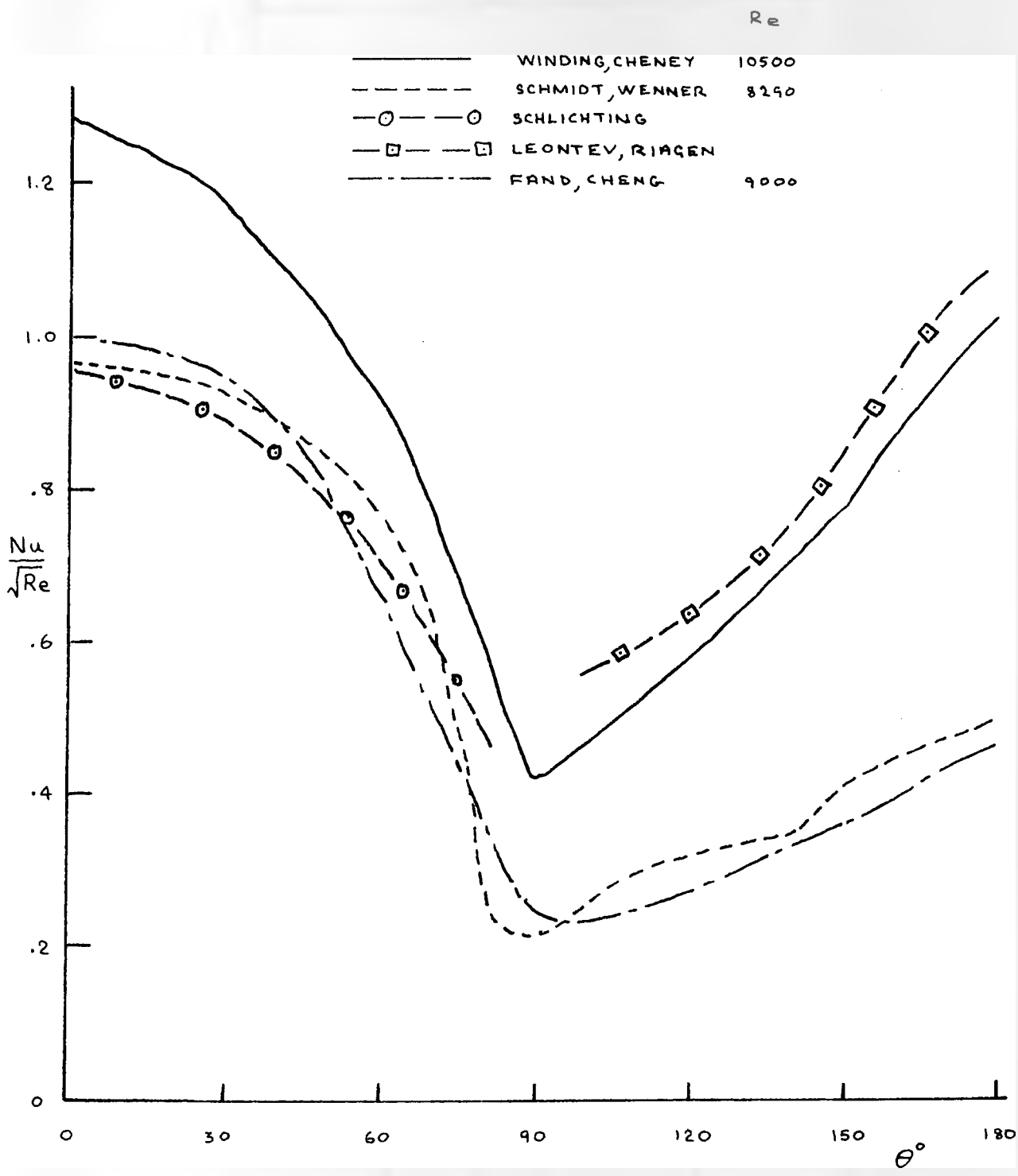
A COMPARISON BETWEEN HORIZONTAL AND HORIZONTAL + VERTICAL ROD GRIDS

FIG 4.3.11



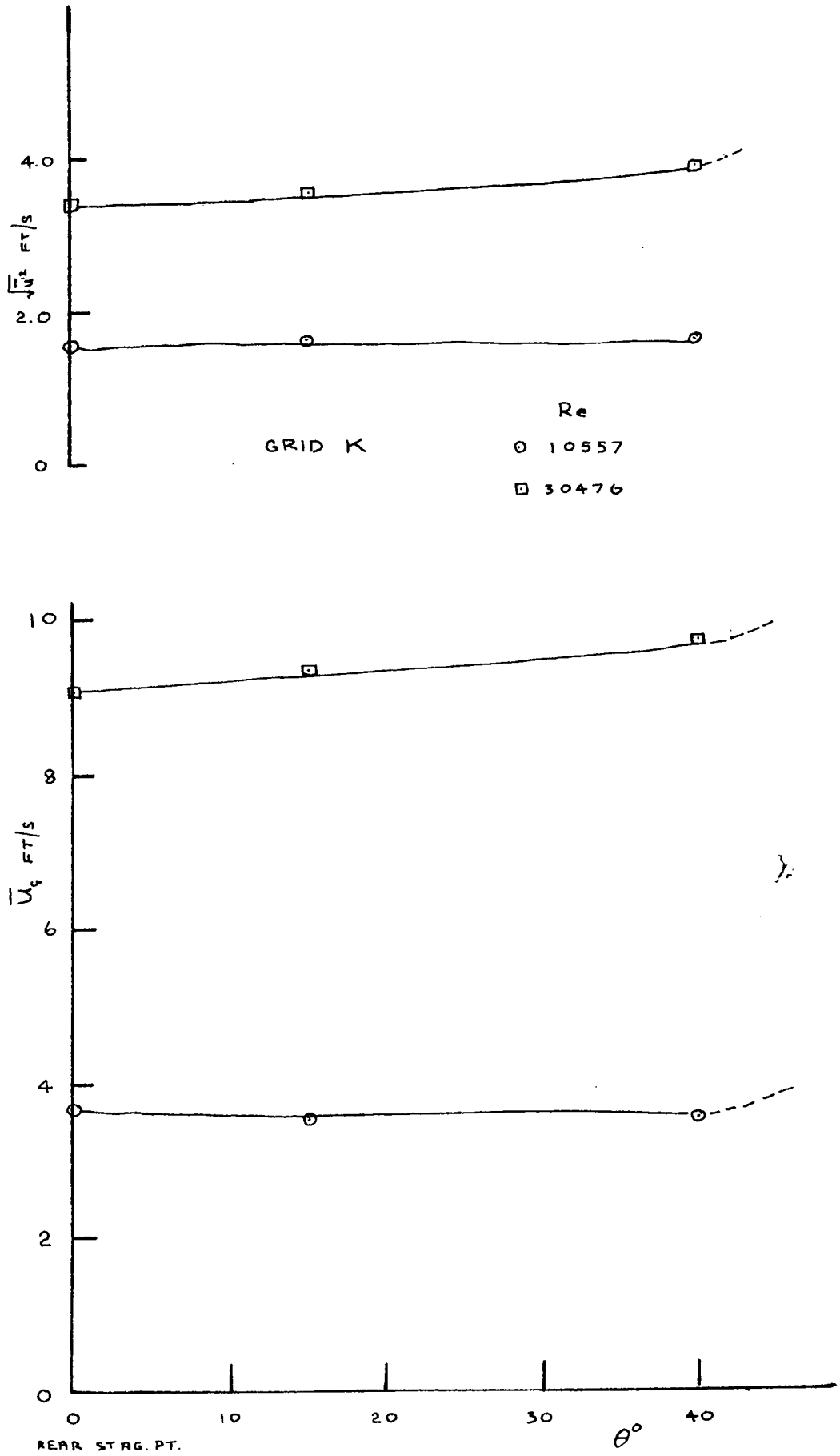
DISTRIBUTION OF LOCAL HEAT TRANSFER : EXPERIMENTAL DATA OF OTHER WORKERS

FIG 4.3.12



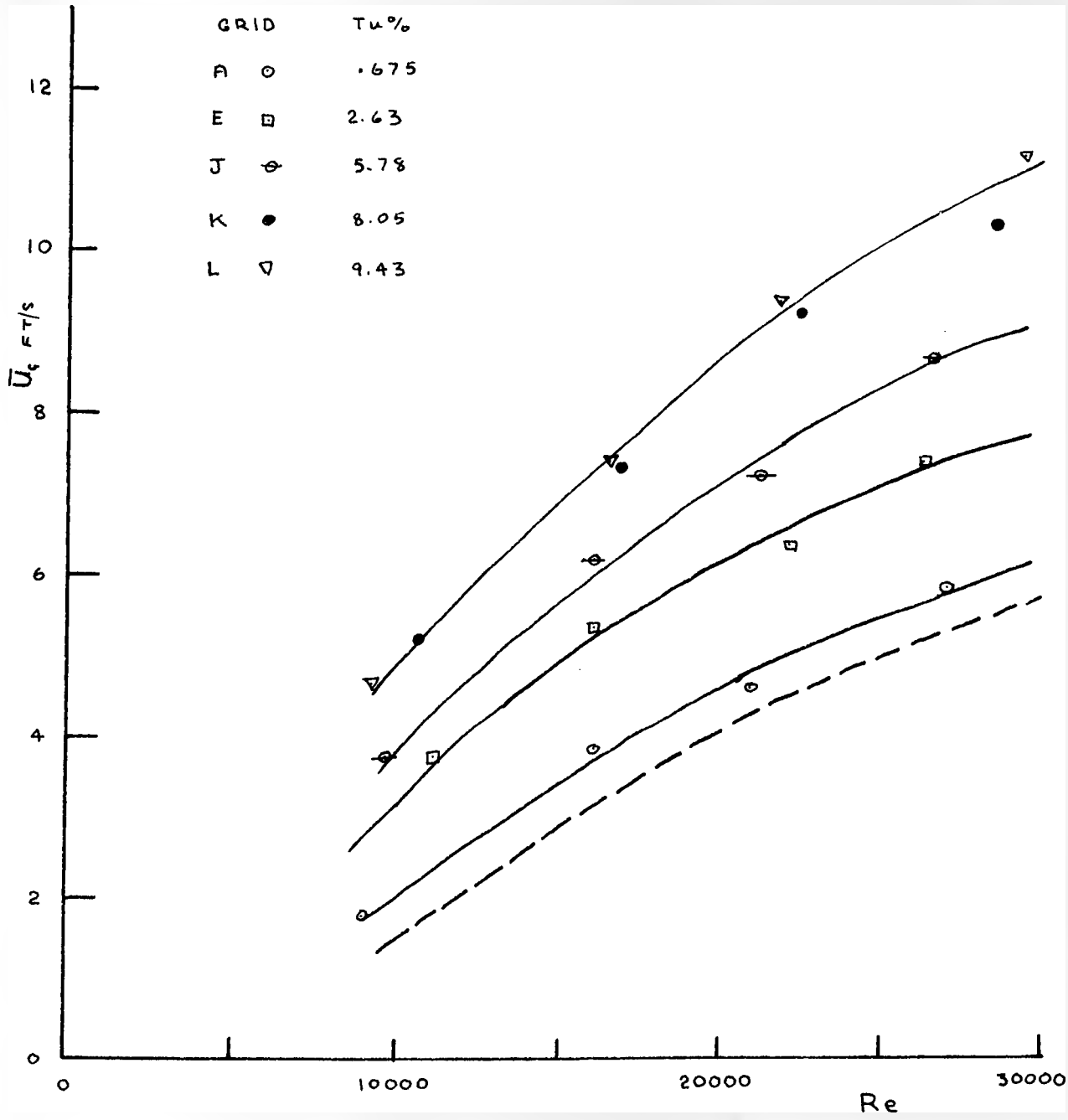
A COMPARISON BETWEEN EXPERIMENTAL DATA AND AVAILABLE THEORIES

FIG4.3.13



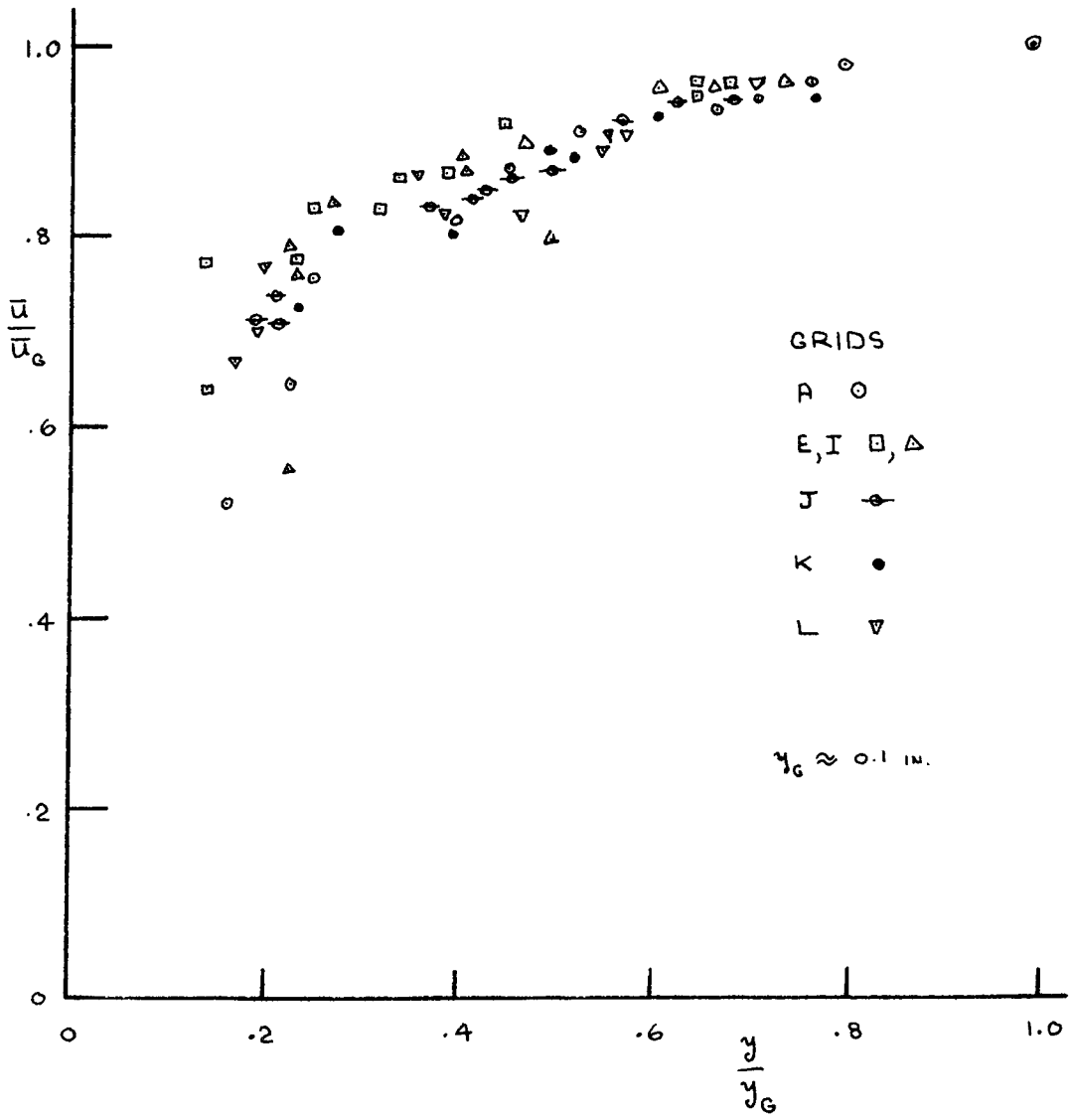
VARIATION OF MEAN AND FLUCTUATING VELOCITY IN THE WAKE REGION OF CYLINDER

FIG 4.4.1



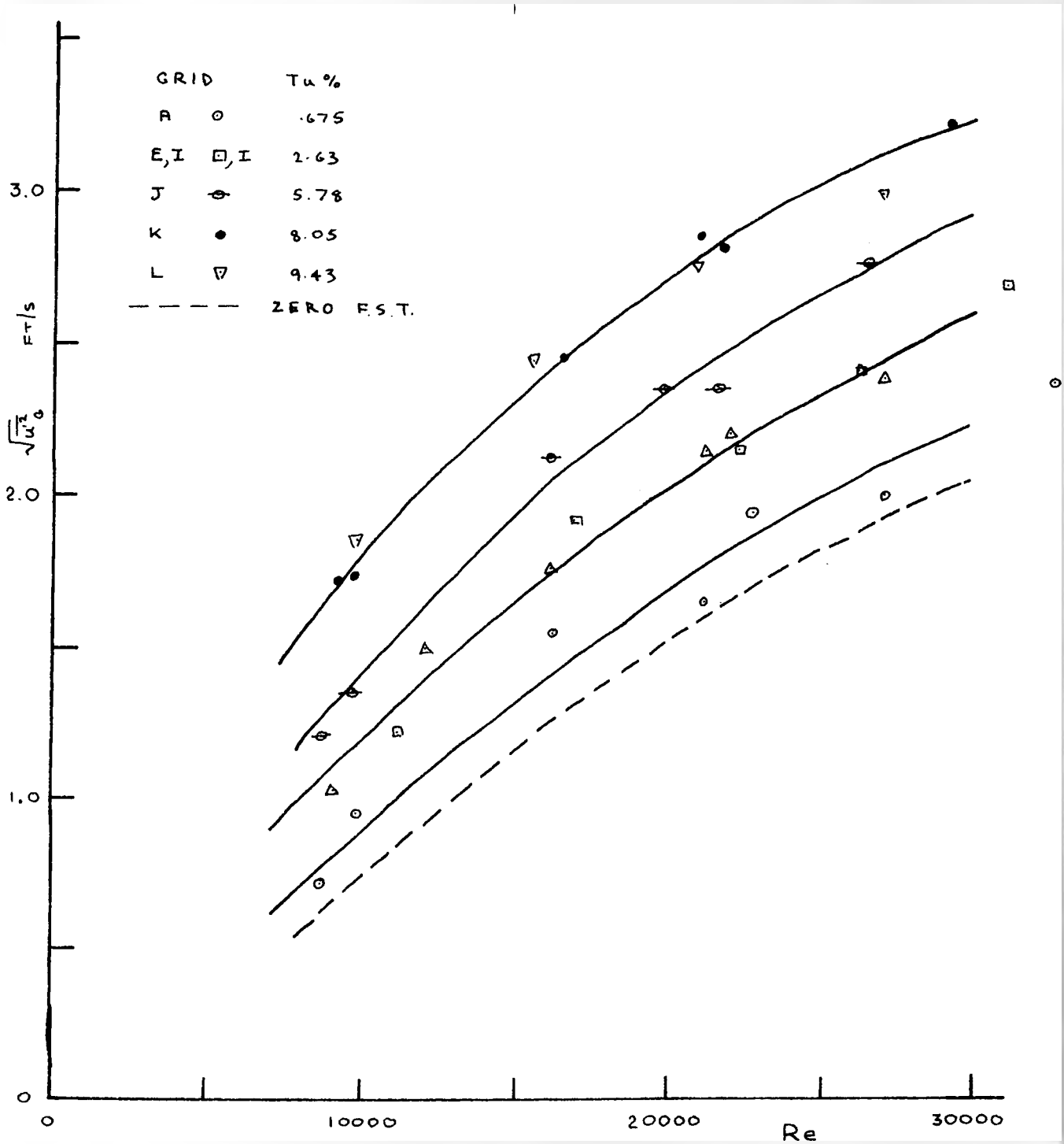
VARIATION OF MEAN VELOCITY($\bar{U}_c$) AT REAR STAGNATION POINT WITH FREE STREAM TURBULENCE

FIG 4.4.2



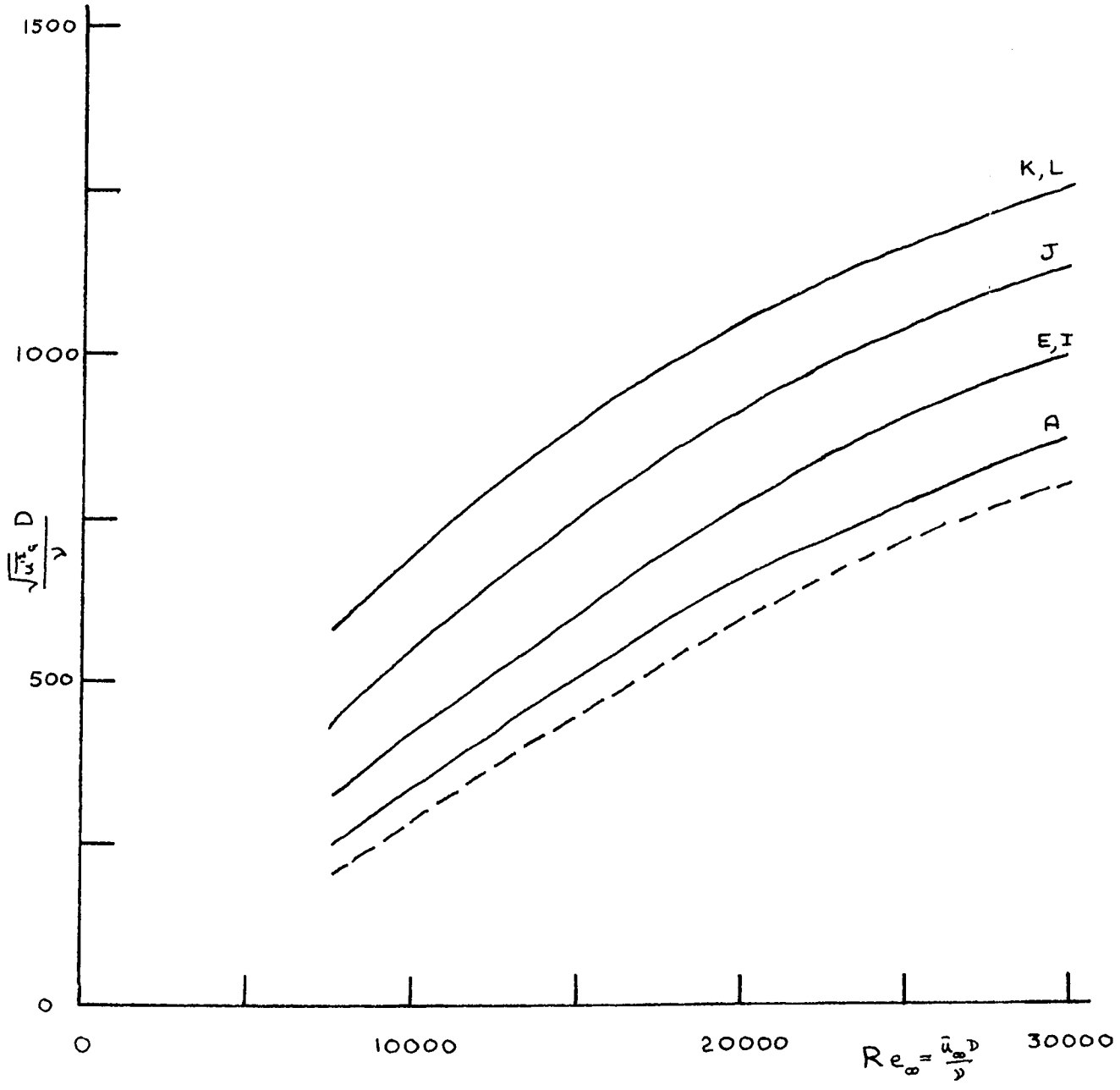
NON-DIMENSIONAL MEAN VELOCITY PROFILES AT REAR STAGNATION POINT

FIG 4.4.3



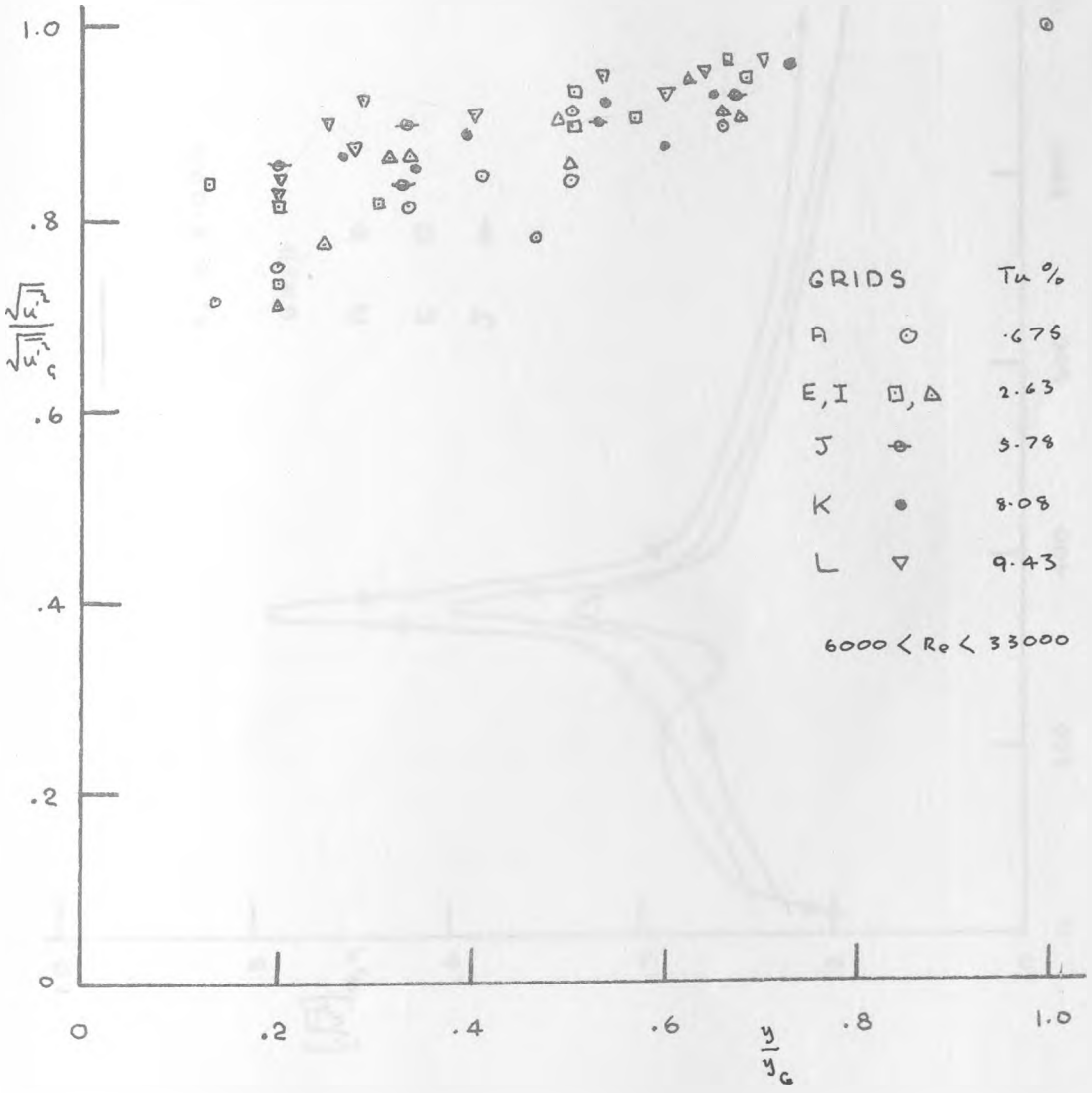
VARIATION OF FLUCTUATING VELOCITY($\sqrt{\overline{u^2}}_c$) AT THE REAR STAGNATION POINT WITH FREE STREAM TURBULENCE

FIG 4.4.4



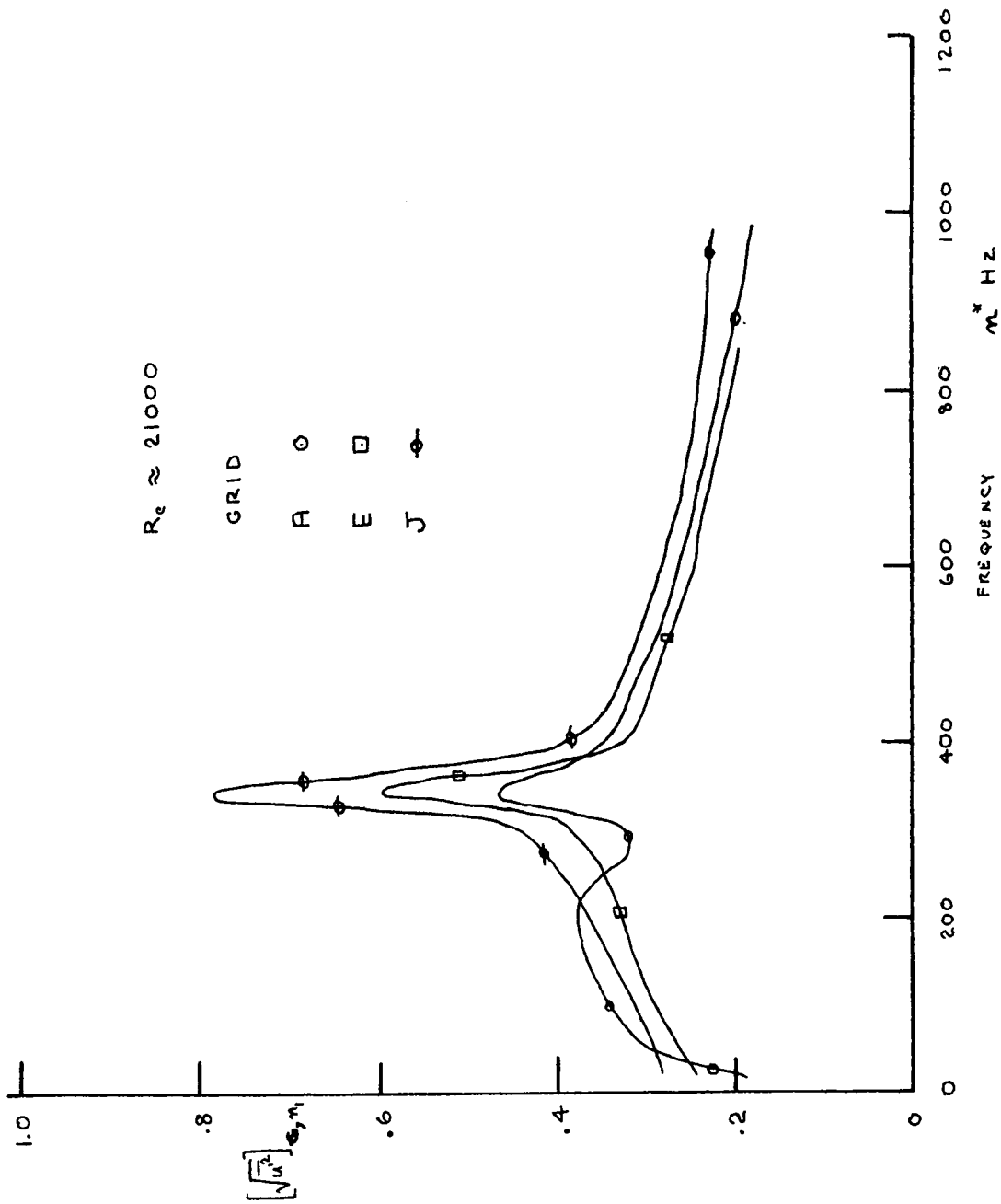
A NON-DIMENSIONAL FORM OF DATA PRESENTED IN FIG 4.4.4

FIG 4.4.5



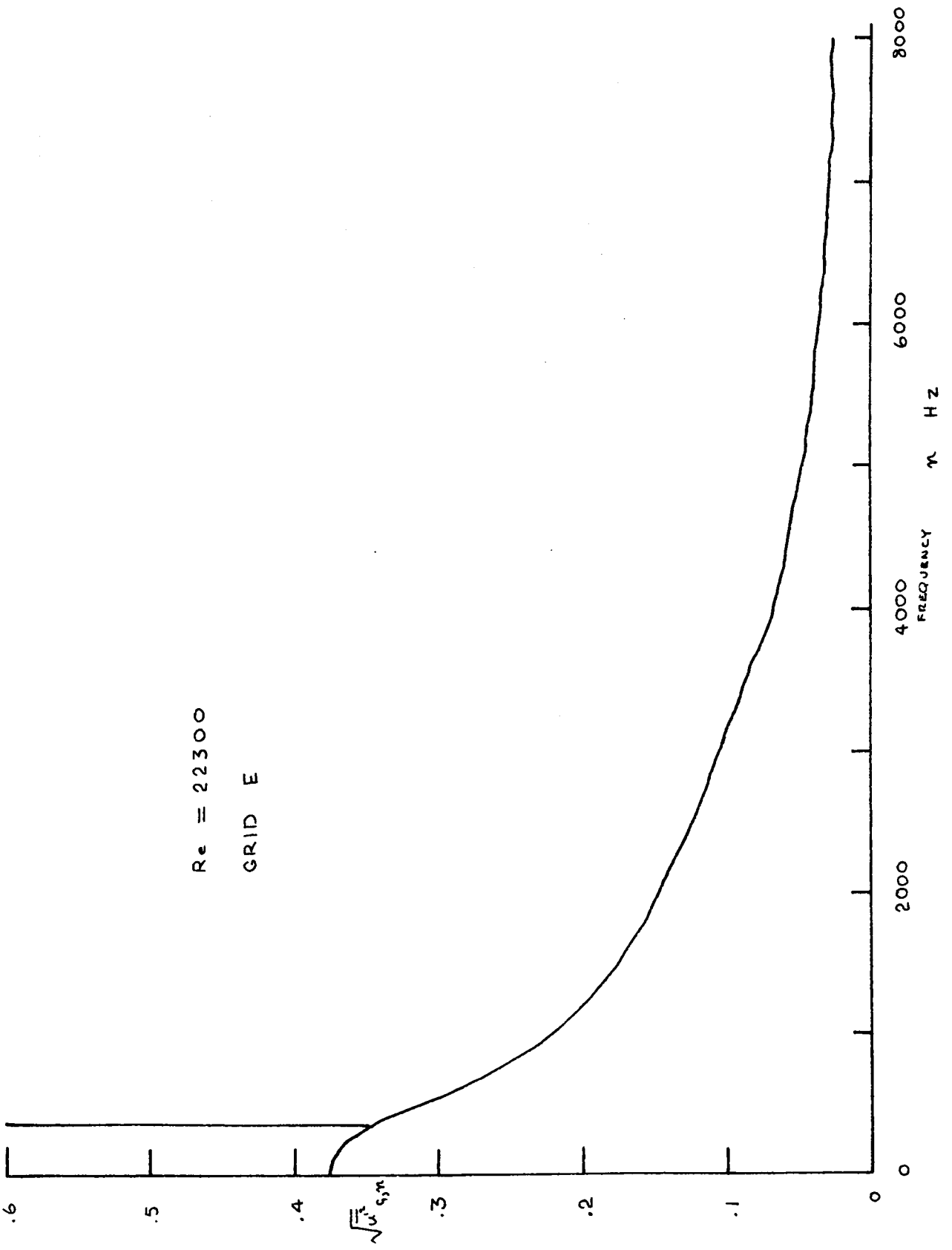
NON-DIMENSIONAL FLUCTUATING VELOCITY PROFILE AT REAR STAGNATION POINT

FIG 4.4.6



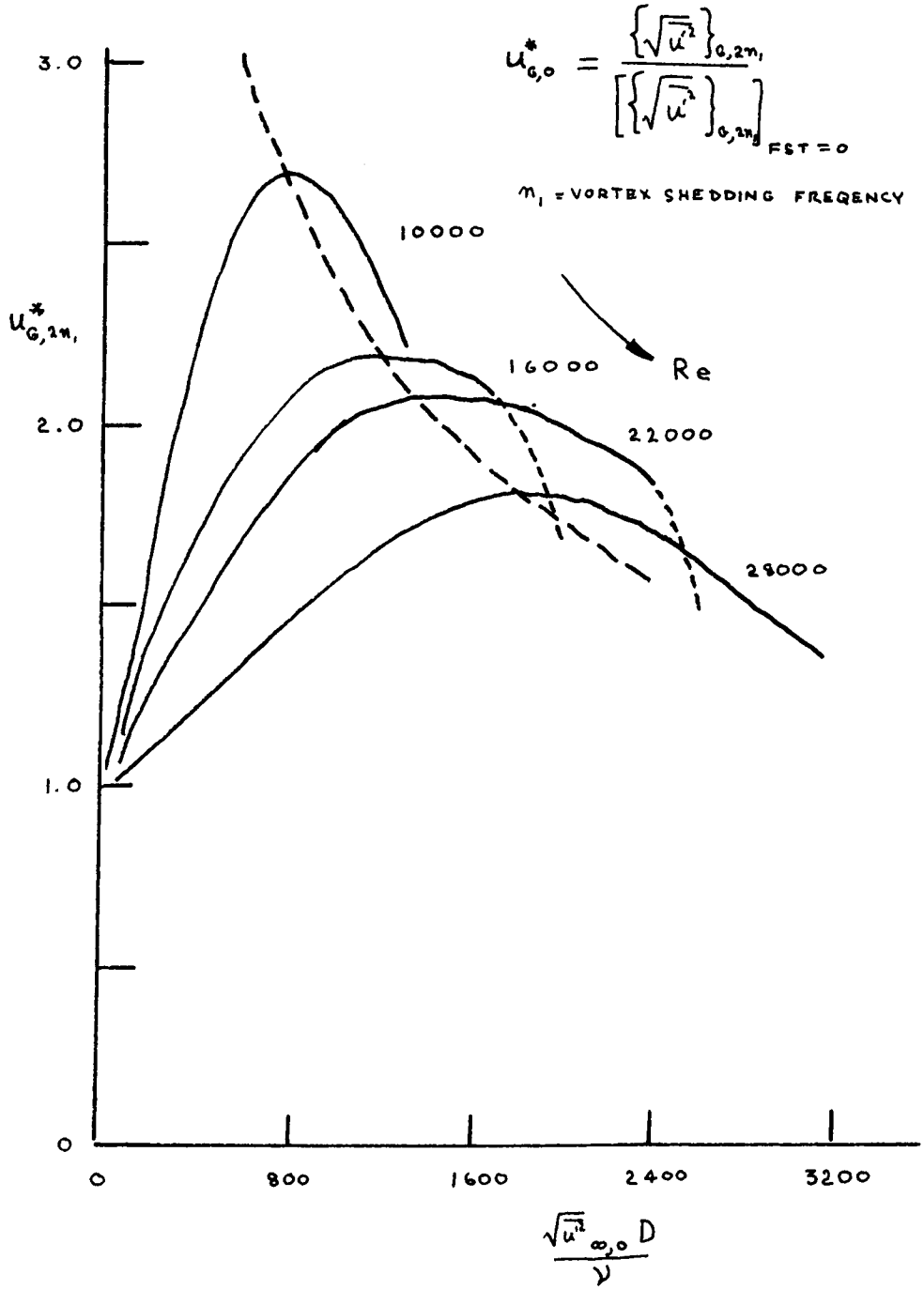
EFFECT OF FREE STREAM TURBULENCE ON THE VORTEX SHEDDING PROCESS IN THE WAKE REGION

FIG 4.4.7



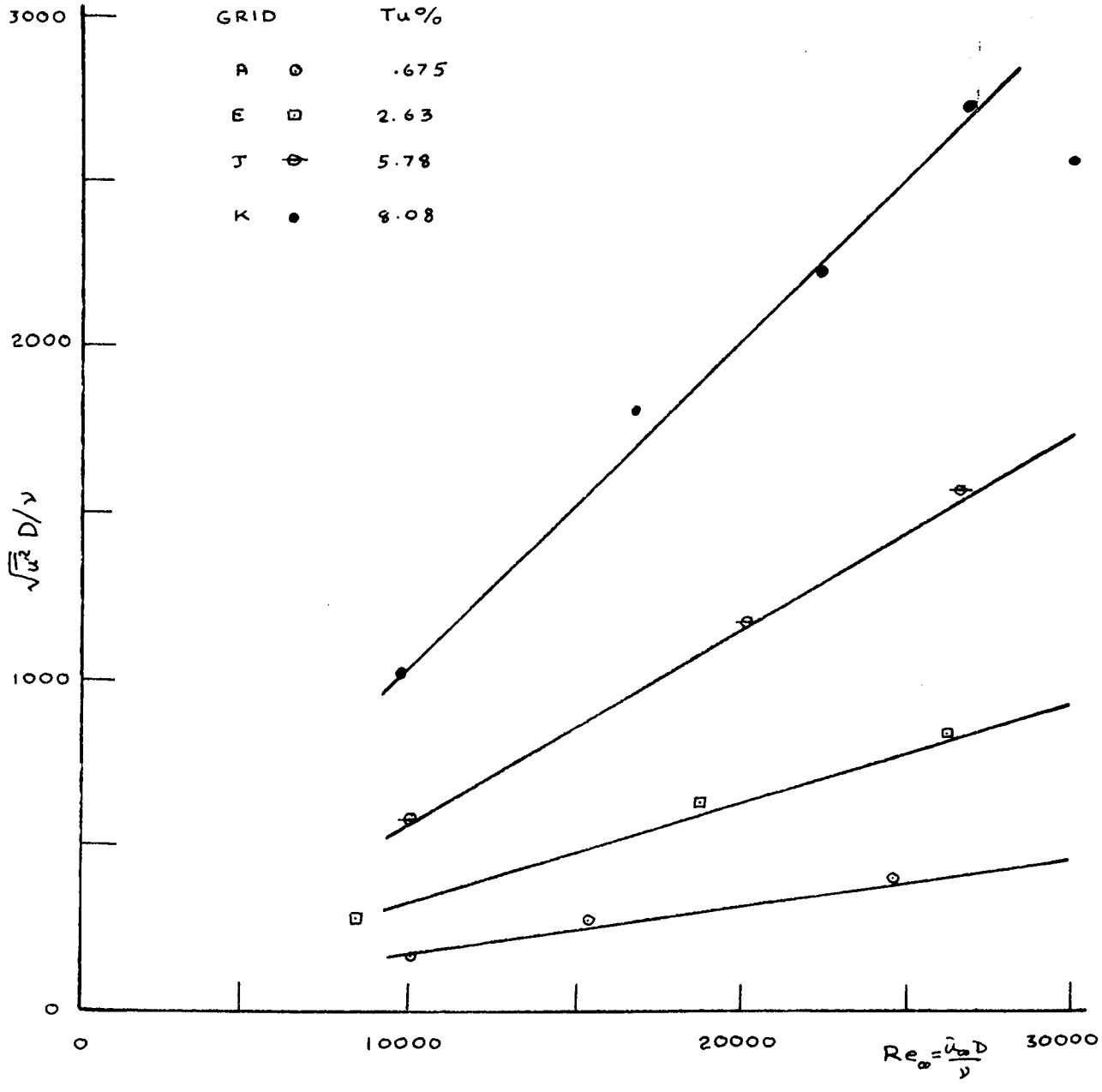
A SPECTRUM OF TURBULENCE AT THE REAR STAGNATION POINT

FIG 4.4.8



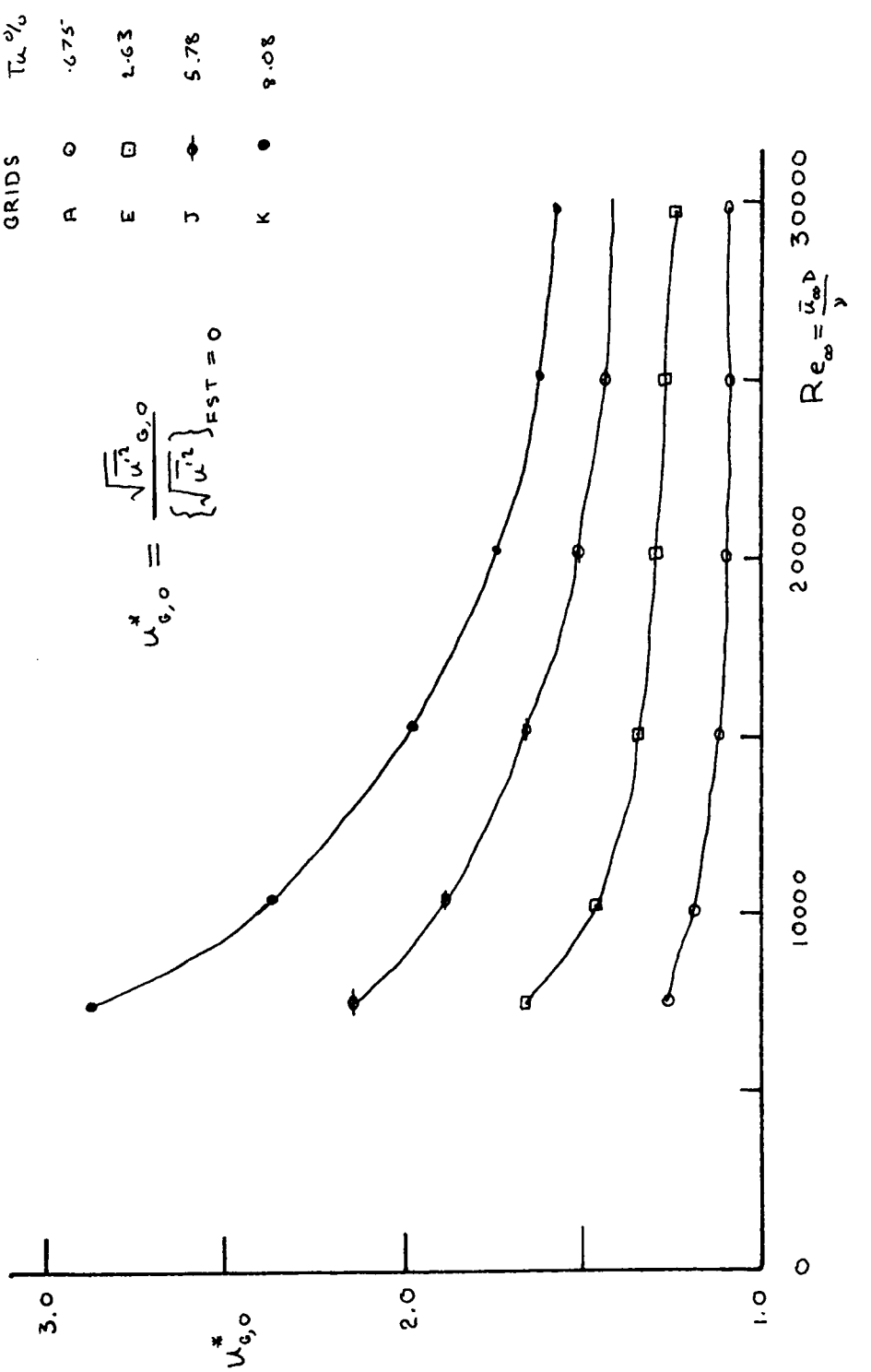
AMPLIFICATION OF R.M.S. VELOCITY WITH FREE STREAM TURBULENCE(MEASURED AT 2×VORTEX SHEDDING FREQENCY)

FIG 4.4.9



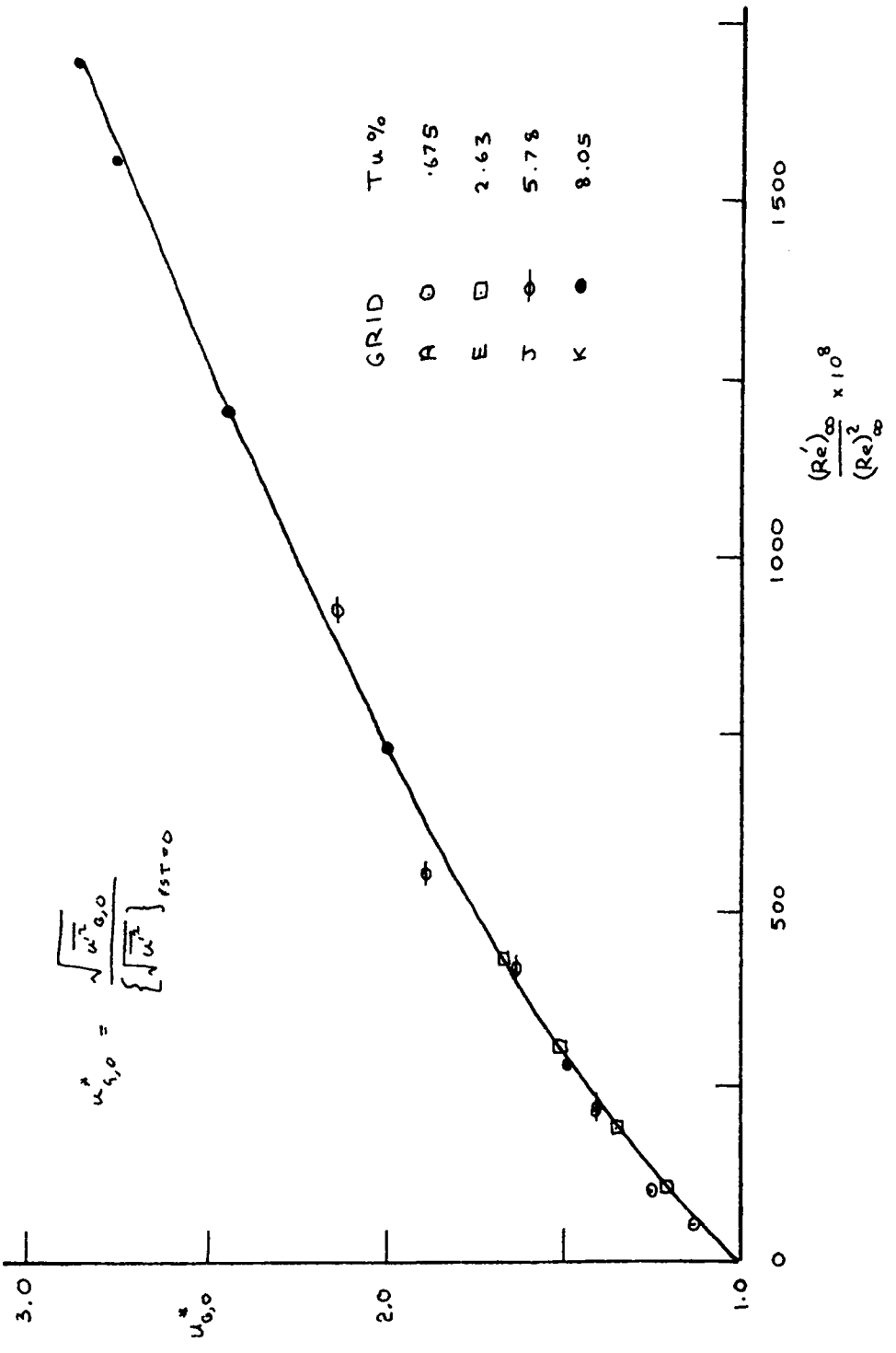
EFFECT OF TURBULENCE ON FLUCTUATIONS AT FRONT STAGNATION POINT

FIG4.5.1



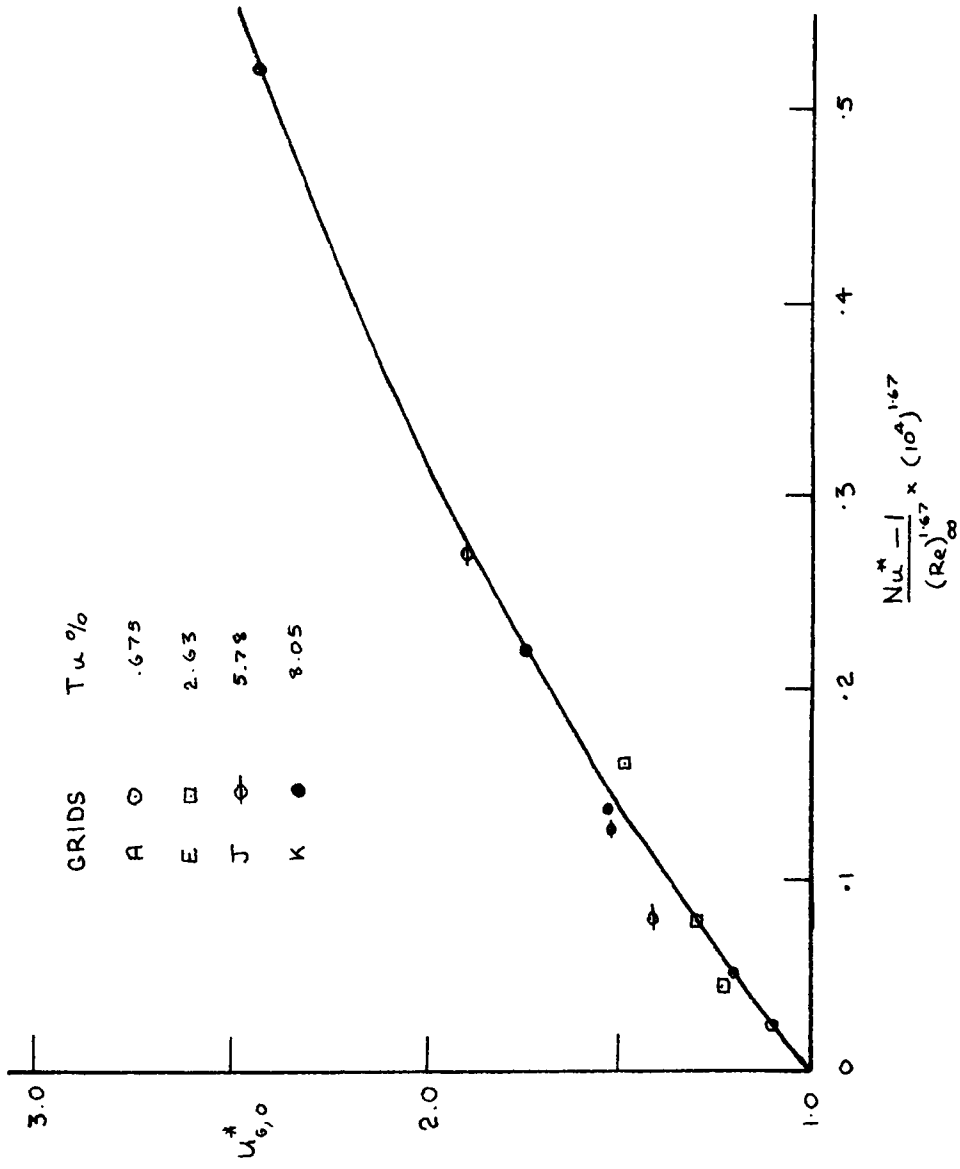
EFFECTIVENESS OF FREESTREAM TURBULENCE ON REAR STAGNATION POINT FLUCTUATIONS

FIG 4.6.1



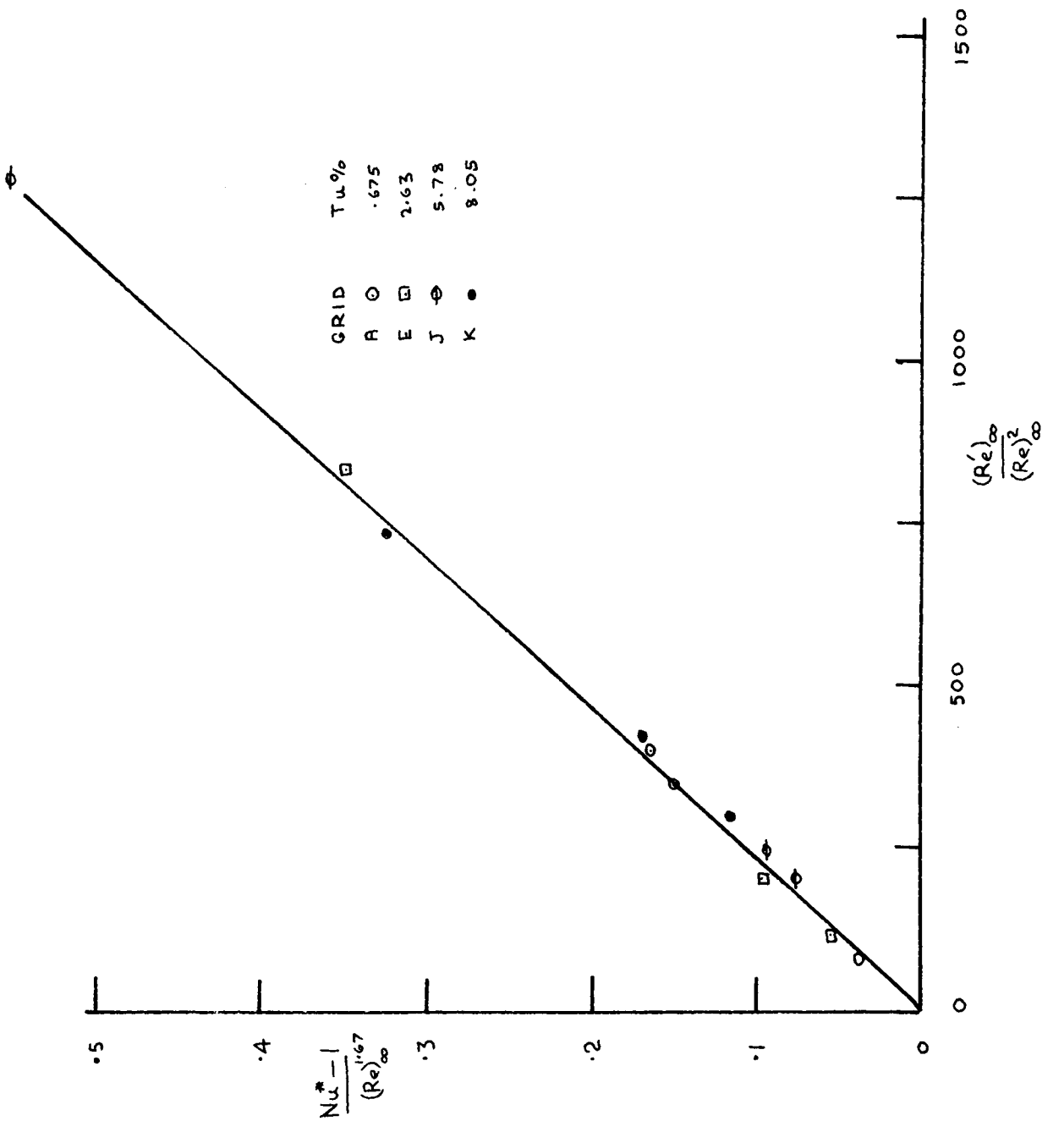
A CORRELATION BETWEEN FREESTREAM TURBULENCE AND THE WAKE FLUCTUATIONS

FIG 4.6.2



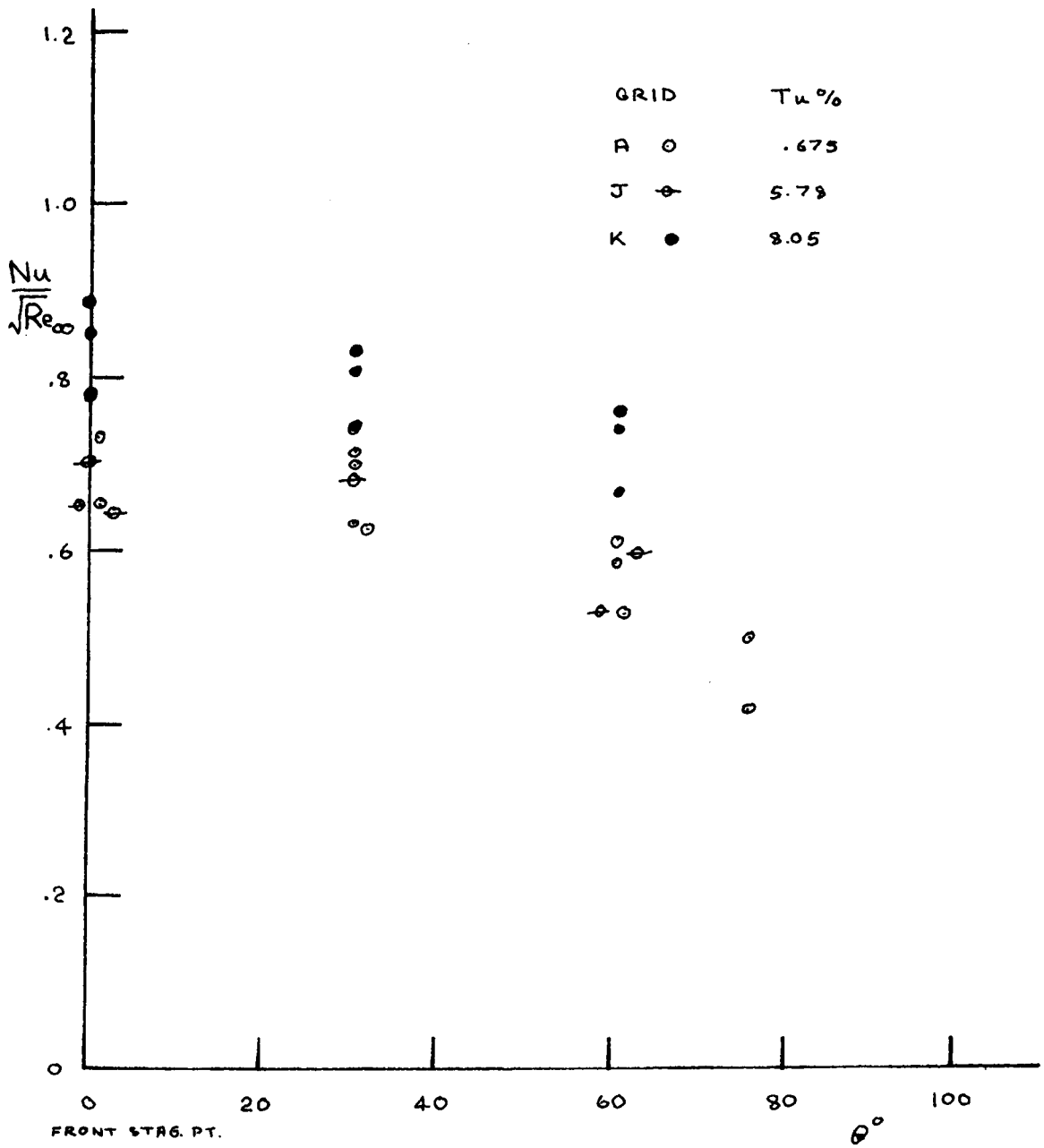
A CORRELATION BETWEEN THE FLUID MOTION AND HEAT TRANSFER AT REAR STAGNATION POINT

FIG4.6.3



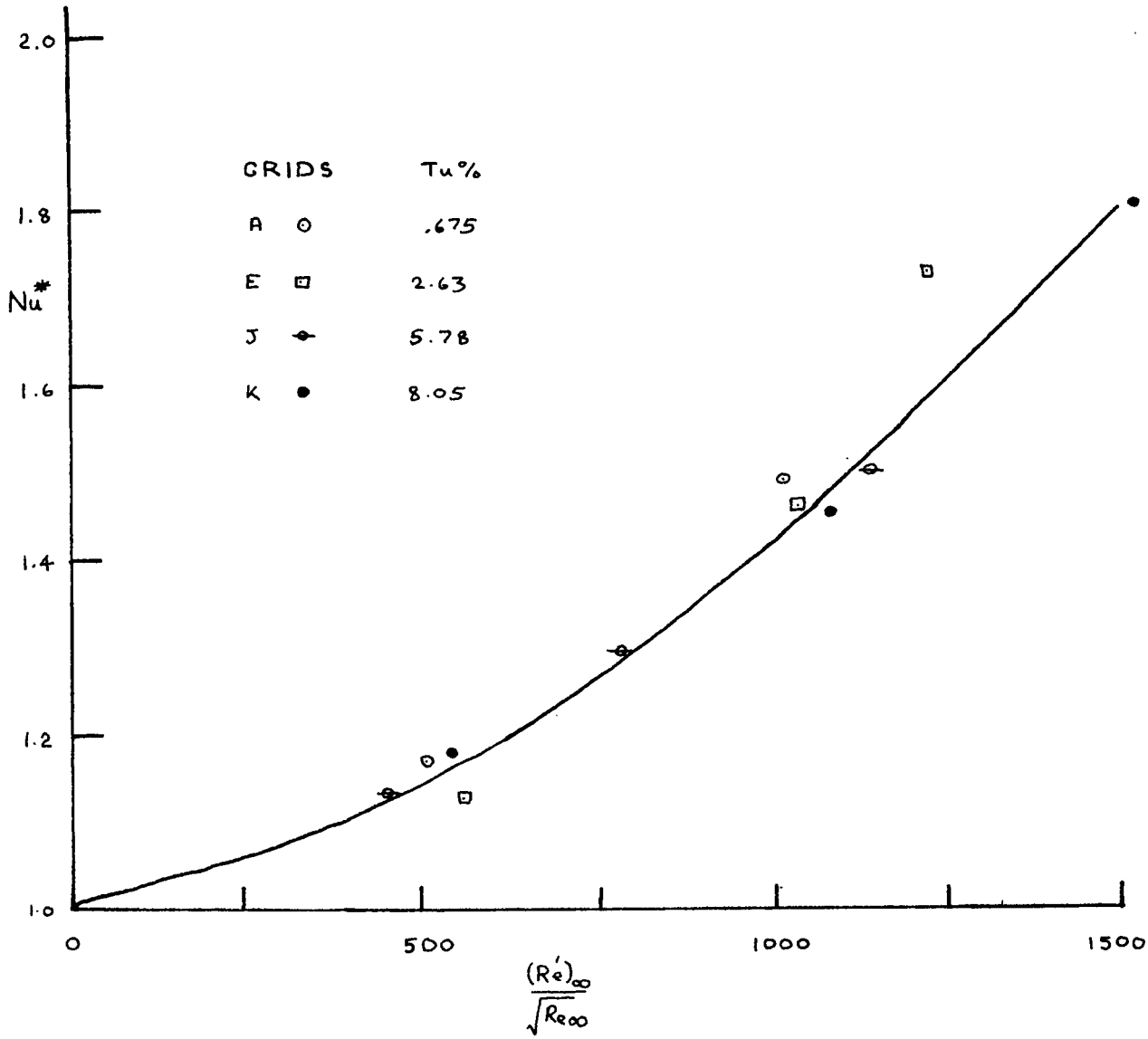
A CORRELATION BETWEEN REAR STAGNATION POINT HEAT TRANSFER AND FREESTREAM MOTION

FIG 4.6.4



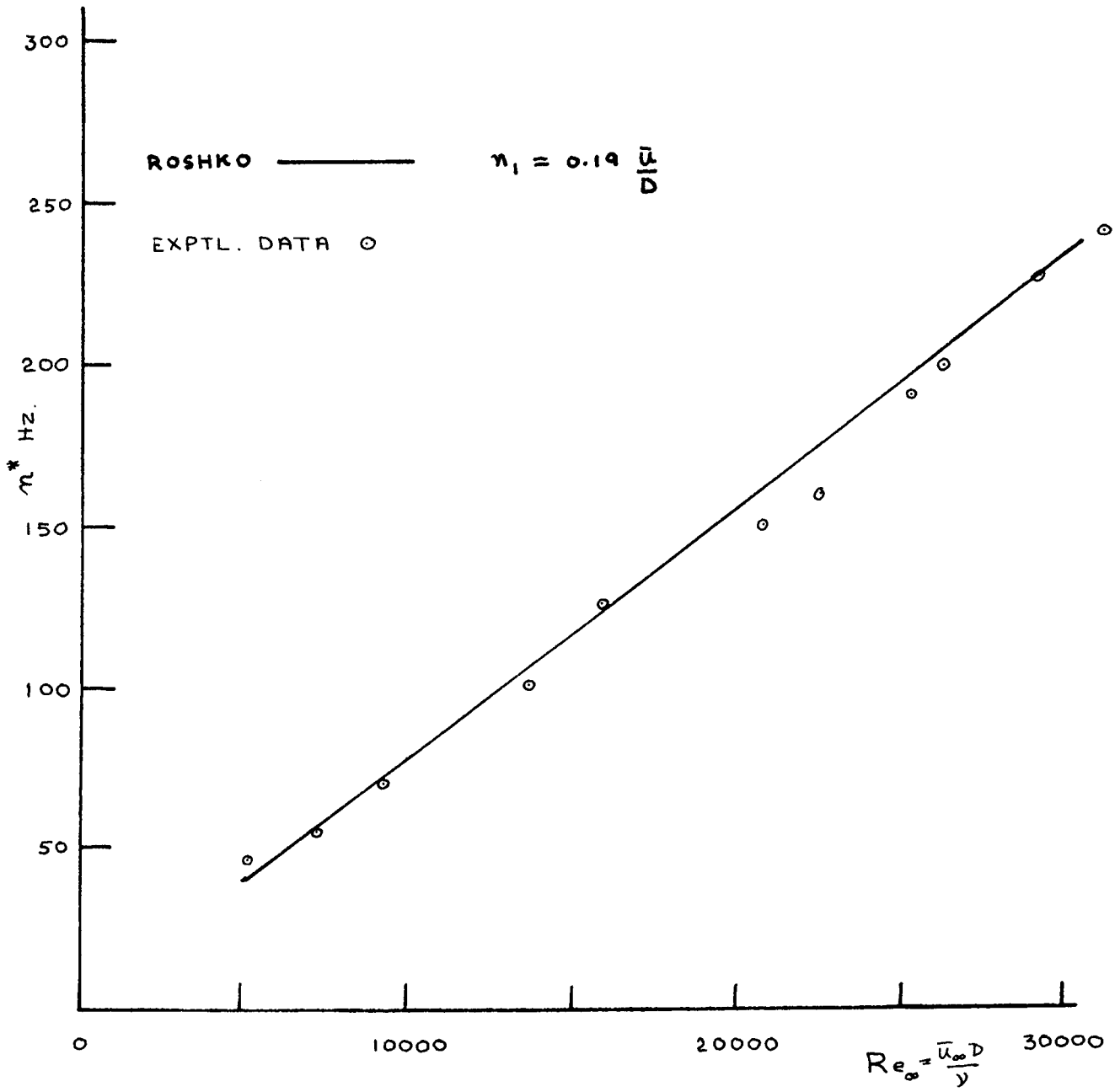
LOCAL HEAT TRANSFER(NON-DIMENSIONAL) ON FRONT PORTION OF CYLINDER

FIG 4.6.5



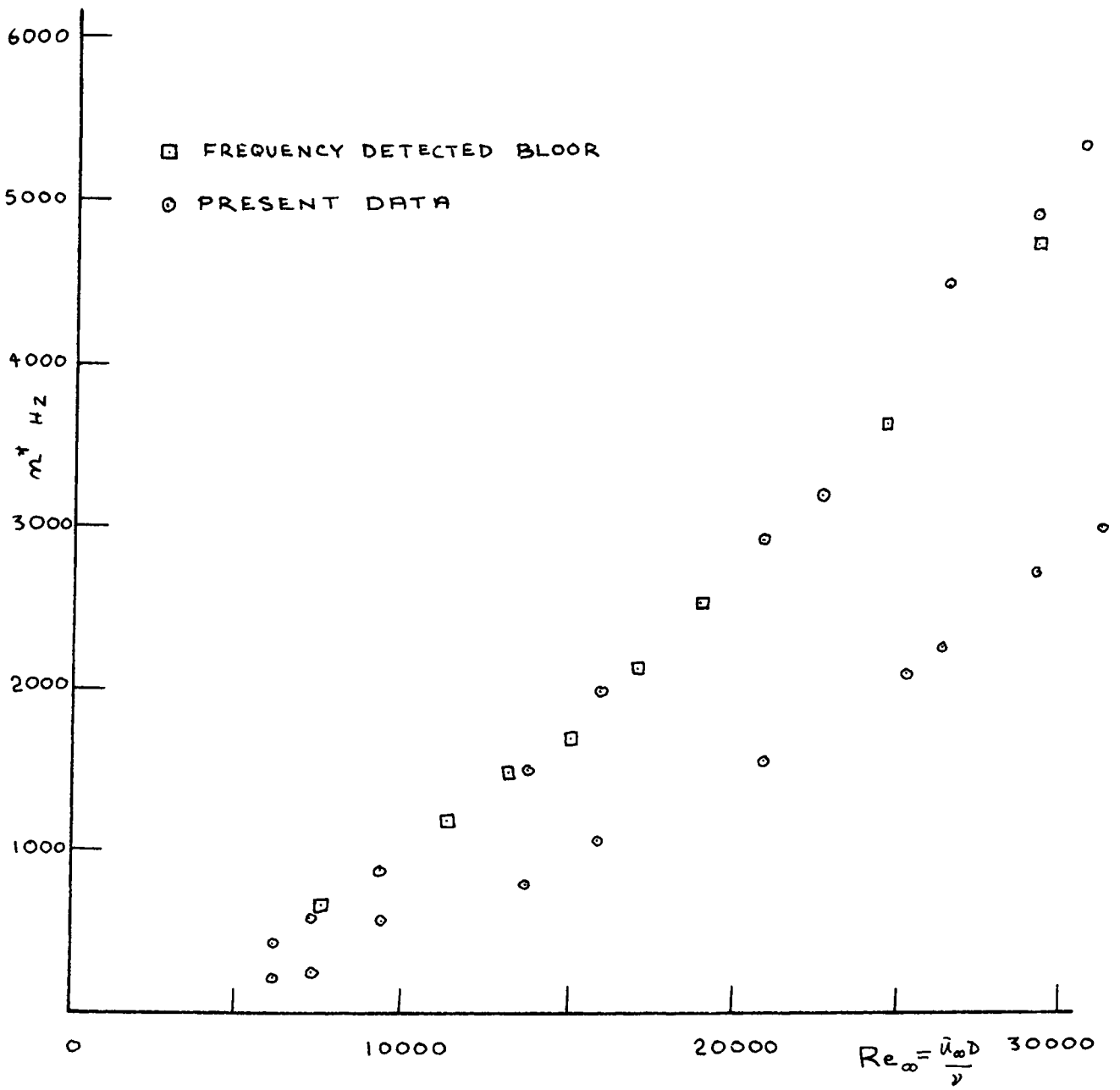
A CORRELATION OF HEAT TRANSFER DATA AT FRONT STAGNATION POINT

FIG 4.6.6



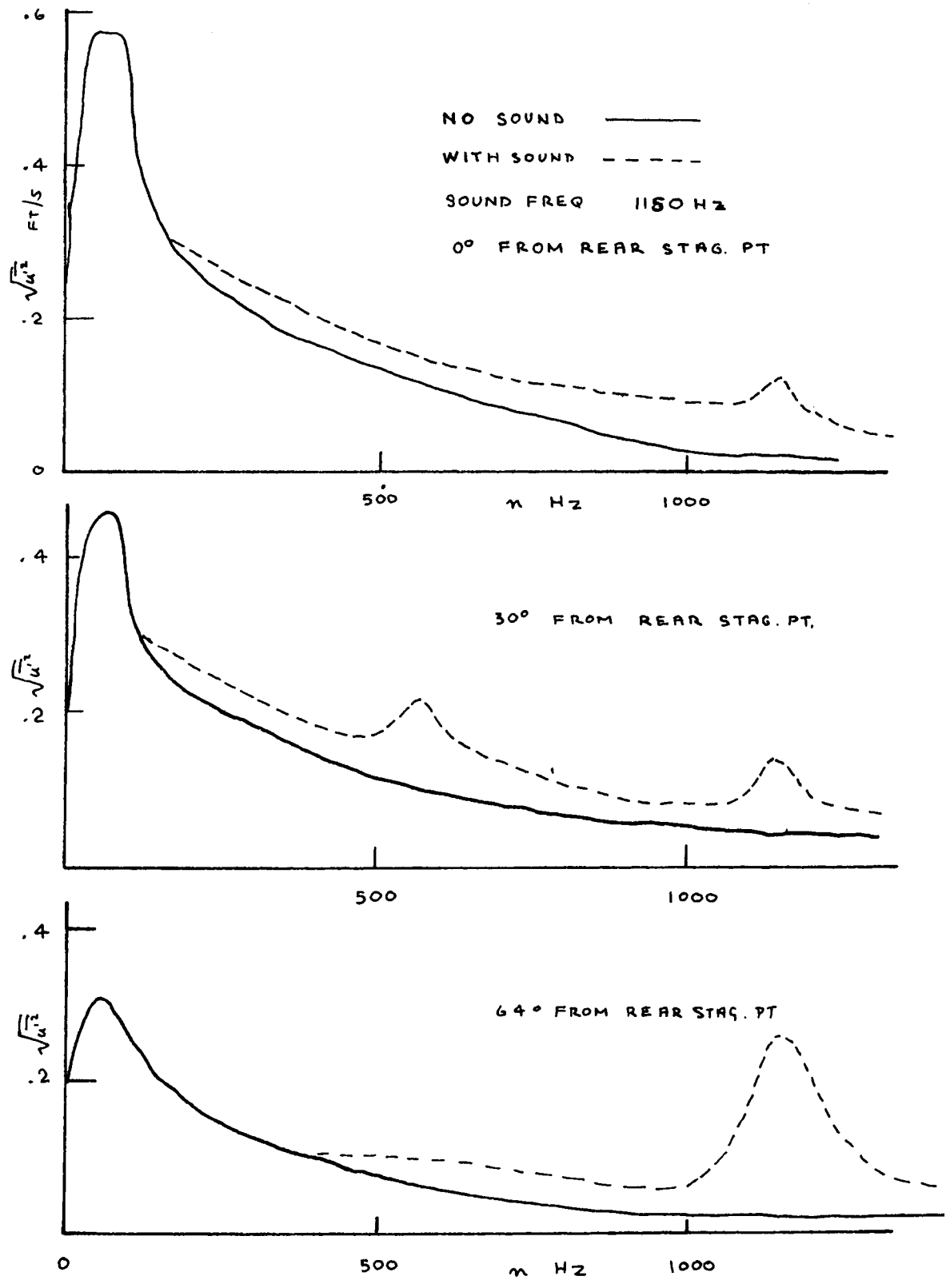
VARIATION OF VORTEX SHEDDING FREQENCY WITH REYNOLDS NUMBER

FIG 4.7.1



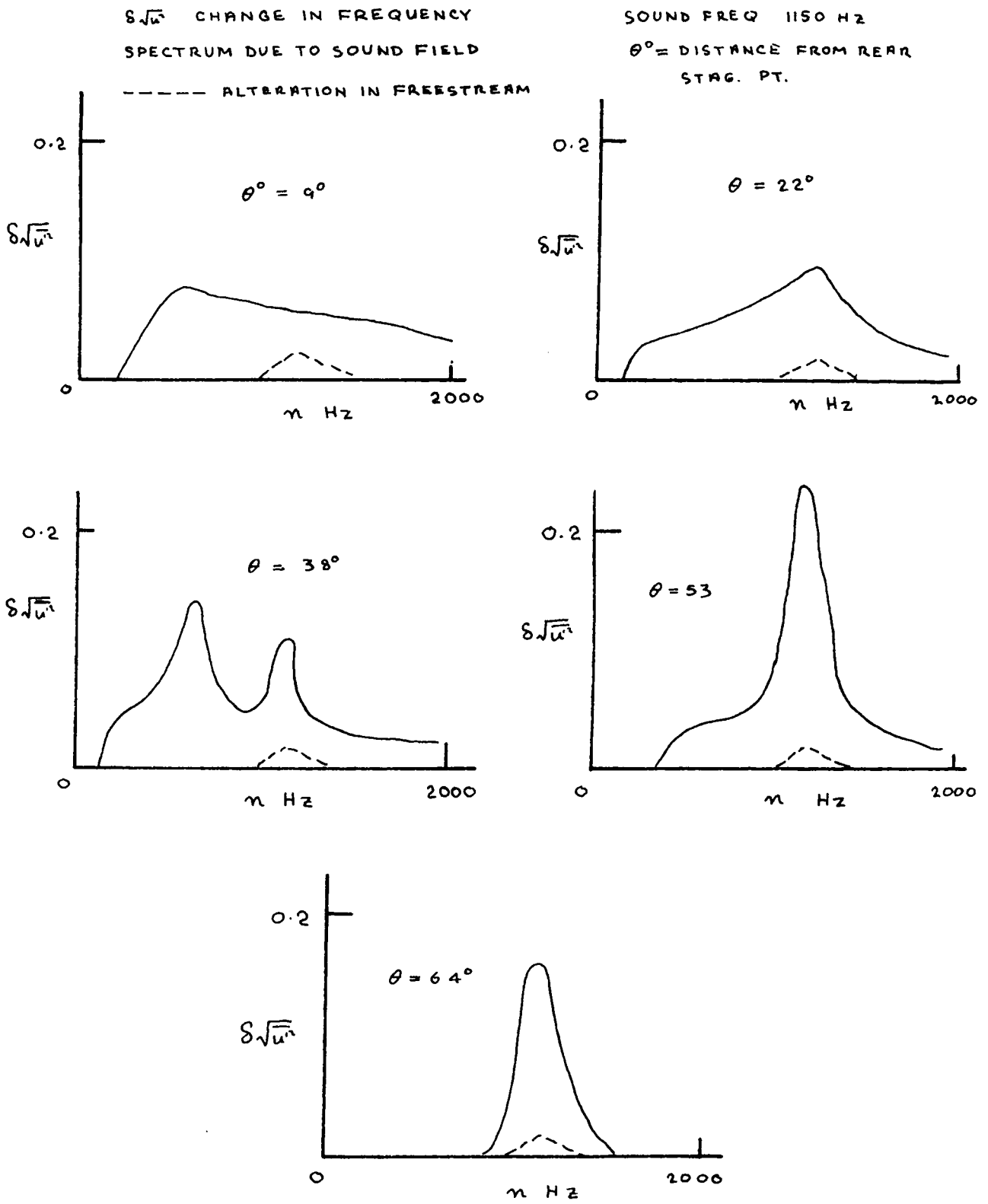
'OTHER' FREQENCIES DETECTED IN WAKE REGION

FIG 4.7.2



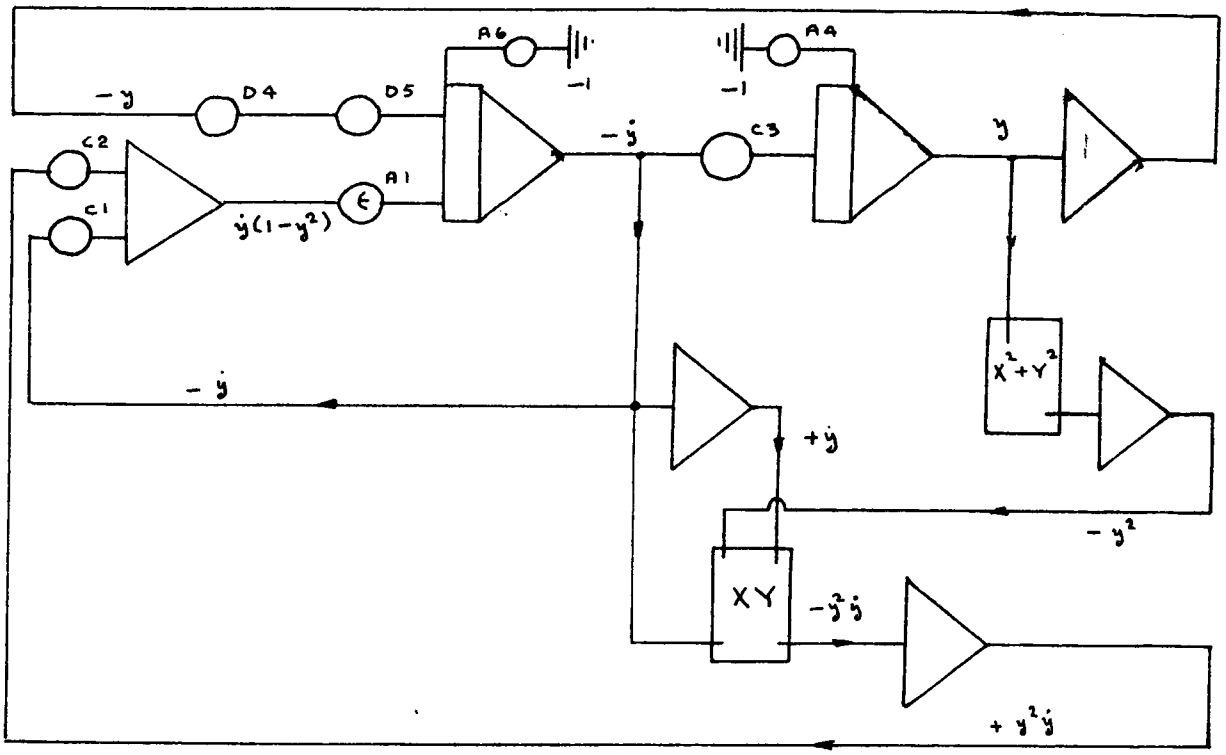
INTERACTION BETWEEN A SOUND FIELD AND WAKE REGION FLUID MECHANICS

FIG 4.7.3



THE AMPLIFICATION OF DISCRETE FREQENCIES IN THE WAKE REGION BY MEANS OF AN APPLIED SOUND FIELD

FIG 4.7.4

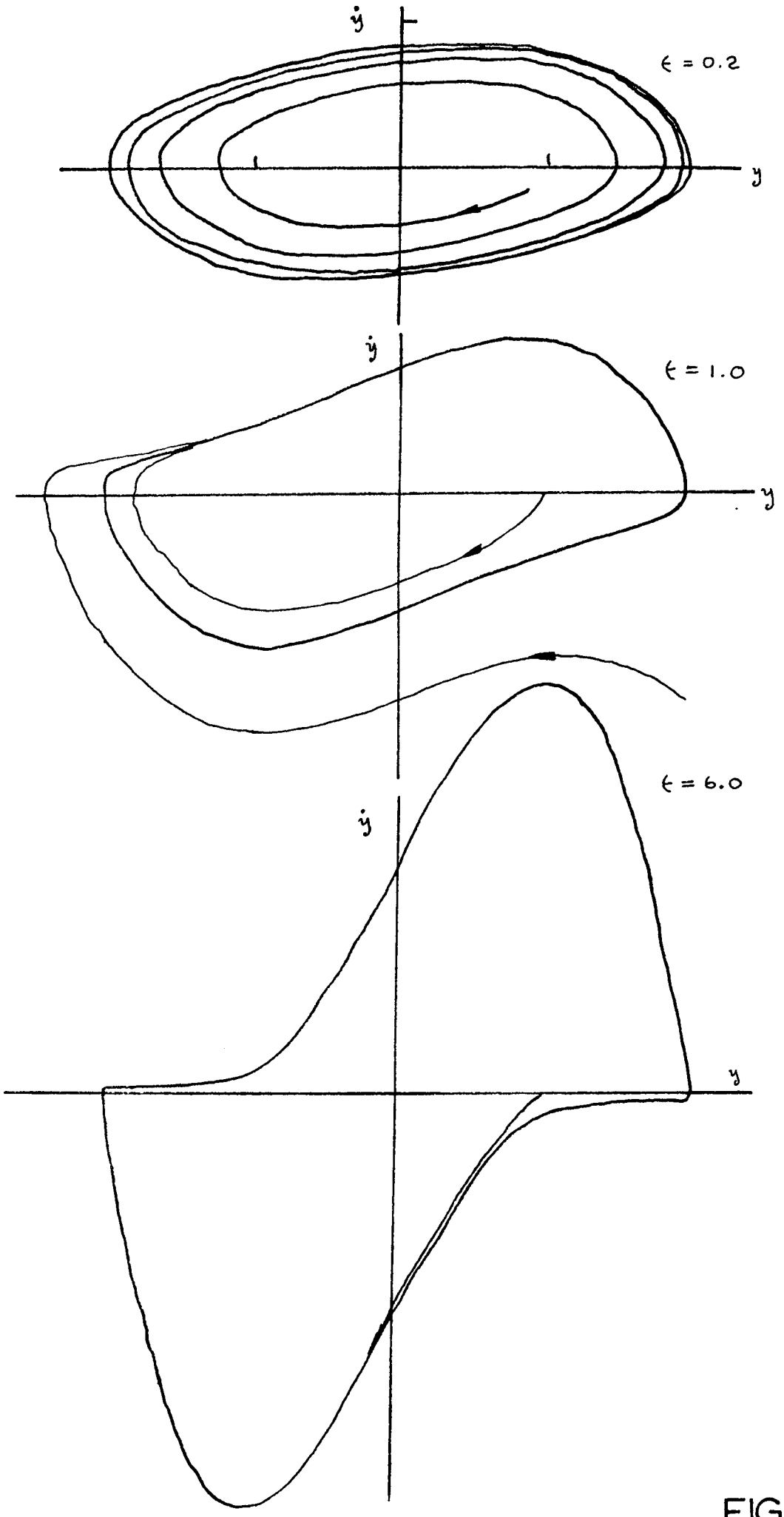


POTENTIOMETER SETTINGS

C1	.2
C2	.125
C3	.8
A1	ϵ
A4	INITIAL CONDITION
A6	" "
D4	.5
D5	.1

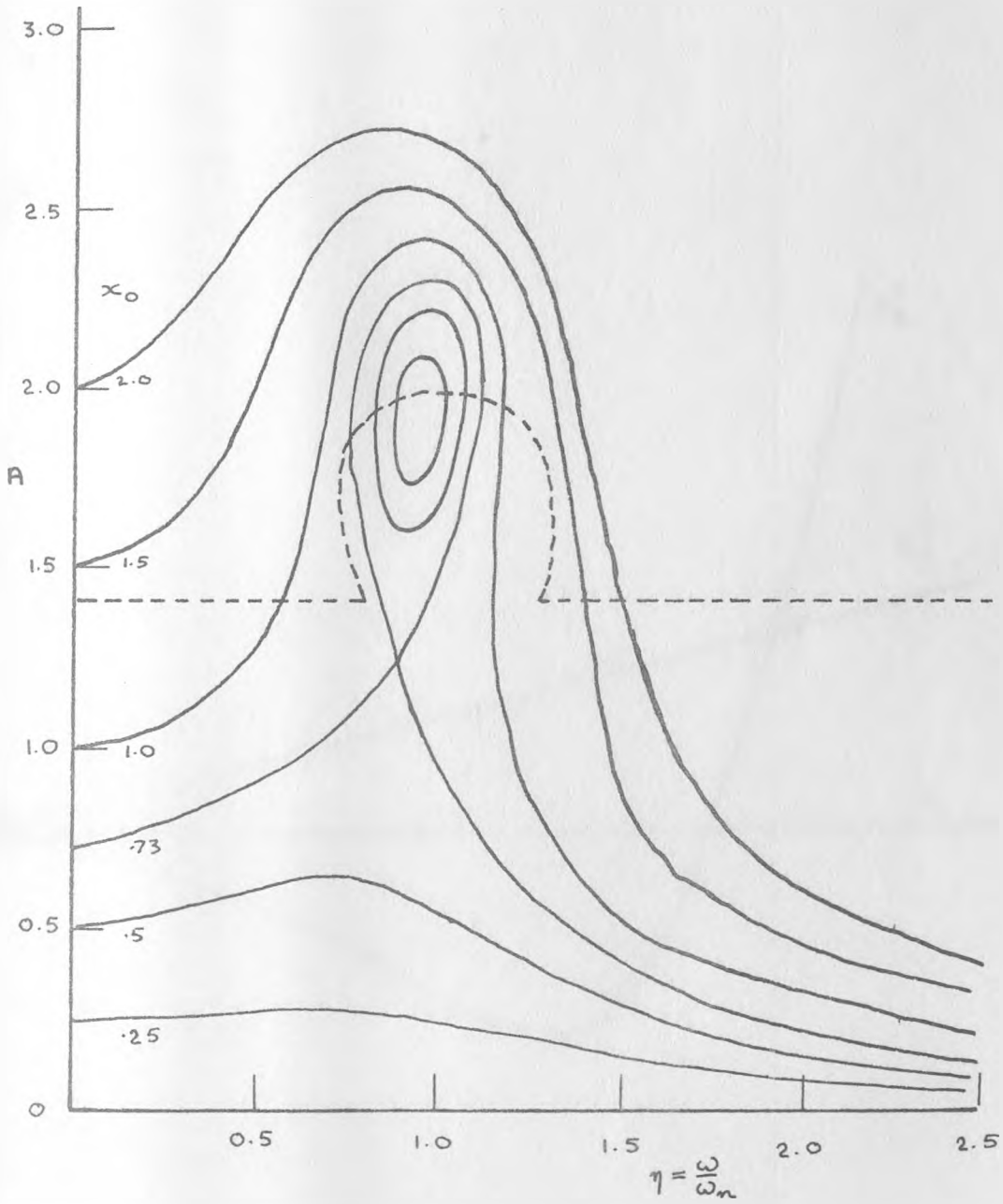
AN ANALOGUE COMPUTER CIRCUIT FOR THE SOLUTION OF VAN DER POLS EQUATION

FIG 5.1



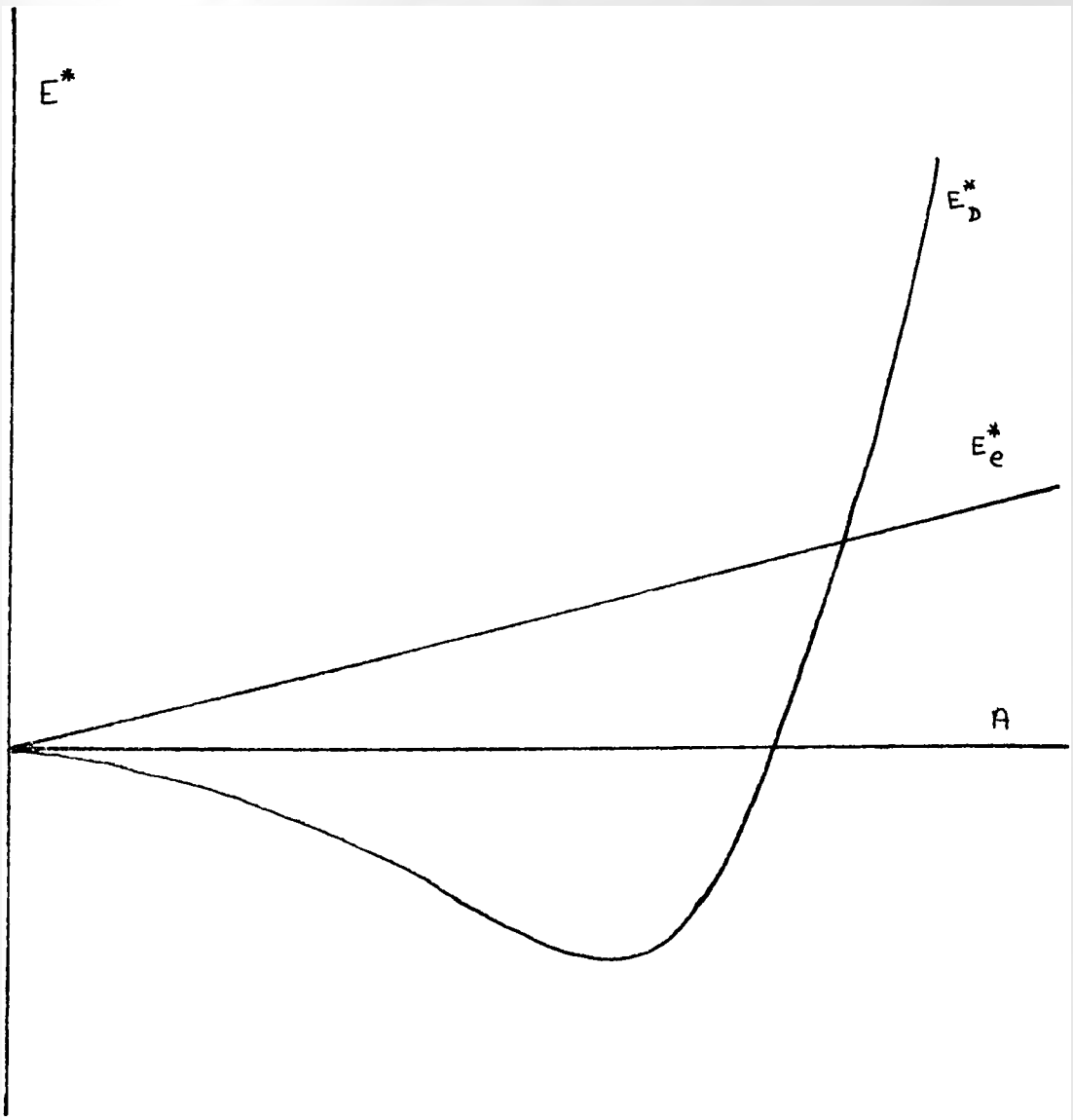
SOLUTIONS OF VAN DER POLS EQUATION

FIG 5.2



EFFECT OF EXTERNAL EXCITATION ON THE SOLUTION OF VAN DER POL'S EQUATION

FIG 5.3



ENERGY RELATIONSHIPS DERIVED FROM

VAN DER POLS EQUATION

FIG 5.4

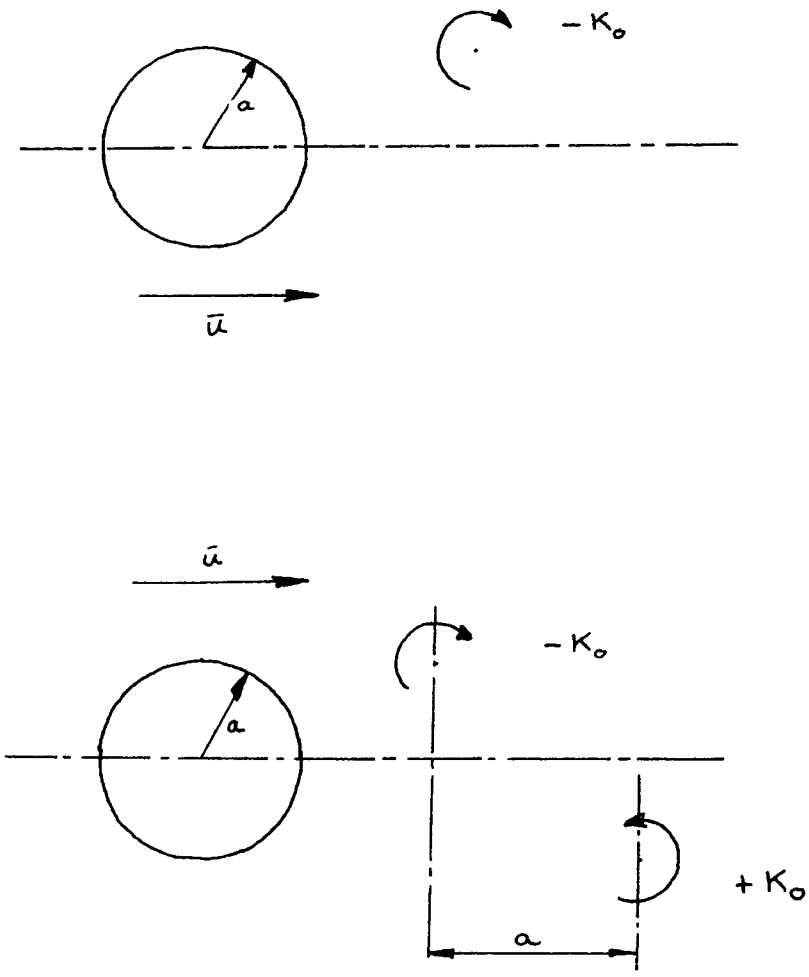
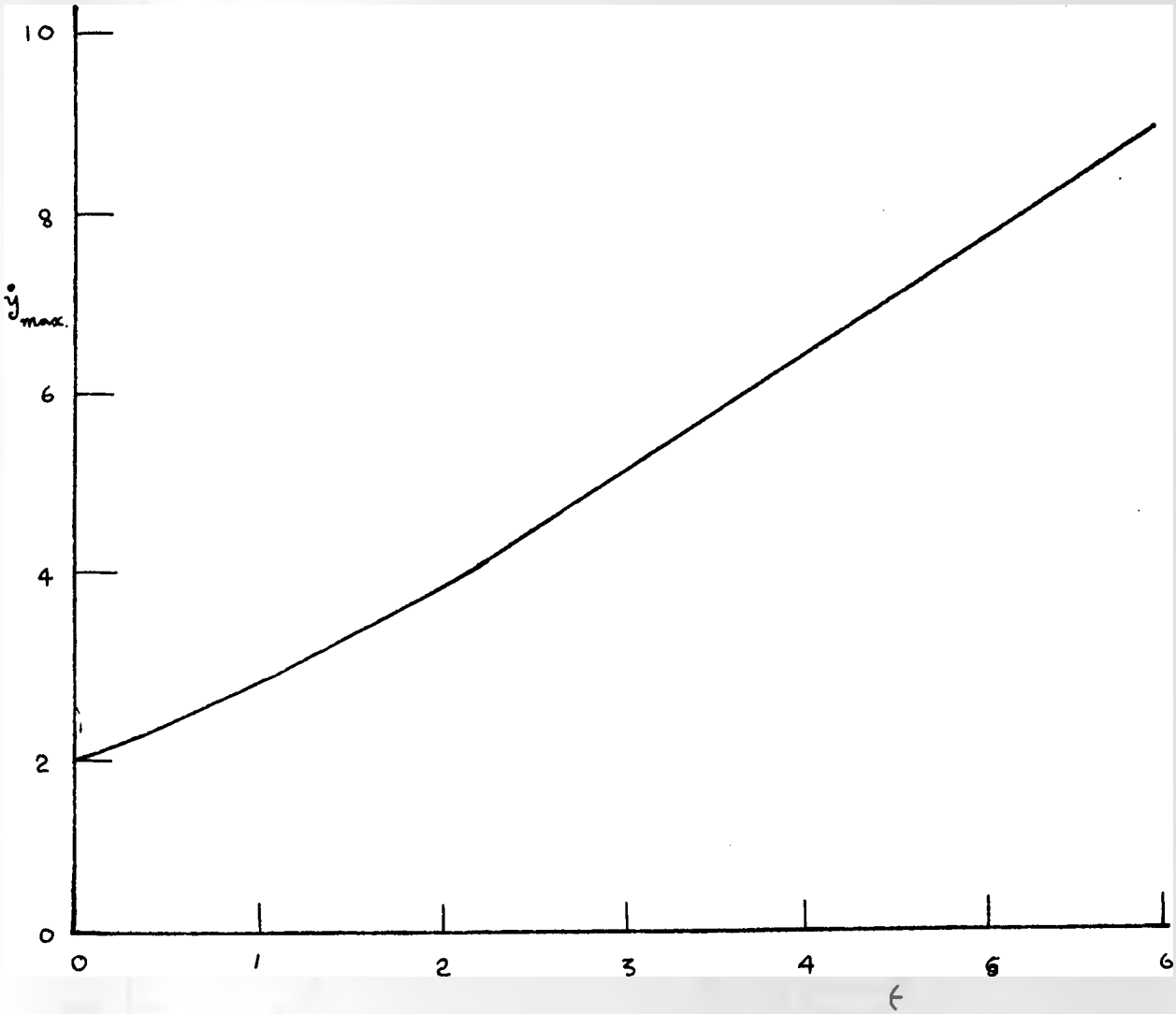
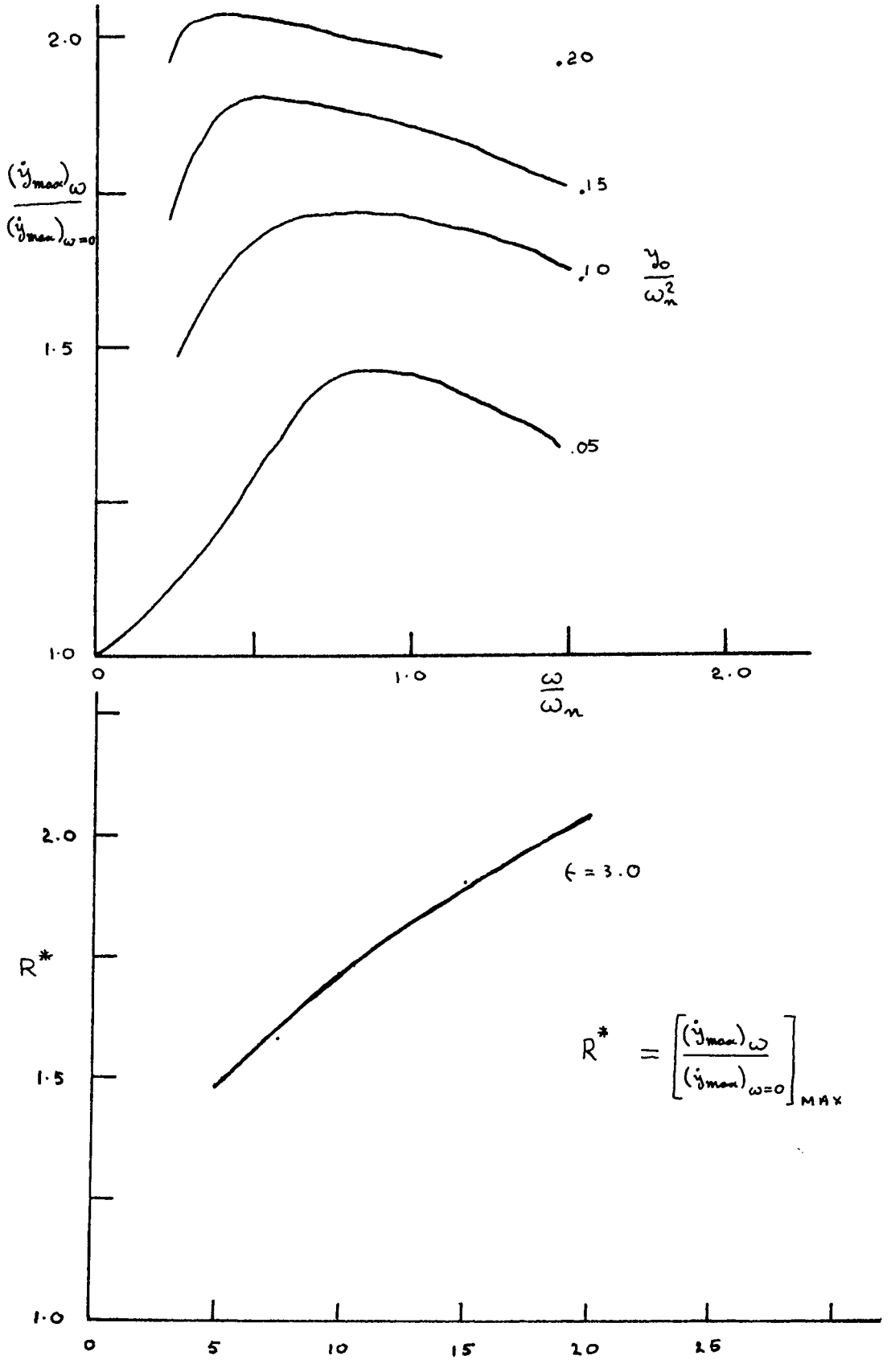


FIG 5.5



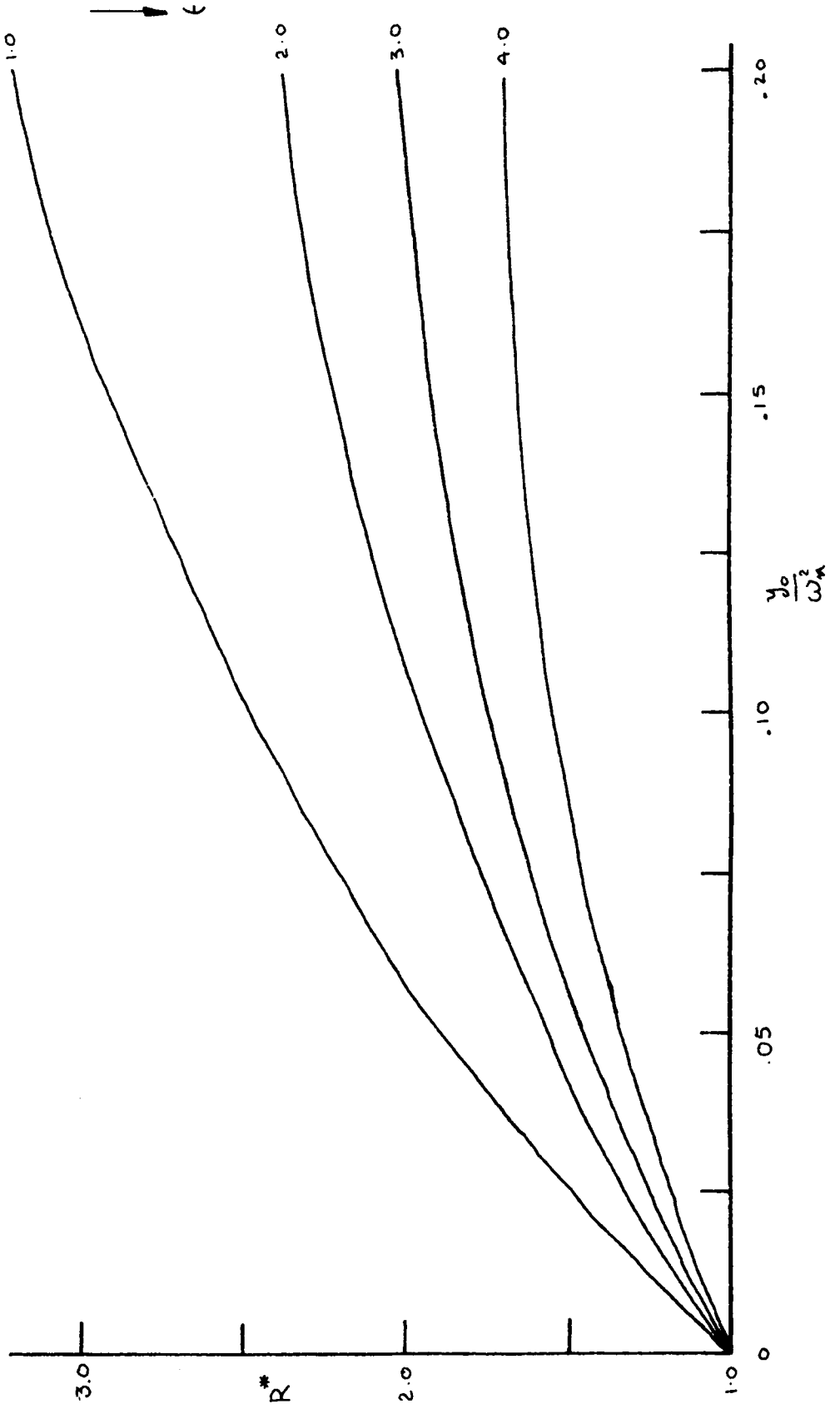
VARIATION OF $\dot{y}_{max.}$ WITH ϵ

FIG 5.6



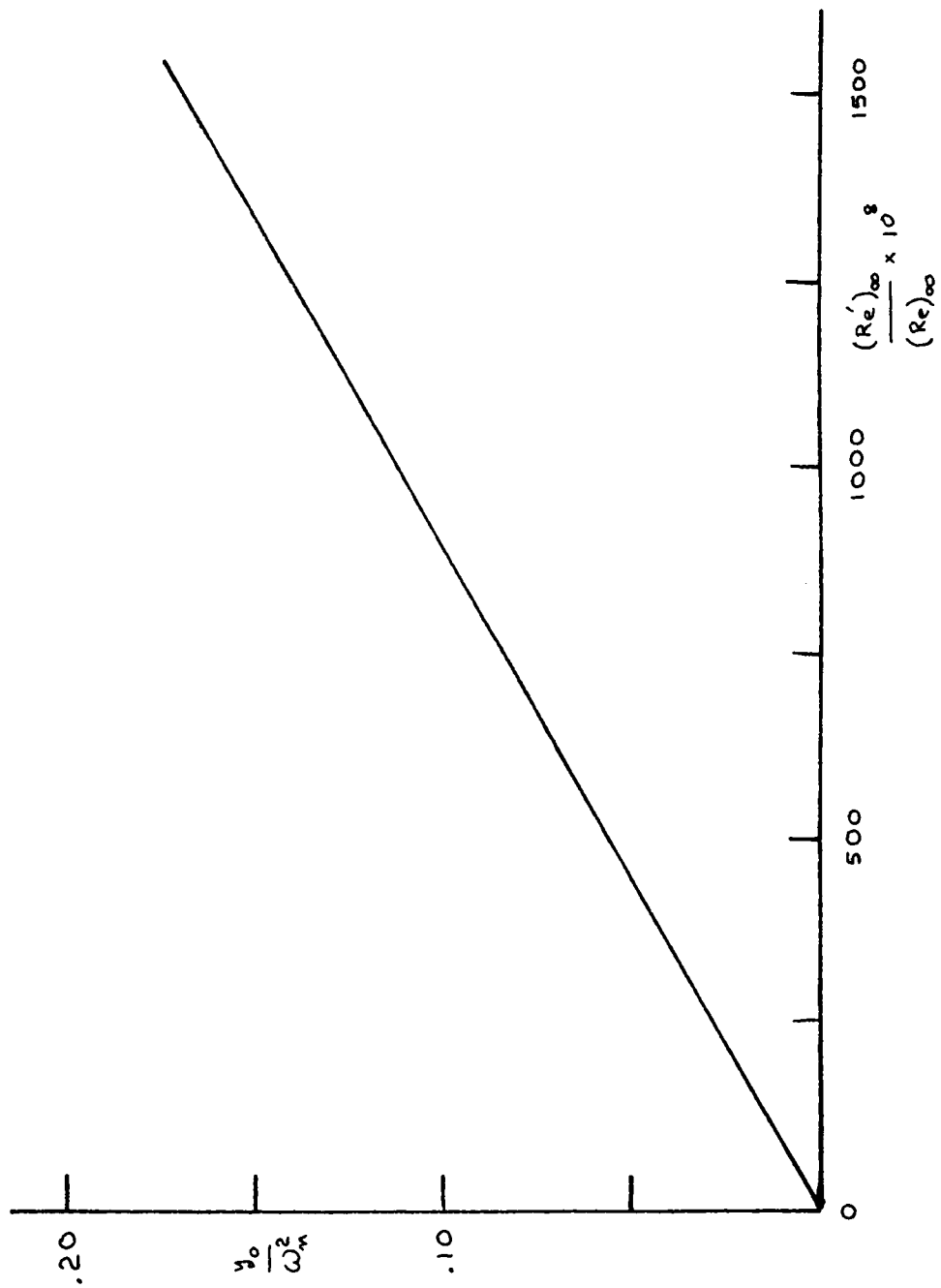
EFFECT OF EXTERNAL EXCITATION ON THE SOLUTION OF VAN DER POLS EQUATION

FIG 5.7



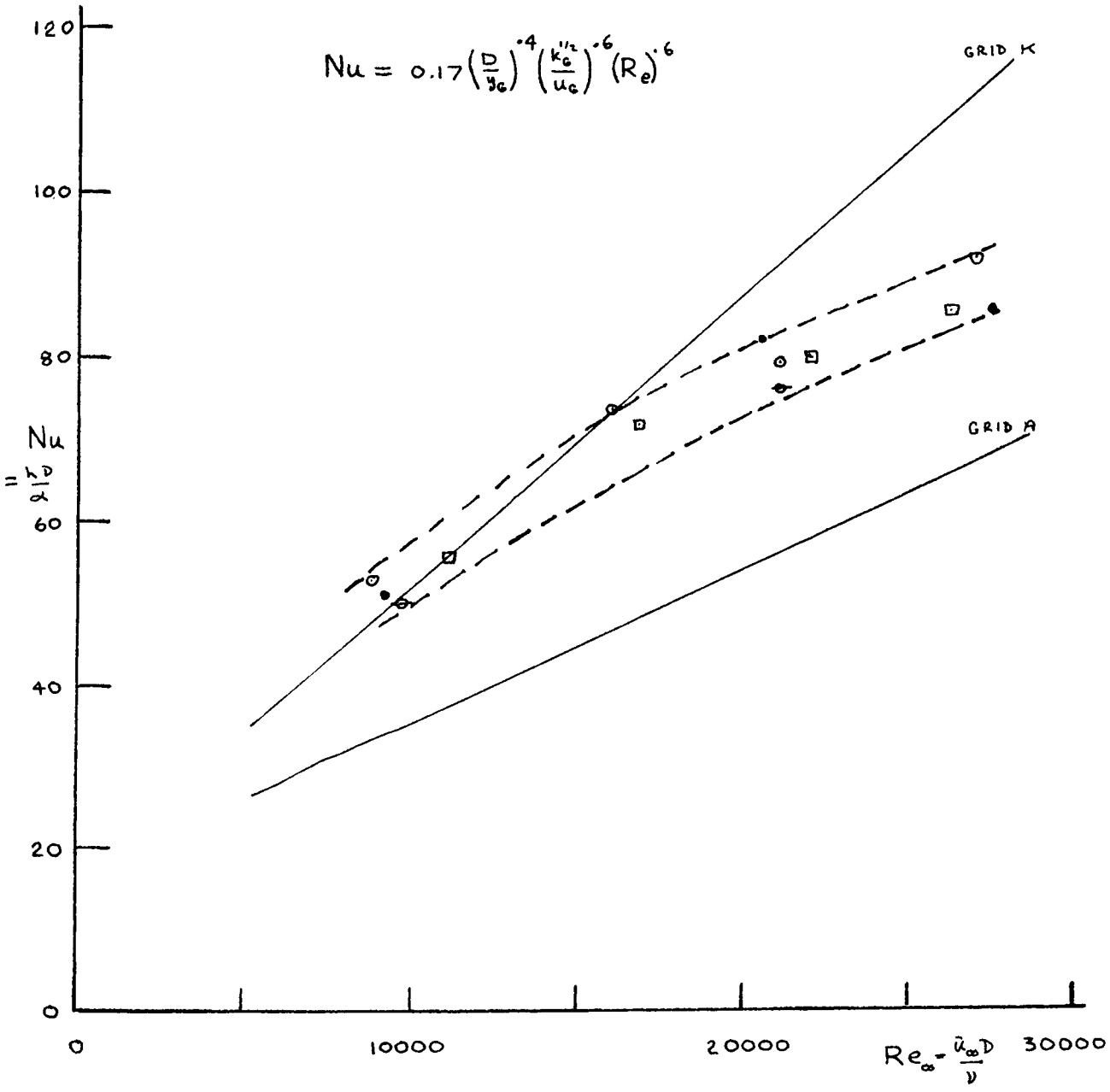
VAN DER POLS EQUATION: VARIATION OF MAXIMUM AMPLIFICATION WITH EXTERNAL EXCITATION AT SEVERAL VALUES OF ϵ

FIG 5.8



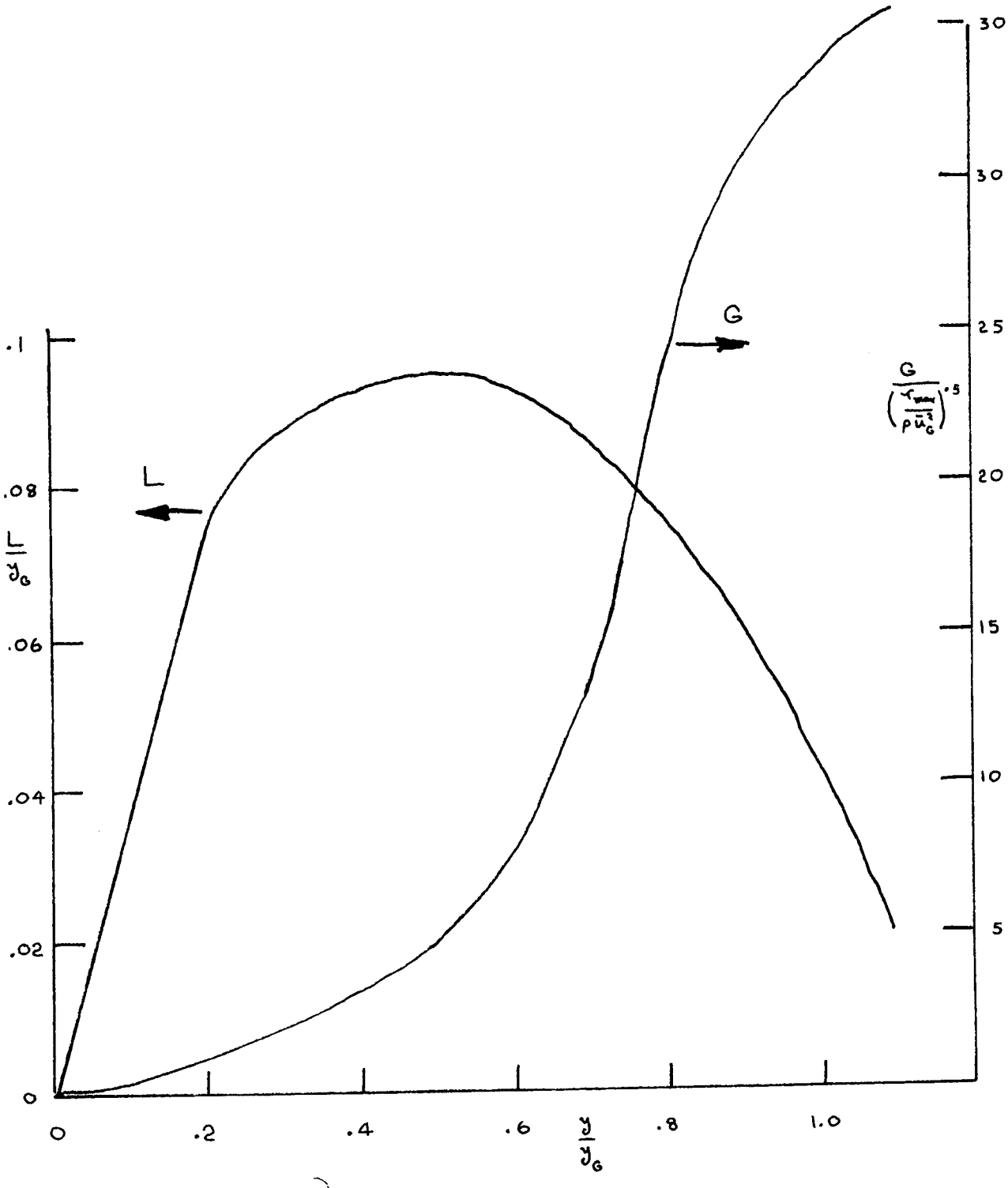
A RELATIONSHIP BETWEEN THEORETICAL AND EXPERIMENTAL DATA

FIG 5.9



A PREDICTION OF HEAT TRANSFER FROM FLUID MOTION IN THE WAKE REGION USING ABOVE RELATIONSHIP

FIG 6.1



L,G FUNCTIONS USED IN EQUATION 6.26

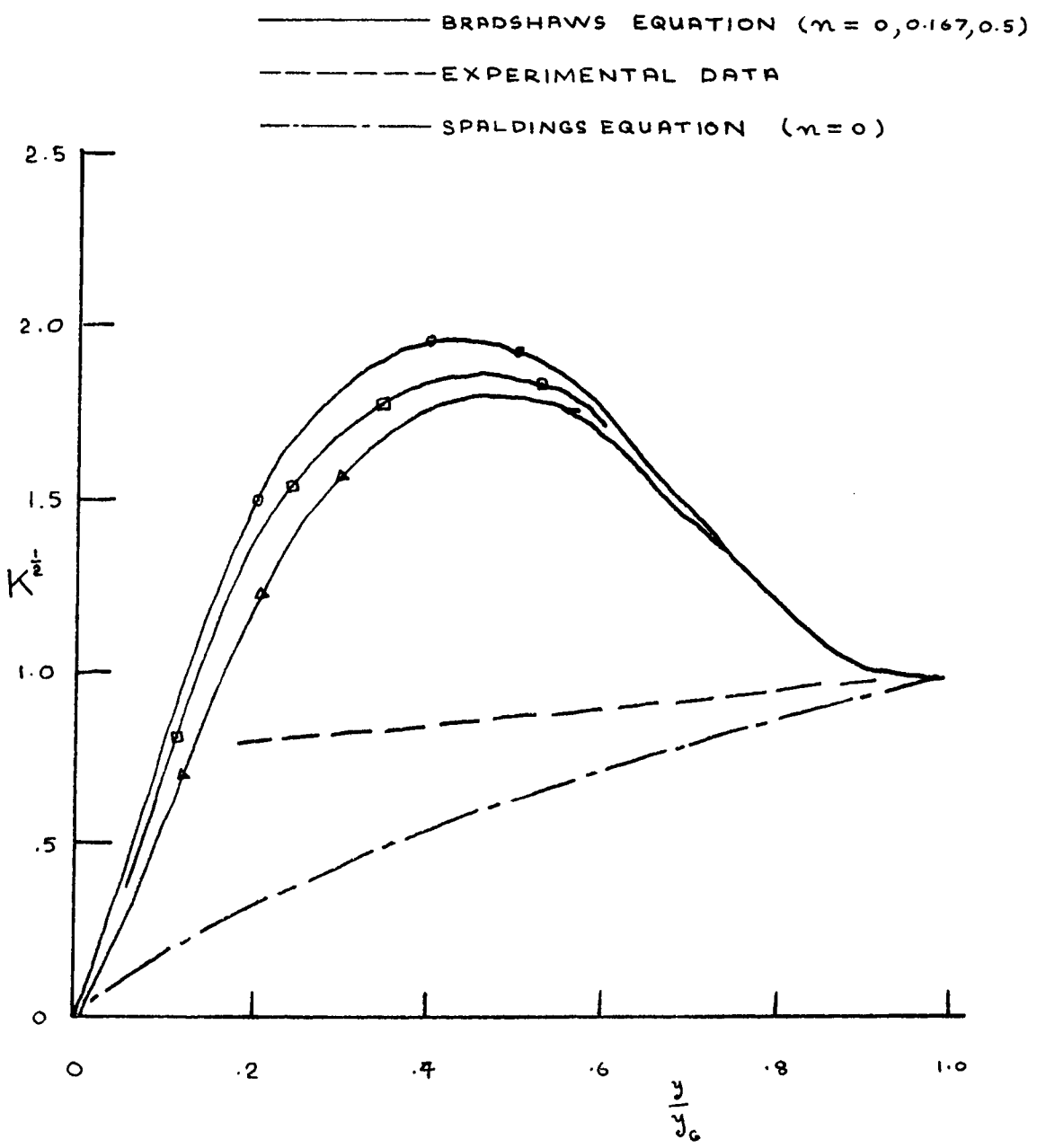
FIG 6.2

$$f(x) = \frac{a_0 + a_1 x + a_2 x^2 + \cdots + a_m x^m}{1.0 + b_1 x + b_2 x^2 + \cdots + b_n x^n}$$

	L		G	
	$0 < y/y_G < 0.2$	$0.2 < y/y_G < 1.1$	$0 < y/y_G < 0.7$	$0.7 < y/y_G < 1.1$
a_0	0.0000	$2.893333333359 \times 10^{-2}$	$2.17902426649 \times 10^{-28}$	$2.50921252241 \times 10^{4}$
a_1	0.375	$3.40845687731 \times 10^{-1}$	$8.74845940436 \times 10^{-1}$	$-1.69097902249 \times 10^{5}$
a_2		$-6.32132864548 \times 10^{-1}$	$-9.91746035501 \times 10^{0}$	$4.72189440563 \times 10^{5}$
a_3		$6.11247082218 \times 10^{-1}$	$4.79887956630 \times 10^{1}$	$-7.00161305504 \times 10^{5}$
a_4		$-4.23076917783 \times 10^{-1}$	$3.25303454517 \times 10^{1}$	$5.81245013397 \times 10^{5}$
a_5		$1.15384611197 \times 10^{-1}$		$-2.57641025552 \times 10^{5}$
a_6		$8.84299927860 \times 10^{-10}$		$4.74074073844 \times 10^{4}$
b_1			$-8.93613445574 \times 10^{0}$	
b_2			$3.14509804104 \times 10^{1}$	
b_3			$-2.53781511277 \times 10^{1}$	

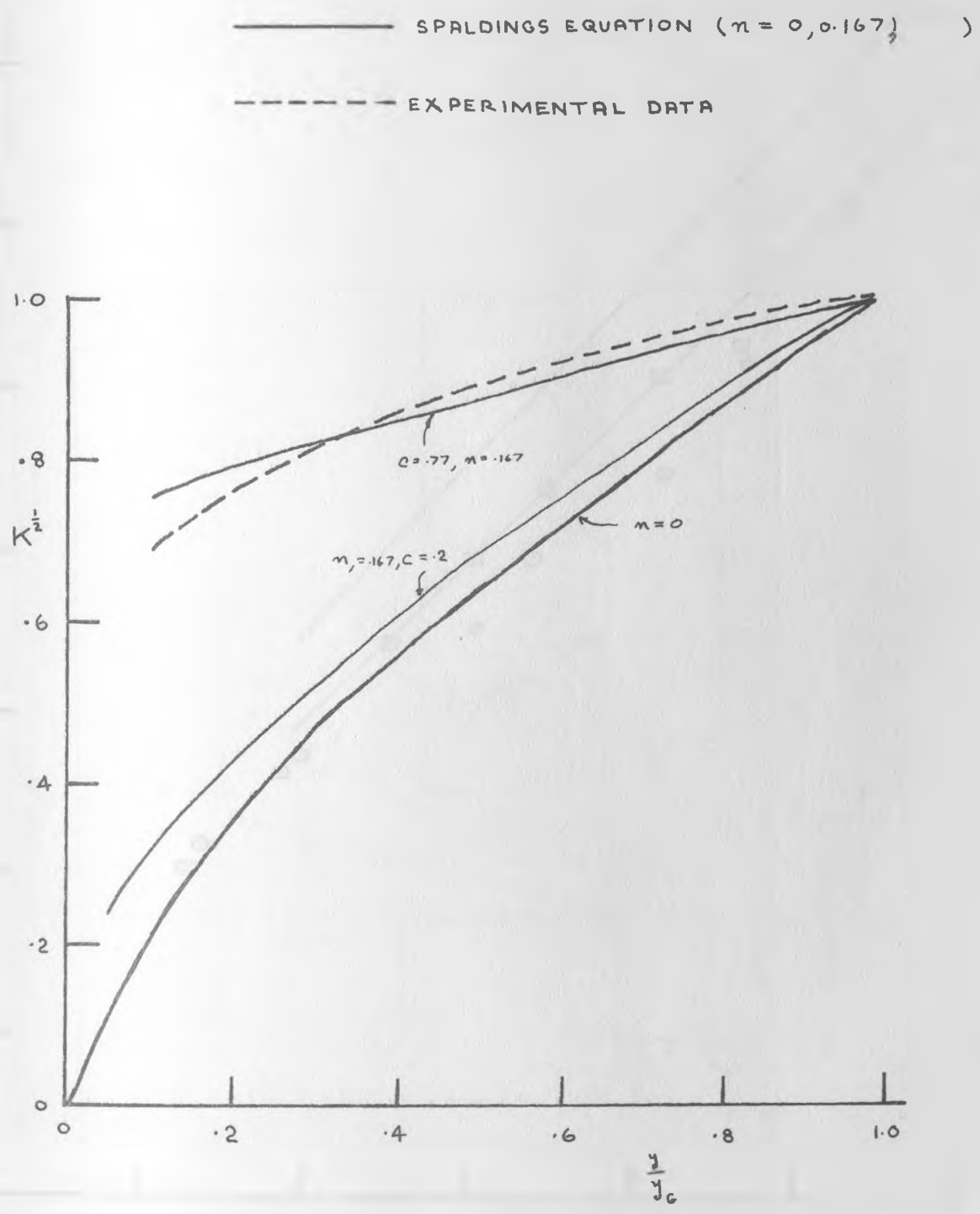
COEFFICIENTS FOR POLYNOMIAL CURVE FITTING FOR L AND G FUNCTIONS

FIG 6.3



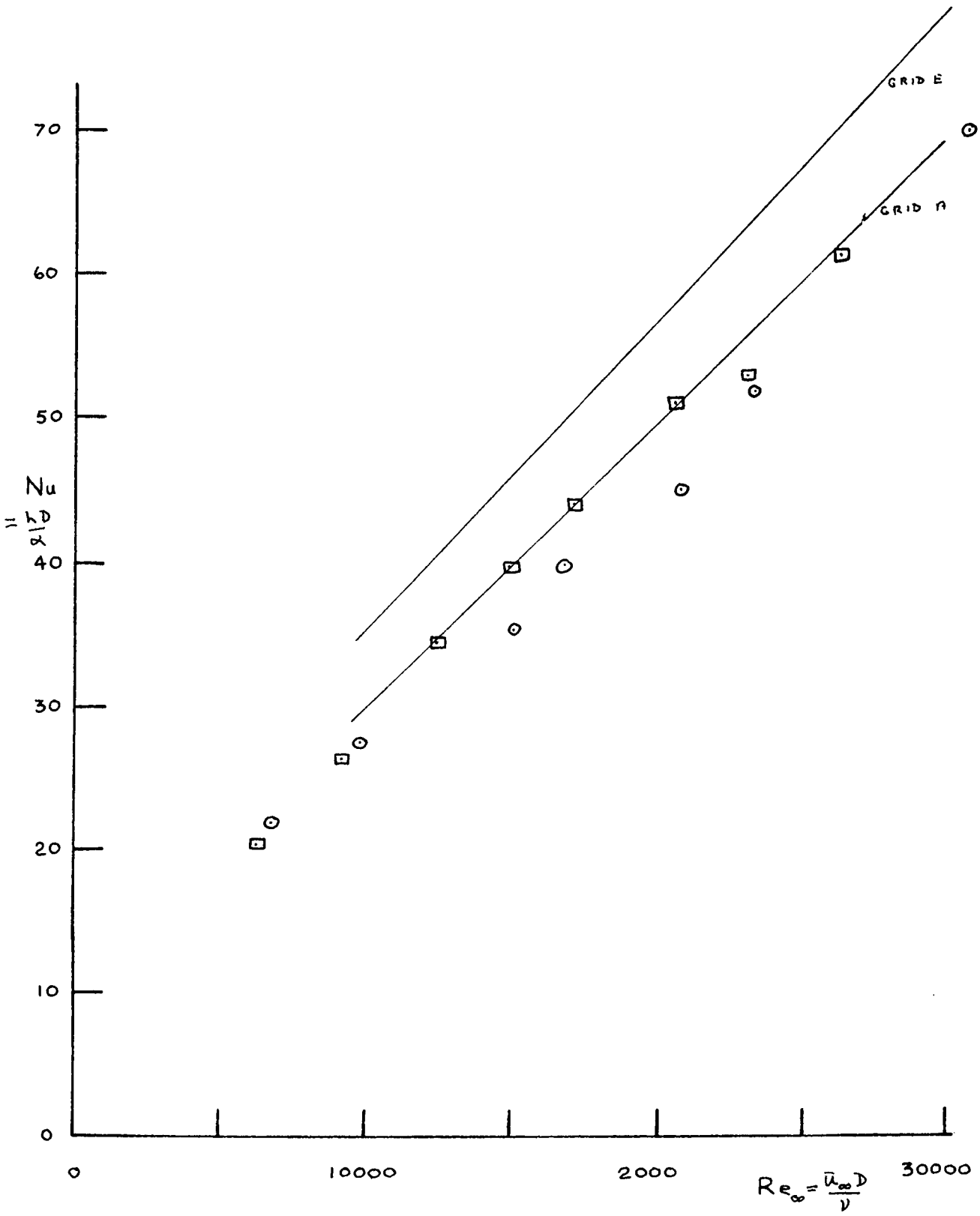
SOLUTIONS OF BRADSHAWS EQUATIONS

FIG 6.4



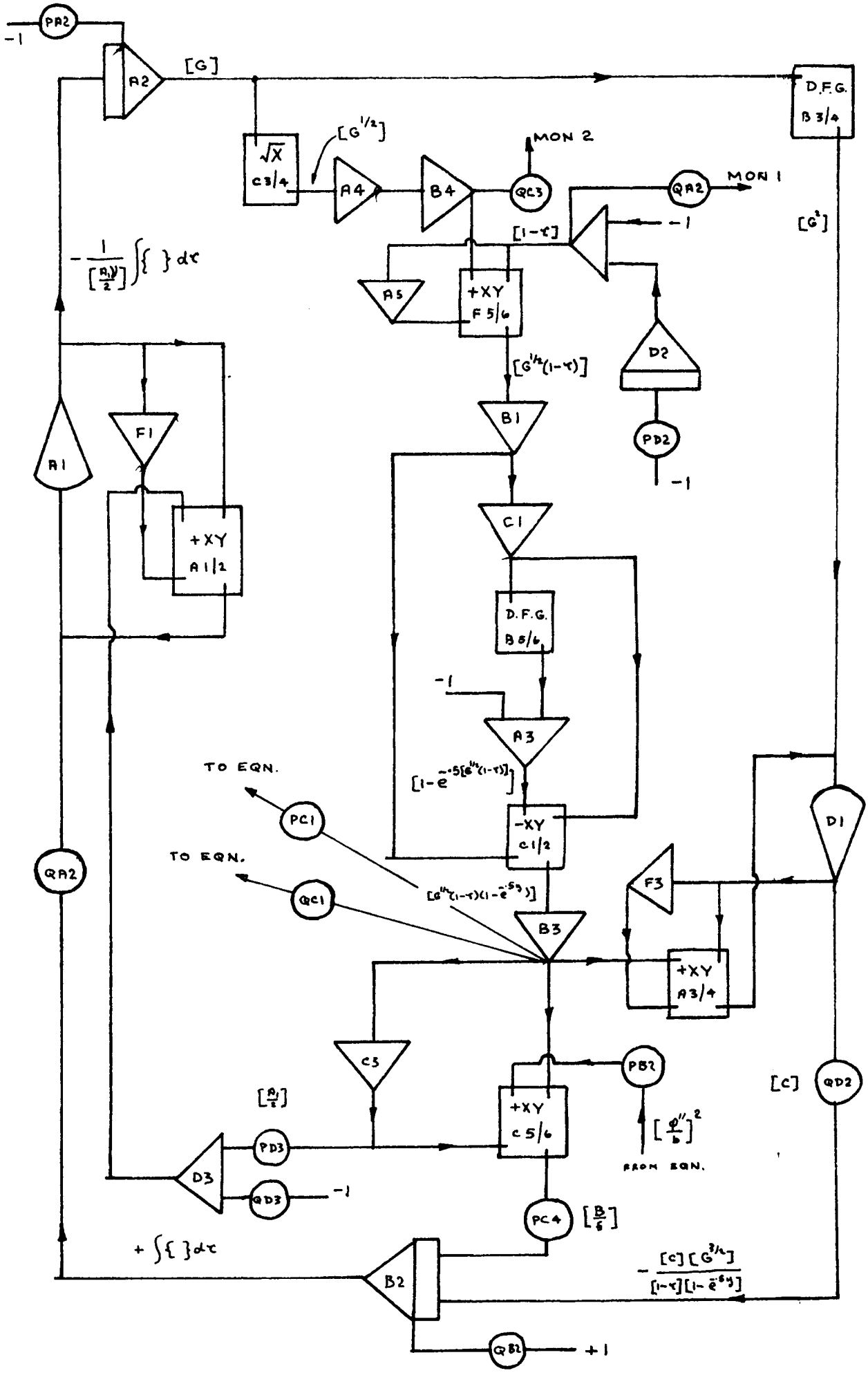
SOLUTIONS OF SPALDINGS EQUATION

FIG 6.5



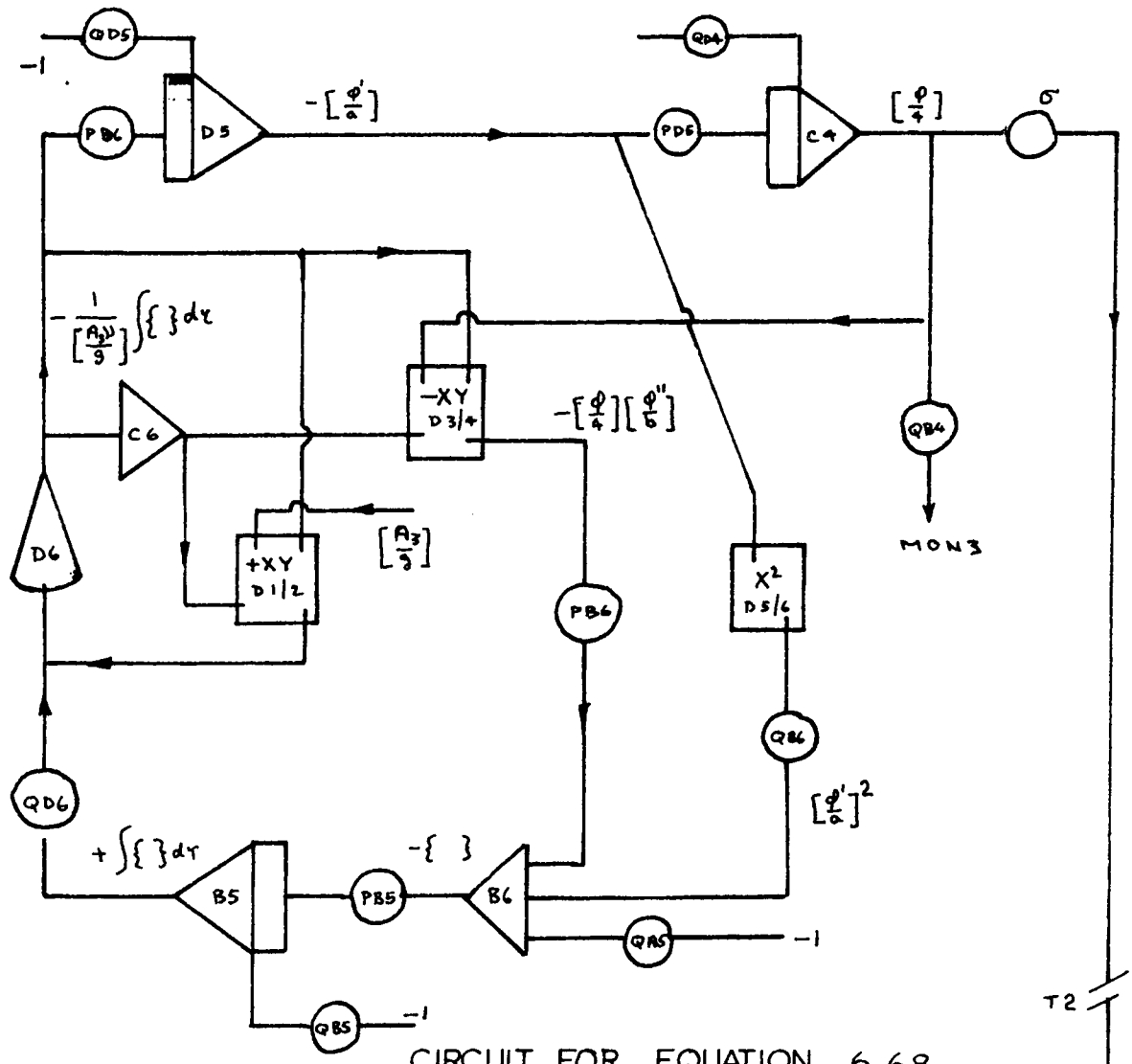
A ONE DIMENSIONAL THEORY TO PREDICT HEAT TRANSFER FROM FLUID MOTION AT REAR STAGNATION POINT

FIG 6.6

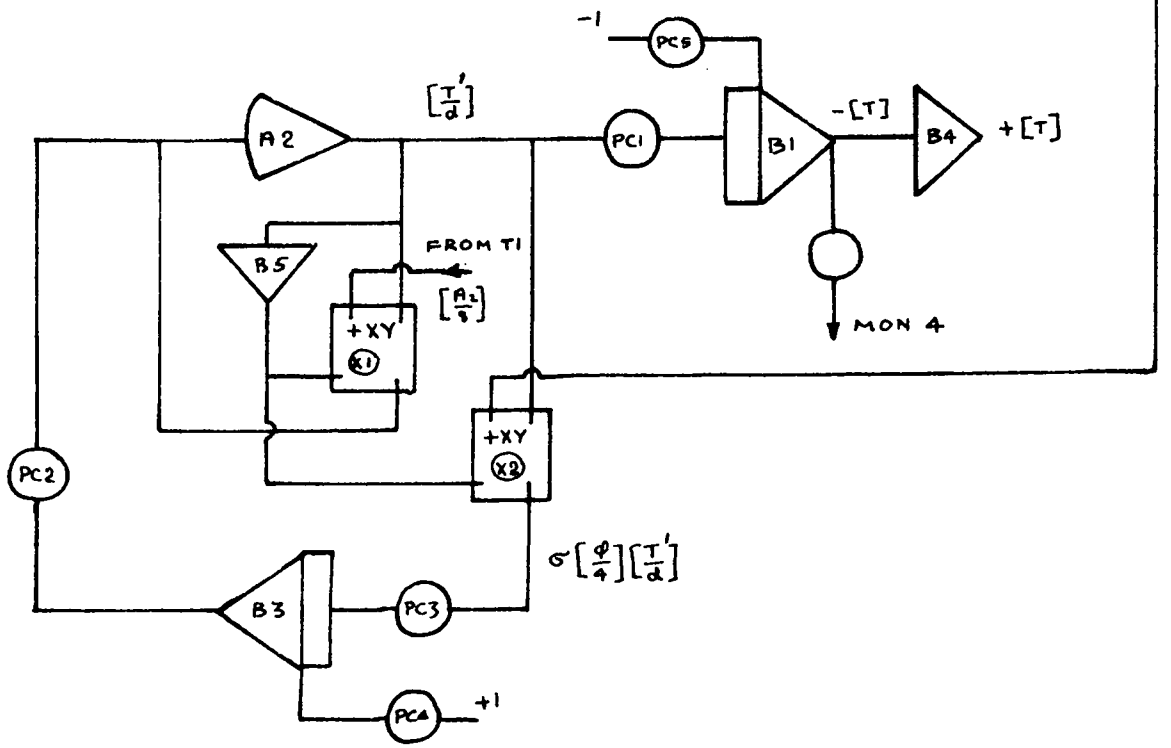


CIRCUIT FOR EQUATION 6.70

FIG 6.7a

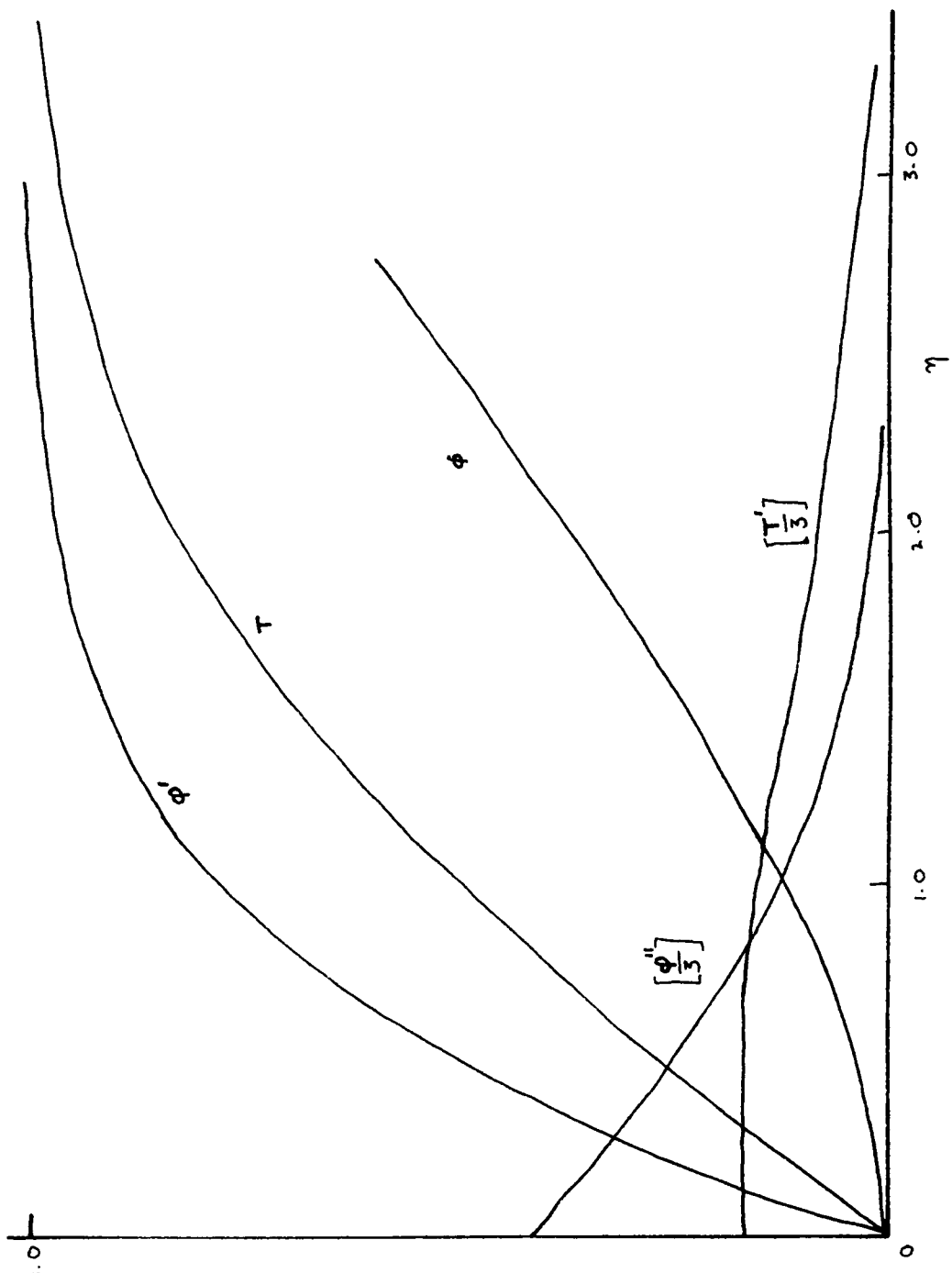


CIRCUIT FOR EQUATION 6.68



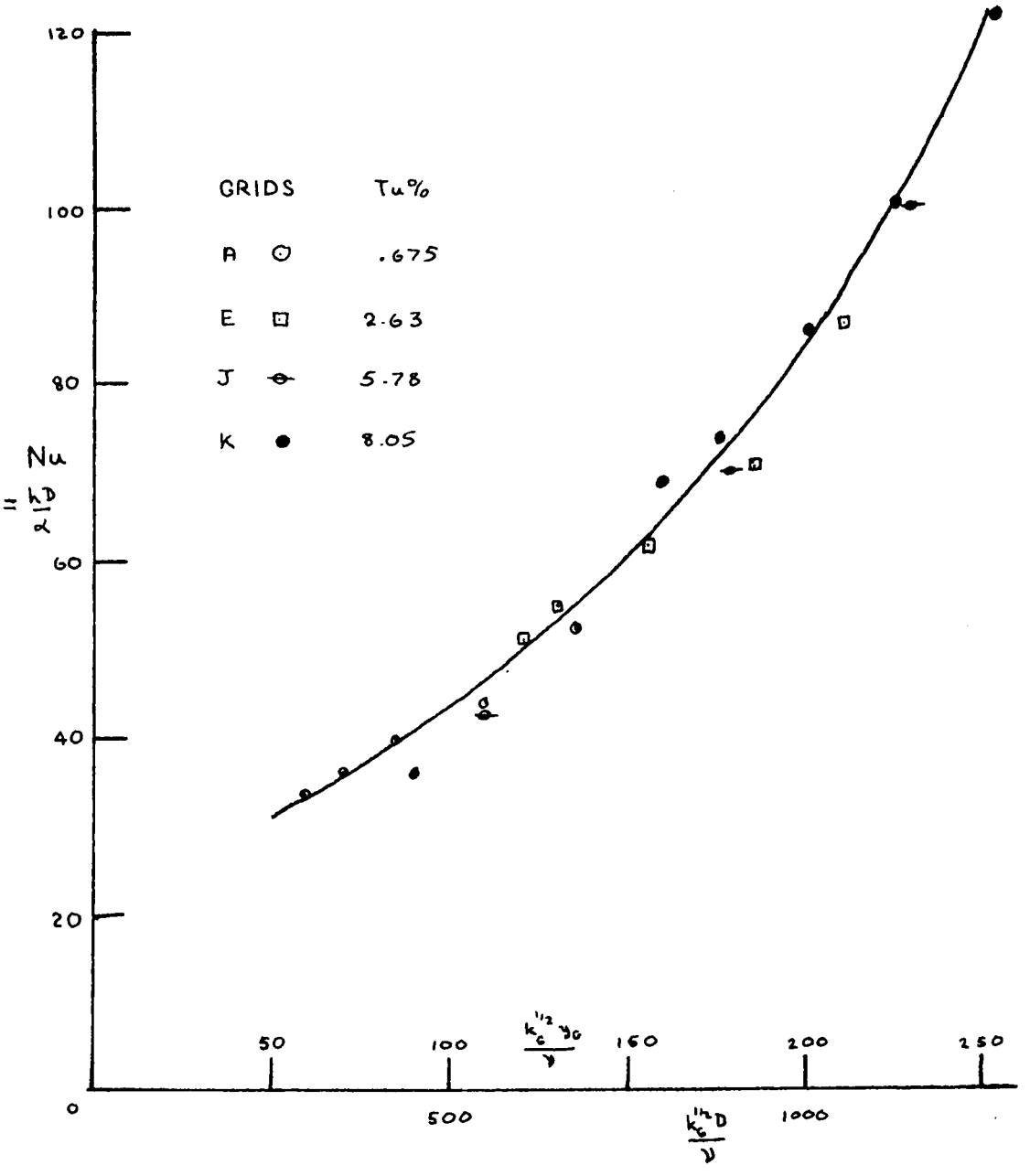
CIRCUIT FOR EQUATION 6.69

FIG 6.7 b



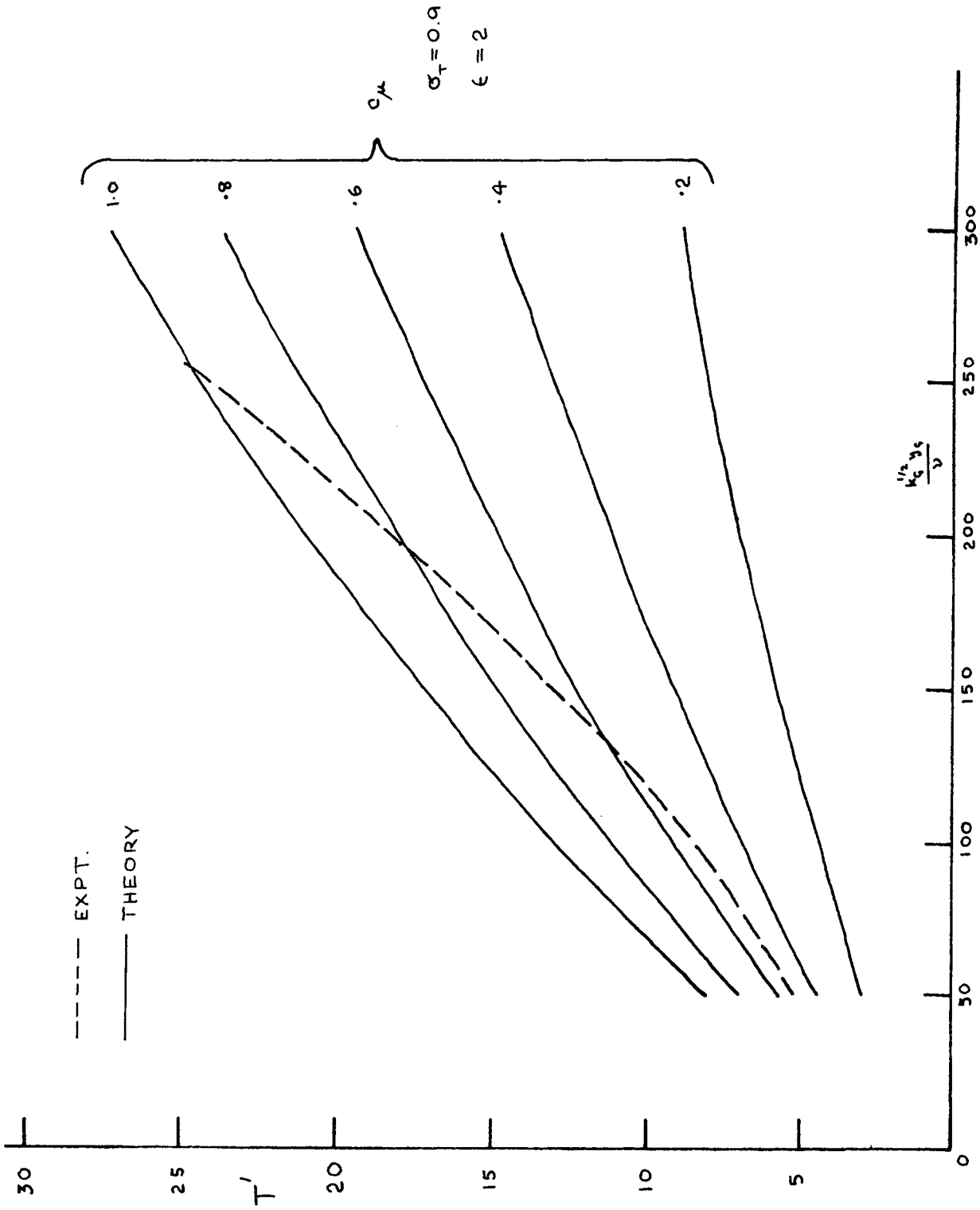
THE SOLUTION OF HIEMENZ EQUATION

FIG 6.8



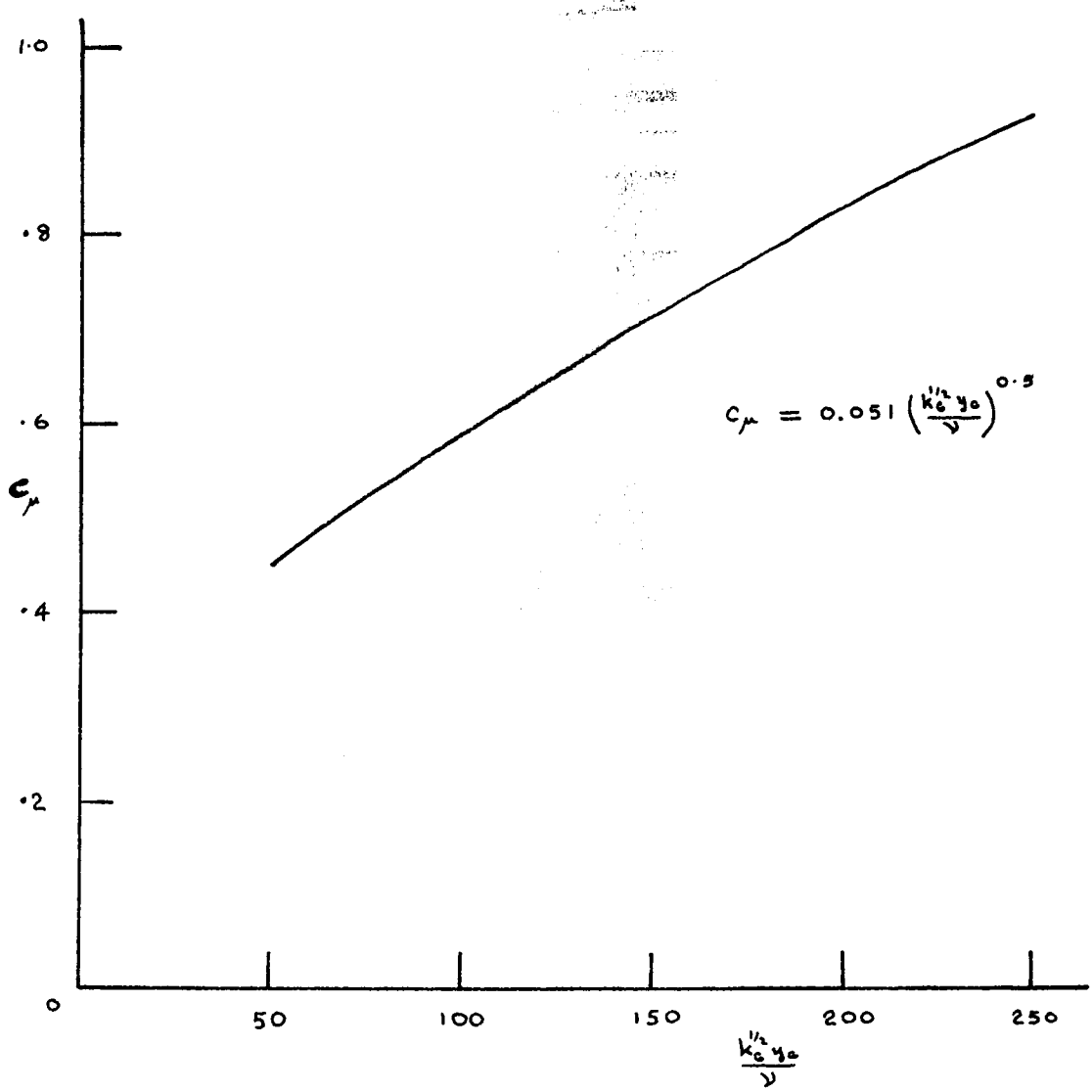
A RELATIONSHIP BETWEEN EXPERIMENTAL HEAT TRANSFER AND TURBULENCE AT REAR STAGNATION POINT

FIG 6.9



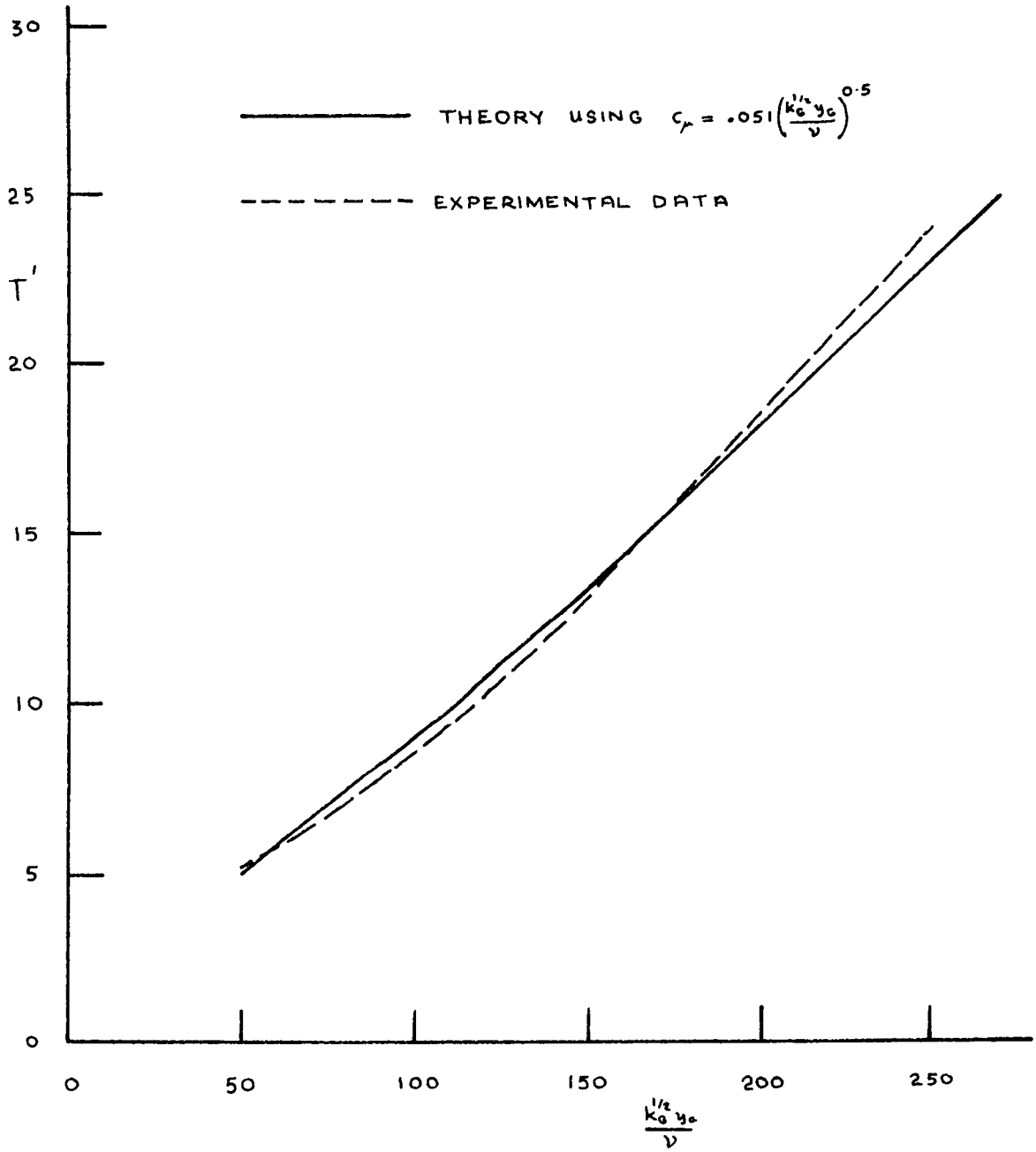
VARIATION OF HEAT TRANSFER WITH TURBULENCE AT REAR STAGNATION POINT FOR A RANGE OF C_μ

FIG 6.10



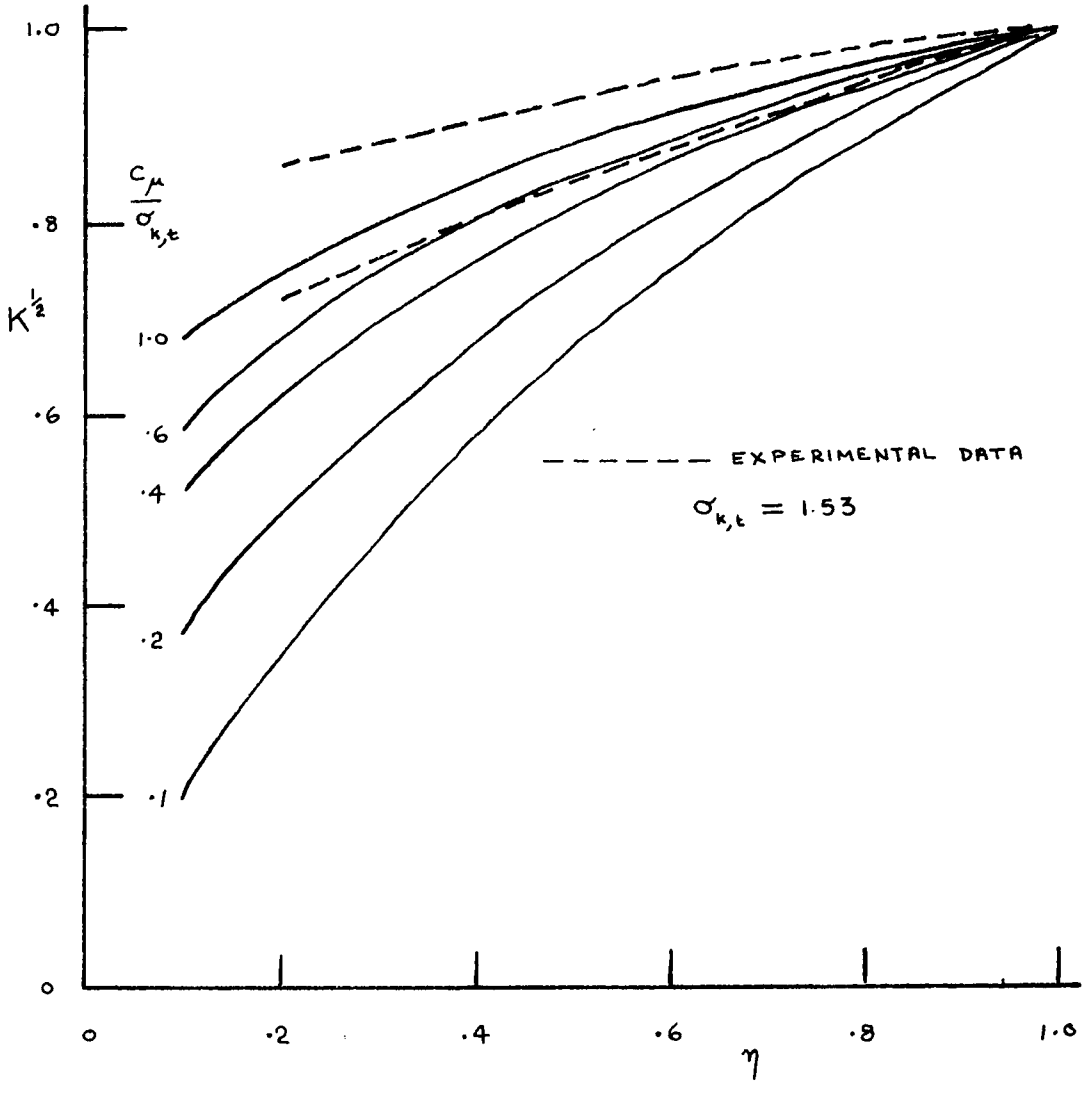
VARIATION OF C_μ WITH R_{osc}

FIG 6.11



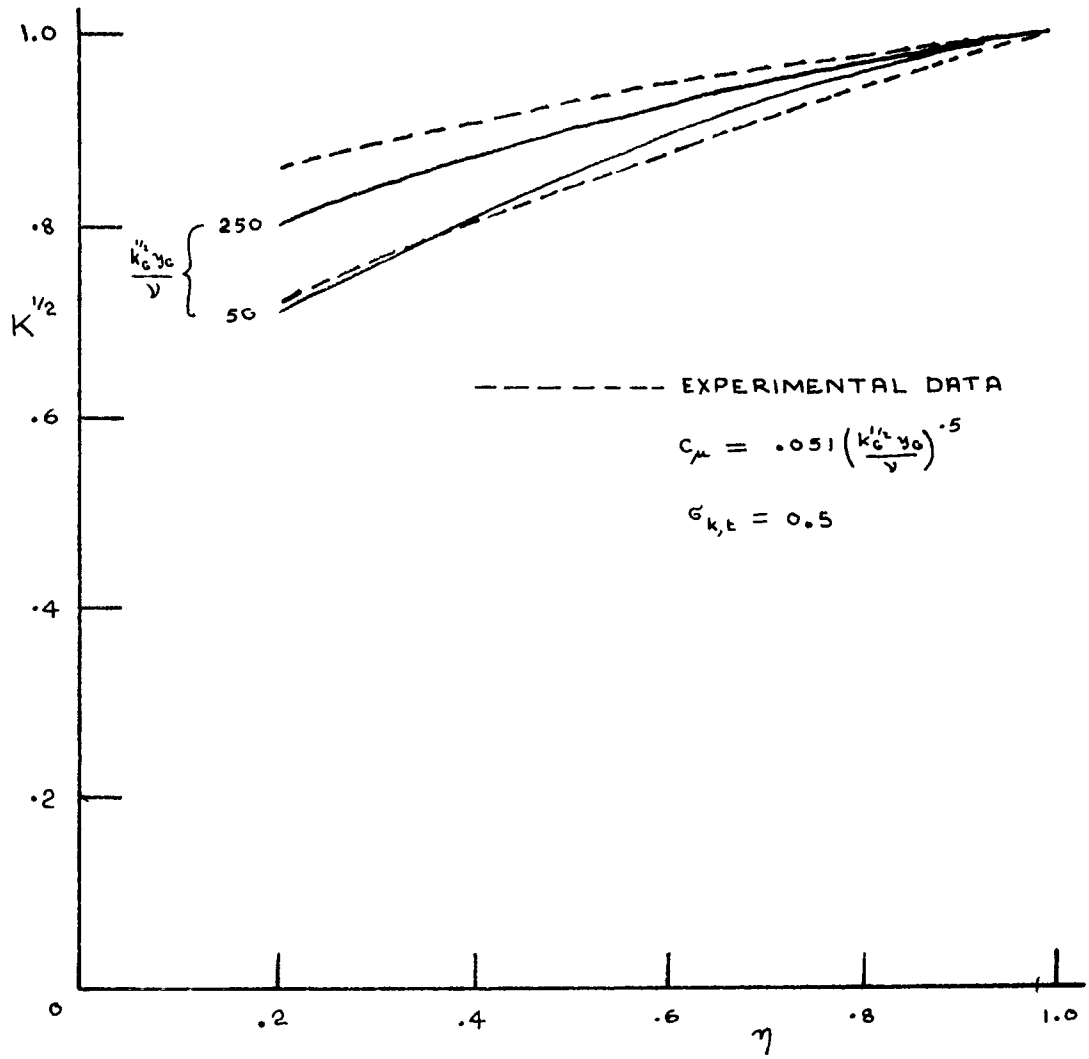
PREDICTION OF HEAT TRANSFER AT REAR STAGNATION POINT : A COMPARISON WITH EXPERIMENTAL DATA

FIG 6.12



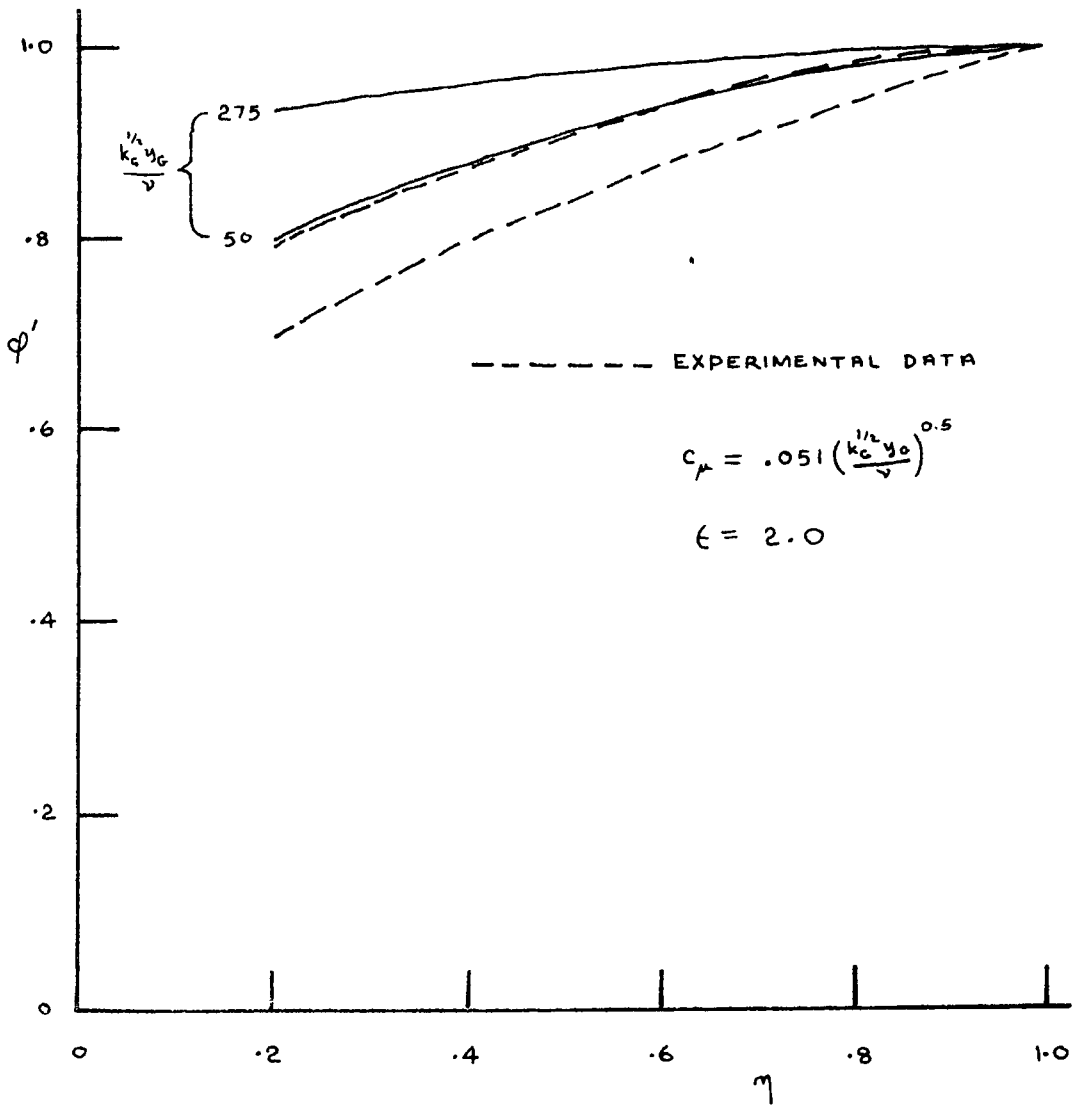
VARIATION OF TURBULENT ENERGY PROFILES WITH PARAMETER C_μ

FIG 6.13



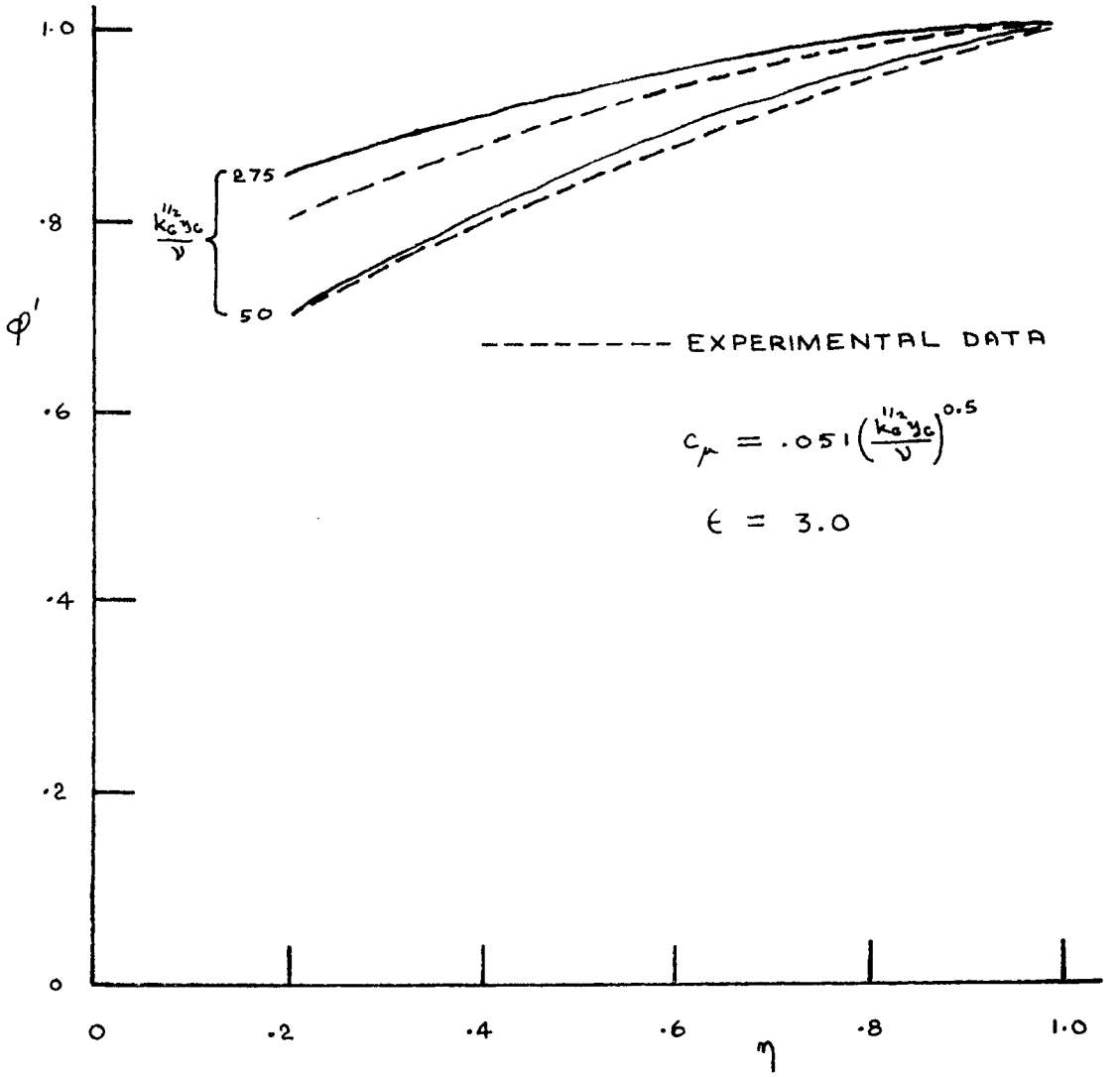
A COMPARISON OF THEORETICAL AND EXPERIMENTAL TURBULENCE PROFILES

FIG 6.14



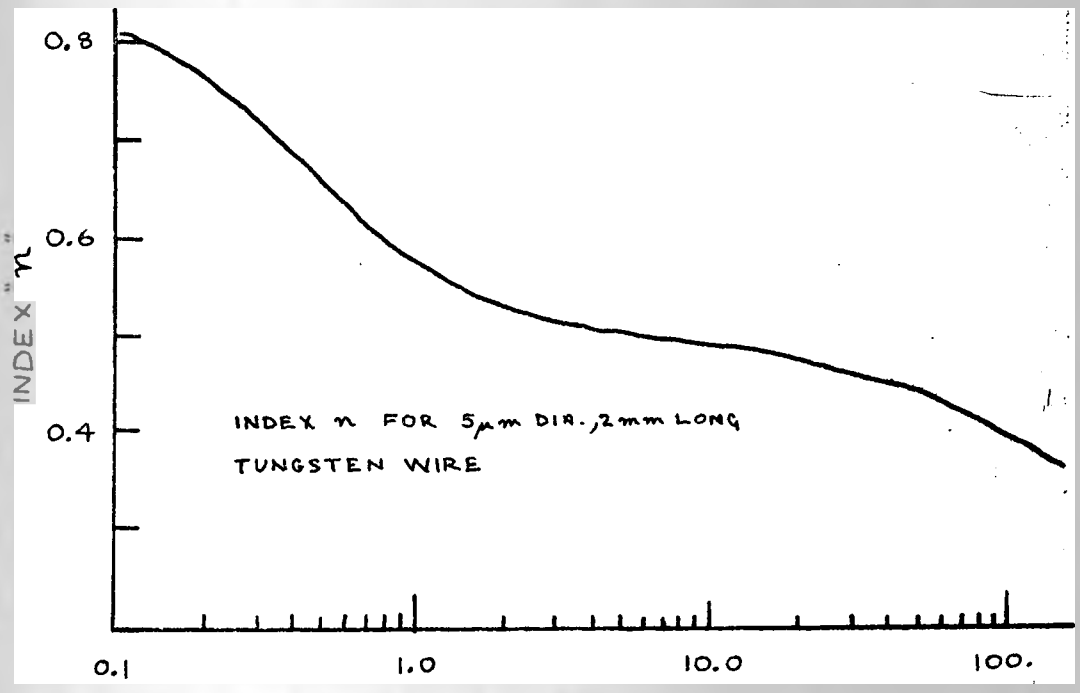
A COMPARISON OF THEORETICAL AND EXPERIMENTAL MEAN VELOCITY PROFILES FOR $\epsilon = 2.0$

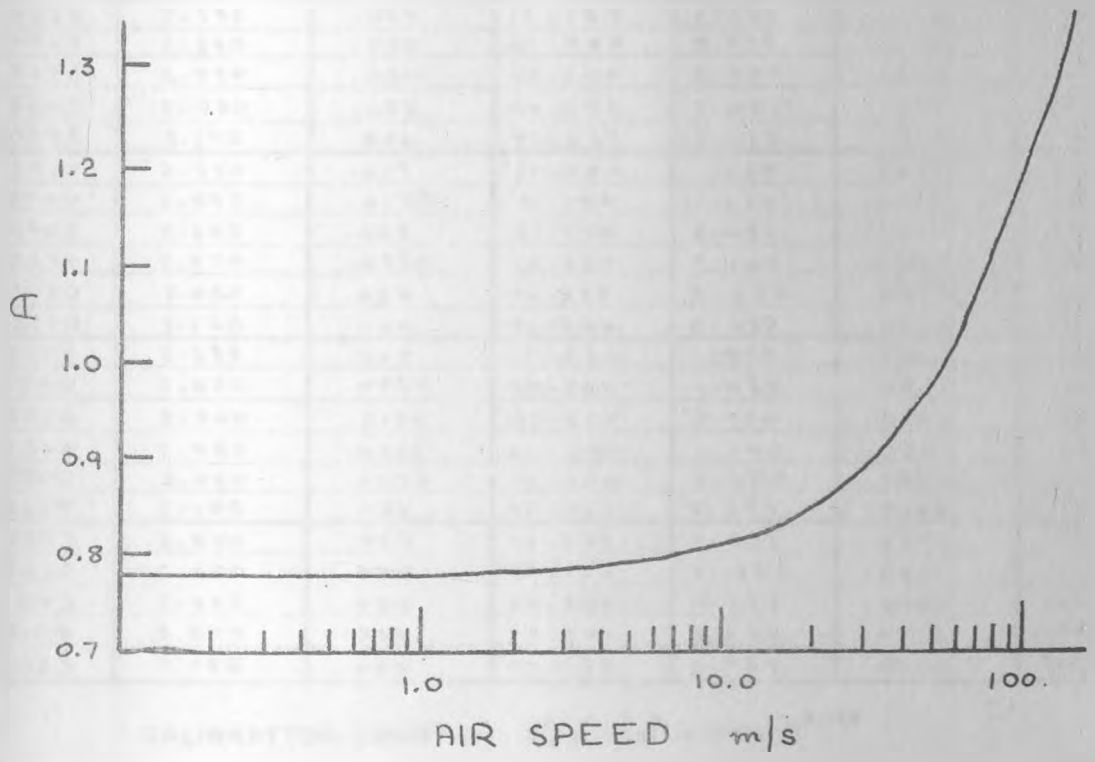
FIG 6.15



A COMPARISON OF THEORETICAL AND EXPERIMENTAL MEAN VELOCITY PROFILES FOR $\epsilon = 3.0$

FIG 6.16





TYPICAL VARIATIONS OF n AND A IN THE CONVENTIONAL FORM OF KINGS LAW

FIG A.1

Re	E_b (V)	$\sqrt{e^2}$ (V)	$\bar{u}$ (FT/S)	$\sqrt{\overline{u'^2}}$ (FT/S)	$\sqrt{\overline{u'^2}}/\bar{u}$	Re.Tu	
4019	2.355	.004	11.288	.175	.0155	64.9	A
6002	2.460	.003	16.502	.167	.0101	61.8	
9652	2.605	.003	25.885	.223	.0086	82.3	
17086	2.745	.004	42.623	.411	.0096	152.1	
23643	2.930	.0027	58.052	.341	.0054	126.0	
28957	3.040	.004	73.082	.589	.0081	219.	
35333	3.165	.0042	93.121	.729	.0078	269.8	
3940	2.350	.008	11.070	.347	.0313	128.2	E
7722	2.570	.010	23.371	.695	.0297	257.	
15261	2.810	.0125	44.183	1.316	.0248	486.6	
23643	2.990	.015	65.962	1.788	.0271	661.2	
25957	3.090	.014	80.740	2.206	.0273	815.9	
31077	3.120	.014	85.526	2.295	.0268	848.7	
3940	2.350	.0085	11.070	.368	.033	136.2	I
8451	2.580	.0095	24.072	.673	.028	248.8	
18398	2.870	.0012	50.803	1.386	.0273	512.5	
26257	3.030	.00135	71.617	1.962	.0274	725.7	
29382	3.080	.0044	79.139	2.177	.0275	805.1	
4317	2.380	.016	12.419	.745	.060	275.5	J
9490	2.630	.020	27.784	1.554	.0559	574.7	
15564	2.790	.028	42.111	2.885	.0678	1056.0	
21366	2.925	.029	57.423	3.634	.0633	1344.0	
25936	3.015	.028	69.461	3.987	.0570	1474.5	
30113	3.080	.026	79.139	4.043	.0511	1495.3	
4527	2.390	.025	12.890	1.191	.0924	440.6	K
11952	2.690	.035	32.704	3.024	.0926	1118.2	
18816	2.865	.039	50.228	4.470	.084	1653.1	
25476	2.998	.040	66.652	5.540	.0831	2048.7	
29906	3.090	.043	80.704	6.776	.084	2506.0	
36201	3.190	.044	97.532	7.887	.0809	2913.8	
4858	2.395	.029	13.129	1.398	.1065	517.6	L
9969	2.590	.039	29.787	2.815	.1136	1040.9	
18483	2.820	.050	45.244	5.347	.1182	1977.4	
26842	2.980	.052	64.596	7.051	.1092	2607.7	
40455	3.190	.056	97.532	10.038	.1029	3712.3	
3940	2.350	.013	11.070	.563	.0509	203.4	M
8740	2.595	.0175	25.150	1.275	.0507	471.5	
16903	2.845	.022	47.970	2.446	.0510	904.4	
23374	2.970	.0235	63.350	3.142	.0497	1161.9	
28030	3.065	.034	76.824	3.658	.0476	1352.9	
32110	3.140	.024	88.848	4.637	.0454	1493.0	
3524	2.335	.010	10.432	.418	.040	154.	N
9744	2.650	.0735	29.366	1.087	.037	402.1	
16074	2.840	.0155	47.417	1.710	.0361	632.3	
21366	2.965	.0165	62.584	2.190	.035	810.1	
25900	3.060	.0172	76.070	2.650	.0348	974.8	
28229	3.105	.018	83.092	2.893	.0348	1070.	
4595	2.400	.022	13.372	1.073	.0802	396.7	P
9652	2.630	.029	27.724	2.253	.0811	833.3	
21293	2.935	.034	58.686	4.323	.0737	1598.8	
28108	3.070	.036	77.594	5.524	.0712	2042.9	
35683	3.185	.038	96.639	6.769	.0700	2503.3	

CALIBRATION EQUATION $E_b^2 = 1.75^2 + 0.761\,\bar{u}^{0.488}$

EXPERIMENTAL DATA: OVERALL FREE STREAM TURBULENCE INTENSITY FOR ALL GRIDS

FIG B.1

$$E_b^2 = 1.75^2 + 0.732\,\bar{U}^{0.499}$$

	Re		E_b (v)		$\sqrt{\overline{e^2}}$ (v)		$\bar{U}$ (ft/s)		$\sqrt{\overline{u^2}}$ (ft/s)		$\sqrt{\overline{u^2}}/\bar{U}$
	9010		2.57		.00139		23.568		.109		.0046
FREQ (Hz)	20	60	80	120	200	300	420	550	630	800	1000	2000	3000
$\sqrt{\overline{e^2}}$	.0004	.0002	.00038	.0002	.00014	.0001	.00016	.0001	.00018	.00005	.00004	.00002	.00001
$\sqrt{\overline{u^2}}$	.027	.01	.012	.024	.014	.01	.007	.01	.007	.011	.003	.003	.002	.001
	14007		2.72		.00245		35.337		.400		.0113
FREQ	20	30	34	60	100	200	600	1200	2500				
$\sqrt{\overline{e^2}}$	.0007	.0006	.00125	.00035	.0005	.00025	.00013	.00005	.00000				
$\sqrt{\overline{u^2}}$	.062	.05	.111	.032	.044	.022	.011	.004	.000				
	21291		2.91		.00375		54.973		.445		.008
FREQ	20	50	85	100	160	200	300	600	1300				
$\sqrt{\overline{e^2}}$	.00113	.00089	.00016	.00036	.00009	.00016	.0005	.0005	.0000				
$\sqrt{\overline{u^2}}$	.133	.106	.019	.042	.009	.019	.006	.006	.0000				
	25750		3.0		.003		66.342		.403		.006
FREQ	20	30	60	85	100	140	200	300	400	700	1400		
$\sqrt{\overline{e^2}}$	.0008	.00125	.001	.00016	.00036	.0007	.0016	.0003	.0007	.0004	.0000		
$\sqrt{\overline{u^2}}$	.107	.168	.134	.021	.048	.009	.021	.005	.009	.005	.000		

EXPERIMENTAL DATA: FREE STREAM TURBULENCE SPECTRA FOR GRID A

FIG B.2

$$E_b^2 = 1.75^2 + 0.732\,\bar{U}^{0.499}$$

	Re		E_b (v)			$\sqrt{e^2}$ (v)		$\bar{U}$ (FT/S)			$\sqrt{u^2}$ (FT/S)		$\sqrt{u^2}/\bar{U}$
	11036		2.67			.016		31.07			1.308		.0421
FREQ (Hz)	20	60	100	200	300	600	1000	2000	3000	6000	11000		
$\sqrt{e^2}$	.0017	.0016	.0022	.0028	.003	.003	.0028	.0022	.0019	.0013	.0006		
$\sqrt{u^2}$	.123	.129	.164	.193	.245	.245	.231	.193	.154	.105	.046		
	18115		2.85			.0178		48.165			1.718		.0357
FREQ	20	60	100	200	300	600	800	2000	3000	6000	11000		
$\sqrt{e^2}$	.0018	.002	.0025	.003	.0035	.0035	.0032	.0024	.0016	.001	.0004		
$\sqrt{u^2}$	.172	.217	.274	.326	.376	.376	.348	.257	.174	.109	.043		
	22750		2.95			.014		59.854			1.782		.0298
FREQ	20	60	100	200	400	700	1000	2000	4000	10000			
$\sqrt{e^2}$	.0016	.0018	.0022	.0025	.0028	.0026	.0024	.0017	.0011	.0002			
$\sqrt{u^2}$	.201	.226	.281	.316	.354	.326	.301	.188	.143	.032			
	26526		3.04			.0132		71.867			1.871		.026
FREQ	20	60	100	200	250	400	700	1400	2000	4000	6000		
$\sqrt{e^2}$	.0018	.002	.0025	.0025	.0028	.0025	.0022	.0016	.001	.0004	.0001		
$\sqrt{u^2}$	.255	.283	.357	.357	.4	.357	.317	.201	.142	.051	.017		

EXPERIMENTAL DATA : FREE STREAM TURBULENCE SPECTRA FOR GRID E

FIG B.3

$$E_b^2 = 1.75^2 + 0.732\,\bar{U}^{0.499}$$

	Re	E_b (v)	$\sqrt{e^2}$ (v)	$\bar{U}$ (ft/s)	$\sqrt{u^2}$ (ft/s)	$\sqrt{u^2}/\bar{U}$
	9378	2.58	.0162	24.259	.991	.0409
FREQ (Hz)	20 60 100 200 300	600 1000	2000 4000 8000			
$\sqrt{e^2}$	.0012 .0018 .0022 .0026 .0026	.0024 .002	.0016 .0018	.0007		
$\sqrt{u^2}$	.084 .126 .156 .181 .181	.168 .14	.112 .078	.05		
	16451	2.79	.0355	41.918	3.524	.0841
FREQ	20 60 100 200 300	600 1000	2000 4000 8000	10000		
$\sqrt{e^2}$	.0016 .002 .0024 .0024 .0028	.0024 .0018	.0013 .0009	.0005 .0003		
$\sqrt{u^2}$	.352 .496 .596 .596 .7	.596 .447	.318 .223	.124 .069		
	22824	2.92	.0335	56.167	4.03	.0718
FREQ	20 60 100 200 300	600 1000	2000 3000	6000 12000		
$\sqrt{e^2}$	.004 .005 .0063 .006 .0063	.005 .004	.003 .0023	.001 .000		
$\sqrt{u^2}$	.481 .602 .758 .722 .758	.602 .481	.361 .271	.12 .000		
	28671	3.04	.063	71.867	8.928	.1242
FREQ	20 50 100 200 250	400 600	1000 2000	3000 6000		
$\sqrt{e^2}$	.0063 .0115 .014 .0125 .0135	.0105 .0089	.0063 .0013	.0019 .0005		
$\sqrt{u^2}$	.893 1.63 1.984 1.771 1.913	1.488 1.261	.893 .184	.255 .071		

EXPERIMENTAL DATA : FREE STREAM TURBULENCE SPECTRA FOR GRID J

FIG B.4

$$E_b^2 = 1.75^2 + 0.732\,\bar{U}^{0.499}$$

	Re		E_b (v)		$\sqrt{e'^2}$ (v)		$\bar{U}$ (FT/S)		$\sqrt{u'^2}$ (FT/S)		$\sqrt{u'^2}/\bar{U}$
	9905		2.59		.041		24.964		2.916		.1167
FREQ (Hz)	20	60	75	100	200	300	600	1000	2000	4000	6000
$\sqrt{e'^2}$	.0056	.01	.0125	.01	.0075	.007	.005	.004	.0025	.001	.0005
$\sqrt{u'^2}$	.398	.711	.889	.711	.533	.501	.355	.284	.179	.071	.032
	17254		2.79		.0855		41.918		5.46		.1307
FREQ	20	60	100	200	300	600	1000	2000	4000	8000	14000
$\sqrt{e'^2}$	.005	.01	.014	.0115	.01	.008	.0055	.004	.00225	.001	.000
$\sqrt{u'^2}$	.496	.993	1.39	1.142	.993	.794	.546	.397	.223	.099	.000
	22898		2.91		.053		54.973		6.286		.1144
FREQ	20	60	100	200	400	800	1600	3000	6000	12000	
$\sqrt{e'^2}$	.0045	.0089	.0113	.0125	.0095	.0075	.005	.004	.0025	.001	
$\sqrt{u'^2}$	.534	1.056	1.334	1.483	1.127	.89	.593	.474	.297	.119	
	29428		3.04		.055		71.869		7.794		.1085
FREQ	20	60	100	200	300	500	1000	2000	4000	8000	10000	20000
$\sqrt{e'^2}$	.0056	.008	.01	.014	.0113	.01	.0075	.006	.004	.0025	.002	.0013
$\sqrt{u'^2}$	.794	1.134	1.417	1.984	1.594	1.417	1.063	.85	.567	.354	.283	.177

EXPERIMENTAL DATA : FREE STREAM TURBULENCE SPECTRA FOR GRID K

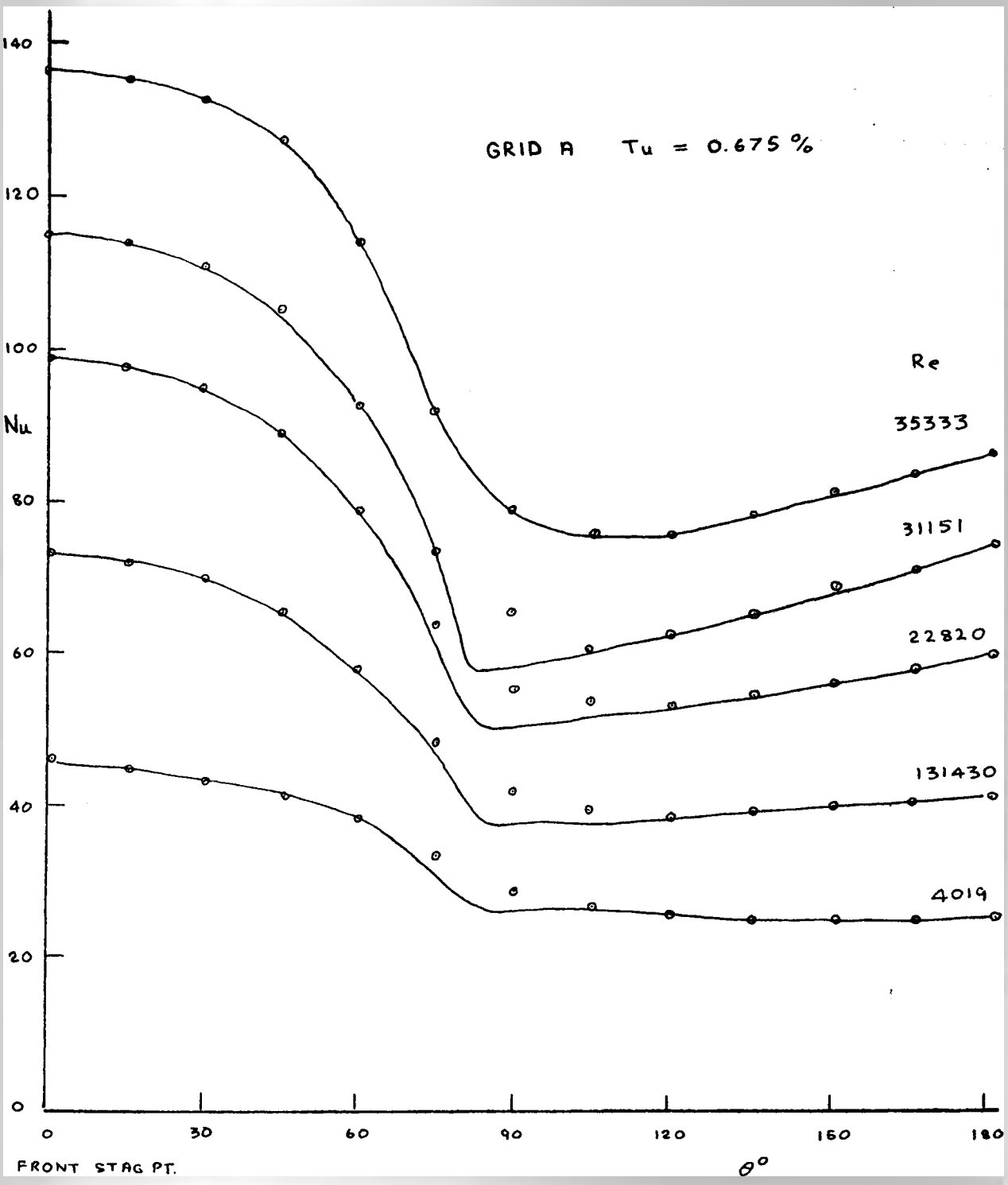
FIG B.5

$$E_b^2 = 1.75^2 + 0.732\,\bar{U}^{0.499}$$

	Re		E_b (V)		$\sqrt{e'^2}$ (V)		$\bar{U}$ (FT/S)		$\sqrt{\overline{u'^2}}$ (FT/S)		$\sqrt{\overline{u'^2}}/\bar{U}$
	10725		2.59		.063		24.964		4.478		.1794
FREQ (Hz)	20	60	100	200	300	600	900	1600	3000	6000	10000
$\sqrt{\overline{e'^2}}$	.005	.0089	.0135	.016	.0125	.0113	.0095	.0075	.0055	.004	.0025
$\sqrt{\overline{u'^2}}$	.355	.633	.96	1.137	.889	.8	.675	.533	.391	.284	.178
	17718		2.78		.063		40.933		6.158		.1504
FREQ	20	60	100	200	300	600	1200	2000	4000	8000	14000
$\sqrt{\overline{e'^2}}$	.0075	.01	.0125	.0126	.0113	.0095	.0075	.005	.0035	.002	.001
$\sqrt{\overline{u'^2}}$	.689	.977	1.222	1.222	1.1	.929	.689	.489	.342	.195	.098
	23265		2.89		.056		52.63		6.454		.1226
FREQ	20	60	100	200	400	800	1600	3000	6000	10000	
$\sqrt{\overline{e'^2}}$	.005	.0089	.013	.0115	.0089	.0075	.005	.0035	.0018	.001	
$\sqrt{\overline{u'^2}}$	.576	1.026	1.498	1.325	1.026	.813	.576	.403	.207	.115	
	29313		3.01		.05		67.701		6.809		.1006
FREQ	20	60	90	200	300	600	1000	2000	4000	6000	
$\sqrt{\overline{e'^2}}$	.005	.01	.0125	.008	.007	.0055	.0045	.003	.001	.0005	
$\sqrt{\overline{u'^2}}$	.681	1.362	1.702	1.089	.953	.749	.613	.409	.136	.068	

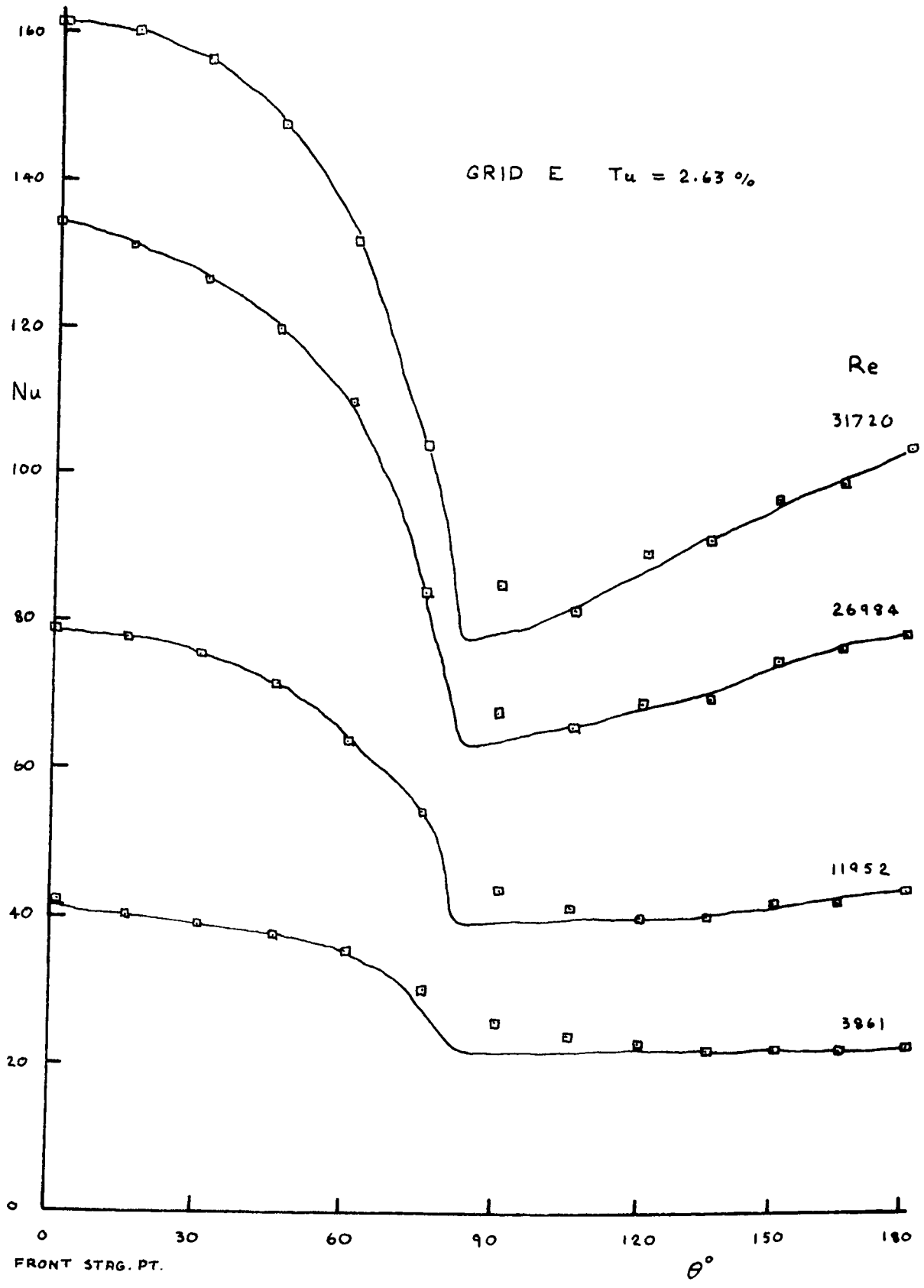
EXPERIMENTAL DATA : FREE STREAM TURBULENCE SPECTRA FOR GRID L

FIG B.6



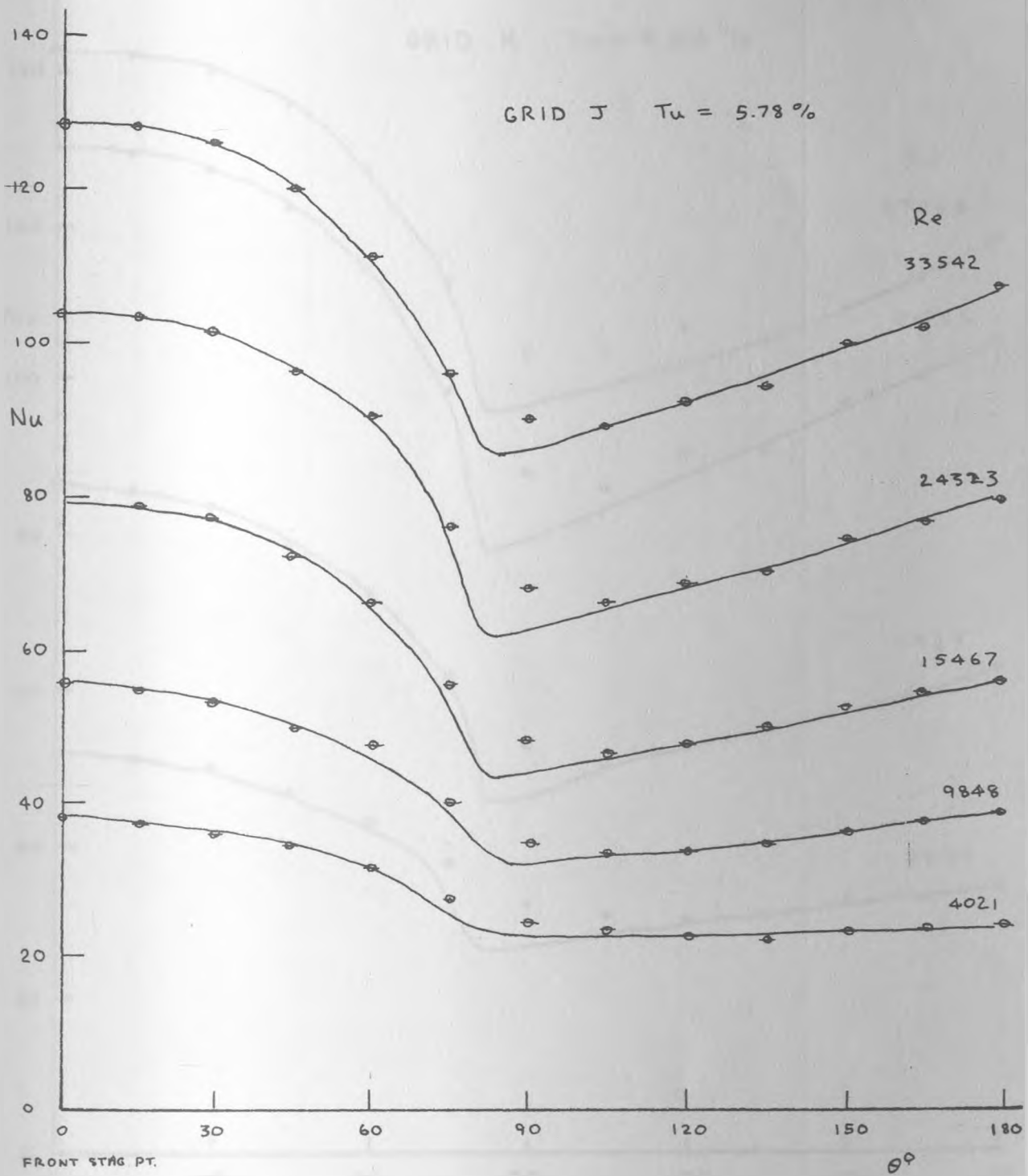
EFFECT OF FREESTREAM TURBULENCE ON LOCAL HEAT TRANSFER

FIG B.7



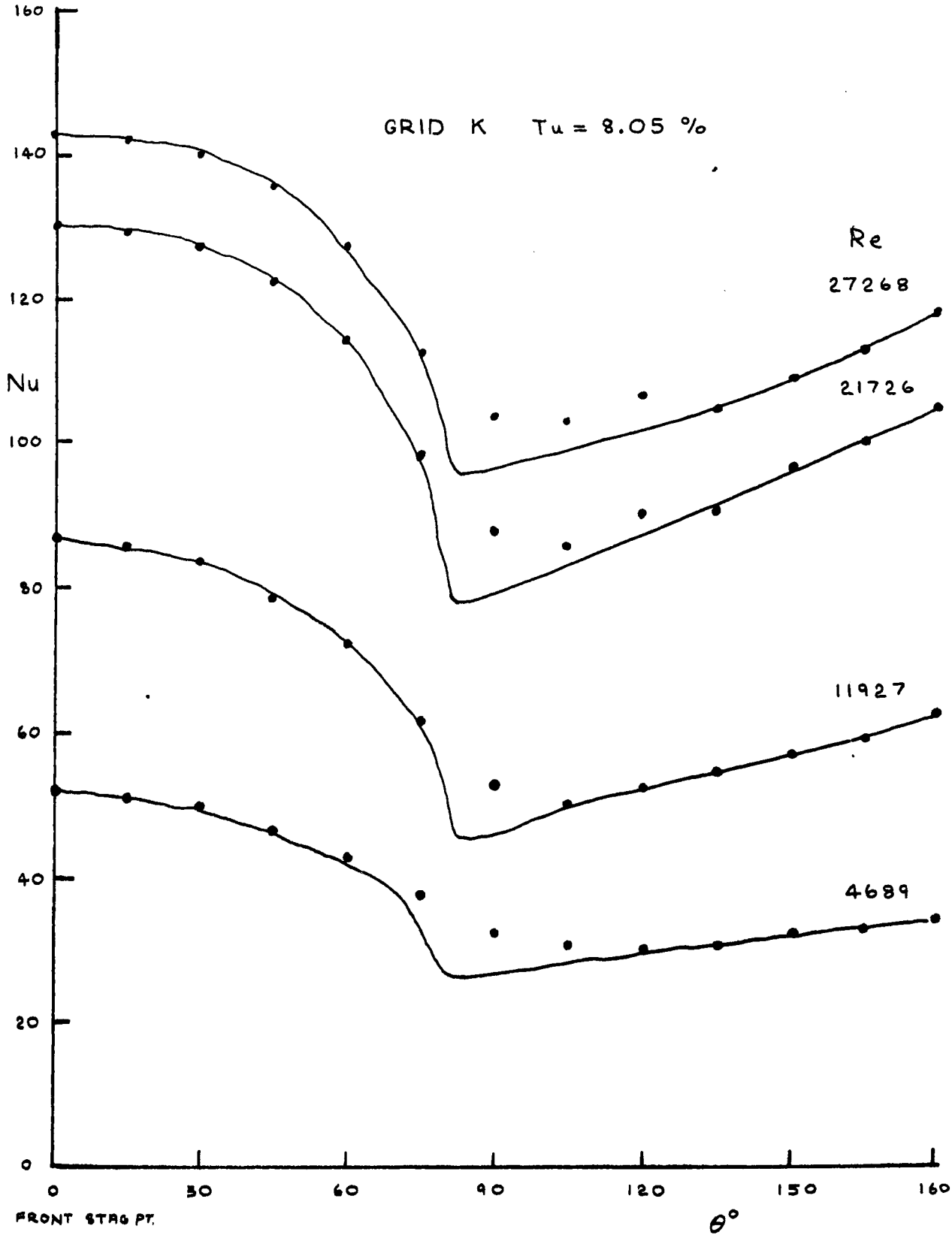
EFFECT OF FREE STREAM TURBULENCE ON LOCAL HEAT TRANSFER

FIG B.8



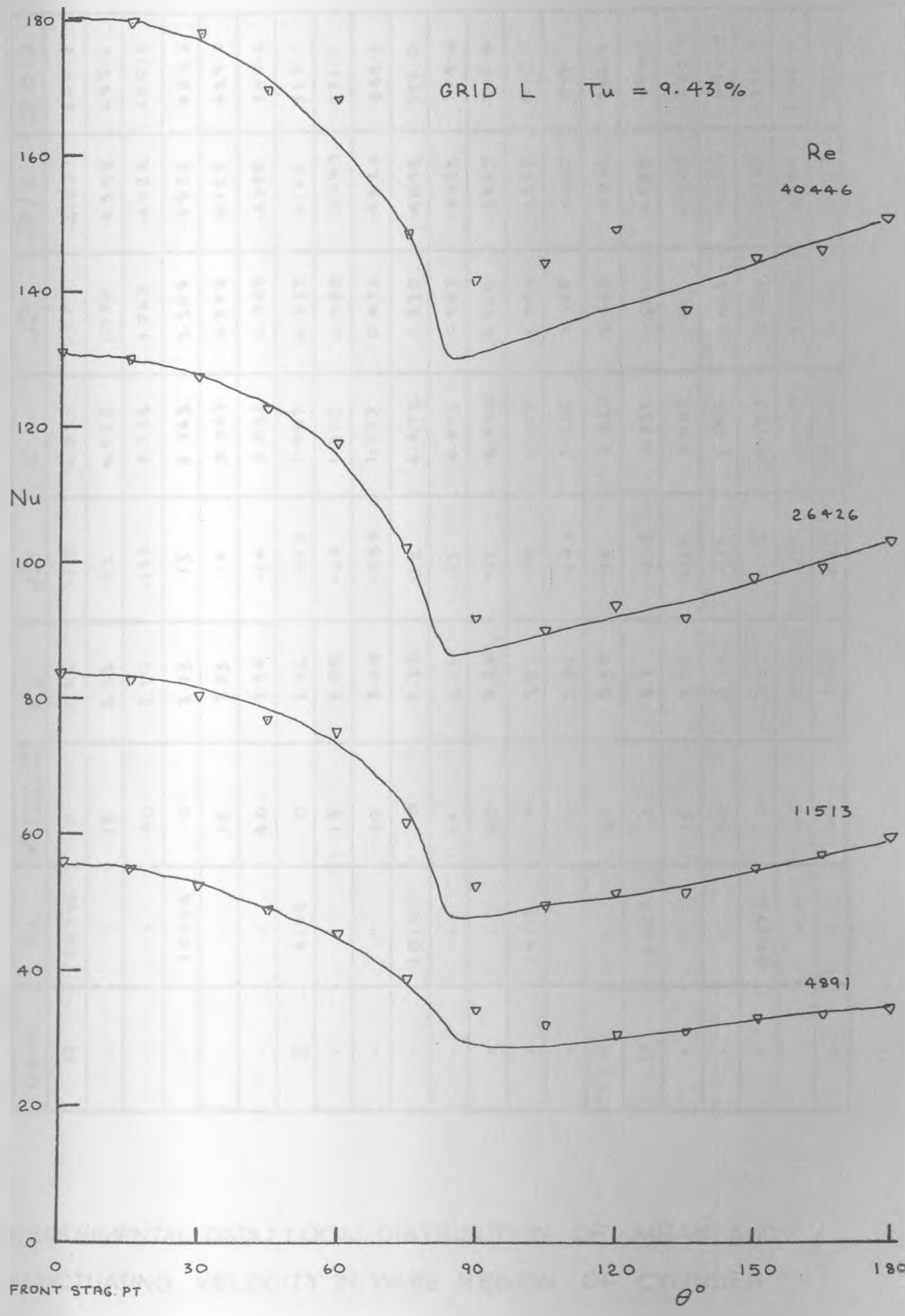
EFFECT OF FREESTREAM TURBULENCE ON LOCAL HEAT TRANSFER

FIG B.9



EFFECT OF FREE STREAM TURBULENCE ON LOCAL HEAT TRANSFER

FIG B.10



EFFECT OF FREE STREAM TURBULENCE ON LOCAL HEAT TRANSFER

FIG B.11

GRID	Re	θ° (MEAS. FROM AERO STN.)	E_b	$\sqrt{\overline{e^2}}$	$\bar{u}$	$\sqrt{\overline{u^2}}$	$\sqrt{\overline{u^2}}/\bar{u}$	$\sqrt{\overline{u^2}}\,D/\nu$
A	20786	0	2.22	.115	4.025	1.677	.4167	655.2
"	"	15	2.22	.12	4.025	1.750	.4348	683.6
"	"	40	2.20	.125	3.738	1.767	.4726	690.1
"	30924	0	2.33	.13	5.763	2.209	.3932	862.6
"	"	15	2.33	.14	5.763	2.378	.4127	929.0
"	"	40	2.34	.14	5.934	2.408	.4058	940.6
I	9199	0	2.06	.077	1.989	0.832	.4185	325.1
"	"	15	2.05	.09	1.882	0.950	.5049	371.1
"	"	40	2.04	.085	1.777	0.876	.4928	342.1
"	20147	0	2.25	.12	4.473	1.830	.4092	715.0
"	"	15	2.25	.13	4.473	1.983	.4433	774.6
"	"	40	2.28	.12	4.940	1.909	.3865	745.8
"	29113	0	2.37	.14	6.459	2.496	.3865	975.1
"	"	15	2.36	.145	6.282	2.555	.4067	998.1
"	"	40	2.39	.14	6.820	2.555	.3746	997.9
K	10557	0	2.2	.115	3.738	1.625	.4348	634.9
"	"	15	2.19	.119	3.598	1.655	.4599	646.4
"	"	40	2.19	.119	3.598	1.655	.4599	646.4
"	30476	0	2.51	.165	9.157	3.413	.3727	1333.0
"	"	15	2.52	.17	9.365	3.550	.3790	1386.6
"	"	40	2.54	.185	9.786	3.936	.4022	1537.4

EXPERIMENTAL DATA: LOCAL DISTRIBUTION OF MEAN AND FLUCTUATING VELOCITY IN WAKE REGION OF CYLINDER

FIG B.12

$$E_b^2 = 1.75^2 + .582\ \bar{U}^{.666}$$

Re	Y (IN)	E_b (V)	$\sqrt{e^2}$ (V)	$\bar{U}_G$ (FT/S)	$\sqrt{\bar{u}^2}$ (FT/S)	$\sqrt{\bar{u}^2}/\bar{U}_c$	$\sqrt{\bar{u}^2}D/\nu$
8821	.110	1.99	.069	1.735	.749	.4317	292
	.090	1.96	.067	1.420	.680	.4791	"
	.070	1.94	.064	1.222	.618	.5058	"
16076	.130	2.16	.110	3.877	1.562	.4028	610
	.070	2.13	.095	3.459	1.298	.3754	"
	.040	2.11	.095	3.189	1.264	.3962	"
	.030	2.07	.092	2.672	1.154	.4317	"
21131	.070	2.21	.110	4.608	1.655	.3591	645
	.050	2.19	.105	4.311	1.545	.3583	"
	.030	2.15	.102	3.736	1.43	.3829	"
	.020	2.12	.100	3.323	1.349	.4058	"
27094	.100	2.29	.125	5.862	2.038	.3476	795
	.070	2.26	.118	5.380	1.869	.3474	"
	.040	2.23	.115	4.912	1.767	.3597	"
			.112				

EXPERIMENTAL DATA: MEAN AND FLUCTUATING VELOCITY PROFILES AT REAR STAGNATION POINT WITH GRID A

FIG B.13

$$E_b^2 = 1.75^2 + .582\ \bar{U}^{.666}$$

Re	Y (IN)	E_b (V)	$\sqrt{e^2}$ (V)	$\bar{U}_0$ (FT/S)	$\sqrt{u^2}$ (FT/S)	$\sqrt{u^2}/\bar{U}_0$	$\sqrt{u^2}D/\nu$
26270	.100	2.38	.138	7.389	2.430	.3289	948
"	.070	2.36	.133	7.040	2.305	.3274	"
"	.050	2.34	.13	6.696	2.215	.3308	"
"	.020	2.29	.13	5.862	2.119	.3615	"
22300	.100	2.32	.127	6.358	2.127	.3345	830
"	.050	2.29	.122	5.862	1.989	.3392	"
"	.030	2.27	.118	5.539	1.887	.3407	"
16977	.110	2.26	.123	5.386	1.948	.3621	760
"	.080	2.24	.115	5.067	1.785	.3524	"
"	.050	2.22	.108	4.759	1.642	.3450	"
"	.030	2.19	.107	4.311	1.574	.3651	"
11188	.100	2.15	.100	3.736	1.402	.3754	546
"	.070	2.13	.095	3.459	1.298	.3752	"
"	.040	2.11	.090	3.189	1.157	.3629	"
"	.030	2.095	.087	2.992	1.133	.3786	"

EXPERIMENTAL DATA: MEAN AND FLUCTUATING VELOCITY PROFILES AT REAR STAGNATION POINT WITH GRID E

FIG B.14

$$E_b^2 = 1.75^2 + .582\,\bar{U}^{.666}$$

Re	Y (in)	E_b (v)	$\sqrt{\overline{e^2}}$ (v)	$\bar{U}_G$ (ft/s)	$\sqrt{\overline{u^2}}$ (ft/s)	$\sqrt{\overline{u^2}}/\bar{U}_c$	$\sqrt{\overline{u^2}}\,D/\nu$
26611	.130	2.45	.15	8.656	2.785	.3218	1086
"	.080	2.41	.14	7.924	2.524	.3185	"
"	.060	2.39	.138	7.566	2.450	.3238	"
"	.030	2.34	.138	6.696	2.352	.3512	"
21257	.110	2.37	.137	7.214	2.358	.3269	920
"	.070	2.328	.128	6.493	2.159	.3325	"
"	.050	2.3	.127	6.026	2.089	.3467	"
"	.030	2.27	.125	5.539	1.999	.3609	"
16009	.130	2.31	.128	6.191	2.125	.3432	829
"	.080	2.28	.121	5.700	1.954	.3428	"
"	.060	2.25	.12	5.223	1.882	.3604	"
"	.030	2.2	.12	4.458	1.785	.4004	"
9717	.110	2.15	.095	3.736	1.332	.3566	520
"	.060	2.12	.087	3.323	1.173	.3531	"
"	.030	2.08	.086	2.799	1.095	.3913	"

EXPERIMENTAL DATA: MEAN AND FLUCTUATING VELOCITY PROFILES AT REAR STAGNATION POINT WITH GRID J

FIG B.15

$$E_b^2 = 1.75^2 + .582\,\bar{U}^{.666}$$

Re	Y (IN)	E_b (V)	$\sqrt{e^2}$ (V)	$\bar{U}_G$ (FT/S)	$\sqrt{\bar{u}^2}$ (FT/S)	$\sqrt{\bar{u}^2}/\bar{U}_c$	$\sqrt{\bar{u}^2}D/\nu$
29428	.130	2.58	.16	11.178	3.236	.2894	1260
"	.070	2.50	.155	9.600	2.979	.3103	"
"	.050	2.47	.152	9.030	2.862	.3170	"
21917	.130	2.49	.148	9.409	2.825	.3003	1100
"	.070	2.41	.143	7.924	2.575	.3253	"
"	.050	2.38	.142	7.389	2.501	.3384	"
"	.030	2.36	.142	7.040	2.461	.3495	"
16553	.110	2.38	.138	7.389	2.430	.3289	948
"	.070	2.34	.132	6.696	2.249	.3359	"
"	.050	2.31	.133	6.191	2.208	.3566	"
"	.030	2.27	.132	5.539	2.111	.3812	"
9378	.110	2.21	.115	4.608	1.730	.3754	675
"	.070	2.19	.11	4.311	1.618	.3754	"
"	.050	2.19	.11	4.020	1.581	.3933	"
"	.036	2.13	.11	3.459	1.503	.4346	"

EXPERIMENTAL DATA: MEAN AND FLUCTUATING VELOCITY PROFILES AT REAR STAGNATION POINT WITH GRID K

FIG B.16

$$E_b^2 = 1.75^2 + .582\ \bar{U}^{.666}$$

Re	Y (IN)	E_b (V)	$\sqrt{\overline{e^2}}$ (V)	$\bar{U}_o$ (FT/S)	$\sqrt{\overline{u^2}}$ (FT/S)	$\sqrt{\overline{u^2}}/\bar{U}_c$	$\sqrt{\overline{u^2}}D/\nu$
28730	.110	2.54	.152	10.379	2.999	.2889	1166
"	.070	2.49	.150	9.409	2.864	.3044	"
"	.050	2.46	.148	8.842	2.767	.3130	"
"	.030	2.43	.148	8.287	2.708	.3268	"
22526	.110	2.48	.147	9.219	2.757	.3024	1086
"	.070	2.42	.140	8.105	2.543	.3137	"
"	.050	2.38	.140	7.389	2.466	.3337	"
"	.025	2.33	.145	6.526	2.450	.3754	"
16655	.130	2.38	.137	7.389	2.413	.3265	940
"	.070	2.33	.130	6.326	2.196	.3365	"
"	.050	2.28	.135	5.700	2.180	.3825	"
"	.035	2.27	.134	5.539	2.143	.3869	"
10725	.130	2.25	.120	5.223	1.882	.3604	734
"	.070	2.21	.115	4.608	1.730	.3754	"
"	.050	2.19	.113	4.311	1.662	.3856	"
"	.030	2.16	.113	3.877	1.604	.4138	"

EXPERIMENTAL DATA: MEAN AND FLUCTUATING VELOCITY PROFILES AT REAR STAGNATION POINT WITH GRID L

FIG B.17

$$E_b^2 = 1.75^2 + .582\ \bar{U}^{.666}$$

	Re		E_b (V)		$\sqrt{e'^2}$ (V)		$\bar{U}$ (FT/S)		$\sqrt{u'^2}$ (FT/S)		$\sqrt{u'^2}/\bar{U}$
	8821		1.99		.07		1.735		.760		.4379
FREQ (Hz)	20	60	100	200	300	500	700	1000	2000		
$\sqrt{e'^2}$	.0079	.0126	.016	.01	.0079	.005	.0028	.0018	.0000		
$\sqrt{u'^2}$	.086	.137	.174	.109	.086	.054	.030	.020	.0000		
	16076		2.16		.11		3.877		1.562		.4028
FREQ	20	60	120	200	250	300	500	800	1600	2500	6000
$\sqrt{e'^2}$	.0126	.016	.0225	.02	.0282	.02	.016	.0112	.043	.025	.000
$\sqrt{u'^2}$	.179	.227	.319	.284	.4	.284	.227	.159	.061	.035	.000
	21131		2.21		0.126		4.608		1.895		.4113
FREQ	20	60	100	200	300	330	400	600	1000	2000	3000	6000
$\sqrt{e'^2}$	.0126	.02	.0225	.025	.024	.029	.0229	.016	.0126	.0075	.0038	.001
$\sqrt{u'^2}$	.190	.301	.338	.376	.361	.436	.338	.241	.190	.113	.057	.015
	27094		2.29		.1		5.862		1.63		.2781
FREQ	20	60	100	200	400	600	1000	2000	3000	6000	10000	
$\sqrt{e'^2}$	.0178	.023	.0282	.0282	.032	.0225	.0178	.0112	.0064	.0023	.0002	
$\sqrt{u'^2}$	.290	.375	.460	.460	.522	.367	.290	.183	.104	.037	.003	

EXPERIMENTAL DATA: TURBULENCE SPECTRA AT REAR STAGNATION POINT USING GRID A

FIG B.18

$$E_b^2 = 1.75^2 + .582\ \bar{U}^{.666}$$

	Re		E_b (V)		$\sqrt{e^{i2}}$ (V)		$\bar{U}$ (FT/S)		$\sqrt{u^{i2}}$ (FT/S)	$\sqrt{u^{i2}}/\bar{U}$
	11188		2.15		.116		3.736		1.627	.4354
FREQ (Hz)	20	60	100	160	180	200	400	1000	2000	6000
$\sqrt{e^{i2}}$	.01	.016	.0178	.0178	.026	.0178	.0141	.0064	.0028	.0000
$\sqrt{u^{i2}}$	.140	.224	.250	.250	.365	.250	.198	.090	.039	.0000
	16977		2.26		.112		5.38		1.774	.3297
FREQ	20	60	200	230	270	300	600	1200	3000	6000
$\sqrt{e^{i2}}$	.0126	.0178	.02	.02	.04	.02	.016	.01	.0036	.0011
$\sqrt{u^{i2}}$	.200	.282	.317	.317	.634	.317	.253	.158	.057	.017
	22300		2.32		.1		6.358		1.675	.2634
FREQ	20	60	200	300	340	400	1000	2000	4000	8000
$\sqrt{e^{i2}}$	.0141	.0141	.02	.0225	.036	.02	.0141	.009	.004	.0013
$\sqrt{u^{i2}}$	.236	.236	.335	.377	.603	.335	.236	.151	.067	.022
	26270		2.38		.08		7.389		1.409	.1907
FREQ	20	100	340	420	500	1000	2000	4000	8000	20000
$\sqrt{e^{i2}}$	.016	.02	.0225	.038	.02	.015	.01	.005	.002	.0000
$\sqrt{u^{i2}}$	.282	.352	.396	.669	.352	.264	.176	.088	.035	.0000

EXPERIMENTAL DATA: TURBULENCE SPECTRA AT REAR STAGNATION POINT USING GRID E

FIG B.19

$$E_b^2 = 1.75^2 + .582\ \bar{u}^{.666}$$

	Re		E_b (V)		$\sqrt{e'^2}$ (V)		$\bar{u}$ (FT/S)	$\sqrt{u'^2}$ (FT/S)	$\sqrt{u'^2}/\bar{u}$
	9372		2.15		0,126		3.736	1.767	.4730
FREQ (Hz)	20	100	140	160	200	400	1000	3000	5000
$\sqrt{e'^2}$	.0126	.0178	.02	.03	.016	.0112	.0045	.0019	.0000
$\sqrt{u'^2}$	.177	.250	.280	.421	.224	.157	.063	.027	.0000
	16034		2.31		.118		6.191	1.959	.3164
FREQ	20	200	240	300	600	1000	2000	4000	8000
$\sqrt{e'^2}$	.016	.02	.045	.02	.015	.01	.0059	.0024	.0008
$\sqrt{u'^2}$	.266	.332	.747	.332	.249	.166	.098	.040	.013
	21291		2.37		.11		7.241	1.922	.2664
FREQ	20	200	300	340	400	1000	2000	4000	10000	20000
$\sqrt{e'^2}$	.016	.021	.025	.045	.0225	.0141	.008	.004	.001	.0000
$\sqrt{u'^2}$	.28	.367	.437	.786	.393	.246	.140	.070	.017	.0000
	26653		2.45		.08		8.656	1.485	.1716
FREQ	20	200	360	420	550	1000	2000	4000	8000	16000
$\sqrt{e'^2}$	.0178	.0225	.025	.045	.02	.015	.01	.0056	.0025	.001
$\sqrt{u'^2}$	.330	.418	.464	.835	.371	.278	.186	.104	.046	.019

EXPERIMENTAL DATA: TURBULENCE SPECTRA AT REAR STAGNATION POINT USING GRID J

FIG B.20

$E_b^2 = 1.75^2 + .582\ \bar{U}^{.666}$

	Re		E_b (V)		$\sqrt{e^{12}}$ (V)		$\bar{U}$ (FT/S)		$\sqrt{u^{12}}$ (FT/S)	$\sqrt{u^{12}}/\bar{U}$
	9378		2.21		.14		4.608		2.106	.4570
FREQ (Hz)	20	120	150	200	400	800	1600	3000	6000	
$\sqrt{e^{12}}$	.016	.02	.03	.019	.015	.0095	.0045	.0016	.0004	
$\sqrt{u^{12}}$	.241	.301	.451	.286	.226	.143	.068	.024	.006	
	16553		2.38		.13		7.389		2.289	.3098
FREQ	20	200	220	250	300	600	1200	3000	6000	9000
$\sqrt{e^{12}}$	.016	.0225	.015	.04	.0225	.017	.0112	.005	.002	.0013
$\sqrt{u^{12}}$	.282	.396	.440	.704	.396	.299	.197	.088	.035	.023
	21417		2.49		.12		9.409		2.291	.2435
FREQ	20	200	300	350	450	600	1200	2000	4000	8000 20000
$\sqrt{e^{12}}$	.015	.025	.025	.04	.023	.02	.014	.0112	.0064	.0032 .0010
$\sqrt{u^{12}}$	.286	.477	.477	.764	.439	.382	.267	.214	.122	.061 .019
	29428		2.58		.1		11.178		2.022	.1809
FREQ	20	100	200	250	400	600	1000	2000	4000	8000 16000
$\sqrt{e^{12}}$	.014	.02	.025	.032	.028	.025	.019	.0141	.0089	.005 .0025
$\sqrt{u^{12}}$	.283	.404	.506	.647	.566	.506	.384	.285	.180	.101 .051

EXPERIMENTAL DATA: TURBULENCE SPECTRA AT REAR STAGNATION POINT USING GRID K

FIG B.21

$$E_b^2 = 1.75^2 + .582\ \bar{u}^{.666}$$

	Re			E_b (V)		$\sqrt{\overline{e'^2}}$ (V)		$\bar{u}$ (FT/S)		$\sqrt{\overline{u'^2}}$ (FT/S)		$\sqrt{\overline{u'^2}}/\bar{u}$	
	10725			2.25		.14		5.223		2.196		.4204	
FREQ (Hz)	20	100	200	400	800	1600	3000	6000	10000				
$\sqrt{\overline{e'^2}}$	.016	.02	.0225	.016	.0105	.0064	.0028	.001	.0000				
$\sqrt{\overline{u'^2}}$	.251	.314	.353	.251	.165	.100	.044	.016	.0000				
	16655			2.38		.13		7.389		2.289		.3098	
FREQ	20	100	200	250	400	800	2000	4000	8000				
$\sqrt{\overline{e'^2}}$	.016	.025	.0225	.032	.0225	.016	.009	.0045	.0012				
$\sqrt{\overline{u'^2}}$	.282	.440	.396	.564	.396	.282	.158	.079	.021				
	22526			2.48		.12		9.219		2.275		.2468	
FREQ	20	200	300	600	1200	2000	4000	8000	16000				
$\sqrt{\overline{e'^2}}$	.0141	.025	.0282	.021	.016	.0126	.0071	.0036	.0016				
$\sqrt{\overline{u'^2}}$	.267	.474	.535	.398	.303	.239	.135	.068	.030				
	28730			2.54		.1		10.379		1.973		.1901	
FREQ	200	200	320	400	600	1000	2000	4000	8000	16000			
$\sqrt{\overline{e'^2}}$	.0126	.025	.025	.032	.025	.02	.0141	.009	.0056	.0025			
$\sqrt{\overline{u'^2}}$	.249	.493	.493	.631	.493	.395	.278	.178	.110	.049			

EXPERIMENTAL DATA: TURBULENCE SPECTRA AT REAR STAGNATION POINT USING GRID L

FIG B.22